

DECIPHERING THE MECHANISMS OF *WT1* GLOMERULOPATHY

Rowan Isabel Asfahani
University College London

*Thesis submitted for the award of
Doctor of Philosophy*

Supervisors

Dr. Aoife Waters
Prof. Peter Scambler

Declaration

I, Rowan Asfahani confirm that the work presented in this thesis is my own. Where information has been derived from other sources, I confirm that this has been indicated in the thesis.

Abstract

Wilms' tumour 1 (WT1) is a transcription factor encoding a zinc finger protein that controls podocyte differentiation and is highly expressed in mature podocytes. *WT1* mutations can lead to renal failure due to glomerular scarring, the underlying mechanisms, of which, are poorly understood. This project explored the mechanisms of glomerulosclerosis by using a tamoxifen-inducible Cre-LoxP system to delete *Wt1* in adult mice. Following the fourth day post-induction with Tamoxifen, podocyte apoptosis was evident and increased as the disease progressed, highlighting *Wt1*'s key role in mature podocyte survival. At disease onset, increased podocyte *Notch1* transcript and its downstream targets, including *Nrarp* and *Hey2* were observed. Decreased expression of podocyte *FoxC2* transcript at the same time-point was noted, thereby supporting previous findings in lower vertebrates for a transcriptional relationship between *Wt1/FoxC2/Notch* in podocyte function. Podocyte Notch1 and Hes1 protein expression was observed in mutant mouse glomeruli at the onset of glomerulosclerosis. Induced podocyte Hes1 expression was associated with an upregulation of *Snai1* and *Slug* transcripts, genes associated with epithelial to mesenchymal transition (EMT), thus proposing a role for Hes1 in mediating podocyte EMT. Moreover, early pharmacological inhibition of Notch, with gamma secretase inhibitors, ameliorated glomerulosclerosis and albuminuria. This data provides evidence that *Wt1* deletion modulates podocyte Notch signalling in mature podocytes, leading to early events in *WT1*-related glomerulosclerosis.

Impact Statement

Nephrotic syndrome is characterised by excessive protein in the urine (proteinuria) and glomerulosclerosis, where children progress towards end-stage kidney disease. The Wilms' tumour 1 (*WT1*) gene is expressed during kidney development and in mature podocytes. *WT1* mutations have been associated with Denys-Drash Syndrome (DDS) and Frasier Syndrome (FS), disorders associated with glomerulosclerosis.

This project aims to explore whether the Notch pathway is implicated in mammalian *Wt1* glomerulopathy, to add further literature on this subject, and to enable future treatments to be found for kidney disease. Mutant murine and patient tissue has been utilised in this project to explore the expression of Notch pathway components during the evolution of glomerulosclerosis. This project achieved its main objectives through the identification of increased expression of Notch transcripts and protein at disease manifestation in mice and provided the rationale for early therapeutic blockade by administration of gamma secretase inhibitors to repress Notch signalling. Harvesting of primary podocytes proved to be valuable in the identification of a Notch-specific signature at disease onset as we were able to investigate a homogeneous population of cells.

The research, described herein, has provided me with the opportunity to present my findings at local, national and international meetings which afforded me the opportunity to network with fellow researchers in related fields of research. Future funding has been secured to investigate the role of Notch in mice carrying mutations relevant to human disease. My research, reported herein, is now published in a well-regarded scientific journal, and provides the foundation for future work to examine Notch as a new therapeutic strategy for *WT1*-related glomerular disease. This project provides a basis for early intervention for treating kidney disease and possible future treatments to prevent disease manifestation.

Publications and Presentations

The results described in Chapter 3 of this thesis are published in:

Asfahani, R.I., Tahoun, M. M, Miller-Hodges, E. V., Bellerby, J., Virasami, A. K., Sampson, R. D., Moulding, D., Sebire, N.J., Hohenstein, P., Scambler, P. J. & Waters, A. M. 2018. Activation of podocyte Notch mediates early Wt1 glomerulopathy. *Kidney Int*, 93, 903-920

Presentations:

Mammalian Genetics and Development Workshop, November 2015: *Elucidating the Mechanisms of Wt1 Glomerulopathy*

UK Kidney Week, June 2016: *Expression of Ascl1, the Proneural Transcription Factor, Precedes Podocyte Notch Activation in Wt1 Glomerulopathy*

Acknowledgements

I would firstly like to thank my primary supervisor, Dr. Aoife Waters, for giving me the opportunity to undertake my PhD and for her support throughout the project. Your guidance has been invaluable. I would also like to thank my secondary supervisor, Prof. Peter Scambler, who has provided continued support on the project, given me direction and offered valuable scientific advice.

My gratitude is extended to Dr. Peter Hohenstein, Prof. Nicholas Hastie and Dr. Eve Miller-Hodges for their collaboration and support on the project, in addition to contributing the transgenic mouse models. I would also like to thank Dr. David Long for his scientific input on the project and for his laboratory team's efforts in supporting my project.

A special mention and thanks to everyone in Prof. Peter Scambler's group for providing me with extensive scientific guidance; you supported me greatly and were always willing to listen and help. Your continued engagement, whether through teaching, assisting, supporting, listening or just even through the simple act of providing great company, amusing anecdotes or general light-heartedness helped me through tough times and provided encouragement in the pursuit of the doctorate. It has been pleasant, it has been fun, it has been a group that I will look back on with fondness. I would like to extend my gratitude to Daniel Dilg; thank you for sharing your sequencing knowledge and for being very supportive and positive throughout this project.

Finally, my deepest gratitude to my family, in particular my parents for your unconditional support and love, your encouragement has always been a reason why I have made it this far. I'd like to thank my father, whilst no longer here, for giving me the confidence when I needed it the most. Your absence has only spurred me to obtain this PhD. I want to thank my mother, for always being there for me when I have needed you and for keeping me positive throughout this journey. Thank you to my siblings for your continued reassurance and inspiration when mostly needed. And finally, I want to thank you Oscar, for being so patient, supportive, encouraging and cheering me up when times were rough. Everyone's combined kindness and care have made this experience manageable and enjoyable and I couldn't have done it without any of you.

Table of Contents

| | |
|--|-----------|
| List of Figures | 10 |
| List of Tables | 12 |
| List of Abbreviations | 13 |
| Chapter 1 - Introduction | 15 |
| 1.1 Glomerular development | 15 |
| 1.1.1 Podocyte morphology and maintenance of the glomerular filtration barrier (GFB) | 15 |
| 1.1.2 Overview of podocytes in kidney development..... | 17 |
| 1.1.3 Podocyte differentiation | 18 |
| 1.1.4 The glomerular filtration barrier..... | 19 |
| 1.2 Podocyte injury | 22 |
| 1.2.1 Nephrotic syndrome (NS) | 23 |
| 1.2.2 Phenotypes of podocyte injury..... | 25 |
| 1.2.3 Mechanisms of podocyte injury | 26 |
| 1.3 Molecular regulation of podocyte differentiation | 29 |
| 1.3.1 Wilms' tumour-1 (<i>WT1</i>)..... | 31 |
| 1.3.2 Forkhead-box C1/2 (<i>FOXC1/2</i>)..... | 41 |
| 1.3.3 Other genes associated with podocyte development | 43 |
| 1.4 Notch Signalling and glomerulogenesis | 45 |
| 1.4.2 Notch signalling activation | 47 |
| 1.4.3 Ligand-independent Notch signalling..... | 50 |
| 1.4.4 Expression of Notch pathway components during kidney development... | 52 |
| 1.4.5 The role of Notch in kidney development | 53 |
| 1.5 Interplay between <i>WT1</i> and Notch in vertebrate nephrogenesis | 61 |
| 1.6 Scope of the thesis | 63 |
| Chapter 2 – Materials and Methods | 64 |
| 2.1 Transgenic mouse strains | 64 |
| 2.2 Genotyping | 67 |
| 2.3 Glomerular isolation | 69 |
| 2.4 Primary podocyte culture | 70 |
| 2.5 RNA extraction | 70 |
| 2.6 Real-time qPCR | 70 |
| 2.7 Phenotype analysis | 74 |

| | | |
|---|--|------------|
| 2.7.1 | Renal histology | 74 |
| 2.7.2 | Urine protein analysis | 74 |
| 2.7.3 | Immunohistochemistry and immunofluorescence multi-labelling..... | 75 |
| 2.8 | Apoptosis Assays | 78 |
| 2.8.1 | Cleaved caspase 3 analysis | 78 |
| 2.8.2 | DeadEnd Fluorometric TUNEL assay..... | 78 |
| 2.8.3 | Caspase 3/7 immunostaining | 79 |
| 2.8.4 | Annexin V staining | 79 |
| 2.8.5 | Fluorescence microscopy | 79 |
| 2.9 | Western blotting..... | 80 |
| 2.10 | Glomerular RNA sequencing | 81 |
| 2.11 | Podocyte shRNA experiments..... | 81 |
| 2.12 | Statistical analysis..... | 82 |
| | | |
| Chapter 3 - Podocyte Notch activation coincides with the onset of <i>Wt1</i> | | |
| | Glomerulopathy | 83 |
| | | |
| 3.1 | Introduction | 83 |
| 3.2 | Results | 84 |
| 3.2.1 | <i>Wt1</i> deletion leads to glomerulosclerosis (GS)..... | 84 |
| 3.2.2 | Apoptosis is evident in <i>Cre-ER^{TM+/-};Wt1^{fl/fl}</i> mutants | 93 |
| 3.2.3 | Podocyte Notch activation precedes GS in <i>Cre-ER^{TM+/-};Wt1^{fl/fl}</i> mutants... | 102 |
| 3.2.4 | Notch inhibition ameliorates disease severity in <i>Wt1</i> glomerulopathy ... | 116 |
| 3.2.5 | Podocyte epithelial-mesenchymal transition (EMT) in <i>Cre-ER^{TM+/-};Wt1^{fl/fl}</i> mutants at the onset of <i>Wt1</i> glomerulopathy..... | 121 |
| 3.3 | Discussion | 123 |
| | | |
| Chapter 4 - <i>Ascl1</i> expression precedes podocyte Notch activation in <i>Wt1</i> | | |
| | glomerulopathy | 132 |
| | | |
| 4.1 | Introduction | 132 |
| 4.2 | Results | 135 |
| 4.2.1 | <i>Ascl1</i> is upregulated in D4 P.I. <i>Cre-ER^{TM+/-};Wt1^{fl/fl}</i> mutant glomeruli | 135 |
| 4.2.2 | Glomerular ASCL1 and HES1 protein in patient <i>WT1</i> glomerulopathies | 139 |
| 4.2.3 | TUNEL is not detected in all ASCL1-positive cells in late GS..... | 140 |
| 4.2.4 | Patterns of ASCL1 expression during glomerulogenesis..... | 141 |
| 4.2.5 | Doxycycline-induced <i>Ascl1</i> expression in <i>TetOAscl1;NPHS2;rtTA</i> mice | 143 |
| 4.3 | Discussion | 148 |

| | |
|--|------------|
| Chapter 5 - Discussion and Future Directions | 153 |
| 5.1 Overall Discussion..... | 153 |
| 5.1.1 Utility of inducible models to study mechanisms underlying disease onset.. | |
| | 153 |
| 5.1.2 Utility of primary podocyte culture..... | 156 |
| 5.1.3 Limitations..... | 156 |
| 5.2 Future work..... | 157 |
| 5.2.1 Pharmacological inhibition of Notch to prevent late stages of disease... | 157 |
| 5.2.2 Investigating Fringe and ligand-mediated Notch signalling in podocytes | 157 |
| 5.2.3 Strategies to investigate transcriptional networks..... | 158 |
| 5.2.4 Genetic rescue strategies | 160 |
| 5.2.5 Transgenic <i>Wt1^{R394W}</i> mutant mice | 161 |
| 5.2.6 Notch pathway analysis in other murine models of GS | 162 |
| 5.3 Summary..... | 162 |
| References | 163 |
| Appendix A | 206 |
| Appendix B | 208 |

List of Figures

| | |
|--|-----|
| Figure 1.1. The kidney glomerulus..... | 15 |
| Figure 1.2. The glomerular filtration barrier (GFB)..... | 16 |
| Figure 1.3. Podocyte morphology | 17 |
| Figure 1.4. Kidney development | 18 |
| Figure 1.5. Podocyte differentiation | 19 |
| Figure 1.6. Components of the podocyte foot process associated with proteinuria | 20 |
| Figure 1.7. Focal segmental glomerulosclerosis..... | 25 |
| Figure 1.8. Diffuse mesangial sclerosis | 26 |
| Figure 1.9. Signalling pathways for induction of podocyte apoptosis | 27 |
| Figure 1.10. Epithelial and mesenchymal features of podocytes | 28 |
| Figure 1.11. Structure of <i>WT1</i> and its isoforms | 32 |
| Figure 1.12. <i>WT1</i> expression during kidney development..... | 33 |
| Figure 1.13. Roles of <i>WT1</i> in transcriptional and post-transcriptional regulation | 40 |
| Figure 1.14. Notch pathway components | 46 |
| Figure 1.15. The Notch pathway | 47 |
| Figure 1.16. Ligand-independent Notch activation | 51 |
| Figure 1.17. Notch expression during podocyte differentiation..... | 52 |
| Figure 1.18. Transcriptional regulation of podocyte development..... | 62 |
| Figure 2.1. <i>Wt1</i> exon 1 deletion. | 65 |
| Figure 2.2. Transgenic <i>TetOAscl1;Nphs2;rtTA</i> experiment outline | 67 |
| Figure 2.3. Real-time qPCR protocol | 72 |
| Figure 3.1. Temporal <i>Wt1</i> deletion in <i>Cre-ER^{TM+/-};Wt1^{ff}</i> mutants. | 85 |
| Figure 3.2. Temporal increase of GS in <i>Cre-ER^{TM+/-};Wt1^{ff}</i> mutants post-tamoxifen induction ... | 87 |
| Figure 3.3. <i>WT1</i> is expressed <i>Cre-ER^{TM+/-};Wt1^{ff}</i> hets transgenic mice post-tamoxifen induction | 88 |
| Figure 3.4. FP effacement at D4 P.I. in <i>Cre-ER^{TM+/-};Wt1^{ff}</i> transgenic mice..... | 89 |
| Figure 3.5. Vascular SMA expressed in <i>Cre-ER^{TM+/-};Wt1^{ff}</i> mutants | 91 |
| Figure 3.6. Podocin-positive cells in kidney tubules of D8 P.I. <i>Cre-ER^{TM+/-};Wt1^{ff}</i> mutants | 93 |
| Figure 3.7. Temporal increase in podocyte apoptosis in <i>Cre-ER^{TM+/-};Wt1^{ff}</i> mutants..... | 95 |
| Figure 3.8. Cleaved-caspase-3/7 is activated in primary <i>Cre-ER^{TM+/-};Wt1^{ff}</i> podocytes | 96 |
| Figure 3.9. TUNEL-positive primary podocytes in D6 P.I. <i>Cre-ER^{TM+/-};Wt1^{ff}</i> mutants..... | 97 |
| Figure 3.10. TUNEL-positive glomeruli in D5 P.I. of <i>Cre-ER^{TM+/-};Wt1^{ff}</i> mutants | 98 |
| Figure 3.11. TUNEL-positive cells in <i>Cre-ER^{TM+/-};Wt1^{ff}</i> glomeruli at D12 P.I. | 99 |
| Figure 3.12. Apoptosis is increased at D8 P.I. in <i>Cre-ER^{TM+/-};Wt1^{ff}</i> mutant podocytes | 100 |
| Figure 3.13. Podocyte apoptosis in pre-proteinuric and GS <i>Cre-ER^{TM+/-};Wt1^{ff}</i> mutants. | 102 |
| Figure 3.14. Podocyte Notch pathway gene expression in pre-proteinuric <i>Cre-ER^{TM+/-};Wt1^{ff}</i> primary podocytes..... | 104 |
| Figure 3.15. Activated cleaved Notch1 at the early onset of disease in <i>Cre-ER^{TM+/-};Wt1^{ff}</i> mutants | 106 |

| | |
|---|-----|
| Figure 3.16. Notch activation coincides with onset of GS in <i>Cre-ER^{TM+/-};Wt1^{ff}</i> mutants..... | 108 |
| Figure 3.17. JAGGED 1 is expressed in <i>Cre-ER^{TM+/-};Wt1^{ff}</i> glomeruli at disease onset | 110 |
| Figure 3.18. Increased Notch pathway transcripts in primary mutant <i>WT1</i> podocytes | 111 |
| Figure 3.19. Podocyte Hes1 expression coincides with onset of GS in <i>Cre-ER^{TM+/-};Wt1^{ff}</i> mutants | 112 |
| Figure 3.20. Upregulation of podocyte EMT genes in <i>TetOHes1</i> -induced podocytes..... | 113 |
| Figure 3.21. Hes1 is increased post-doxycycline treatment in <i>Nphs2;rtTA</i> -transduced podocytes | 114 |
| Figure 3.22. JAGGED1 and HES1 are expressed in <i>WT1</i> c.1390G>T (p.Asp464Asn) human glomeruli..... | 115 |
| Figure 3.23. γ -secretase inhibition of Notch ameliorates early <i>Wt1</i> glomerulopathy | 117 |
| Figure 3.24. <i>Wt1</i> transcript and protein levels are comparable in <i>Cre-ER^{TM+/-};Wt1^{ff}</i> mutants post- γ -secretase inhibition and vehicle treatment | 118 |
| Figure 3.25. γ -secretase inhibition in <i>Cre-ER^{TM+/-};Wt1^{ff}</i> at D8 P.I. does not rescue GS..... | 120 |
| Figure 3.26. <i>Mfng/Rbpj</i> shRNA knockdown in <i>Cre-ER^{TM+/-};Wt1^{ff}</i> podocytes repress Notch bHLH transcripts..... | 122 |
| Figure 4.1. Interplay between <i>Ascl1</i> and Notch signalling during neurogenesis | 133 |
| Figure 4.2. Upregulation of <i>Ascl1</i> mRNA and protein in D4 P.I. <i>Cre-ER^{TM+/-};Wt1^{ff}</i> mutant glomeruli..... | 137 |
| Figure 4.3. <i>Ascl1</i> and <i>Hes1</i> mRNA levels oscillate in <i>Cre-ER^{TM+/-};Wt1^{ff}</i> mutants from D4 to D6 P.I. | 139 |
| Figure 4.4. ASCL1 and HES1 are expressed in <i>WT1</i> glomeruli | 140 |
| Figure 4.5. ASCL1 protein is expressed in D12 P.I. <i>Cre-ER^{TM+/-};Wt1^{ff}</i> glomeruli | 141 |
| Figure 4.6. ASCL1 protein expression during early glomerulogenesis..... | 142 |
| Figure 4.7. ASCL1 protein expression during late glomerulogenesis..... | 143 |
| Figure 4.8. Upregulation of <i>Ascl1</i> mRNA and protein in doxycycline-induced <i>TetOAscl1;NPHS2rtTA</i> primary podocytes | 145 |
| Figure 4.9. Doxycycline-induced <i>TetO:Ascl1;NPHS2;rtTA</i> exhibit normal glomerular morphology | 147 |
| Figure 5.1. Experimental design for Manic Fringe overexpression in podocytes | 158 |
| Figure 5.2. Binding domains within the <i>WT1</i> promoter for Notch bHLH genes..... | 160 |
| Figure 5.3. Experimental strategy to genetically inhibit Notch target genes in <i>Wt1</i> glomerulopathy..... | 161 |

List of Tables

| | |
|---|----|
| Table 1.1. Genes implicated in human NS | 23 |
| Table 1.2. Genes regulating early podocyte differentiation | 30 |
| Table 1.3. Early nephrogenesis in transgenic mouse models of <i>Wt1</i> gene manipulation | 37 |
| Table 1.4. Late nephrogenesis in transgenic mouse models of <i>Wt1</i> gene manipulation | 39 |
| Table 1.5. Nephrogenesis in transgenic models of <i>FoxC</i> gene manipulation | 42 |
| Table 1.6. List of glycosyltransferases that modify Notch ECD | 49 |
| Table 1.7. Fringe-mediated glycosylation of Notch 1 | 50 |
| Table 1.8. Expression of the Notch components during glomerulogenesis..... | 53 |
| Table 1.9. Early nephrogenesis in transgenic mouse models of Notch gene manipulation | 57 |
| Table 1.10. Late nephrogenesis in transgenic mouse models of Notch gene manipulation | 58 |
| Table 1.11. Inhibition of Notch signalling in murine glomerular disease..... | 60 |
| Table 2.1. Tail lysis buffer | 68 |
| Table 2.2. Genomic primers for genotyping..... | 68 |
| Table 2.3. PCR programme for genotyping <i>Cre-ERT2</i> and <i>Wt1</i> floxed alleles | 69 |
| Table 2.4. PCR Programme for genotyping <i>TetOAscl1;rtTANPHS2</i> transgenic mice..... | 69 |
| Table 2.5. qPCR reagents..... | 71 |
| Table 2.6. Real-time qPCR primers | 72 |
| Table 2.7. Antibodies for IHC, ICC, IFC..... | 77 |

List of Abbreviations

| | |
|----------------|---|
| BC | Bowman's capsule |
| BHLH | Basic Helix Loop Helix |
| BS | Bowman's space |
| CG | Collapsing glomerulopathy |
| CKD | Chronic kidney disease |
| CL | Capillary loops |
| CMV | Cytomegalovirus |
| CNS | Congenital Nephrotic Syndrome |
| DDS | Denys-Drash syndrome |
| DEPC | Diethyl pyrocarbonate |
| DLL | Delta-like |
| DMS | Diffuse Mesangial Sclerosis |
| DT | Distal tubule |
| EGF | Epidermal growth factor |
| EMT | Epithelial to mesenchymal transition |
| ESRD | End-stage renal disease |
| EtOH | Ethanol |
| F-actin | Filamentous actin |
| FA | Folic Acid |
| FGF | Fibroblast growth factor |
| FP | Foot process |
| FS | Fraser Syndrome |
| FSGS | Focal Segmental Glomerulosclerosis |
| GBM | Glomerular Basement Membrane |
| GFB | Glomerular filtration barrier |
| GO | Gene ontology |
| GS | Glomerulosclerosis |
| HBSS | Hank's balanced salt solution |
| HIVAN | Human Immunodeficiency Virus-associated Nephropathy |
| IM | Intermediate mesoderm |
| LB | Lysogeny broth |
| MCD | Minimal change disease |
| MET | Mesenchymal to Epithelial transition |
| MM | Metanephric mesenchyme |
| NECD | Notch extracellular domain |

| | |
|--------------|--|
| NICD | Notch intracellular domain |
| NLS | Nuclear localising sequence |
| NPC | Nephron progenitor cells |
| NRR | Negative regulatory region |
| NS | Nephrotic syndrome |
| PAS | Period acid-Schiff stain |
| PBS | Phosphate-buffered saline |
| PCR | Polymerase chain reaction |
| PEC | Parietal epithelial cell |
| PEST | Proline/glutamic acid/serine/threonine-rich motifs |
| PFA | Paraformaldehyde |
| P.I. | Post-induction |
| PT | Proximal tubule |
| PTA | Pre-tubular aggregate |
| PVDF | Polyvinylidene difluoride |
| qPCR | Quantitative polymerase chain reaction |
| RV | Renal vesicle |
| SD | Slit diaphragm |
| SDS | Sodium dodecyl sulphate |
| SRNS | Steroid-resistant nephrotic syndrome |
| SSC | Saline sodium citrate |
| TAD | Transactivation domain |
| TEM | Transmission electron microscopy |
| TIF | Tubulointerstitial fibrosis |
| TMD | Transmembrane domain |
| TUNEL | Terminal deoxynucleotidyl transferase-mediated deoxyuridine triphosphate nick-end labelling |
| UB | Ureteric bud |
| WT1 | Wilms' tumour 1 |

Chapter 1 - Introduction

The mammalian kidney plays a crucial role in fluid homeostasis by preserving pH and electrolyte balance. Each human kidney comprises about one million nephrons, consisting of a glomerulus which filters plasma to the proximal nephron (Figure 1.1) (Quaggin and Kreidberg, 2008).

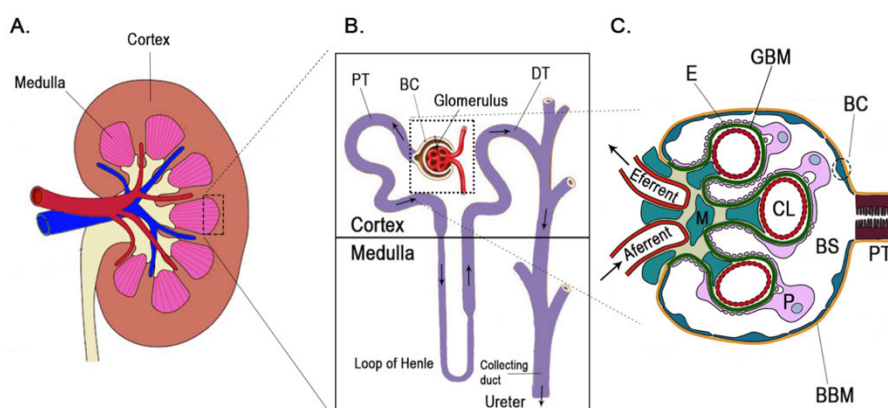


Figure 1.1. The kidney glomerulus

(A) Sagittal section demonstrating the gross structure of the mammalian kidney. **(B)** Cortex: the nephron, showing the glomerulus, along with the Bowman's capsule (BC), Proximal tubule (PT), Distal tubule (DT). Medulla: loop of Henle, collecting duct and ureter. **(C)** Kidney glomerulus: Endothelial cells (E), glomerular basement membrane (GBM), BC, capillary loops (CL), mesangial cells (M), podocytes (P), Bowman's space (BS), PT. Adapted from (Mimura and Nangaku, 2010, Quaggin and Kreidberg, 2008)

1.1 Glomerular development

1.1.1 Podocyte morphology and maintenance of the glomerular filtration barrier (GFB)

Podocytes are terminally differentiated specialised epithelial cells that comprise the outer layer of the GFB (Figure 1.2) (Quaggin and Kreidberg, 2008, Asanuma, 2015). They exert their function through a unique architecture consisting of a cell body from which cytoplasmic processes (primary) extend and further branch into secondary and tertiary foot processes (FPs), which then interdigitate with adjacent FPs of neighbouring cells (Figure 1.3A, B, D).

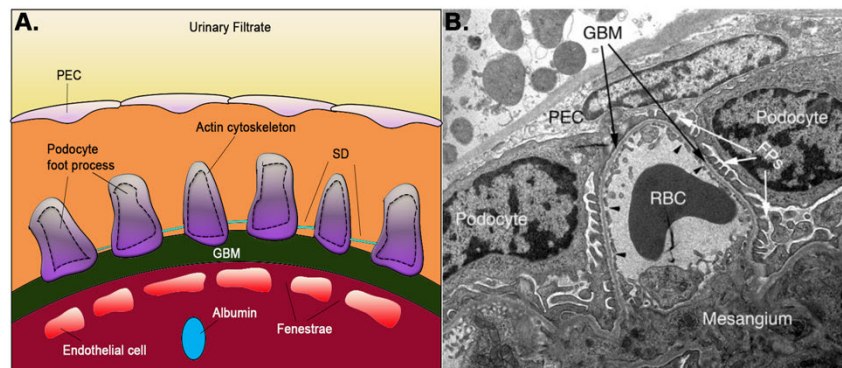


Figure 1.2. The glomerular filtration barrier (GFB)

(A) The GFB is comprised of the podocytes, endothelial cells, and GBM. The slit diaphragm (SD) between the interdigitating podocyte FPs control plasma filtration. The glomerular capillaries filter blood through the endothelium and GBM into the SD to produce primary urinary filtrate. (B) TEM demonstrating the layers of the GFB: The GBM lies between the podocytes and endothelium. The endothelial cells are fenestrated (black arrows) and line the capillary lumen. The glomerulus also contains parietal epithelial cells (PECs), which line the Bowman's capsule and the mesangium. Adapted from (Miner, 2012).

Primary processes are composed of predominantly intermediate filaments and microtubules, while a tightly regulated actin cytoskeleton underlies the architecture of secondary and tertiary FPs (Reiser et al., 2000, Schell and Huber, 2017). The podocytes encase the glomerular basement membrane (GBM) with their FPs through integrins and dystroglycans, namely α and β -dystroglycan, giving them structural support (Jefferson et al., 2011). The podocyte slit diaphragms (SDs), along with the endothelia and GBM, allow filtration of small solutes and plasma water, whilst retaining larger molecules in the plasma. Figure 1.3C illustrates a 3-dimensional reconstitution of the podocyte SD. Under normal conditions, cell membranes extend as cross-strands to form pores, preventing large proteins from entering the urine.

Loss of glomerular permselectivity is associated with leakage of plasma proteins into the urine (proteinuria) (Schell et al., 2014, Greka and Mundel, 2012, Jefferson et al., 2011, Scott and Quaggin, 2015). Proteinuric diseases are associated with a loss of podocyte interdigitations (effacement), (Figure 1.3D), which are morphologically considered to represent a reversal to an immature cellular phenotype. (Grahammer et al., 2013).

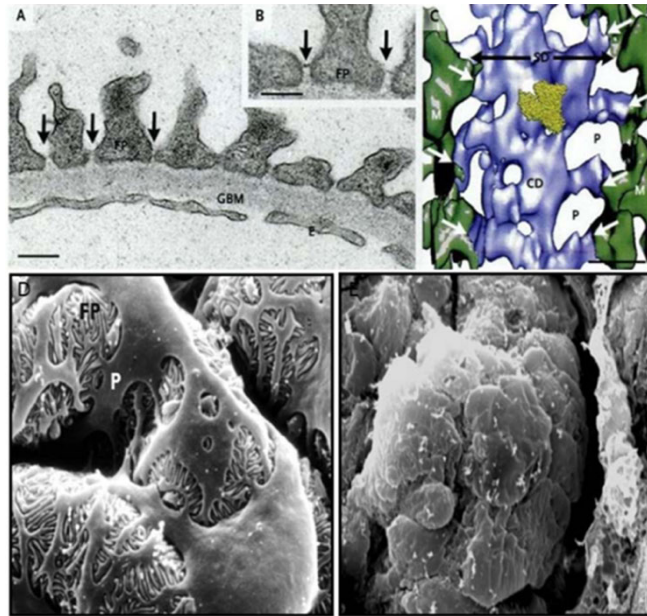


Figure 1.3. Podocyte morphology

(A, B) Transmission Electron Micrograph (TEM) representing FPs enwrapping the glomerular basement membrane (GBM); **(B)** Highlighting the FP, with the SD. **(C)** Electron tomography displaying a 3D reconstitution of the SD (blue) spanning the filtration slit between FPs (green). The podocyte cell membranes extend as cross-strands (white arrows), forming lateral pores and merge centrally into a longitudinal central density (CD), preventing proteins larger than the pores to enter the urine. **(D)** Scanning electron micrograph (SEM) of normal podocyte structure in mice; primary and secondary processes interdigitate forming FPs, which cover the GBM and capillaries, allowing filtration to take place. **(E)** SEM displaying FP effacement due to podocyte injury (Waters et al., 2008, Wartiovaara et al., 2004)

1.1.2 Overview of podocytes in kidney development

Podocyte precursors are cuboidal in shape and are first identified within the S-shaped body at the onset of glomerulogenesis. A series of morphological events occurs during kidney development, following induction of the metanephric mesenchyme (MM) (Costantini and Kopan, 2010, Seely, 2017). Condensation of the MM around each UB tip ensues forming the pretubular aggregate (PTA) (Saxen and Sariola, 1987, Kreidberg et al., 1993, Stark et al., 1994, Carroll et al., 2005) (Figure 1.4). The PTAs undergo mesenchymal-to-epithelial-transition (MET) to develop into the epithelial renal vesicle (RV), subsequently morphing into the comma-shaped bodies, developing a cleft at their distal end to form S-shaped bodies. Cells which proximate to the S-shape cleft give rise to the podocyte cells, while cells in the caudal region are specified towards the proximal tubule. The S-shaped body vascularises at the proximal end to form a single capillary loop, eventually forming a network of capillary loops to become the glomerulus, assisted by endothelial and mesangial cells (Figure 1.4) (Stark et al., 1994, Saxen and Sariola,

1987). The distal RV develops into proximal and distal tubules; proximal polarity establishes the proximal tubule segments and loop of Henle, distal segments form the distal tubules, which connect to the collecting duct (Kreidberg, 2010, Kreidberg et al., 1993, Saxen and Sariola, 1987, Quaggin and Kreidberg, 2008).

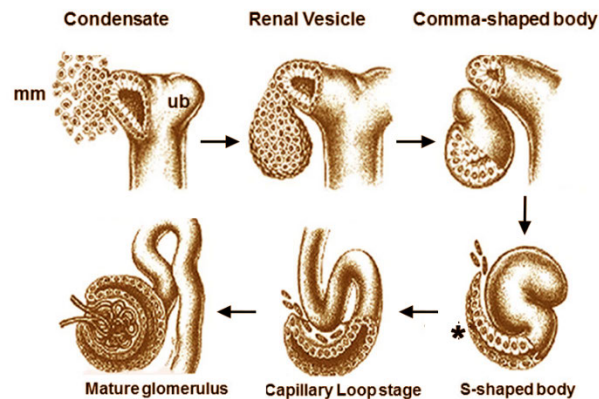


Figure 1.4. Kidney development

Condensation of the metanephric mesenchyme (MM) leads to the formation of the renal vesicle, eventually becoming the comma- and S-shaped bodies. The podocyte precursors are expressed in the proximal medial region of the S-shaped body cleft (asterisk). Vascularisation of the S-shaped body leads to a single capillary loop, ultimately forming a mature glomerulus through a network of capillaries. Adapted from (Saxen and Sariola, 1987).

1.1.3 Podocyte differentiation

The primitive podocytes are located within the inner aspect of the proximal cleft of the S-shaped body (Figure 1.4). Columnar in shape, they are connected to each other at their lateral margins by tight junctions (Kreidberg, 2003, Quaggin and Kreidberg, 2008) (Figure 1.4, Figure 1.5) (Kreidberg, 2003, Quaggin and Kreidberg, 2008, Brunskill et al., 2011). As the glomerular capillary loops develop, the podocyte precursors develop primary FPs which are anchored to the underlying GBM (Kreidberg, 2003) (Figure 1.5). Primary processes develop into secondary and tertiary FPs and become interdigitated with FPs of neighbouring podocytes (Figure 1.5C).

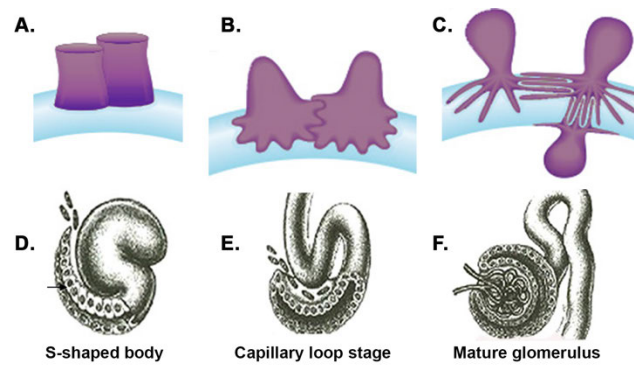


Figure 1.5. Podocyte differentiation

(A) Podocyte progenitors (purple) begin as columnar epithelial cells adhered at their lateral margins, lying on the underlying developing glomerular capillary loop (blue). (B) Podocyte differentiation involves the dissociation of the podocyte cell bodies from one another, with cytoplasmic extensions arising from the basal aspect of the cell bodies. (C) Neighbouring foot processes become interdigitated with each other, wrapping around the capillary loops and forming the mature glomerulus. (D-F) Representative images showing corresponding stages of glomerular development. Adapted from (Quaggin and Kreidberg, 2008).

1.1.4 The glomerular filtration barrier

The formation of the GFB involves coordinated reciprocal interactions between the podocyte precursors and the developing capillary vasculature with interposition of the GBM. A single capillary loop is initiated in the glomerular cleft of proximal S-shaped body following the secretion of vascular endothelial growth factor-A (VEGF-A) by the podocyte precursors (Quaggin and Kreidberg, 2008, Eremina et al., 2003). The capillary loop further develops into six to eight loops whilst the podocytes produce structural components of the underlying GBM, which provides support to the developing glomerular vasculature. Platelet-derived growth factor- α and β (PDGF), produced by mesangial cells, also contributes to mesangial interposition in between developing capillary loops during glomerular development (Jefferson et al., 2011). Ultimately, the GBM lies interposed between the underlying fenestrated endothelium and an epithelial sheet composed of interdigitating podocyte FPs.

Interaction between podocyte $\alpha 3\text{-}\beta 1$ integrin and GBM $\beta 2$ laminin mediates the attachment of the podocytes to the GBM (Foster et al., 2003, Eremina and Quaggin, 2004, Sir Elkhatim et al., 2014, Eremina et al., 2007) (Figure 1.2). Podocyte precursors produce and secrete laminin-1 ($\alpha 1\beta 1\gamma 1$) and collagen IV ($\alpha 1$ and $\alpha 2$). As the GBM develops, the $\beta 1$ chain of laminin is progressively lost and there is a shift to laminin 11 ($\alpha 5\beta 2\gamma 1$) and collagen IV subunits ($\alpha 3$, $\alpha 4$, $\alpha 5$) at the capillary loop stage (Miner and Sanes, 1994, Abrahamson and St John, 1993, Miner, 1998). The $\alpha 6$ chain of collagen

IV is located in the Bowman's capsule basement membrane. Mutations in collagen IV $\alpha 3$ and $\alpha 4$ chains lead to Alport syndrome, a proteinuric kidney disease that arises from a defective GBM (Hudson et al., 1992). Mutations in LAMB2 are associated with Pierson syndrome, a proteinuric kidney disease which presents in the first year of life and is associated with glomerulosclerosis and defective GBM (Liapis, 2008).

The podocyte SD comprises the size-selective layer of the GFB. Lying between the connecting FPs, SDs are composed of proteins such as nephrin (*NPHS1*), podocin (*NPHS2*) and CD2-associated protein (CD2AP) (Figure 1.6).

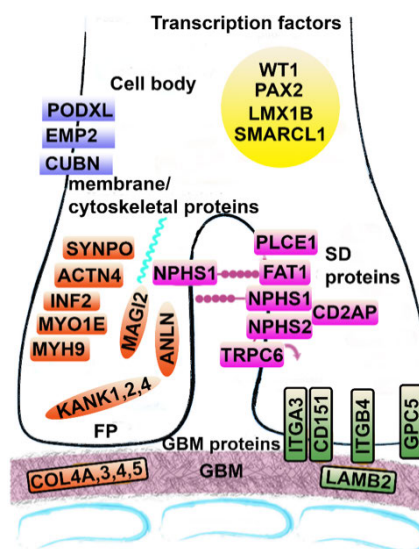


Figure 1.6. Components of the podocyte foot process associated with proteinuria

Proteinuria is a heterogeneous disease which can be associated with mutations in genes encoding transcription factors involved in podocyte differentiation, cytoskeletal proteins important for FP integrity and SD function. Adapted from (Preston et al., 2017).

1.1.4.1 Composition and function of podocyte foot processes

Tertiary podocyte FPs play a critical role in the maintenance of glomerular permselectivity. In podocyte injury, proteinuria is associated with a broadening and flattening of podocyte FP, known as FP effacement (Ronco, 2007, Kerjaschki, 1994, Salant, 1994). FP morphology is regulated by a tightly structured intracytoplasmic network of cytoskeletal proteins such as actin, synaptopodin and myosin. Integrins, heterodimeric transmembrane receptors connect the FP actin cytoskeleton to the extracellular matrix of the GBM (Kikkawa et al., 1998, Kreidberg, 2000, Hynes, 2002). The main integrins that bind laminins are integrins $\alpha 3\beta 1$ and $\alpha 6\beta 1$, whereas integrins that bind to collagen are integrins $\alpha 1\beta 1$ and $\alpha 2\beta 1$. Deletion of integrin $\alpha 3$ in transgenic mice is associated with proteinuria and FP effacement in their first week of life (Sachs et

al., 2006). Moreover, deletion of integrin $\alpha 3$ and $\alpha 5$ laminin in mice leads to an inability to form FPs (Kreidberg et al., 1996).

1.1.4.2 Development of the slit diaphragm (SD)

SDs are located at the basolateral region of the podocyte FPs and prevent large molecular weight proteins such as albumin [MW 50kDa] from entering the urinary filtrate in Bowman's capsule. SDs initiate as junctional complexes at the apical region of podocyte precursors within the proximal region of the S-shaped body. During podocyte maturation, these cell-cell junctions migrate to the basal aspect of the cell where the composition changes from that of a tight junction to a modified adherens junction at the basolateral aspects of the FPs. Numerous proteins participate in the formation of the SD, giving it its unique structure (Fukasawa et al., 2009).

Nephrin

Nephrin (encoded by *NPHS1*) is one of the structural components of the SD. A member of the immunoglobulin superfamily, nephrin, consists of a short intracellular domain, a transmembrane domain and a long extracellular domain with a proximal fibronectin type III-like motif (Tryggvason et al., 2006, Martin and Jones, 2018). The nephrin extracellular domain forms the main outline of the SD by forming homo and heterodimers with itself and NEPH1 to maintain SD integrity (Gerke et al., 2003, Sellin et al., 2003). NEPH1 has shown to impact podocyte integrity; earlier work revealed that in murine models, *Neph1* deficiency resulted in proteinuria and loss of kidney function (Donoviel et al., 2001). Tyrosine phosphorylation of the intracellular domain of nephrin regulates its interaction with the adaptor proteins, NCK1 and NCK2, which interact with the actin cytoskeleton and regulate FP morphology (Verma et al., 2006, Qin et al., 2009). Mutations in *NPHS1* causes congenital nephrotic syndrome (CNS), characterised by proteinuria in the first 3 months of life and progressive kidney failure (Kestila et al., 1998, Ruotsalainen et al., 1999, Holthofer et al., 1999, Holzman et al., 1999). CNS is a heterogenous condition associated with mutations in a variety of genes such as *NPHS2*, which encodes podocin, a known interactor of nephrin (Boute et al., 2000).

Podocin

Podocin (*NPHS2*) is a hairpin-like integral membrane 42kDa protein localised at the SD (Boute et al., 2000). It forms oligomers with the intracellular domains of nephrin and NEPH1, as well as with CD2AP (Schwarz et al., 2001, Huber et al., 2003b). Around 10-

28% of all non-familial childhood recessive mutations of *NPHS2* exhibit proteinuria and result in postnatal death (Roselli et al., 2002). Steroid-resistant nephrotic syndrome (SRNS) has been associated with the missense mutation, R138Q in *NPHS2*. *Nphs2*^{R140x/R140x} transgenic mice exhibit proteinuria by postnatal day 10 and represent a useful mouse model of CNS (Philippe et al., 2008).

CD2AP

CD2AP, an intracellular protein that interacts with the C-terminus of nephrin, forms a network with both nephrin and podocin to connect the actin cytoskeleton to the SD (Shih et al., 2001, Schwarz et al., 2001). Structurally, it consists of a coiled coil domain and 3 Src homology 3 domains (SH3). CD2AP interacts with p85, an intermediary protein and prevents podocyte apoptosis through Nephrin-induced AKT signalling (Huber et al., 2003a, Dustin et al., 1998, Welsch et al., 2001). New-born *Cd2ap*^{-/-} mice develop proteinuria and FP effacement during their first week of life (Shih et al., 1999).

Other SD proteins

SD maintenance is further supported by additional proteins, including membrane-associated guanylate kinase inverted 2 (MAGI-2), calcium/calmodulin-dependent serine protein kinase (CASK), α -actinin, ZO-1 (Patrakka and Tryggvason, 2007). Large transmembrane proteins, FAT1 and FAT2, are also necessary for SD structure (Inoue et al., 2001). *Fat1*^{-/-} mice lack assembled FPs and SDs and suffer from proteinuria. *Fat2*^{-/-} mice also develop proteinuria (Ciani et al., 2003). Myosin 1E (MYO1E), a protein which binds actin during podocyte synthesis, is required for the filtration barrier. Mutations in this gene in both humans and mouse knockout models cause FP effacement and proteinuria (Krendel et al., 2009, Chase et al., 2012). SD proteins implicated in human proteinuric conditions are highlighted in Table 1.1.

1.2 Podocyte injury

Podocyte injury plays a major role in glomerulosclerosis (GS), the scarring of the glomerulus (Marshall and Shankland, 2006, Liapis et al., 2013, Dimke et al., 2015). GS is a leading global cause of end-stage renal disease (ESRD) and accounts for 5% to 10% of paediatric and adult ESRD. GS can recur in 30% to 50% of kidney transplants and therefore, represents a major economic health burden (Saran et al., 2016). Podocyte injury results in proteinuria (specifically albuminuria) which, when associated with oedema and hypoalbuminaemia, manifests as nephrotic syndrome (NS).

1.2.1 Nephrotic syndrome (NS)

NS is a clinical entity characterised by albuminuria, oedema, hypoalbuminaemia, and hyperlipidaemia. It affects 1-2 per 100,000 children (Liebeskind, 2014, McKinney et al., 2001). Classification is often based on clinical response to steroid therapy; NS can either be steroid-sensitive or steroid-resistant (SRNS). SRNS is more typically associated with GS which is a progressive kidney disease for which there are no specific treatments available (Tasic et al., 2015, Hostetter, 2001). Four genes (*NPHS1*, *NPHS2*, *LAMB2*, *WT1*) have been linked to 85% of SRNS in patients aged less than 3 months and 66% 1-year olds (Sadowski et al., 2015). Table 1.1 outlines genes encoding podocyte proteins identified in human NS.

Table 1.1. Genes implicated in human NS

| Gene | Protein | Expression pattern | Phenotype-associated mutations | Reference |
|-----------------------|------------------------------------|--|---|---|
| SLIT DIAPHRAGM | | | | |
| <i>NPHS1</i> | Nephrin | Podocyte SD | Autosomal recessive NS at birth or early life, congenital NS of the Finnish type, <i>NPHS2</i> knockdown: FP effacement, mild proteinuria, narrowing of filtration slit | (Kestila et al., 1998, Bierzynska et al., 2014, Xu et al., 2014, Li et al., 2015) |
| <i>NPHS2</i> | Podocin | Podocyte FP | Autosomal recessive NS, SRNS, minimal glomerular disease, familial FSGS | (Relle et al., 2011) |
| <i>PLCE1</i> | Phospholipase CE1 | S-shape, cap loop, Cytoplasm of podocyte cell body | Proteinuria, truncating mutations: DMS, missense mutations: FSGS | (Jefferson and Shankland, 2007, Hinkes et al., 2006) |
| <i>CD2AP</i> | CD2-associated protein | Anchors SD to actin cytoskeleton | Familial FSGS, progressive renal failure leading to death | (Tolvanen et al., 2015, Yaddanapudi et al., 2011, Perico et al., 2016) |
| <i>TRPC6</i> | Short transient receptor channel 6 | Podocyte membrane | Familial FSGS, failed SD formation, proteinuria, GS Overexpression of TRPC6: podocyte injury, glomerular lesions | (Dattilo et al., 2008, Abkhezr and Dryer, 2014, Krall et al., 2010) |

| Gene | Protein | Expression pattern | Phenotype-associated mutations | Reference |
|---------------------|---|---------------------------------------|--|---|
| <i>ZO-1</i> | Zonula Occludens-1 | SD | Human diabetic kidney disease, global GS | (Itoh et al., 2014) |
| <i>LMX1B</i> | LIM homeobox TF 1 β | Regulates FP & SD development | Nail patella syndrome (NPS) Low no. glomeruli and glomerulosclerosis, over thickening of GBM & abnormal podocytes lacking FP & SD | (Zhou and Qin, 2012, Burghardt et al., 2013) |
| CYTOSKELETAL | | | | |
| <i>SYNPO</i> | Synaptopodin | Actin filaments in podocyte FP | FSGS, HIV-associated nephropathy, idiopathic NS, DMS hypercellularity, MCD | (Barisoni et al., 1999, Yu et al., 2016) |
| <i>ACTN4</i> | α -actinin-4 | Podocyte FP, bundling actin filaments | AD Familial FSGS | (Kaplan et al., 2000, Dandapani et al., 2007, Khurana et al., 2012) |
| <i>MYO1E</i> | Myosin IE | SD & FP | Proteinuria, FP effacement, delamination of GBM, autosomal recessive SRNS, FSGS | (Bi et al., 2013, Sanna-Cherchi et al., 2011, Krendel et al., 2009, Chase et al., 2012) |
| <i>INF2</i> | Inverted formin 2 | Actin filaments | AD FSGS | (Subramanian et al., 2016) |
| <i>KANK2</i> | KN motif and Ankyrin repeat domain-containing protein 2 | Basement membrane | FSGS | (Gee et al., 2015) |
| <i>MYH9</i> | Myosin-9 | Podocyte primary FP | Severe glomerular disease, cytoskeletal damage & podocyte detachment | (Miura et al., 2013, Yuan et al., 2016) |

*MET, Mesenchymal-epithelial transition; DDS, Denys-Drash syndrome; FS, Frasier syndrome; MM, metanephric mesenchyme, UB, ureteric bud; FSGS, Focal segmental glomerulosclerosis; DMS, Diffuse mesangial sclerosis; GBM, Glomerular basement membrane; FP, Foot process; SD, Slit diaphragm; SRNS, Steroid-resistant nephrotic syndrome; MCD, Minimal change disease; AD, Autosomal dominant

1.2.2 Phenotypes of podocyte injury

Histological characterisation of podocyte injury based on light microscopy and ultrastructural analysis by electron microscopy includes minimal change disease (MCD), focal segmental glomerulosclerosis (FSGS), diffuse mesangial sclerosis (DMS), and collapsing glomerulopathy (CG) (Waldman et al., 2007, D'Agati, 2008).

1.2.2.1 Minimal change disease (MCD)

MCD is a condition where NS occurs in the context of normal kidney histology as assessed by light microscopy. Ultrastructurally, however, FP effacement is evident by electron microscopy. 90% of paediatric patients are steroid responsive and are considered to have MCD (Braden et al., 2000, Bahiense-Oliveira et al., 2004). Several studies have supported an immunological basis for MCD. In particular, the efficacy of rituximab in steroid-dependent NS points to a central role for B-lymphocytes in mediating podocyte dysfunction in MCD (Vivarelli et al., 2017)

1.2.2.2 Focal segmental glomerulosclerosis (FSGS)

FSGS is characterised by a segmental scar within the glomerulus, occurring in a focal part of the kidney cortex. Around 5-10% of children and adults with FSGS progress to ESRD (Malaga-Dieguez et al., 2015). Other features include hyalinosis, podocyte hyperplasia/hypertrophy, apoptosis and capillary tuft collapse (Figure 1.7).

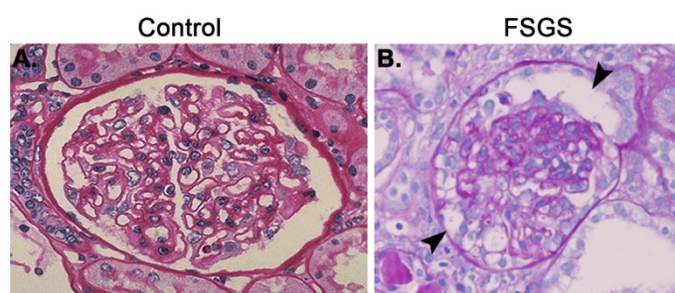


Figure 1.7. Focal segmental glomerulosclerosis

Periodic acid-Schiff (PAS)-stained kidney biopsies demonstrating (A) Normal glomerulus with normal thin capillary loops and tubular epithelium (Ramidi et al., 2011); (B) FSGS tip variant.

Five histologic variants of FSGS have been proposed: collapsing, tip, cellular, perihilar and non-specific (D'Agati et al., 2004). Collapsing variant includes global mesangial expansion and extracapillary epithelial proliferation/hypertrophy. Tip lesions affect the glomerular tuft region, showing abnormal cell adhesion to the Bowman's capsule and tip;

sclerosis and hypercellularity are also displayed in this phenotype. Cellular lesions are present as segmental endocapillary hypercellularity (Meehan et al., 2013). Peri-hilar variants are characterised by segmental sclerosis of the capillary loops with matrix expansion near the hilum (Rosenberg and Kopp, 2017).

1.2.2.3 Diffuse mesangial sclerosis (DMS)

DMS is characterised by global expansion of the mesangial matrix, hypertrophic capillary walls and podocyte hyperplasia and involving all glomeruli (Figure 1.8). DMS can be isolated or part of a *WT1*-mutation syndrome, Denys-Drash syndrome (DDS), a SRNS with severe proteinuria, gonadal dysgenesis with male pseudohermaphroditism (Kucinskas et al., 2005, Patek et al., 1999). DDS patients have a tendency to develop Wilm's tumour, leading to renal failure during the first three years of life.

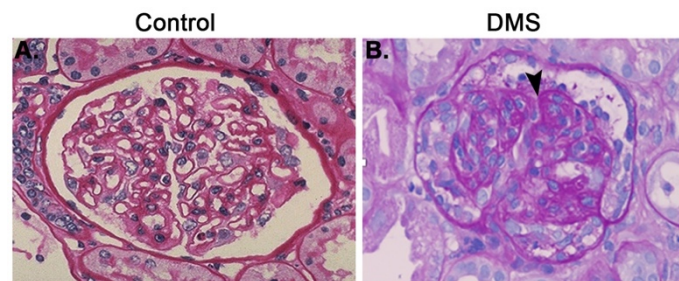


Figure 1.8. Diffuse mesangial sclerosis

Periodic acid-Schiff (PAS)-stained kidney biopsies demonstrating (A) Normal glomerulus with normal thin capillary loops and tubular epithelium (Ramidi et al., 2011); (B) Mesangial sclerosis with capillary lumen obliteration and patent Bowman's space.

1.2.3 Mechanisms of podocyte injury

Several mechanisms of podocyte injury exist and include apoptosis, dedifferentiation, detachment, epithelial-to-mesenchymal-transition (EMT) and occasionally cell cycle re-entry with proliferation, all of which can lead to GS (Marshall and Shankland, 2006).

1.2.3.1 Podocyte apoptosis

Podocyte apoptosis plays a central role in the pathogenesis of FSGS (Niranjan et al., 2008). High doses of diphtheria toxin administered to rats expressing the diphtheria toxin receptor in podocytes leads to podocyte loss (Wharram et al., 2005). A 20-40% reduction in podocyte number results in FSGS, highlighting a crucial role for podocyte number in the pathogenesis of FSGS (Wharram et al., 2005). Podocytopenia has also been

associated with diabetic nephropathy (Meyer et al., 1999, Steffes et al., 2001). Over-expression of TGF- β 1 in podocytes results in podocyte apoptosis and FSGS, implying that podocyte apoptosis is mediated by TGF- β 1 activation (Schiffer et al., 2001). Several mouse models of GS show increased expression of podocyte TGF- β 1 such as CD2AP-deficient mice as well as streptozotocin-induced (STZ) murine diabetic nephropathy (Schiffer et al., 2004, Niranjan et al., 2008). Podocyte apoptosis has also been observed in animal models of type 1 and type 2 diabetes following AngII and TGF- β 1 treatment (Jia et al., 2008). Mouse models of diabetes show a correlation between podocyte apoptosis and the onset of albuminuria (Susztak et al., 2006). Increased podocyte apoptosis was demonstrated in ROS/NADPH oxidase induced rat models of diabetes, where p38-MAPK and caspase-3 were activated to stimulate podocyte apoptosis. TGF- β 1 exerts its function through p38-MAPK and caspase-3, inducing podocyte apoptosis (Susztak et al., 2006) (Figure 1.9).

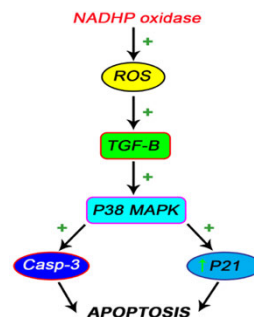


Figure 1.9. Signalling pathways for induction of podocyte apoptosis

Reactive oxygen species (ROS) generated from NADHP can induce podocyte apoptosis by activating signalling pathways via TGF- β , including p38-MAPK and Caspase-3. Podocyte apoptosis is also triggered through TGF- β facilitated p21. Adapted from (Fakhruddin et al., 2017).

Streptozotocin (STZ)-induced rat models of diabetes, and high glucose podocyte cultures with increased podocyte apoptosis, express high levels of *Vegfa*, *Ap1* and *Bcl-2*. Inhibition of *Vegfa* regulated *Ap1* and *Bcl-2* expression, ameliorating podocyte apoptosis (Bai et al., 2014). Collagen 4a3-deficient mouse models of Alport nephropathy show increased expression of tumour necrosis factor- α (TNF- α) in the podocytes and other glomerular cells, with podocyte apoptosis (Ryu et al., 2011).

Podocyte apoptosis is a feature of adriamycin (ADR) and puromycin aminonucleoside (PAN) nephropathy; treatment with a selective cAMP/PKA activator reduces podocyte apoptosis and caspase-3 activation (Li et al., 2014). Patients with membranous nephropathy show reduced miR-186 with elevated levels of caspase-3 (Sha et al., 2015). Coactivator-associated arginine methyltransferase 1 (CARM1) degradation via

ubiquitination has been shown to promote podocyte apoptosis through *Notch1* activation in diabetes, and preservation of this enzyme may prevent podocyte apoptosis (Kim et al., 2014).

1.2.3.2 Epithelial to mesenchymal transition (EMT)

EMT is a process by which epithelial cells lose their epithelial features and gain mesenchymal characteristics. Podocytes are visceral epithelial cells which retain mesenchymal features (spindle shape morphology, vimentin), therefore they may not necessarily undergo EMT in a diseased state unless it is extremely severe (Figure 1.10). Podocyte EMT results in loss of epithelial polarity and altered SD, along with a rearrangement in the actin cytoskeleton (Valcourt et al., 2005). A key feature of podocyte EMT is represented by loss of the SD and effaced FP in diseased podocytes.

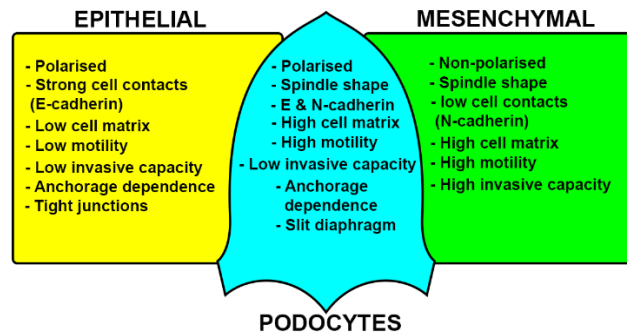


Figure 1.10. Epithelial and mesenchymal features of podocytes

Podocytes exhibit both epithelial and mesenchymal characteristics, as highlighted above. Adapted from (May et al., 2014).

TGF- β 1 triggers podocyte EMT in human immortalised podocytes, increasing levels of α -smooth muscle actin (α -SMA), causing a switch of P-cadherin to N-cadherin, and upregulating the EMT transcription factors *SNAIL* and *SLUG* (Ghiggeri et al., 2013). Mouse podocytes *in vitro* demonstrate the same phenotypic transformations when exposed to TGF- β 1, showing suppressed *P-cadherin*, *Zo-1*, and *Nphs1* expression and an upregulation of *Desmin*, along with Collagen I and Fibronectin, which may contribute to GBM thickening, a distinct feature of diabetic nephropathy (Li et al., 2008, Jefferson et al., 2008). The mesenchymal marker, Desmin, has also been observed in podocytes of glomerular diseases associated with podocyte injury (Zou et al., 2006).

1.2.3.3 Podocyte proliferation

Podocyte cell cycle re-entry has been reported in both human and murine tissue sections characterised by GS (Barisoni et al., 2000, Wang et al., 2004, Srivastava et al., 2003). Cyclins are regulatory subunits that mediate kinase activity by partnering with cyclin-dependent kinases (CDKs). There are 20 members of the CDK family and they consist of a serine/threonine-specific catalytic core, allowing them to associate themselves with cyclins (Lim and Kaldis, 2013). Histological analysis of kidney sections of collapsing FSGS has revealed increased podocyte cyclin A expression (Barisoni et al., 2000, Wang et al., 2004). Cyclin D expression has also been observed in podocytes of FSGS biopsies (Srivastava et al., 2003). Upregulation of cyclin-dependent kinase inhibitors (CKI) has been seen in patients and in *in vivo* models of glomerulopathy, suggesting a role for podocytes to maintain cell cycle quiescence. CKI upregulation of *p21* and *p27* was observed in podocytes of Zucker diabetic fatty (ZDF) rats (Hoshi et al., 2002). Moreover, patients with collapsing glomerulopathy (CG), FSGS, and MCD all had altered *p27* and *p21* expression (Srivastava et al., 2003).

1.2.3.4 Circulating factors associated with podocyte injury

Mechanisms of podocyte injury can also be associated with circulating factors, resulting in specific phenotypes, including primary FSGS (Rosenberg and Kopp, 2017). Recurrent FSGS with FP effacement and proteinuria was demonstrated in a patient with primary FSGS receiving a kidney transplant, whilst another patient with ESRD receiving the paired kidney did not develop the same phenotype (Gallon et al., 2012). Recurrent FSGS has been linked to circulating factors, cardiotrophin-like cytokine factor 1 (Savin et al., 2015), apoA1b (Lopez-Hellin et al., 2013), anti-CD40 antibody (Delville et al., 2014), and suPAR (serum urine-type plasminogen activator receptor) (Wei et al., 2011).

1.3 Molecular regulation of podocyte differentiation

Transcriptional regulation of podocyte differentiation requires a complex interplay of several genes (highlighted in Table 1.2).

Table 1.2. Genes regulating early podocyte differentiation

| Gene | Protein | Expression pattern | Phenotype-associated mutations | Reference |
|--|---|---|--|--|
| <i>WT1</i> | Wilms' tumour 1 | MET, comma and S-shape, mature podocytes | DDS, FS, WAGR syndrome Null <i>Wt1</i> : MM degeneration, no kidneys Truncated zinc finger 3: DDS Intron 9 splice donor site mutation: lack of +KTS – FS Homozygous mice lacking – KTS isoform: small kidneys FSGS, DMS | (Kreidberg et al., 1993, Miller-Hodges and Hohenstein, 2012) |
| <i>POD1</i> (<i>capsulin</i> , <i>epicardin</i>) | Podocyte-expressed 1 | Condensing MM, reappears in S-shape | Arrested glomerular development at capillary loop, hypoplastic kidneys | (Quaggin et al., 1999, Sadl et al., 2002, Schell et al., 2014) |
| <i>Kreisler</i> (<i>MAFB2</i>) | Kreisler MAF-related leucine zipper homolog | Capillary loop | Arrested glomerular development at capillary loop stage Podocytes remain columnar shaped | (Chugh, 2007, Quaggin, 2002, Sadl et al., 2002) |
| <i>FOXC2/MF2</i> | Mesenchyme/mesoderm forkhead 2, Forkhead Box C2 | Condensed mesenchyme Late S-shape | Renal defects, no abnormal podocytes <i>Foxc2</i> mutations mouse: FPs are absent | (Kreidberg, 2003, Quaggin, 2002), (Takemoto et al., 2006) |
| <i>HES, HEY1</i> | bHLH TF | S-shape | Ectopic expression in mature & differentiated podocytes: DMS, FSGS | (Niranjan et al., 2008) |
| <i>PAX2</i> | Paired Box 2 | Renal vesicle | FP effacement and proteinuria, FSGS | (Wagner et al., 2006, Chugh, 2007, Dressler et al., 1993) |
| <i>OSR1</i> | Odd-Skipped Related TF | Patterning of MM and podocyte development | <i>Osr1</i> knockout – lack of MM | (Tomar et al., 2014) |

*MET, Mesenchymal-epithelial transition; DDS, Denys-Drash syndrome; FS, Frasier syndrome; WAGR, Wilms tumour aniridia syndrome; MM, Metanephric mesenchyme; FSGS, Focal segmental glomerulosclerosis; DMS, Diffuse mesangial sclerosis; FP, Foot process

1.3.1 Wilms' tumour-1 (*WT1*)

WT1 was initially discovered in 1990 as a predisposition gene for Wilms' tumour (Call et al., 1990, Gessler et al., 1990); a paediatric cancer affecting 1 in 10,000 children (Charlton and Pritchard-Jones, 2016). Around 15-20% of Wilms' tumour-associated diseases have been linked to mutations in *WT1* (Charlton and Pritchard-Jones, 2016). While *WT1* classically behaves as a tumour suppressor gene, collective research has revealed *WT1* to be active in specific types of cancer, suggesting its role as an oncogene (Miller-Hodges and Hohenstein, 2012, Hastie, 2017). Extensive research has revealed *WT1*'s critical role in development, homeostasis, and disease (Kreidberg et al., 1993, Pelletier et al., 1991, Wagner et al., 2002, Kreidberg, 2010, Parenti et al., 2015, Hastie, 2017). Moreover, its alternative isoforms allow *WT1* to participate in diverse activities.

1.3.1.1 *WT1* structure and isoforms

WT1 spans approximately 50KB on chromosome 11p13 with 10 exons, encoding a transcript of about 3KB. The mammalian *WT1* is composed of at least 36 isoforms, all of which carry four carboxy-terminal Kruppel- type (Cys2-His2) zinc fingers on their C-terminus that bind to both RNA and DNA (Call et al., 1990, Gessler et al., 1990, Hastie, 2017) (Figure 1.11). *WT1* has numerous isoforms, however the main focus has been on 3 different amino acids: lysine, threonine, and serine (KTS) at the end of exon 9 that may be included or excluded and as a consequence determine function in relation to RNA (+KTS) or DNA binding (-KTS and +KTS). *WT1* protein usually exists at an approximately 2:1 ratio of +KTS:-KTS in humans (Dong et al., 2015a). Mutations in +KTS and -KTS isoforms, resulting in an imbalanced +KTS/-KTS ratio, were identified in patients with Frasier syndrome; a syndrome associated with FSGS and male-to-female sex reversal, highlighting the importance of the KTS isoforms (Barboux et al., 1997).

The alternatively spliced exon 5, resulting in proteins with or without the central 17 amino acids, and the upstream CTG start codon in exon 1 have also been explored. No phenotypes were identified in these murine models and further research in this area is required to assess the function of these isoforms (Ozdemir and Hohenstein, 2014, Natoli et al., 2002b). Likewise, phenotypes were not observed in mice lacking *WT1* extended isoforms, including the alternative translation start site (Miles et al., 2003).

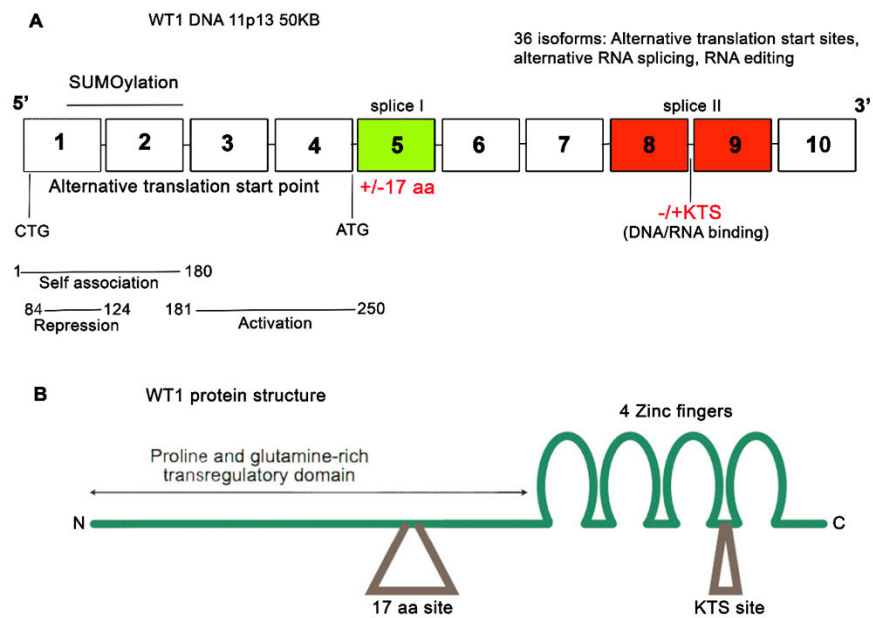


Figure 1.11. Structure of *WT1* and its isoforms

(A) *WT1* comprises 10 exons, which generate a 3Kb mRNA. There are at least 36 isoforms derived from alternative splicing, RNA editing and alternative start translation sites. Two major splice site forms include proteins having/or lacking 17 amino acids at exon 5, and proteins including or lacking the three amino acids +/-KTS between zinc fingers 3 and 4, encoded by exons 7 to 10. **(B)** *WT1* protein highlighting the N-terminus containing proline- and glutamine- rich domains involved in transcriptional regulation, self-association and RNA recognition. Zinc finger domains show the KTS sites at the C-terminal. Two alternative splice sites: +17aa in the trans-regulatory domain and +/- KTS between the third and fourth zinc fingers (brown triangles). Adapted from (Brown and Malik, 2001).

1.3.1.2 *Wt1* expression during kidney development

Wt1 is first detected at low levels in the undifferentiated mesenchyme of the intermediate mesoderm at E9 in mice, and dramatically increases in the condensed mesenchyme before MET (Mundlos et al., 1993). Expression levels remain high during nephrogenesis, becoming restricted to the proximal region of the S-shaped body after the RV morphs into the comma- and S-shaped bodies. *Wt1* expression is sustained in the podocytes throughout adult life (Kreidberg et al., 1993, Armstrong et al., 1993, Guo et al., 2002, Hastie, 2017) (Figure 1.12).

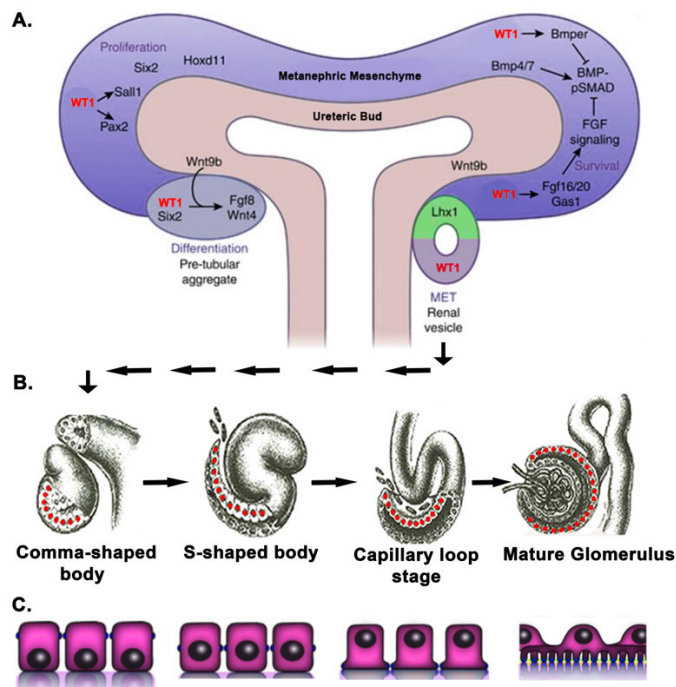


Figure 1.12. *WT1* expression during kidney development

(A) At the early stages of development, *WT1* is highly expressed in the condensing metanephric mesenchyme, along with other transcription factors. *WT1* expression is increased in the epithelial cells and is continually expressed in the mature kidneys. (B) Stages of podocyte maturation highlighting *WT1* presence. (C) Podocyte morphology at each stage of development. Adapted from (Dong et al., 2015a, Schell et al., 2014, Saxen and Sariola, 1987).

WT1 is crucial for the survival and proliferation of the mesenchyme and MET by activating genes, including *Wnt4*, forming the nephron from the cap mesenchyme (Davies et al., 2004, Essafi et al., 2011). It is upstream of transcription factors, *Pax2*, *Sal1*, which are required for MM proliferation and self-renewal, along with *Six2* and *Hoxd1*. Moreover, *WT1* regulates *Bmper*, an inhibitor of BMP-pSMAD signalling that promotes apoptosis in the mesenchyme and activates FGF signalling by regulating *Fgf16/20* and *Gas1*; this permits MM survival. Wnt signalling is also increased via *Wnt9* expression, localised beneath the ureteric tip near the MM; at this stage, the β -catenin-LEF/TCF complex collaborates with *Six2* and *Wt1* to activate *Fgf8* and *Wnt4*, inducing PTA formation (Dong et al., 2015a).

1.3.1.3 Human *WT1*-associated disorders

WT1 mutations result in a wide range of renal manifestations, which eventually lead to ESRD. The renal disorders associated with *WT1* mutations include DDS, FS, WAGR (Wilms' tumour, Aniridia, Genitourinary malformation and mental retardation), and SRNS, all of which are congenital mutations (Bielinska et al., 2017). As previously stated, *WT1* +KTS and -KTS isoforms are expressed at a ratio of around 2:1 in healthy human

kidneys (Hohenstein and Hastie, 2006). Mutations of this gene in humans have been associated with urogenital abnormalities. FS and DDS are rare inherited diseases characterised by SRNS, resulting in kidney failure, gonadal tumour and male pseudohermaphroditism (Ezaki et al., 2015).

DDS is a rapidly progressive glomerular disease with renal failure that may occur before the age of 1. It is caused by *WT1* point mutations, typically missense mutations within exons 8 or 9, which encode zinc fingers 2 or 3, resulting in an abnormal *WT1* protein (Saylam and Simon, 2003, Miller-Hodges and Hohenstein, 2012, Drash et al., 1970). It is characterised by DMS. Phenotypes associated with this syndrome include genitourinary abnormalities, specifically male pseudohermaphroditism. DDS has also been linked to mutations in *WT1* DNA-binding domains, affecting its function as a transcription factor and resulting in DDS phenotypes (Little et al., 1995). Histological analysis of DDS kidneys reveals effaced podocytes with regions of continued proliferation, where there is reduced *WT1* protein expression, as well as increased expression of PDGFA and TGF- β 1 (Yang et al., 2004a). Furthermore, subsequent data has revealed that DDS podocytes do not fully differentiate; they continue to express VEGF-A, a component which induces glomerular endothelial cell proliferation and differentiation, and is only expressed at the S-shaped body stage. Mature podocytes normally express the inhibitory isoform VEGF165b during podocyte differentiation. DDS patient biopsies completely lack this isoform, resulting in a delay in podocyte maturation with expression of the early podocyte S-shaped body components, including collagen IV and laminin B1 (Schumacher et al., 2007).

FS is characterised by male pseudohermaphroditism and FSGS, leading to NS and renal failure by the age of 20. It is caused by splice-site point mutations in exon 9 of *WT1*, where patients develop gonadoblastoma (Barbosa et al., 1999). FS KTS isoforms are imbalanced, resulting in a lower expression of the +KTS isoform and a higher expression of the -KTS isoform, affecting the post-transcriptional regulation of *WT1* and its binding partners and subsequently leading to gonadal and renal abnormalities (Hammes et al., 2001, Hastie, 2001, Larsson et al., 1995, Barbaux et al., 1997, Koziell and Grundy, 1999, Klamt et al., 1998) (Figure 1.11).

WAGR syndrome was the first disease linked to *WT1*, resulting from 11p13 deletions and leading to the loss of *WT1* and *PAX6* (Fischbach et al., 2005). WAGR patients commonly show FSGS in their biopsies, and around 50% develop Wilms' tumour (Fischbach et al., 2005, Muto et al., 2002). Patients with FSGS who do not develop

Wilms' tumour do not display proteinuria or NS, suggesting that the absence of one *WT1* allele may promote FSGS (Iijima et al., 2012).

1.3.1.4 Transgenic mouse models highlighting the role of Wt1 during podocyte development

WT1-associated kidney disease has been extensively investigated *in vivo* and *in vitro*, highlighting *WT1*'s relevance during podocyte differentiation and its role in kidney development and disease.

A model for urogenital abnormalities was developed by Kreidberg by generating mice carrying a targeted mutation of the *Wt1* gene (Kreidberg et al., 1993). Homozygotes of *Wt1* mutation led to embryonic lethality. Furthermore, the UB ceased to develop at day 11 gestation due to apoptosis of the metanephric blastema. A later study performed RNAi experiments in culture to repress *Wt1* expression at different stages during kidney development; early inhibition of *Wt1* mimicked the *Wt1*^{-/-} mouse of Kreidberg's team. When *Wt1* was ablated at a later stage, nephrons were incapable of differentiating and instead, proliferated aberrantly (Davies et al., 2004). Moreover, a gain of function study performed by another group examined the significance of *Wt1* during the condensed mesenchyme stage in early kidney development; microinjection and electroporation of *Wt1* in null murine kidney organ cultures resulted in normal nephron growth, highlighting *Wt1*'s importance during nephrogenesis (Gao et al., 2005).

More recently, Kreidberg's team examined *Wt1* and fibroblast growth factor (FGF) signalling in nephron progenitor cells (NPC); they concluded that *Wt1* controls FGF signalling by triggering a downstream target of *Wt1*, growth arrest-specific 1 (*Gas1*). ChIP-on-chip and ChIP-qPCR analysis revealed that *Wt1* binds directly to a conserved DNA binding motif within the *Gas1* promoter. *In situ* hybridisation (ISH) showed reduced *Gas1* expression following oligonucleotide morpholino (MO) inhibition of *Wt1*. Loss of *Gas1* expression *in vivo* resulted in hypoplastic kidneys with decreased nephron number, highlighting the requirement of *Wt1* for *Gas1* expression in the kidneys and its significance during kidney development (Kann et al., 2015a).

ChIP and high-throughput sequencing using DNA from mouse glomeruli was performed to identify targets of *Wt1* during podocyte differentiation. Deletion of *Wt1* in a podocyte-specific Cre-inducible mouse resulted in kidney haemorrhage and death 24 hours post-birth (Dong et al., 2015b). Functional zebrafish studies identified *wf1* targets, including *nphs2*, *mafb* and *magi2* that were necessary for podocyte development (Dong et al.,

2015b). Moreover, Kreidberg's team investigated podocyte development and viability by performing RNA and ChIP sequencing; WT1 was found to regulate the podocyte transcriptome through binding to enhancers and promoters of target genes. Additionally, a podocyte transcriptional network between *Wt1*, *Lmx1b*, *Tcf21*, *Fox-c* and *Mafb* was identified, controlling podocyte gene expression (Kann et al., 2015b).

Three different Cre-inducible systems to knockout *Wt1* in transgenic mice were analysed before and after MET: 1) *Nes-Cre;Wt1^{co/co}*; *Nes* encodes the intermediate filament protein Nestin and is a transcriptional target of *Wt1*, 2) *Pax8^{+Cre};Wt1^{co/co}*; *Pax8* encodes the paired box gene 8, which is initially expressed at the renal vesicle stage and maintained until the end of nephrogenesis (Bouchard et al., 2004), 3) Cre-GFP fusion construct inserted into the endogenous *Wnt4* locus (*Wnt4-Cre;Wt1^{co/co}*) (Shan et al., 2010); *Wnt4* is expressed in epithelial progenitors in the developing kidney. The loss of *Wt1* at each stage of kidney development resulted in disrupted kidneys and post-natal death within 24 hours (Berry et al., 2015). *Wt1* transcriptionally activates *Wnt4* to induce MET, leading to nephron differentiation (Davies et al., 2004, Essafi et al., 2011), and deletion of *Wt1* prior to MET results in the formation of aberrant kidneys that resemble human Wilms' tumours, emerging from *WT1* mutations (Berry et al., 2015).

Mosaic and somatic ablation of *Wt1* with constitutive expression of *Igf2* were studied in mice to mimic a set of human Wilms tumours. *H19* and *Igf2* are closely linked and are from a large group of imprinted genes, located on chromosome 7 (Zemel et al., 1992). Their monoallelic expression patterns are conserved between humans and mice. In this study, a truncated form of WT1 was produced following Cre-knockout of the endogenous gene; mice also contained an *H19*- allele, resulting in the upregulation of the normally silenced copy of the maternal *Igf2* known to be a target of WT1 activity (*CreERTM;Wt1^{-f}H19^{+/-m}*). Ablation of *Wt1* blocked kidney development, with the formation of Wilms tumours at E13.5 following tamoxifen induction in experimental animals, but not controls (*CreERTM;Wt1^{+f}H19^{+/-m}*, *Wt1^{+f}H19^{-m};Wt1^{+f}H19^{+/-m}*). At E19, mutant kidneys displayed complete lack of nephron development with no glomeruli in comparison to the controls (Hu et al., 2011). *In vivo* mouse studies on *Wt1* during early nephrogenesis and late nephrogenesis are summarised below (Table 1.3).

Table 1.3. Early nephrogenesis in transgenic mouse models of *Wt1* gene manipulation

| Mouse strain | Phenotype | Reference |
|---|---|---|
| <i>Wt1</i> ^{-/-} | Bilateral renal agenesis, embryonic lethality | (Kreidberg et al., 1993) |
| <i>Wt1</i> ^{R362X/+} | DDS: Abnormally large capillaries, few capillary loops, present but irregular FP shape – no adverse effect on kidney development (E18) | (Natoli et al., 2002a) |
| <i>Nes-Cre;Wt1</i> ^{Co/Co} | Disturbed nephron development, inhibited ureteric branching, reduced MM condensation; Intermediate cortex: reduced formation of RV, comma and S-shaped bodies; Inner cortex: reduced glomerulogenesis, tubulogenesis (E18.5) | (Essafi et al., 2011, Berry et al., 2015) |
| <i>Wnt4</i> ^{+creGFP} ; <i>Wt1</i> ^{co/co} <i>Pax8</i> ^{+Cre} ; <i>Wt1</i> ^{co/co} | MET stage reduced, mesenchyme expansion; lack of glomerulogenesis and tubular maturation (E18.5); Normal levels of condensation, epithelisation; lack of glomerulogenesis and early tubulogenesis (E18.5) | (Berry et al., 2015) |
| <i>CreER</i> TM ; <i>Wt1</i> ^{-fl} <i>H19</i> ^{+m} | No glomeruli, no differentiation of condensed mesenchyme after comma-shaped body, block in nephron development (E19) | (Hu et al., 2011) |

*DDS, Denys-Drash syndrome; MM, Metanephric mesenchyme; FP, Foot process; RV, Renal vesicle; MET, Mesenchymal to epithelial transition

Hammes et al. studied the KTS domain between zinc fingers 3 and 4 (Hammes et al., 2001). Heterozygous mutants of the +KTS isoform (+KTS^{+/-}) developed GS and died 3 months after birth. Homozygous mutants of both +KTS^(-/-) and -KTS^(-/-) did not survive longer than 24 hours post-birth due to a low number of glomeruli, reduced kidney size and haemorrhage. Conversely, Natoli et al. showed that no phenotypes were observed in mice lacking the 17 amino acid domain of exon 5 (Natoli et al., 2002b).

An early study generated mice with amino acid substitution S395R, within exon 9. This resulted in a premature termination within zinc finger 3 of the WT1 protein, where a stop codon was introduced at 396, *Wt1*^{tmT396} (Patek et al., 1999). The truncated protein lacked the KTS insertion and zinc finger 4. Heterozygous mice exhibited global sclerosis and

protein casts within the tubules at four months of age compared to the wildtypes (Patek et al., 1999). A later study generated transgenic mice that carried the mutant form of *Wt1* in podocytes, where zinc fingers 3 and 4 were deleted (R362X truncation), and the constructs either contained or omitted exon 5 (Ex5/or Ex5-). Mice with the mutant form of *Wt1*, lacking exon 5 at E18, demonstrated abnormally large capillaries in the glomeruli with irregular shaped FPs (Natoli et al., 2002a). A subsequent study developed a mouse strain carrying the missense mutation *Wt1* R394W (*Wt1*^{+/^{R394W}) to recapitulate the genetic defect seen in DDS patients (Gao et al., 2004). By four months of age, all male heterozygotes exhibited proteinuria and GS compared to the wildtypes (*Wt1*^{+/+}). The podocyte-specific genes and proteins, nephrin, podocin and podocalyxin were also reduced in the mutants compared to the wildtypes, with increased TGFβ1 and IGF1 expression (Gao et al., 2004).}

Induced FSGS was reported in transgenic mice overexpressing the micro-RNA, miR-193a. Doxycycline induction in 2-month old mice increased the expression of the miRNA by ten-fold, which repressed *Wt1* expression resulting in FP effacement, glomerular lesions and albuminuria at 10 weeks of age. Rapidly progressive FSGS and death was observed at 12 weeks of age (Gebeshuber et al., 2013). Next, the investigators deleted *Wt1* to test whether this excision would result in the same FSGS phenotype as the increased miR-193a. A *Wt1* floxed gene (flanking exons 2 and 3, resulting in a premature stop) was combined with a podocyte-specific doxycycline inducible transcriptional activator (rtTA) and an rtTA-inducible *Cre* (LC1) in the transgenic mice, where *Wt1* deletion was induced by doxycycline treatment (*Wt1*^{fl/fl};*Nphs2*rtTA;LC1). *Wt1* deletion at 12 weeks post-doxycycline led to a downregulation of its target genes, *Podxl* and *Nphs1* as well as other podocyte-specific genes, and an FSGS phenotype with progressive albuminuria similar to that caused by miR-193a overexpression in comparison to the controls (*Wt1*^{fl/+}) (Gebeshuber et al., 2013). Thus, WT1 is a master regulator of podocyte differentiation and targeting miR-193a might be a potential therapeutic target in FSGS.

WT1 targets have been investigated in differentiating podocytes by ChIPseq, exon arrays and genetic studies in mice (Lefebvre et al., 2015), where FOXC1 (Forkhead box C1), a transcriptional activator of WT1, was revealed to possess binding sites in a large section of WT1-bound regions. The SD protein, membrane-associated guanylate kinase (MAGI2), was also only seen when the +KTS isoform was predominant. Mice lacking this isoform resulted in glomerular injury (Lefebvre et al., 2015). This highlights the importance of WT1 KTS isoforms in podocyte differentiation and maintenance. *In vivo* mouse studies on *Wt1* during late nephrogenesis are summarised below (Table 1.4).

Table 1.4. Late nephrogenesis in transgenic mouse models of *Wt1* gene manipulation

| Mouse strain | Phenotype | Reference |
|--|--|--|
| <i>WT1(+KTS^{+/-})</i> Frasier heterozygote | Severe mesangial sclerosis, proximal tubule dilation, protein casts, death 3 months after birth | (Hammes et al., 2001, Lefebvre et al., 2015) |
| <i>WT1 (+KTS^{-/-})</i> Frasier homozygote | Mildly reduced kidney size, local haemorrhage within kidney, less developed glomerular tufts, death within 24hrs after birth | |
| <i>WT1 (-KTS^{+/-})</i> KTS heterozygote | Normal kidneys | |
| <i>WT1 (-KTS)</i> KTS homozygote | Severely reduced kidney size, reduced number of glomeruli, severe glomerular contraction, death within 24hrs after birth | |
| <i>Wt1^{ex5n/ex5n}</i> | No phenotypes reported in adult mice | (Natoli et al., 2002b) |
| <i>Nphs2-Cre; Wt1^{fl/fl}</i> | Reduced glomeruli, kidney haemorrhage and death (24h post-birth) | (Dong et al., 2015b) |
| <i>Wt1^{+R394W}</i> | Proteinuria and GS (4 months old) | (Gao et al., 2004) |
| <i>Wt1^{fl/fl};Nphs2rtTA;LC1</i> | FSGS, albuminuria FP effacement (2 weeks post-doxycycline) | (Gebeshuber et al., 2013) |
| <i>Wt1^{tmT396/+}</i> | Global sclerosis, podocyte hyperplasia, protein casts in dilated tubules (4 months) | (Patek et al., 1999) |
| <i>Cre-ER^{TM+/-};Wt1^{fl/fl}</i> | GS, protein casts in tubules, proteinuria, gonadal dysgenesis | (Chau et al., 2011) |

* GS, Glomerulosclerosis; FSGS, Focal segmental glomerulosclerosis; FP, Foot process;

1.3.1.5 Molecular mechanisms of *WT1* action

While WT1 acts as a transcriptional regulator by enabling the activation or repression of genes, reports have revealed an additional role as a post-transcriptional regulator where it can interact with RNA (Morrison et al., 2008). Most research proposes that the WT1 -KTS isoforms are linked to DNA binding, whilst the +KTS isoforms interact with RNA (Toska and Roberts, 2014, Ullmark et al., 2018). That being said, DNA binding has also been associated with the +KTS isoforms, and -KTS isoforms can interact with RNA.

WT1 transcription and chromatin

WT1 contains both transrepression and transactivation domains, which can repress or activate certain gene targets via WT1 dimerisation at the promoters (Toska and Roberts, 2014) (Figure 1.13A). Wang et al. found that WT1 functioned as a repressor of a *PDGFA* promoter reporter when binding to elements both upstream and downstream of the transcription start site (TSS), whereas when it bound to only one of the sites it acted as an activator (Wang et al., 1993). WT1 not only self-interacts at its C-terminal region but has also been shown to bind via its N-terminus.

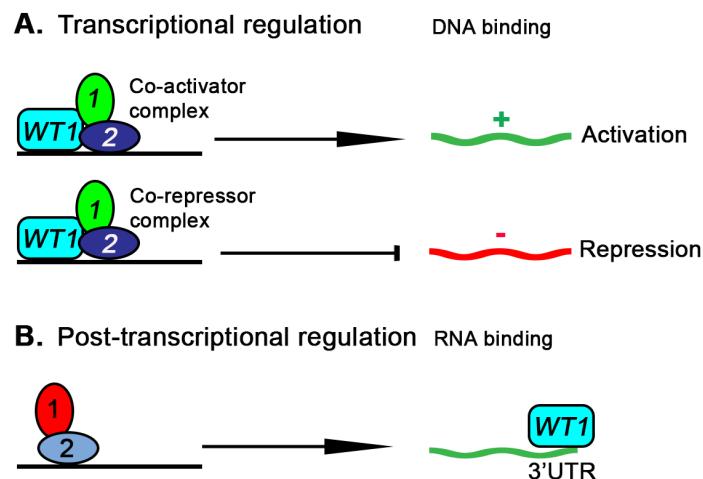


Figure 1.13. Roles of WT1 in transcriptional and post-transcriptional regulation

(A) WT1 can either transcriptionally activate or repress target genes depending on its binding partners. **(B)** Post-transcriptional regulation; WT1 can directly bind to mRNA 3'UTR regions, regulating RNA stability.

Recent ChIP-ChIP and ChIP-sequencing data have revealed a number of WT1 transcriptional target genes that interact with its -KTS isoform during kidney development, including *Mafb*, *Nphs1*, *Nphs2* (Motamedi et al., 2014, Kann et al., 2015b, Lefebvre et al., 2015, Dong et al., 2015b, Hastie, 2017). Specific domains of WT1 can mediate transcriptional regulation or repression by interacting with transcriptional co-regulators. One example is BASP1, which is expressed during kidney development. The interaction of BASP1 with the activator domain of WT1 leads to the formation of a repressor complex (Toska and Roberts, 2014). Additionally, WT1 has been shown to be sumoylated within its N-terminus, within its transcriptional repression domain. Small ubiquitin-related modifier-1 (SUMO-1) and ubiquitin-conjugating enzyme 9 (Ubc9) have been shown to interact with WT1. Phosphorylation of WT1 by protein kinase A and C (PKA, PKC) have also been identified in zinc fingers 2 and 3, affecting the ability of WT1 to bind to DNA. WT1 phosphorylation can also influence the localisation pattern of WT1

from the nucleus to the cytoplasm, suggesting that WT1 transcriptional regulation can be negatively regulated by phosphorylation (Toska and Roberts, 2014).

RNA binding and post-transcriptional regulation

Early studies have shown that the WT1 +KTS isoform can bind to certain RNA sequences. Zinc fingers 1 and 4 have been associated with RNA binding. In particular, *Igf2* has been found to bind to zinc finger 1 (Caricasole et al., 1996) as has Actinin alpha 1 (*Actn1*) (Ladomery et al., 2003, Caricasole et al., 1996, Nurmemmedov et al., 2010, Bardeesy and Pelletier, 1998). During olfactory development, the proneural transcription factor, achaete-scute complex homologue-1 (*Ascl1*) mRNA is upregulated by WT1 +KTS (Wagner et al., 2005), highlighting the role of WT1 +KTS in mRNA regulation. Furthermore, the WT1-associated protein, WTAP and RBM4 (RNA binding motif protein 4) interact with +KTS (Little et al., 2000, Ortega et al., 2003, Markus et al., 2006). UV crosslinking and sequencing in M15 kidney cells revealed a group of endogenous mRNA binding sites that are regulated by WT1 during kidney and cardiovascular development (Bharathavikru et al., 2017) (Figure 1.13B).

1.3.2 Forkhead-box C1/2 (*FOXC1/2*)

The mesenchyme/mesoderm forkhead 2-transcription factor/Forkhead box protein 2 (MF2/*FOXC2*) is a member of the forkhead/winged helix family expressed in various embryo tissues (Kume et al., 2000). It is highly expressed during mesenchyme condensation and persists within podocytes at the late S-shaped body stage, and overlaps with *FoxC1* (Kume et al., 2000).

FOXC1 and *FOXC2* transcription factors play critical roles in non-renal tissues, including the lymphatic system, eye and cardiovascular system (Motojima et al., 2017).

1.3.2.1 Transgenic models of FoxC1/2 mutations

Earlier studies revealed the involvement of *FOXC2* in podocyte differentiation and GBM development (Takemoto et al., 2006). Former research in *Xenopus* uncovered a network of transcription factors involved in podocyte specification, including *foxc2*, *wt1*, *hey1*, *tcf21* (*pod1*), *Imx1b* and *mafb* (Carroll and Vize, 1996, Ishibashi and Yasuda, 2001, Haldin et al., 2003, Simrick et al., 2005, Taelman et al., 2006). One particular study investigated the role of *wt1* and *foxc2* during podocyte development in *Xenopus* (White et al., 2010). Combined knockdown of *wt1* and *foxc2* using morpholinos resulted in

reduced podocyte gene expression and notch signalling during podocyte development was necessary for the accurate spatiotemporal arrangement of podocyte gene expression. Glomerular abnormalities have been associated with *FoxC2* in *FoxC2*-null murine models (Motojima et al., 2016b). Reduced podocyte number was associated with double knockdown of either *wt1a/rbpj* or *wt1a/foxc1a* in zebrafish, when compared to just single knockdown of the respective genes (O'Brien et al., 2011), demonstrating the importance of their interactions in podocyte maintenance. Conditional knockout of *Foxc2* using Pax2-Cre mice results in kidney hypoplasia and glomerular cysts (Motojima et al., 2016a). While reduced expression of *Foxc2* leads to injured podocytes, overexpression of the gene results in disrupted SD protein markers, including ZO-1, as well as increased β -catenin activity, a pathway related to podocyte dysfunction (Datta et al., 2016). Mice carrying null-*FoxC1* mutations, where both *Foxc1* alleles (*Foxc1^{ch/ch}*) lead to a truncated form FOXC1 protein, displayed hypoplastic kidneys with fewer glomeruli than controls (Komaki et al., 2013). Furthermore, increased *FoxC2* expression induces EMT within the kidney tubular cells (Hader et al., 2010). Deletion of *FoxC1/2* in adult mice leads to podocyte injury and glomerular sclerosis associated with increased proteinuria, proteinaceous casts and dilated tubules (Motojima et al., 2017). Table 1.5 summarises nephrogenesis in transgenic models of *FoxC* gene manipulation.

Table 1.5. Nephrogenesis in transgenic models of *FoxC* gene manipulation

| Mouse model | Phenotype | Reference |
|---|---|--------------------------|
| <i>Foxc2^{-/-}</i> | Abnormal glomerular tufts | (Takemoto et al., 2006) |
| <i>Foxc1^{ch/ch} null</i> | Ectopic budding and kidney hypoplasia | (Komaki et al., 2013) |
| <i>Pax2-Cre;FoxC2^{fllox/fllox}</i> | Glomerular cysts and kidney hypoplasia | (Motojima et al., 2016a) |
| <i>Foxc1^{+/-};FoxC2^{+/-}</i> <i>Foxc1^{-/-}</i> | Duplex urinary system Hydronephrosis megaureter | (Motojima et al., 2016b) |
| <i>ROSA26-CreER;Foxc1^{fl/fl};Foxc2^{fl/fl}</i> <i>Nphs1-Cre;Foxc1^{fl/fl};Foxc2^{fl/fl}</i> | Albuminuria and segmental sclerosis Massive non-selective proteinuria Proteinaceous casts Mild tubular dilation Died before weaning | (Motojima et al., 2017) |

1.3.3 Other genes associated with podocyte development

1.3.3.1 PAX2

PAX2 (Paired Box 2) is a transcription factor member of the paired box family present in the mesoderm, giving rise to the metanephros. *Pax2* expression is strong in the nephric duct before and during MM induction (Patel et al., 2014). *Pax2* is expressed at the RV stage, and downregulated at the S-shaped body stage (Eccles, 1998, Sharma et al., 2015, Dong et al., 2015a, Dressler and Woolf, 1999).

Transgenic mice ubiquitously expressing *Pax2* under the control of the cytomegalovirus (CMV) promoter show FP effacement and proteinuria (Dressler et al., 1993). Homozygous mutants of *Pax2* results in a lack of UB development, eventually leading to renal agenesis (Patel et al., 2014). Human *PAX2* mutations have also been linked to kidney abnormalities, including CAKUT (Congenital anomalies of the kidney and urinary tract) (Harshman and Brophy, 2012). Frameshift mutations of *PAX2* can lead to papillorenal syndrome (PRS), an autosomal dominant disorder caused by a truncated *PAX2* protein. This syndrome results in reduced nephrons and UB branching, leading to renal hypoplasia (Dureau et al., 2001).

Both *Pax2* and *WT1* are believed to regulate one another following induction of the condensing MM. This relationship was assessed using mice carrying heterozygous mutations in both genes. Hypoplastic kidneys were observed in the compound heterozygotes compared to the wildtypes and fewer nephrons developed. Pelletier's group discovered that the compound heterozygous mice, as well as *Wt1*-null mice, resulted in *Pax2* phenotypes, suggesting that *Wt1* and *Pax2* interact with one another to form a molecular complex and the *Wt1* alleles may be one of the modifiers of *Pax2* alleles (Discenza et al., 2003). Earlier *in vitro* work showed that *Pax2* contains *WT1* binding sites and during kidney development, it may be a potential target of *WT1* negative regulation (Dehbi et al., 1996, McConnell et al., 1997).

1.3.3.2 POD1

The basic-loop-helix-loop (bHLH) proteins are another family of transcriptional regulators of podocyte development. *POD1* (capsulin/epicardin/Tcf21) was the first bHLH protein found in the developing kidney (Lu et al., 1998, Robb et al., 1998, Quaggin et al., 1999). *POD1* is highly expressed during MM condensation and is downregulated in the renal vesicles during epithelialisation. It is re-expressed at the S-shaped stage within the

podocyte precursors. This gene is continuously expressed in fully differentiated podocytes in the adult kidney (Quaggin et al., 1998). *Pod1*-null mice have major renal abnormalities with arrested glomerular differentiation at the capillary loop stage and die at birth due to lung and cardiac defects (Quaggin et al., 1999). Selective knockout of *Pod1* using the Cre-loxP system in mature podocytes in mice results in underdeveloped glomerulus with proteinuria and FSGS (Maezawa et al., 2014).

1.3.3.3 *Kreisler*

Kreisler (*MAF-1*, *MAFB*), a member of the basic domain leucine zipper family of transcription factors, is significantly expressed in the developing and mature podocytes at the capillary loop stage (Imaki et al., 2000). Mice homozygous for *Maf1* mutation exhibit proteinuria and podocyte FP effacement with reduced *Nphs1* and *Nphs2* expression (Sadl et al., 2002). *Mafb* has been found to be significant for podocyte differentiation and FP development (Moriguchi et al., 2006). An *in vivo* experiment overexpressing *Mafb* in podocytes of mice with diabetic nephropathy ameliorated albuminuria and protected podocyte number (Morito et al., 2014). Furthermore, transcriptomic analyses identified *mafb* to be a target gene of *wt1* in zebrafish models (Dong et al., 2015b). ChIP sequencing data has also revealed strong WT1-associated peaks at *Mafb*, highlighting WT1's importance in regulating *Mafb* (Lefebvre et al., 2015, Bharathavikru et al., 2017).

1.3.3.4 *LMX1B*

LMX1B, a member of the LIM-homeodomain family, is limited to differentiating podocytes from the capillary loop stage onwards. It is important during GBM development by regulating the type IV collagen gene as well as regulating other genes during podocyte maintenance (Morello and Lee, 2002). *LMX1B* mutations result in nail patella syndrome with 30-50% of patients developing kidney disease and around 5% developing ESRD (Sweeney et al., 2003). Chen et al. examined *Lmx1b*'s function in mouse limb and kidney, as dorsal-ventral limb patterning is known to be controlled by this gene. They showed that *Lmx1b* is necessary for dorsal limb fate specification and targeted disruption of this gene leads to nail and patellae absence, with glomerular proteinuria, GBM thickening and convoluted proximal tubules (Chen et al., 1998). *LMX1B* can interact with other podocyte genes to maintain normal podocytes; double knockdown of *Lmx1b* and *foxc* using morpholinos in zebrafish interrupts podocyte development and co-overexpression of both genes induces *nphs2* expression in podocytes, emphasising *LMX1B*'s importance in podocyte integrity (He et al., 2014).

1.4 Notch Signalling and glomerulogenesis

The Notch pathway is a highly conserved cell-signalling pathway essential for the spatial patterning and homeostasis in embryonic and adult tissues and is important during renal organogenesis and podocyte differentiation (Bray, 2006, Bray, 2016).

1.4.1.1 Notch components

In mammals, there are four Notch receptors NOTCH 1-4 (N1-4) which are transmembrane type 1 proteins (Kovall and Blacklow, 2010, Kopan and Ilagan, 2009); in contrast only one Notch homolog exists in *Drosophila* (Figure 1.14). The extracellular domain of the Notch receptors (NECD) contains around 29-36 EGF-like tandem repeats (epidermal growth factor) and is glycosylated by glycosyltransferases in the endoplasmic reticulum (ER) post-cleavage of the N-terminus (Rana and Haltiwanger, 2011). Sugar modifications include O-fucosylation by Ofut1 (Pofut1 in mammals) followed by Fringe elongation with O-GlcNAc in the Golgi complex (Munro and Freeman, 2000, Moloney et al., 2000, Bruckner et al., 2000) (Figure 1.15). Receptor activation occurs in the ER by Rumi O-glycosylation (Poglut in mammals) (Acar et al., 2008). C-terminal to the ECD is a negative regulatory region (NRR) consisting of the Lin-12 Notch repeats (LNR) and HD (heterodimeric) motifs (Figure 1.14). The EGF domain of the receptor allows ligand interaction to take place between neighbouring cells (trans) and within the same cell (cis).

Both proteolytic cleavage sites, S1 and S2, reside in the cysteine-rich LNR within the negative regulatory region (NRR). In the absence of the Notch ligand, the proteolytic cleavage site (S2) of the receptor is masked by the NRR, preventing activation of the Notch pathway (Weinmaster and Fischer, 2011). Cleavage of the S3 site takes place in the transmembrane domain (TMD) (Figure 1.14). The intracellular domain of the Notch receptor (NICD) consists of the RBPj association module (RAM), and nuclear localising sequence (NLS), which links the RAM to seven ankyrin repeats (ANK). Another NLS (NLS2) is located after the ANK repeats, followed by a transactivation domain (TAD) (Figure 1.14). The stability of the NICD is controlled by proline/glutamic acid/serine/threonine-rich motifs (PEST), located at the C-terminus (Kopan and Ilagan, 2009, Yamamoto et al., 2014). The NICD also contains numerous post-translational modification sites for phosphorylation and ubiquitination (Fryer et al., 2004). The *Drosophila* NICD contains a poly-glutamine (Q)-rich domain, OPA domain, within the TAD (Wharton et al., 1985).

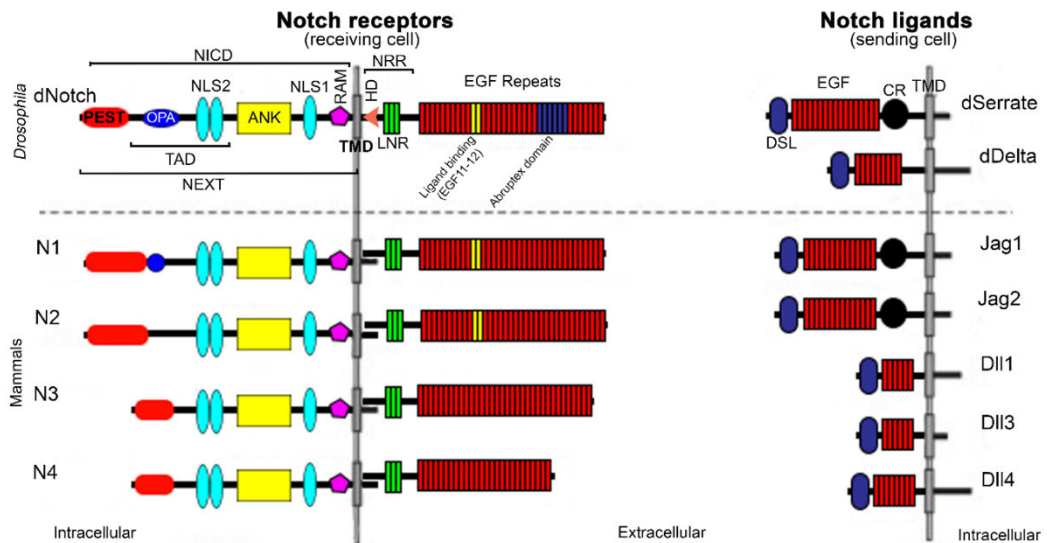


Figure 1.14. Notch pathway components

Notch receptors contain Intracellular (NICD) and extracellular (NECD) domains. NICD: PEST (proline, glutamate, serine, threonine rich degradation motif), essential for proteasome-facilitated degradation of NICD; OPA (opa repeats); TAD (transactivation domain), involved in recruiting additional coactivators; NLS (nuclear localisation signals), ANK, seven ankyrin repeats and RAM, RAM domain, which interact with CSL (CBF, suppressor of Hairless, Lag-1) and Mam (Mastermind). NECD: NRR (Negative regulatory region) contains three LNR domains and a HD motif, where the S1 and S2 cleavage sites reside; TMD (transmembrane domain) is the S3 cleavage site; EGF (epidermal growth factor) repeats, EGF 11-12 are essential for ligand binding, EGF 8 is associated with ligand selectivity, EGF 24-29 (Abruptex domain) negatively regulate signalling. The receiving cell contains Notch receptors that bind to Notch ligands. Notch ligands also contain EGF repeats; DSL (Delta-serrate-Lag2 domain); CR (cysteine rich region), TMD. Adapted from (Schwanbeck et al., 2011, Yamamoto et al., 2014).

The Notch pathway consists of two families of ligands; the Delta-like family members, Delta-like 1, 3 and 4 (DII1, DII3, DII4), and Jagged/serrate family members Jagged 1 and 2 (Jag1, Jag2). The Notch ligands are also transmembrane type 1 proteins, which contain a DSL (Delta/serrate/LAG-2) motif at their N-terminus, the DOS domain (Delta and OSM-11) and EGF repeats (Kopan and Ilagan, 2009, D'Souza et al., 2010) (Figure 1.14). Both ligands contain a PDZ (PSD-95/Dlg/ZO-1) binding domain at their C-terminus, apart from Jag2 and DII3 (Adam et al., 2013). Jagged ligands contain more EGF-like repeats than Delta-like ligands, and a cysteine-rich domain near the transmembrane domain (Sjoqvist and Andersson, 2017).

1.4.2 Notch signalling activation

The Notch pathway is activated by inter-cellular cross-talk between a signal-sending cell and a signal-receiving cell, resulting from initiation of signalling in the Golgi Apparatus with eventual translation of Notch to the nucleus (Figure 1.15). The EGF domains of the NECD receptors undergo glycosylation by fucosyltransferases, including POFUT1 (protein o-fucosyltransferase), subsequently followed by Fringe modification in the Golgi complex, where specific Fringes (Manic Fringe [Mfng], Lunatic Fringe [Lfng] and Radical Fringe [Rfng]) elongate the o-fucose chains, modifying the Notch receptors and allowing them to bind their ligands.

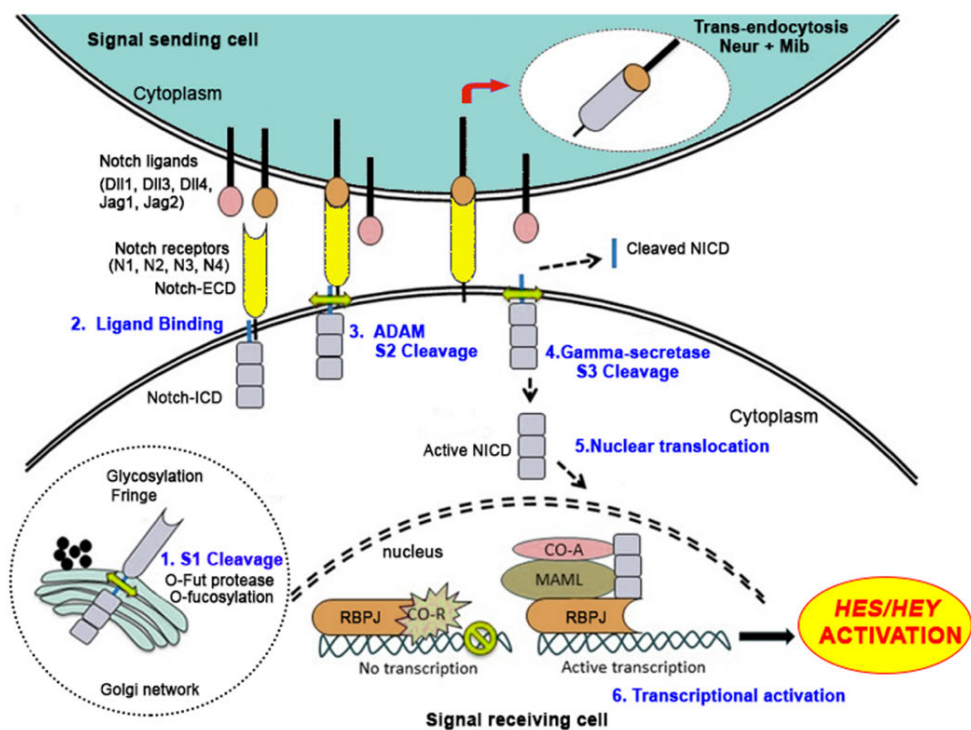


Figure 1.15. The Notch pathway

(1) Notch signalling is initiated in the Golgi apparatus where the receptor undergoes proteolytic cleavage at its S1 site, facilitated by furin proteases. (2) It is then transported to the cell surface membrane, where its extracellular domain binds with Notch ligands from the adjacent cell. (3) The Notch receptor is then proteolytically cleaved by ADAM metalloproteases, leading to endocytosis of the ECD into the ligand-expressing cell, followed by the release of the NICD with a hitched membrane. (4) NICD undergoes cleavage by gamma-secretase, leading to an active NICD. (5) Activated NICD translocates to the nucleus, interacting with CSL, forming a complex with MAML, RBPJ. (6) The active complex releases canonical Notch targets HES and HEY. Lack of NICD binding leads to CSL interacting with co-repressor. Adapted from (Suresh and Irvine, 2015).

The NECD undergoes its first proteolytic cleavage (S1) in the Golgi complex, where the LNR is cleaved by furin-like proteases and a heterodimeric receptor with the NECD is

formed in the HD (Lake et al., 2009, Gordon et al., 2009) (Figure 1.15). The Notch ligands are translated in the ER and travel to the cell surface through the Golgi complex. Following Fringe modification, the Notch receptor transfers to the cell surface where it interacts with the ligand, and trans-endocytosis is activated into the signal-sending cell. Trans-endocytosis is triggered by E3 ubiquitin ligases, Neuralized (Neu), recognising delta-ligands or Mindbomb (Mib), recognising jagged ligands, which are necessary for ligand endocytosis (Yamamoto et al., 2014). This process creates a conformational change in the Notch receptor and reveals its S2 cleavage site, normally masked by NRR, which is cleaved by ADAM proteases. This allows Notch extracellular truncation (NEXT) to enter the active site where S3, within the TMD, is sequentially cleaved by γ -secretase (Jorissen and De Strooper, 2010). This cleavage releases the NICD, which translocates into the nucleus and forms a complex with the DNA-binding transcription factor CSL (*RBP-jk* in mammals, *Su(H)* in *Drosophila*) and coactivator mastermind (*MAML1*, *MAML2*, *MAML3* in mammals, *Mam* in *Drosophila*) through its domains, RAM and ANK (Borggreffe and Liefke, 2012, Tanigaki and Honjo, 2010). Downstream canonical transcription factors, including Hairy/enhancer of split (*HES* and *HEY*) genes are then activated (Kopan and Ilagan, 2009, Liu et al., 2013, van Tetering and Vooijs, 2011, Yamamoto et al., 2014) (Figure 1.15). NICD absence results in the binding of CSL to its analogous sequence, leading to a recruitment of transcription corepressors, including Hairless, CtBP (C-terminal Binding Protein), and Groucho. These corepressors negatively regulate Notch target gene expression.

Notch receptors are initially cleaved during exocytosis at site 1 (S1), regulating signal activity (Figure 1.15). Ubiquitination of the ligand takes place in the ICD and is controlled by E3 ubiquitin ligases including Mindbomb and Neuralized (Kopan and Ilagan, 2009). Lateral patterning during Notch signalling depends on positive (lateral induction) or negative (lateral inhibition) feedback.

1.4.2.1 Notch glycosylation

Notch modification by glycosyltransferases takes place in the Golgi complex where glycans are added to the EGF domains of NECD. The addition of glycans can either reduce or potentiate Ligand-mediated Notch signalling, depending on which EGF domain is being modified (Taylor et al., 2014). Table 1.6 highlights the glycosyltransferases that modify the ECD of Notch1.

Table 1.6. List of glycosyltransferases that modify Notch ECD

| Glycosyltransferase (drosophila/ mammals) | Function | EGF modification |
|---|--|--|
| <i>Ofut1/Pofut1</i> | O-fucosyltransferase/ Chaperon activity | Adds fucose to EGF 11-12 |
| <i>Fringe/ Lunatic, Manic, Radical Fringe</i> | N-acetylglucosaminyl- transferase | Adds GlcNAc to 3'-OH groups of O-fucose EGF 11-12 |
| <i>Rumi (Ogut1)/ Poglut1</i> | O-glycosyltransferase | Add glucose to EGF 16-20 |
| <i>Shams/ (GXylT)1, (GXylT)2</i> | O-xylosyltransferase | Adds first xylose to xylose on O-glucose |

*EGF, epidermal growth factor; GlcNAc, N-acetylglucosamine. Adapted from (Rana and Haltiwanger, 2011)

Notch O-fucosylation

Notch modification involves addition of O-fucose or O-glucose to the EGF repeats within the extracellular domain of the receptor. Enzymes involved in this process include POFUT1 (Protein O-Fucosyltransferase 1), which are located and function within the Golgi complex (Figure 1.15, Table 1.6). O-glucose addition is carried out by the enzyme O-glycosyltransferase, POGLUT, encoded by *Rumi*, and finally, O-GlcNAc, a type of O-glycosylation occurring on hydroxyl amino acids of the EGF repeat, is added by Fringe. (Rana and Haltiwanger, 2011). O-fucosylation can occur on EGF12 as well as other EGF repeats, which may play a vital role in Notch activation (Ge and Stanley, 2008). Amongst the 36 EGF repeats of the Notch receptors, 20 of them have O-fucosylation sites, thus Fringe modifications can take place in any of these residues.

The Fringe proteins (β 3-N-acetylglucosaminyltransferases)

Fringes are β 3-N-acetylglucosaminyltransferases that transfer a GlcNAc to O-fucose residues in the Golgi complex, and play a crucial role in activating the Notch pathway through specific ligand binding (Okajima et al., 2003, Moloney et al., 2000, Taylor et al., 2014, Bruckner et al., 2000). There are three Fringe proteins that mediate Notch signalling; Lunatic (LFNG), Manic (MFNG) and Radical Fringe (RFNG), all of which elongate the O-fucose chain of the Notch transmembranes (Table 1.6, Table 1.7).

Table 1.7. Fringe-mediated glycosylation of Notch 1

| Fringe proteins | Notch 1 EGF domains | | | | |
|-----------------|---------------------|--------|---------------|--------------|--------------------|
| | EGF6 | EGF8 | EGF12 | EGF26 | EGF36 |
| <i>Lfng</i> | - Jag1 | + Dll1 | +Dll1, +Jag1 | -Dll1, -Jag1 | - Jag1 |
| <i>Mfng</i> | - Jag1 | + Dll1 | + Dll1, +Jag1 | -Dll1, -Jag1 | - Jag1 |
| <i>Rfng</i> | NM (+Jag1, +Dll1) | + Dll1 | + Dll1 | +Dll1, +Jag1 | NM (+Jag1, + Dll1) |

*NM, not modified by Fringe; +/-, ligand binds/ligand does not bind. Adapted from (Kakuda and Haltiwanger, 2017)

1.4.3 Ligand-independent Notch signalling

1.4.3.1 Deltex-induced Notch activation

Notch ligand-independent signalling is activated through the binding of Notch ICD and Deltex (Dx), promoting Notch endocytosis (Baron, 2012) (Figure 1.16). Notch endocytosis can be blocked by an early endosome component, RAB5, downregulating Notch signalling. Dx-induced Notch activation requires assistance of particular components to allow Notch trafficking into the late endosome. These components are the Adaptor-protein-3 (AP-3) complex and the HOPS (Homotypic fusion and vacuole protein sorting); AP-3 transfer NICD to the late endosomal and lysosomal vesicle membranes (Peden et al., 2004), HOPS is involved in late endosome maturation and fusion to the lysosome (Rink et al., 2005). With the help of these complexes, Notch is co-expressed with a constitutively active form of RAB7, allowing Notch to relocate to the late endosomes and upregulating Notch activity (Wilkin et al., 2008, Morohashi and Tomita, 2013, Baron, 2012).

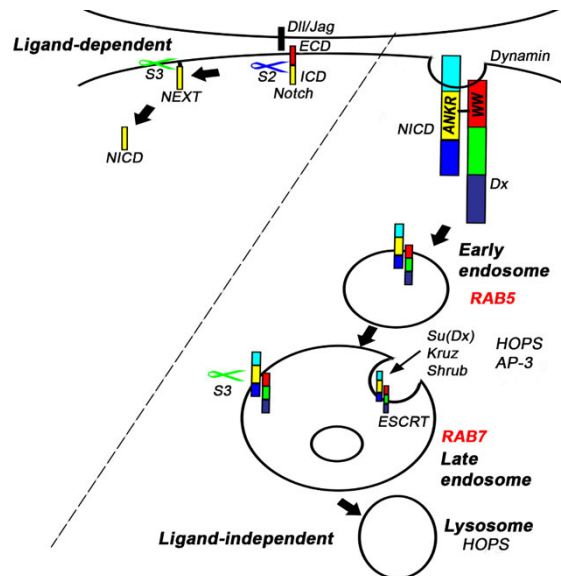


Figure 1.16. Ligand-independent Notch activation

The Notch pathway can be triggered through ligand-receptor binding (left) or ligand-independent activation (right). Ligand-independent activation of Notch involves the binding of Deltex (Dx) with NICD, inducing endocytosis of NICD from the early endosome (RAB5) to the late endosome (RAB7), promoted by HOPS and AP-3, regulating endosome maturity. The interaction of Dx with Su(Dx), Kurtz (Krz), and Shrub localises Notch into internal vesicles of the multivesicular bodies, downregulating Notch activity. Notch activity can also be triggered by S3 cleavage by presenilin post-NECD removal, where Notch is sorted to the late endosome, further requiring Rab7 and HOPs-fusion to the lysosome. During late endosomal maturation, ESCRT complexes are required to transfer Notch into multivesicular bodies, downregulating Notch signalling.

1.4.3.2 Notch trafficking destinations associated with up or downregulation of signalling

When Notch is no longer required for cell-to-cell signalling, it is marked for degradation. Coexpression of Dx with the suppressor of Deltex (Su(dx)) relocates Notch into the multivesicular body and results in a downregulation of Notch activity (Wilkin et al., 2008). Without Su(dx), Dx induces Notch endocytosis and allows it to remain at the periphery of the late endosome, preventing it from relocating to the multivesicular bodies (MVB) (Wilkin et al., 2008). Kurtz (Kz) is another protein that downregulates Notch activity through its co-expression with Dx. This stimulates receptor poly-ubiquitination of Notch and decreases the activity of the ESCRTIII (endosomal sorting complex required for transport) complex named Shrub, resulting in Notch downregulation (Mukherjee et al., 2005). Polyubiquitinated proteins are recognised by the ESCRT complexes, which are known to regulate numerous membrane-bound receptors (Palmer and Deng, 2015). The distinct ESCRT complexes function in a serial manner to sort Notch into intraluminal vesicles (ILVs) of the MVB. Here, the MVB lumen cargo is transported to the lysosome lumen, where it becomes degraded (Palmer and Deng, 2015, Hori et al., 2012).

1.4.4 Expression of Notch pathway components during kidney development

Notch plays a crucial role in podocyte cell fate induction and is involved in the initial patterning of the nephron, determining proximal versus distal fates in both mouse and *Xenopus* (White et al., 2010, Hartwig et al., 2010).

Notch pathway components including NOTCH1-4, HES1 and HEY1 are expressed in podocyte progenitors at the S-shaped body stage. All components are no longer detected in terminally-differentiated podocytes (McCright et al., 2001) (Figure 1.17). Notch homologues and ligands involved in podocyte differentiation are highlighted in Table 1.8.

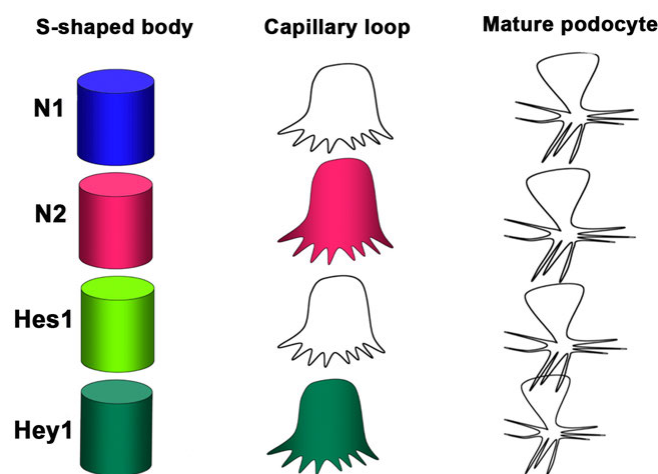


Figure 1.17. Notch expression during podocyte differentiation

At the S-shaped body of glomerulogenesis, Notch components Notch1 (N1), Notch2 (N2), *Hes1*, *Hey1* are expressed. At the capillary loop stage of the differentiating podocytes, *N1* and *HES1* become downregulated, while *N2* and *Hey1* expression remains. When the podocytes are terminally differentiated, all Notch components are downregulated. Adapted from (Aoife Waters, 2009).

During glomerulogenesis, numerous Notch components are expressed, including NOTCH1, NOTCH2 and the Notch ligands, DLL1 and JAG1. HES1 and HEY1 are expressed in the proximal domain of the S-shaped body and become increasingly reduced during terminal podocyte differentiation. NOTCH3 is mainly present in the major kidney blood vessels and glomerular tuft, whilst NOTCH4 is found in the vascular endothelia. JAG1 is seen in the proximal part of the S-shaped body along with DLL1, which is usually restricted to the middle segment (Table 1.8). *Notch2* mRNA has also been detected in the comma-shaped bodies and tubules (McCright et al., 2001) and earlier work revealed that *Notch2* was essential for proximal tubule fate during nephrogenesis (Cheng et al., 2007).

Table 1.8. Expression of the Notch components during glomerulogenesis

| Notch component | S-shaped body | Podocyte progenitors | Endothelial progenitors | Mesangial progenitors |
|-----------------|---------------|----------------------|-------------------------|-----------------------|
| Notch 1 | Middle | + | + | - |
| Notch 2 | Proximal | + | - | - |
| Notch 3 | Proximal | - | + | + |
| Notch 4 | - | - | + | - |
| Jag1 | Middle | - | + | + |
| Jag2 | - | - | + | - |
| Dll1 | Middle | - | + | - |
| Dll3 | - | - | - | - |
| Dll4 | - | - | + | - |
| Hes 1 | Middle | + | + | - |
| Hes 5 | Middle | - | - | - |
| Hes 6 | - | - | - | - |
| Hey 1 | Middle | + | + | - |
| Hey 2 | - | - | - | - |
| HeyL | Middle | - | + | - |
| Lfng | Middle | - | - | - |

*Adapted from (Leimeister et al., 2003, Piscione et al., 2004, Chen and Al-Awqati, 2005)

1.4.5 The role of Notch in kidney development

1.4.5.1 Transgenic mouse models of Notch in kidney development and disease

Numerous studies have investigated the role of the Notch pathway in mouse models during early (summarised in Table 1.9) and late nephrogenesis (summarised in Table 1.10).

Cheng et al., demonstrated the significance of Notch expression in the comma- and S-shaped bodies (Cheng et al., 2003) by blocking the Notch pathway with a γ -secretase inhibitor; UB branching, renal epithelial structures, glomerular podocytes and proximal tubules were reduced. Likewise, targeted deletion of the EGF repeat 14 in *Notch2* homozygotes (*Notch2^{del1}/Notch2^{del1}*) from the MM stage resulted in hypoplastic kidneys with no comma- nor S-shaped bodies and lack of mature glomeruli at E16.5 compared to wildtype glomeruli (McCright et al., 2001). Subsequent research revealed that NOTCH1 and NOTCH2 (N1 and N2) displayed differential expression patterns in the developing kidney; NOTCH1 was mainly expressed in the endothelial cells whilst

NOTCH2 was largely expressed in the MM, UB and vascular smooth muscle cells (Liu et al., 2013). By switching the NICD genomic sequences, new mice were generated carrying the genes *N12* (N1 locus carrying N2ICD) and *N21* (N2 locus carrying N1ICD), where they discovered that the ICDs were interchangeable and their ECDs were more responsible for the abundance of NOTCH2 during nephrogenesis. NOTCH2 binding affinity was higher than NOTCH1 at the cell surface and NOTCH2 ECD produced more NICD than NOTCH1 ECD. Heterozygous mice *N1^{+/-};N2^{21/-}* and homozygous *N2^{21/21}* carrying the *N2* locus and lacking the N2ICD, still developed nephrons that were functional, however, *Pax3-Cre;N2^{fl/fl};N1^{12/12}* mice lacking the *N2* locus altogether did not develop nephrons and died within 24 hours of birth, suggesting a role for the ECD's rather than ICDs during kidney development (Liu et al., 2013). *Notch1* and *2* cleavage were further assessed using a Cre reporter mouse line (*N1;Cre^{Lo}* and *N2;Cre^{Lo}*), where the release of Cre depended on the release of the Notch ECD. Epithelial cells in the S-shaped bodies and RV were detected in *N2;Cre^{Lo};Rosa^{CAG-EYFP}* mice, but not seen in *N1;Cre^{Lo};Rosa^{CAG-EYFP}* mice, indicating that *Notch2* ECD is released more efficiently than *Notch1* in developing nephrons.

Additionally, Tomino's team investigated the role of NOTCH2 during nephrogenesis in ADR-treated mice, representing models of NS and GS. NOTCH2 agonistic monoclonal antibody (mAB), NOTCH1 agonistic mAB and JAG1 antagonistic mAB were administered independently in mice post-ADR-induction. Proteinuria and GS were both improved following *Notch2* activation by the mAB but no improvement was seen using the NOTCH1 agonistic mAB or JAG1 antagonistic mAB. Likewise, when NOTCH2 activation was decreased *in vitro*, apoptosis was increased in the podocytes (Tanaka et al., 2014). Similarly, an increase in *Notch2* activation has been linked with enhanced activation of the transcription factor *Mafb* (essential for podocyte differentiation), which has been shown to ameliorate albuminuria and phenotypes associated with diabetic diseases (Morito et al., 2014). NOTCH3 has also been detected in podocyte nuclei of patients with FSGS or lupus nephritis (Lasagni et al., 2010). Mice injected with nephrotoxic sheep serum (NTS) develop a rapid progressive glomerulonephritis (RPGN) with increased expression of *Notch3* and its canonical targets. NTS-induced mice lacking *Notch3* (*Notch3^{-/-}*) resulted in reduced renal inflammation, proteinuria and uremia compared to the NTS/Wildtype mice (El Machhour et al., 2015).

Presenilins (PSEN1 and PSEN2) are transmembrane proteins that are catalytic components of γ -secretase, which proteolytically cleave the Notch receptors to regulate Notch signalling. *Psen1*-deletion in mice leads to pre- or perinatal death, with somite segmentation defects associated with *Notch1* (Wong et al., 1997). Mice with a double

knockout of *Psen1* and *Psen2* die at E9.5, with absence of somite patterning, similar to the *Notch1* loss of function model and *Notch1* and *Notch4* double knockout mouse phenotypes (Conlon et al., 1995, Donoviel et al., 1999, Herreman et al., 1999, Krebs et al., 2000). Double knockout of *Psen1* and *Psen2* with a human *PSEN1* transgene introduced into mice (*Psen1*^{-/-};*Psen2*^{-/-};*PSEN1*) supported the survival of the null embryos up until the perinatal stage, however, the mutant embryos were slightly smaller in size. Moreover, no S- or comma-shaped bodies were observed in E13.5 mutant kidneys compared to their littermate controls, suggesting that presenilins may play a role in the progression of pretubular aggregates towards the S- and comma-shaped bodies. By P0, kidneys lacked glomeruli and mice died within 24 hours (Wang et al., 2003). Notch signalling is also activated by E3 ubiquitin ligases. Mindbomb is an E3 ubiquitin ligase known to promote endocytosis of the Notch ligands during Notch signalling. Inactivation of the Mindbomb gene (*Mib1*) was induced specifically in the renal collecting duct by crossing *Hoxb7-Cre* mice, where Cre recombinase was expressed only in the UB, and exons 2 and 3 of *Mib1* were floxed (*Hoxb7-Cre;Mib1*^{fl/fl}). P17 mice showed disrupted Notch activation with unilateral or bilateral hydronephrosis that had become more evident at P30 (Jeong et al., 2009).

A former study analysed *Notch1* and *Notch2* function during nephron development and showed that *Notch2* was more essential than *Notch1* for proximal tubule fate (Cheng et al., 2007). Cre-mediated knockout of *Notch2* in the kidney mesenchyme using a *Pax3-Cre* mouse line was used to study the formation of proximal tubules (*Pax3-cre*^{tg/+};*Notch2*^{fl/fl}). The mutant mice died 48 hours after birth, with smaller kidneys compared to the control heterozygote littermates (*Pax3-cre*^{tg/+};*Notch2*^{fl/+}). Haemorrhage was detected in the interstitial spaces of the mutant kidneys, as well as a collapsed renal pelvis and flattened papilla. Furthermore, the *Notch2*-deficient kidneys formed distal tubules without developing podocytes or proximal tubules. To examine whether *Notch2* was adequate for nephron segmentation, without *Notch1*, a mouse model to delete *Notch1* was generated, using a *Pax2-cre;Notch1*^{fl/Δ1} line (where Δ1 represents a null allele). *Notch1*-deficient mice contained normally developed proximal tubules, suggesting that *Notch1* is not required for proximal patterning of the nephron. Furthermore, *Rbpj* knockouts (*Pax2-cre;Rbpj*^{fl/fl}) lacked glomeruli and proximal patterning, mimicking the *Notch2*-deficient mice. Constitutive expression of *Notch1* ICD in undifferentiated nephron progenitors using *Six2GFPcre* line, at the cap stage before RV formation (*Rosa*^{Notch/+};*Six2-GFP:Cre*^{tg/+}), was used to test whether *Notch1* was able to compensate for the loss of *Notch2* in the kidneys. Although proximal tubules developed, mice at E17.5 displayed severely hypoplastic kidneys, with reduced UB branching and repressed distal tubule formation (Cheng et al., 2007). Subsequent research was performed on models

of DKD to identify the roles of *Notch1* and *Notch2* during the development of diabetic nephropathy (Sweetwyne et al., 2015). Conditional deletion of *Notch1* in podocytes of *NPHS2^{cre};Notch1^{fl/fl}* mice protected the kidneys from streptozotocin-induced DKD with reduced podocyte dedifferentiation, whereas controls only carrying the *Notch1* floxed gene (*Notch1^{fl/fl}*) and *Notch2* knockout did not rescue DKD (*NPHS2^{cre};Notch2^{fl/fl}*), suggesting a distinctive role for *Notch1* in podocytes during DKD progression. This was also supported by *in vitro* deletion of *Notch1*, resulting in reduced podocyte apoptosis and dedifferentiation. *Notch1* deletion led to an increase in *Notch2* expression, highlighting an interaction between both receptors (Sweetwyne et al., 2015).

Recent research reported that the Notch pathway is not only important for proximal tubule formation but necessary for proximal-distal segmentation of the nephron (Chung et al., 2017). Chung et al. carefully examined the Notch pathway during the late stages of nephrogenesis by deleting both exon 1 of *Notch1* (*Notch1^{c/c}*) and exon 3 of *Notch2* (*Notch2^{c/c}*) using a *Wnt4GFPcre*-activated Rosa EYFP reporter. The loss of function (LOF) experiment revealed a reduction in nephron markers, including the podocyte marker, Podocin, and proximal tubule marker, SLC34A1, and all nephron segments failed to develop. Although loss of Notch signalling still allowed epithelial cell transition, S-shaped bodies were not able to form compared to the controls. Transcription factors, LHX1 and HNF1B, both important for correct nephron segmentation, were expressed in lower amounts in the LOF mutant cells compared to the controls. A gain of function (GOF) experiment was subsequently carried out using the *Six2GFPcre*-activated Rosa EYFP/b-gal where NICD1 was constitutively activated. Following up on this study, Park's team (Chung et al., 2017) used the same reporter line to see whether the nephron progenitors would only convert to proximal tubules and no other nephron segment. GOF Notch activated SIX2 progenitor cells not only developed into proximal cells, but a heterogeneous population of cells, including podocyte marker positive cells (WT1+ and MAFB+) were observed. *Lhx1* and *Hnf1b* were ectopically expressed following GOF Notch expression, highlighting the importance of Notch signalling for the differentiation of nephron progenitors. To conclude, Notch is not only important for proximal tubule formation, but is required for the segmentation of the nephron.

Hairy/enhancer of split (HES) play a significant role during early nephrogenesis; they are expressed in UB tips, condensed mesenchyme, and the comma- and S-shaped bodies. Haematoxylin/PAS-stained kidneys of *Hes1* and *Hes5* mutant mice (*Hes1^{-/-}*, *Hes5^{-/-}*, *Hes1^{-/-};Hes5^{+/-}*, *Hes5^{-/-};Hes1^{+/-}*, *Hes5^{+/-};Hes1^{+/-}*) at E15-E17.5 showed no morphological difference in the kidneys compared to the wildtype mice. LTA-stained proximal tubules and E-cadherin-stained distal tubules/collecting ducts in all the mutants were similar to

the wildtypes. Double knockouts (*Hes1^{-/-};Hes5^{-/-}*) were not analysed as they did not survive past E11.5, i.e. before nephron formation (Chen and Al-Awqati, 2005).

Table 1.9. Early nephrogenesis in transgenic mouse models of Notch gene manipulation

| Mouse model | Phenotype | Reference |
|--|---|---|
| <i>Notch2^{del1}/Notch2^{del1}</i> | - UB branching with formation of metanephric vesicles (E13.5) - Arrested glomerular differentiation, absent capillary tuft and disorganised clumped cells, capillary tuft replaced by capillary aneurysm structure within Bowman's capsule (E16.5) | (McCright et al., 2001) |
| <i>Psen1^{-/-};Psen2^{-/-};PSEN1</i> | - Normal induction of UB and condensed mesenchyme (E12.5) - S- and comma-shaped bodies absent, only PTA/RV present (E13.5) - Absent mature glomeruli (E15.5-P0). Death within 2hrs of birth | (Wang et al., 2003) |
| <i>Hes1^{+/-};Hes5^{-/-}, Hes1^{-/-};Hes5^{+/-} Hes1^{-/-}, Hes5^{-/-}, Hes1^{+/-};Hes^{+/-}</i> | No obvious morphological difference; smaller kidneys (E15-E17.5) | (Chen and Al-Awqati, 2005) |
| <i>Pax2-cre^{tg/+};N1^{f/Δ1}</i> <i>Pax2-cre^{tg/+};Rbp-j^{ff}</i> <i>Rosa^{Notch/+};Six2-GFP;Cre^{tg/+}</i> | - No impact on proximal fates; histologically normal (E12.5) - Failure to produce proximal tubules, death (E13.5) - Hypoplastic kidneys, reduced UB branching | (Cheng et al., 2007) |
| <i>N1^{12/12};N2^{21/21}</i> <i>N2-Cre^{Lo};Rosa^{CAG-EYFP}</i> <i>N1-Cre^{Lo};Rosa^{CAG-EYFP}</i> | - Normal RV, SSB, endothelial cells (E17.5) - Normal RV and SSB development (E17.5) - Reduced RV and SSB cell expression (E17.5) | (Liu et al., 2013) |
| <i>R26^{EYFP/+};N1^{c/c};N2^{c/c};Wnt4^{Cre}</i> | Failed nephron segment formation, both proximal and distal, failed S-shaped body formation (E16.5) | (Chung et al., 2017, Yang et al., 2004b, McCright et al., 2006) |

* UB, Ureteric bud; PTA, Pretubular aggregate; RV, Renal vesicle; SSB, S-shaped body

Table 1.10. Late nephrogenesis in transgenic mouse models of Notch gene manipulation

| Mouse model | Phenotype | Reference |
|---|---|----------------------------|
| <i>Notch2^{del1}/Notch2^{del1}</i> | - Perinatal death, hypoplastic kidneys, capillary aneurysms (P0) | (McCright et al., 2001) |
| <i>Notch2^{del1}/Jag1^{dDSL}</i> | - Hypoplastic kidneys, reduced number of glomeruli, absent capillary tufts, capillary aneurysms (P6) | |
| <i>Pax3-cre^{tg/+};Notch2^{ff}</i> | Glomeruli and proximal tubules lost. Distal tubules lacking podocytes, spotty haemorrhage in interstitial space, collapsed renal pelvis, flattened papilla (P2) | (Cheng et al., 2007) |
| <i>NPHS2-rtTA; tetO-ICN1</i> | Podocyte apoptosis, FSGS, proteinuria, advanced stage of tubular dilation (4weeks old) | (Niranjan et al., 2008) |
| <i>Nphs1-Cre(+);Notch-IC</i> | DMS, podocyte proliferation, FP effacement, reduced podocyte gene and protein expression (P0-P42) | (Waters et al., 2008) |
| <i>Hoxb7-Cre;Mib^{ff}</i> | Unilateral and bilateral hydronephrosis, distal renal tubular defects (P17) | (Jeong et al., 2009) |
| <i>Pax8-rtTA;tetO-ICN1</i> | Sever tubule degeneration, dilation, interstitial fibrosis (10 weeks old) | (Bielez et al., 2010) |
| <i>N1^{+/-};N2^{21/-} & N2^{21/21}</i> <i>Pax3-Cre;N2^{ff};N1^{12/12}</i> | - Normal nephron formation (P0) - No nephron development, death within 24hrs of birth | (Liu et al., 2013) |
| <i>Notch3⁻ NTS-induced nephropathy</i> | Significant decrease in proteinuria and uremia, decreased crescentic glomeruli and fibrin deposits, reduced renal inflammation | (El Machhour et al., 2015) |
| <i>NPHS2^{cre};Notch1^{fl/fl} vs</i> <i>NPHS2^{cre};Notch2^{fl/fl}</i> STZ-induced DKD | -N1 reduction leads to podocyte apoptosis and dedifferentiation reduced, mesangial expansion ameliorated (20 weeks old) - Proteinuria and increased mesangial expansion (20 weeks old) | (Sweetwyne et al., 2015) |

* FSGS, Focal segmental glomerulosclerosis; DMS, Diffuse mesangial sclerosis; FP, Foot process; NTS, nephrotoxic sheep serum; STZ, streptozotocin

Overexpression of Notch activity is associated with renal disorders

Ectopically activating Notch in developing and terminally differentiated podocytes in murine models can lead to proteinuria and GS (Niranjan et al., 2008, Waters et al., 2008). Tubulointerstitial fibrosis has been demonstrated in *Pax8rtTA;tetOICN1* doxycycline

induced mice, where NOTCH1 ICD was overexpressed in mature tubular epithelial cells. Histological analysis revealed severe tubular dilation and degeneration with interstitial fibrosis, similar to that of patient TIF phenotypes (Bielez et al., 2010). Genetic and pharmacological inhibition of the Notch pathway has been tested in several models of kidney disease (summarised in Table 1.11).

Pharmacological inhibition of the Notch pathway using a γ -secretase inhibitor in PAN-induced NS rats prevents podocyte apoptosis and albuminuria (Niranjan et al., 2008). Additional research however, revealed that γ -secretase inhibition exacerbated GS in ADR-induced FSGS mice (Lasagni et al., 2010) instead of ameliorating the disease. Niranjan et al. also deleted the canonical Notch target, *Rbpj* in DN mice and revealed a reduction in podocyte injury with less proteinuria (Niranjan et al., 2008).

Immunohistochemistry of human kidney biopsies with proteinuric nephropathy show expression of NOTCH1, NOTCH2 and JAG1 expression in the podocytes (Murea et al., 2010). Patients with HIVAN show an increase in NOTCH1 and NOTCH4 in their kidney, and γ -secretase inhibition of this pathway ameliorates kidney injury and hinders podocyte proliferation in a Tg26 mouse model of HIVAN (Sharma et al., 2013). Xiao et al. used γ -secretase inhibition with Dibenazepine (DBZ) in unilateral ureteral obstructed (UUO) C57/Bl6 mice, where upregulation of *Notch1*, 3, 4, *Nicd* and the downstream targets *Hes1* and *HeyL* were observed (Xiao et al., 2014). DBZ treatment post-UUO significantly reduced Notch expression, ameliorated renal fibrosis and inhibited the TGF- β pathway. A more recent study conditionally-deleted podocyte-specific *Notch1* in mice with DKD induced by uninephrectomy and STZ injection. *Notch1* deletion protected the mice from DKD. Podocyte dedifferentiation was prevented by maintaining *Nphs1*, as well as reducing levels of *snai1* observed post-TGF β 1 treatment. *Notch2*-deleted mice did not show improved podocyte dedifferentiation nor apoptosis; on the contrary, *Notch2* deletion enhanced podocyte apoptosis. These results revealed that *Notch1* plays a non-redundant role in podocytes during DKD progression (Sweetwyne et al., 2015). Likewise, constitutive activation of *Notch1* in the podocytes resulted in albuminuria and GS (Niranjan et al., 2008).

Table 1.11. Inhibition of Notch signalling in murine glomerular disease

| Treatment | Outcome | Reference |
|--|---|-------------------------|
| Tg(NPHS2-cre);Rbpj^{fl/fl} STZ-induced GSIXX-treated PAN-rats | - Reduced albuminuria, mild mesangial expansion, reduced diabetic kidney injury - Reduced albuminuria, effaced FPs rescued, reduced GS | (Niranjan et al., 2008) |
| GSIXX-treated TG mice | - Improved glomerular lesions, reduced scarred glomeruli and cystic dilatations, improved tubulointerstitial disease, reduced proteinuria | (Sharma et al., 2013) |
| Nphs1-Cre/ROSA26-loxP/NEP25 (cFSGS) DBZ-treated | - Urinary casts in cortex, tubulointerstitial damage, increased histological damage- worse than vehicle | (Ueno et al., 2013) |
| DBZ treatment on UUU-induced C57BL6 | - Collagen deposition decreased in kidney tissues; renal fibrosis prevented | (Xiao et al., 2014) |
| DBZ treatment on FA-induced TIF DBZ treatment on UUU-induced TIF PEPCK^{cr};Rbpj^{fl/fl} genetic deletion in FA-induced | - Reduced tubular dilatation and TIF - Less severe fibrosis, attenuated TIF - Reduced TIF | (Bielez et al., 2010) |
| ADR- induced nephropathy J1 antagonistic mAb and N1, N2 agonistic mAb | - Reduced proteinuria, glomerulosclerosis, and podocyte apoptosis | (Tanaka et al., 2014) |

* FP, Foot process; GS, Glomerulosclerosis; TIF, Tubulointerstitial fibrosis; FA, Folic acid; ADR, Adriamycin; PAN, Puromycin aminonucleoside; STZ, Streptozotocin; DBZ, Dibenzazepine; GSI, γ -secretase inhibitor; UUU, Unilateral ureteral obstruction

Morrissey et al. showed an upregulation of *Jag1/Notch1* in CKD and fibrosis through early gene expression profiling in mice (Morrissey et al., 2002). Folic Acid (FA) administration into mice causes acute renal failure and tubulointerstitial fibrosis (Bielez et al., 2010). *Jag1* and *Notch1* transcripts were upregulated in FA-treated mice. Notch

target, *HeyL*, was reduced following γ -secretase inhibition using DBZ. To validate the effect of DBZ, another tubulointerstitial model was tested UUO, resulting in increased Notch pathway transcript levels. DBZ again reduced Notch target expression and tubulointerstitial fibrosis. They followed this up by looking at tubular epithelial cell (TEC)-specific *Rbpj* deletion, where floxed *Rbpj* mice were crossed with PEPCK Cre mice in order to knockout *Rbpj* in TECs (*PEPCK^{cr};Rbpj^{fl/fl}*). After FA treatment, tubulointerstitial fibrosis was ameliorated in *Rbpj* knockout mice compared to FA-treated *wildtype* controls (Bielez et al., 2010). Further research discovered that *NOTCH1* expression was amplified in hyperplastic parietal epithelial cells (PECs) of human collapsing FSGS (cFSGS) and in mouse models of cFSGS (*Nphs1-Cre/ROSA26loxP/NEP25*). Transgenic mice expressing human CD25 on the podocyte (NEP25) develop progressive proteinuria and GS following administration of the immunotoxin (LMB2). Pharmacological inhibition of Notch with γ -secretase inhibitors did not influence disease (Ueno et al., 2013).

1.5 Interplay between *WT1* and Notch in vertebrate nephrogenesis

Notch and *WT1* both play a vital role during spatiotemporal kidney development and temporal deletion of these genes can severely impact the kidney. The expression of the Notch signalling genes, *notch1*, *serrate1*, and *delta1* has been examined in developing pronephros of *Xenopus* (McLaughlin et al., 2000). Overexpression of Notch signalling in the pronephric anlage disrupts tubule formation and results in an increase of both *pax2* and *wt1* expression (McLaughlin et al., 2000), highlighting the relationship between Notch signalling and *WT1* expression.

Davidson's team (O'Brien et al., 2011) examined the correlation between transcription factors *wt1* and *hes1* during podocyte differentiation in the zebrafish pronephros. Whole mount *in situ* revealed an expression pattern of both genes at different stages of development; an increase in *wt1* was associated with a downregulation of *hey1* (O'Brien et al., 2011). Moreover, the significance of Notch during early kidney development was demonstrated in the *Xenopus* pronephros. *Xenopus* hairy-related transcription factor (*xhrt*) and *xhes* genes had distinct dynamic patterns during glomerulus development. *xwt1* antisense morpholinos (MO) in the *Xenopus* resulted in reduced levels of *xhrt1* expression in the pronephros, highlighting the relationship between *WT1* and Notch signalling during glomerular development (Taelman et al., 2006). Furthermore, as previously cited, earlier work in mice investigated the role of *Notch* in podocytes at various stages of development by inducing the Notch1 ICD in mature and embryonic podocytes at the capillary loop stage (*NPHS2-rtTA;tetO-ICN1* and *Nphs1-Cre(+);Notch-IC*). Depending on the time-point, either FSGS (mature podocytes) or DMS (capillary

loop) manifested in the kidney, which was caused by podocyte apoptosis or dedifferentiation (Niranjan et al., 2008, Waters et al., 2008). These mice also showed a downregulation of podocyte genes, *Wt1*, *Nphs1* and *Nphs2*. *Wt1* knockdown in embryonic mouse kidney explants results in a significant reduction of *HeyL* transcript, highlighting the association between *Wt1* and the Notch pathway (Hartwig et al., 2010). *Xenopus* morpholino studies demonstrating spatiotemporal expression through the systemic elimination of podocyte transcription factors (*wt1*, *foxc2*, *hey1*, *mafb*, *Imx1b*) discovered that podocyte maturation required three main participants, *wt1*, *foxc2* and Notch signalling (White et al., 2010). Likewise, *WT1* and the *Notch* homologue, along with sonic hedgehog (SHH) and *Wnt* pathways, have been shown to function as part of a molecular network during nephrogenesis (Dormoy et al., 2012). Figure 1.18 illustrates the interplay between the Notch pathway and *WT1* during podocyte differentiation.

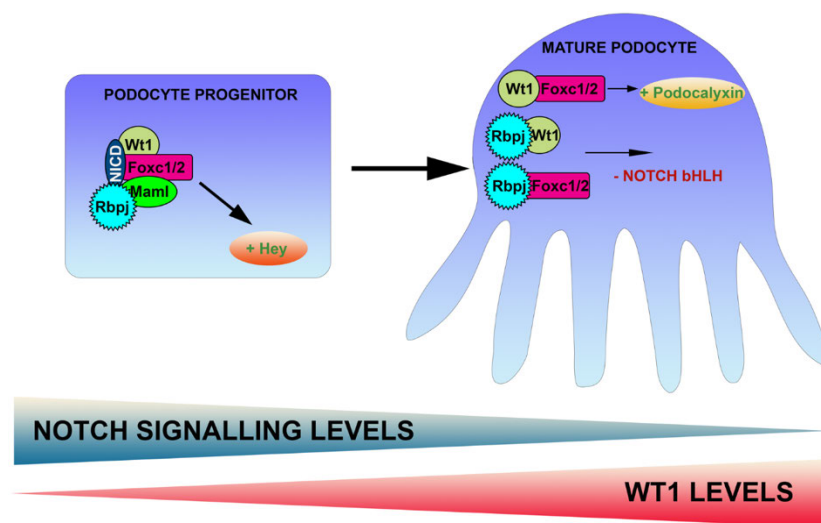


Figure 1.18. Transcriptional regulation of podocyte development

Podocyte progenitors express high levels of Notch signalling components including *Rbpj* and *NICD*, as well as *Wt1* and *FoxC1/2*, which induce *Hey* expression. Notch signalling decreases as podocytes mature, whilst *Wt1* expression levels increase. Higher levels of *Wt1* complexing with *FoxC1/2* trigger the activation of *Podocalyxin*. *Wt1* expression may regulate the Notch pathway by sequestering *Rbpj*, inhibiting downstream expression of Notch signalling. Adapted from (O'Brien et al., 2011).

Valsartan, an angiotensin II type 1 receptor antagonist, was investigated on STZ-induced diabetic mice, where Notch signalling was upregulated (Gao et al., 2016). Following Valsartan treatment, podocyte injury was ameliorated with reduced expression of the Notch signalling genes and increased *Wt1* gene expression (Gao et al., 2016). Opposing findings recently revealed that overexpression of Notch activity during pronephros development in *Xenopus* increased *wt1* expression (Katada and Sakurai, 2016). Further research examined Notch signalling during zebrafish kidney development and identified

that *jag1b*, *rbpj*, *jag2b*, *notch1a* and *notch3* are necessary to control the separation of *wt1* expressing podocytes and interrenal cells (Chou et al., 2017).

1.6 Scope of the thesis

Reciprocal interaction between WT1 and Notch has been documented during kidney development. Moreover, specific mutations in the *WT1* gene cause SRNS in humans and manifest as glomerular damage characterised by two distinct histological patterns – FSGS and DMS. Studies have also shown that ectopic activation of Notch in both mature and differentiating podocytes can also lead to FSGS and DMS in animal models.

As such, the aim of this study was to investigate whether podocyte Notch activation participates in *Wt1* glomerulopathy in both early and late stages of glomerulosclerosis. An inducible mouse model whereby podocyte-specific deletion of *Wt1* occurred following Tamoxifen administration was used for experiments.

The objectives were to:

- Establish and characterise the histological and biochemical phenotype of a *Wt1*-deleted model at different stages of disease;
- Functionally characterise Notch pathway expression in the inducible model of glomerulosclerosis;
- Determine the underlying mechanisms of podocyte injury;
- Determine whether pharmacological inhibition of Notch could abrogate GS in the inducible *Wt1*-floxed model; and
- Characterise Notch activation in human NS.

Chapter 2 – Materials and Methods

2.1 Transgenic mouse strains

Breeding and maintenance

Breeding pairs were set up once mice reached sexual maturity; females at 6 weeks of age and males at 8 weeks. Pups were then ear clipped 10 days post-birth and genotyped.

CAGG promoter-driven Cre-ERT2TM mice (*Cre-ERTTM±/±*, MGI 2182767) were crossed with homozygous *Wt1* conditional mice, where the first exon of *Wt1* is flanked by loxP sites (*Wt1^{loxP/loxP}*, MGI 4849364) (Chau et al., 2011). Following tamoxifen induction, the *Wt1* gene is excised through the Cre-recombinase mechanism and the kidneys are examined.

Frozen embryos were sent from Professor Hohenstein's group and were re-derived at the Kathleen Lonsdale Building (KLB), UCL. Cre-ERT2;*Wt1* mice were from a C57Bl/6j background.

Nphs2;rtTA transgenic mice were used for primary podocyte cultures and Hes1 overexpression experiments. These mice carry the reversed tetracycline transactivator under the human Podocin (*NPHS2*) promoter, which targets expression in the podocytes of the kidney. *Nphs2;rtTA* transgenic mice (MGI 3629962) were given to us from Dr. David Long's group in the Nephro-Urology Unit, Institute of Child Health, Great Ormond Street Hospital.

Nphs2;rtTA mice were also crossed with the transgenic mice carrying the tetracycline-responsive promoter element (tetO) achaete-scute family BHLH Transcription Factor (*Ascl1*), which was kindly sent to us from Professor Thomas Reh's group, University of Washington (Ueki et al., 2015).

All animal work was carried out under the permission of the Home Office project license 2518, PIL 70/23192. After the mice were re-derived at the KLB, UCL, Mice were housed and bred in the animal facilities at the Western Labs, UCL Institute of Child Health, Great Ormond Street.

***Wt1* deletion in *Cre-ERTM±;Wt1^{loxP/loxP}* transgenic mice**

In vivo *Wt1* deletion was achieved through tamoxifen induction (1mg/40g body weight for 3 days; Sigma) using 21G syringe needles in 5-week-old mice. Following tamoxifen induction, Cre-recombinase induced site-specific recombination between the loxP sites of the *Wt1* gene, resulting in a ubiquitous *Wt1* null allele. Recombination PCR was carried out in order to confirm successful *Wt1* deletion (Figure 2.1). Mice were sacrificed at days (D) 4, 5, 6, 8 and 12 post-tamoxifen induction (P.I.) and both kidneys were removed under sterile conditions. Mice were injected for three consecutive days with a low dose of tamoxifen in order to facilitate recombination of *Wt1* and to minimise tamoxifen toxicity and maximise survival. This time-course was established following a careful examination of the phenotype at every time-point until D12 P.I. Mice were too sick to be examined after D12 P.I., therefore were sacrificed at this time-point for humane reasons. Urine was collected at each time-point in order to measure albumin/creatinine protein levels at the pre-proteinuric, proteinuric and GS stages.

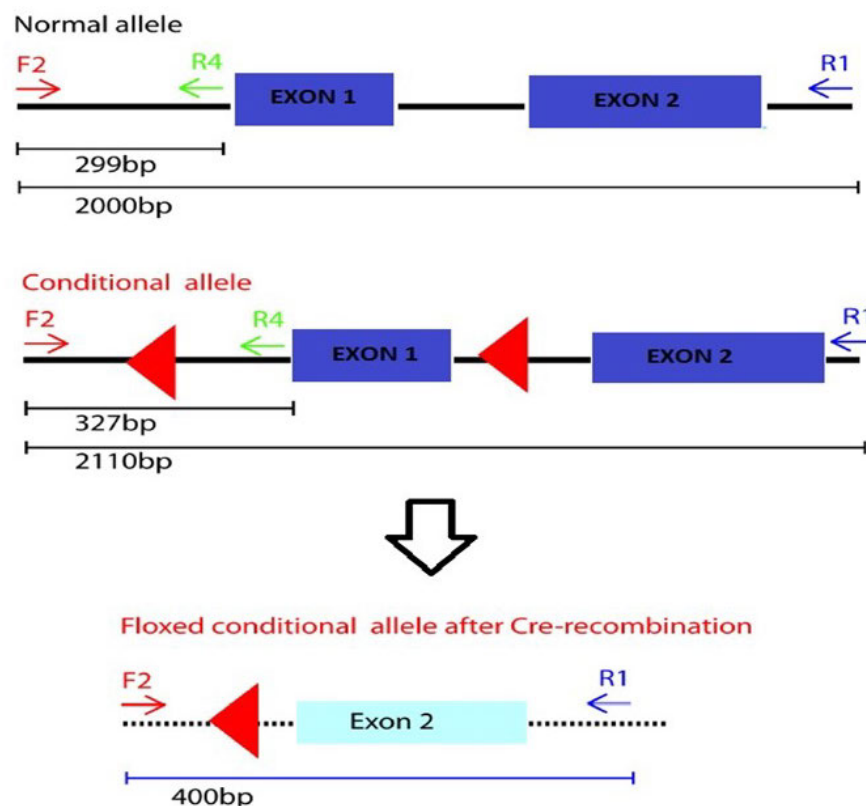


Figure 2.1. *Wt1* exon 1 deletion.

Following tamoxifen I.P., the floxed *Wt1* exon 1 is deleted by Cre-recombinase binding with loxP sites, resulting in a 400bp fragment. Primers F2 and R4 span loxP at 5' site of the conditional *Wt1* exon 1, giving a 327bp size. Pre-Tamoxifen, F2 and R1 display the full 2110bp. Post-tamoxifen, F2 and R1 result in 400bp.

GSI-IX treatments in *Cre-ER^{TM+/-};Wt1^{loxp/loxp}* transgenic mice

In this study, podocyte Notch activation has been shown to be a feature of early disease, therefore, γ -secretase inhibitor was introduced to mice to prevent Notch signalling at the onset of GS. IP treatments of γ -secretase inhibitor, GSI IX (N-[N-(3,5-difluorophenylacetyl-L-alanyl)]-S-Phenylglycine t-butyl ester (DAPT) (Sigma-Aldrich D5942) were given late D4 P.I. in 5-week old *Cre-ER^{TM+/-};Wt1^{loxp/loxp}* (*Cre-ER^{+/-};Wt1^{ff}*) mutants as a prophylactic intervention (100 μ g GSI IX/40g body weight) and again the next morning (16 hours later). Vehicle controls were treated with Dimethyl sulfoxide (DMSO, W387520 Sigma-Aldrich) administered by IP (100 μ g GSI IX/40g body weight) at the same time point (D4 P.I.) to *Cre-ER^{+/-};Wt1^{ff}* mutants as controls. For late treatments, an IP injection with the γ -secretase inhibitor-GSI-IX DAPT was given to *Cre-ER^{+/-};Wt1^{ff}* mutants (100 μ g/40g mouse body weight) on the evening of day 7 post-tamoxifen induction (D7 P.I.) and treated again with DAPT the next morning (16hrs later). Urine was collected from the metabolic cages at least 8 hours post-second DAPT treatment and mice were then sacrificed. PAS-stained specimens were scored for severity of glomerulosclerosis following nephrectomy. GSI-DAPT and vehicle-treated *Cre-ER^{+/-};Wt1^{ff}* transgenic mice were compared.

Overexpression of *Ascl1* in *TetOAscl1;NPHS2;rtTA* transgenic mice

Doxycycline treatment was achieved orally by either water or chow (2mg/ml in 5% sucrose water, 4mg in chow) in 4 week-old mice. The aim was to overexpress *Ascl1* in the podocytes (podocin-specific) by using a nuclear mCherry reporter under the tetracycline-responsive element (tetO-*Ascl1*-ires-mCherry) (Ueki et al., 2015) to investigate whether overexpression of *Ascl1* induces a glomerular phenotype. Following doxycycline treatment, the *NPHS2*-rtTA system stimulates *Ascl1* expression in the podocytes. Mice were treated with 2mg/ml doxycycline in 5% sucrose water for 2 weeks and sacrificed. Urine and nephrectomies were collected to examine the phenotype. Furthermore, 4 week-old mice were treated with 4mg doxycycline in chow for 2, 4 and 6 weeks and then sacrificed. It was hard to control the amount of doxycycline intake in each mouse, however, to ensure that all mice were receiving doxycycline, levels of water and chow were checked daily and replaced every other day. Urine and kidneys were then collected and examined for a phenotype. *Ex vivo* experiments were also performed where podocytes from the doxycycline-treated mice were isolated following kidney harvest (described later in this chapter). Following 6 days of podocytes in culture, cells were treated with doxycycline (4 μ g/ml) to overexpress *Ascl1*. RNA and protein analyses

were performed to confirm overexpression. The schematic of the experiment is presented in Figure 2.2.

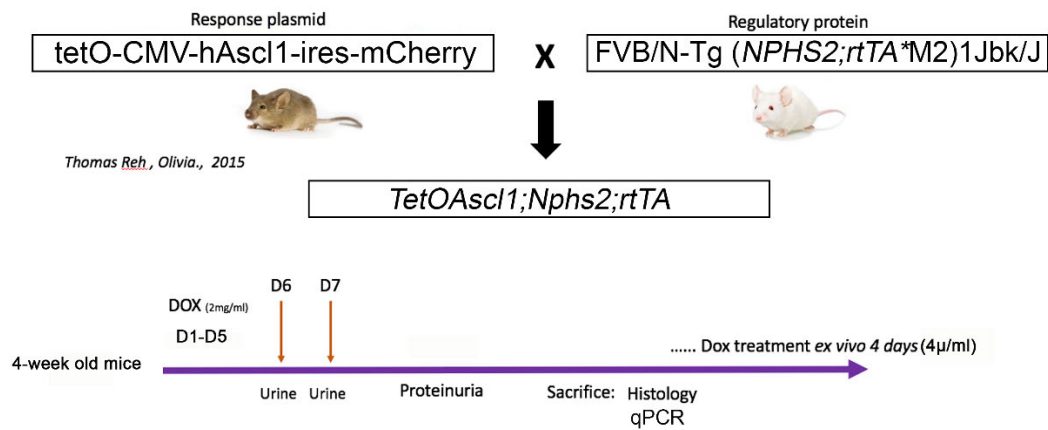


Figure 2.2. Transgenic *TetOAscl1;Nphs2;rtTA* experiment outline

2.2 Genotyping

To confirm *Wt1* floxed genotypes, mice were ear-clipped 10 days post-birth and earclips were incubated in tail lysis buffer (Table 2.1) + 400 µg/ml proteinase K (Sigma P6556-500mg) overnight at 56°C, followed by enzyme inactivation at 95°C for 5 minutes. Isopropanol was then added at equal volumes for precipitation and centrifuged at 4°C for 25 minutes at 16,000xg. The supernatant was discarded and 70% ice-cold ethanol was added to each sample and centrifuged at 4°C for 5 minutes at 16,000xg. The supernatant was carefully removed and the DNA were air-dried for one hour at room temperature (RT) upside down. 150µl Milli-Q H₂O was added to each pellet. Samples were genotyped using polymerase chain reaction (PCR). The remaining samples were stored at 4°C.

Genotyping post- in vivo treatments

Mouse tail tips were collected and lysed (Table 2.1) to determine recombination and *Wt1* deletion using the genomic primers (Table 2.2) and the same PCR programme as genotyping (Table 2.3). A combination of 3 primers were used to amplify the floxed region of *Wt1* and to highlight Cre-recombination and *Wt1* excision following tamoxifen induction (Figure 2.1).

Table 2.1. Tail lysis buffer

| Tail lysis buffer | Total 500ml | Final conc. |
|--------------------|--------------|-------------|
| 1M Tris pH 8.0 | 5ml | 10mM |
| 5M NaCl | 10ml | 100mM |
| 0.5M EDTA pH 8.0 | 10ml | 10mM |
| 10% SDS | 25ml | 0.5% |
| ddH ₂ O | 450ml | 450ml |
| | 500ml | |

Polymerase Chain Reaction (PCR) and genotyping

The Illustra beads kit (GE Healthcare; 27-9559-01) was used to genotype the conditional *Wt1* floxed alleles (Table 2.2) with a final concentration of 1 μ M primers and <100ng genomic DNA in a total volume of 25 μ l. Primers were used to amplify CreERT2 DNA sequence using the BIOTAQ DNA polymerase kit (Bioline, BIO-21040) containing <100ng genomic DNA, 0.4 μ M primers, 1XNH₄ buffer, 1.5mM MgCl₂, 0.8mM dNTP, 0.2 μ l/ μ l Taq DNA polymerase in a total volume of 25 μ l. PCR reactions were run using a thermocycler with the programme shown in Table 2.3 and products were run on a 2% agarose gel to identify their sizes. *TetOAscl1;rtTANPHS2* mice were genotyped using genomic primers amplifying *Nphs2rtTA* and *IRES-Ascl1* (Table 2.2) and the PCR programme shown in Table 2.4.

Table 2.2. Genomic primers for genotyping

| Gene | Primer Sequence (5'-3') | Target | Size (bp) |
|--------------|---------------------------------|--|--|
| Cre_F | GCATTACCGGTGCGATGCAACGAGTGATGAG | | Cre expressing 300 |
| Cre_R | GAGTGAACGAACCTGGTCGAAATCAGTGCG | | |
| Nphs2;rtTA F | CGCACTTCAGTTACTTCAGGTCCTC | | 455 |
| Nphs2;rtTA R | GCTTATGCCTGATGTTGATGATGC | | |
| hAscl1 F | CATCTCCCCCAACTACTCCA | | Ascl1 IRES 400 |
| IRES R | GAGGAACTGCTTCCTTCACG | | |
| Wt1_F | TGGGCATTTCTGCTAAGCG | | |
| Wt1_R4 | AGCTGCGGGGTCACCTTAG | Wt1_F + Wt1_R4 spanning 5' loxP | Wildtype 299 Mutant 327 |
| Wt1_R1 | TAAGAGTCAACGCCTGGTG | Wt1_F + Wt1_R1 | Wildtype 2000 Mutant 2110 Recombination 400 |

Table 2.3. PCR programme for genotyping *Cre-ERT2* and *Wt1* floxed alleles

| Cycle Step | Temp | Time | No. cycles |
|------------------|------|------------|------------|
| Initial denature | 94°C | 2 minutes | 1 |
| Denaturation | 94°C | 15 seconds | 35 |
| Annealing | 58°C | 30 seconds | |
| Extension | 72°C | 1 minute | |
| Final Extension | 72°C | 5 minutes | 1 |
| | 4°C | Hold | |

Table 2.4. PCR Programme for genotyping *TetOAsc1;rtTANPHS2* transgenic mice

| Cycle Step | Temp | Time | No. cycles |
|------------------|------|------------|------------|
| Initial denature | 94°C | 1 minute | 1 |
| Denaturation | 94°C | 30 seconds | 35 |
| Annealing | 58°C | 30 seconds | |
| Extension | 72°C | 30 seconds | |
| Final Extension | 72°C | 10 minutes | 1 |

2.3 Glomerular isolation

Four week-old mice, both male and female from available litters (controls, heterozygotes and mutants), were sacrificed. Dissected fresh kidney cortices were decapsulated and minced in ice-cold Hank's balanced salt solution (HBSS; Gibco/Invitrogen 24020-133). Following a thorough rinse with fresh HBSS, they were filtered through a 100µm cell strainer (BD Falcon 352360) into a chilled 50ml falcon tube in order to remove any large tubular fragments from passing through. HBSS was added to a total of 6mls, which was then divided amongst 2 chilled 15ml falcon tubes. Each tube contained 2.2ml Percoll (Amersham 17-0891-02) and was mixed thoroughly. Glomeruli were separated across the Percoll gradient by centrifugation at 200xg for 10 minutes at 4°C (Johns et al., 1987). The top layer of the gradient contained glomeruli, which was verified microscopically. The top 1-2mls of the gradient was passed again through a 100µm cell strainer to prevent any large tubule fragments from filtering through in order to achieve pure glomeruli. The filtrate was then passed through a 40µm cell strainer (BD Falcon 352340) to trap the glomeruli. Glomeruli were either lysed on the cell strainer to collect RNA and protein, or used to isolate primary podocytes.

2.4 Primary podocyte culture

For podocyte culture, minced cortices were digested in 1mg/ml collagenase A (Sigma C2674) in HBSS medium for 30 minutes at 37°C. Glomeruli were obtained following the above protocol. Harvested glomeruli were placed onto culture dishes coated with Matrigel (Corning; 35423) Culture medium was RPMI 1640 containing 15% foetal bovine serum (FBS; Atlanta Bio), 1% penicillin/streptomycin (P/S), 1% Insulin, transferrin, selenium (I/T/S) and amphotericin B. On day 3 of culture, unattached glomeruli were washed away and fresh medium was added. Podocytes were examined on day 6 of culture post-harvest and were verified by immunofluorescence using the podocyte marker, Nestin.

2.5 RNA extraction

RNA was extracted using the RNeasy mini kit for cells or RNeasy Micro Kit for glomerular isolates (Qiagen; 74104). Total RNA was isolated following the manufacturer's instructions. Podocyte cell RNA concentrations from both kidneys/mouse gave a good yield of around 100-300ng/μl whilst glomerular isolates (from two kidneys) gave between 20-100ng/μl eluted in 50μl water and an optical density of 1.8-2.0, measured by the Nanodrop spectrophotometer ND1000 (Lab Tech).

2.6 Real-time qPCR

cDNA synthesis

cDNA was generated from the total RNA using the high capacity cDNA synthesis kit (Thermo Fisher 4387406). RNA was normalised before synthesising cDNA, where approximately 1μg RNA was added to the 2X RT buffer and 20X RT enzyme in a total volume of 20μl. cDNA synthesis ran for one hour at 37°C followed by 95°C incubation for 5 minutes.

Real-time qPCR

Real-time qPCR primers were designed using the NCBI primer blast website (<https://www.ncbi.nlm.nih.gov/tools/primer-blast/>). To ensure pure cDNA amplification, primers designed spanned the exon-exon junction, and product size was set to a

maximum 150bp. Primers for qPCR were also taken from published papers, where their efficiency had been tested.

To ensure maximum efficiency of the primers designed, a relative standard curve method was carried out where all the cDNA samples were pooled together and diluted in a 10-fold dilution series to generate the standard curve ($y=mx+c$). The efficiencies of each primer were analysed relative to GAPDH. This particular method is useful as the housekeeping control gene, (GAPDH in this case), is only required once if running multiple plates and the efficiency of the primers is measured relative to GAPDH. Due to low yields of cDNA and already optimised primers, the $\Delta\Delta CT$ Livak method was also used to analyse qPCR data. In this case, the efficiency is approximately 100% between the genes and the housekeeping control gene, and the control gene is required each time a plate is run.

Real-time qPCR was carried out using the SYBR Green PCR mix (BIORAD 1708882) on the CFX96 touch thermal cycler (BIORAD) machine. Samples were analysed on a 96-well plate in the SYBR Green Master Mix volumes (Table 2.5) using the programme illustrated in Figure 2.3. Real-time qPCR primers are summarised in Table 2.6. Primers that are not referenced in the table were designed in-house using Ensembl blast, Primer3Plus or the NCBI primer design tool, primer-BLAST. These were tested for efficiency using the standard curve method.

Table 2.5. qPCR reagents

| SYBR Green Mastermix | Total 24μl |
|-----------------------------|----------------------------------|
| cDNA | 2 μ l |
| 20uM Primer F | 1 μ l |
| 20uM Primer R | 1 μ l |
| SybrGreen | 12.5 μ l |
| ddH2O | 7.5 μ l |

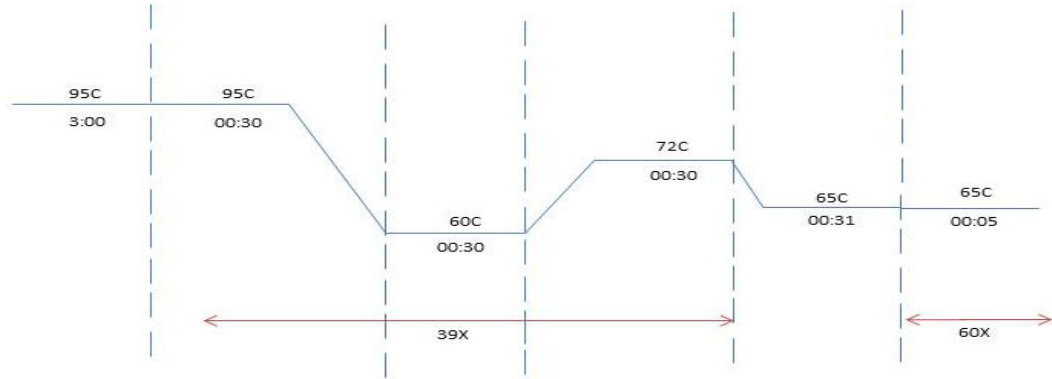


Figure 2.3. Real-time qPCR protocol

Table 2.6. Real-time qPCR primers

| Gene | Primer sequence (5'-3') | Reference |
|-----------------|-------------------------|-------------------------|
| <i>Apaf1 F</i> | GGGTGGGTCACCATCTATGG | (Niranjan et al., 2008) |
| <i>Apaf1 R</i> | TTCCGCAGCTAACACAGACTTG | |
| <i>Bax F</i> | CCAAGAAGCTGAGCGAGTGTCT | |
| <i>Bax R</i> | AGCTCCATATTGCTGTCCAGTTC | |
| <i>Bcl2 F</i> | TGGGATGCCTTTGTGGAAC | |
| <i>Bcl2 R</i> | CAGCCAGGAGAAATCAAACAGA | |
| <i>Cdkn1c F</i> | CAATCAGCCAGCAGAACAGC | |
| <i>Cdkn1c R</i> | CAGCTCCTCGTGGTCTACAG | |
| <i>Dll1 F</i> | CATGAACAACCTAGCCAATTGC | |
| <i>Dll1 R</i> | GCCCAATGATGCTAACAGAA | |
| <i>Dll4 F</i> | GACCTGCGGCCAGAGACTT | |
| <i>Dll4 R</i> | GAGCCTTGGATGATGATTTGG | |
| <i>Hes1 F</i> | CCCCAGCCAGTGTC AACAC | |
| <i>Hes1 R</i> | TGTGCTCAGAGGCCGTCTT | |
| <i>Hes3 F</i> | AAGGGAGCAGAAAAGCATCA | |
| <i>Hes3 R</i> | CTATGGCAGGGAGCTTTGAG | |
| <i>Hes5 F</i> | TGGGCACATTTGCCTTTTGT | |
| <i>Hes5 R</i> | CAGGCTGAGTGCTTTCCTATGA | |
| <i>Hes6 F</i> | GAAGTGGCCAATCTTGAGACTGA | |
| <i>Hes6 R</i> | GGATTGCTGTGGCCTGTGT | |
| <i>Hey1 F</i> | GGGAGGGTCAGCAAAGCA | |
| <i>Hey1 R</i> | GCTGCGCATCTGATTTGTCA | |
| <i>Hey2 F</i> | CACATCAGAGTCAACCCCATGT | |
| <i>Hey2 R</i> | GTGAGGAGAGCAGAGCCATGA | |
| <i>HeyL F</i> | AGATGCAAGCCCGGAAGAA | |
| <i>HeyL R</i> | CGCAATTCAGAAAGGCTACTGTT | |
| <i>Jag1 F</i> | ACACAGGGATTGCCCACTTC | |

| Gene | Primer sequence (5'-3') | Reference |
|----------------------|--------------------------|-------------------------|
| <i>Jag1 R</i> | AGCCAAAGCCATAGTAGTGGTCAT | (Niranjan et al., 2008) |
| <i>Jag2 F</i> | CRACTCACACTGCGCTTCA | |
| <i>Jag2 R</i> | TCGGATTCCAGAGCAGATAGC | |
| <i>Notch1 F</i> | CCAGCAGATGATCTTCCCCTAC | |
| <i>Notch1 R</i> | TAGACAATGGAGCCACGGATGT | |
| <i>Notch2 F</i> | TCTATCCCCCGTCGATTCCG | |
| <i>Notch2 R</i> | GATGTGATCATGGGAGAGGATGT | |
| <i>Notch3 F</i> | CCAGGGAATTCAGGTGCAT | |
| <i>Notch3 R</i> | GCCGTCGAGGCAAGAACA | |
| <i>Npfs1 F</i> | GCCAATCAATGACAGGAGGT | |
| <i>Npfs1 R</i> | GTCAGGTTGTTGGGCTTGT | |
| <i>Npfs2 F</i> | AGGGATGACAAGAAGGCAAA | |
| <i>Npfs2 R</i> | ACCTCGTCCACGTCCACTAC | |
| <i>p53 F</i> | CTCTCCCCCGCAAAGAAA | |
| <i>p53 R</i> | CGCCCGCGGATCTTG | |
| <i>Rbpsuh F</i> | GCGGATAAAGGTCATCTCCA | |
| <i>Rbpsuh R</i> | TTCCTGAAGCAATGCACAAG | |
| <i>Trp53 F</i> | AGCGCTGCTCCGATGGT | |
| <i>Trp53 R</i> | TTCCTTCCACCCGGATAAGA | |
| <i>Wt1 F</i> | GGTGCCACAGTTGTCAGAAA | |
| <i>Wt1 R</i> | GGTGAGTGGGAGGAATTTCA | |
| <i>Ascl1/Mash1 F</i> | CCAATACTCCAACGACTTGAAC | Designed in house |
| <i>Ascl1/Mash1 R</i> | TCCTGCCATCCTGCTTCCAAAG | |
| <i>Gapdh F</i> | AGGTCGGTGTGAACGGATT | |
| <i>Gapdh R</i> | TCTAGACCATGTAGTTGAGGTCA | |
| <i>Lfg F</i> | CGAGCACAAAGTGAGACCTG | |
| <i>Lfg R</i> | TGCCGTGCTCATGAAGTGTC | |
| <i>Mfg F</i> | AGACTACCTGGGCCTTCCAT | |
| <i>Mfg R</i> | TGAATGTCTGTTGCCTGATCCT | |
| <i>Mib2 F</i> | CTAGGATGGCAGAGATGGGC | |
| <i>Mib2 R</i> | ACCCAGAAGCTGTTGTGCTT | |
| <i>Neurb1 F</i> | AATCGTCTCTGGTGACAGCC | |
| <i>Neurb1 R</i> | GTGCACTCTCCATTCTGCT | |

2.7 Phenotype analysis

2.7.1 Renal histology

Histomorphometrical semi-quantitative analysis of glomerulosclerosis from 0-3 was achieved (Score 0-3, 0, < 25%, 1, 25-50%, 2, 50-75%, 3, >75% sclerosis) by scoring the severity of 30 PAS-stained glomeruli/sample where *Cre-ER^{TM-/-};Wt1^{fl/fl}* and *Cre-ER^{TM+/-};Wt1^{fl/+}* controls were compared to *Cre-ER^{TM+/-};Wt1^{fl/fl}* mutants. Scoring was based on formed adhesions, mesangial expansion and capillary obliteration in one segment.

2.7.1.1 Paraffin and cryo- tissue preparation

Mouse kidneys were dissected, cut in half lengthwise, and fixed overnight in 4% paraformaldehyde (PFA, Sigma 158127) in PBS. For paraffin-embedding, kidneys were dehydrated through different Ethanol (EtOH) concentrations reaching 100% EtOH and then transferred to Histo-Clear (National Diagnostics). Kidneys were then infiltrated with paraffin for 3 hours, overnight at 60°C, then embedded sagittally in paraffin. Kidneys were sagittally sectioned using a microtome at 5-10µm thickness and transferred onto 3-(Triethoxysilyl)propylamine (TESPA)-coated SuperFrost® microscope slides (VWR) overnight to dry. Paraffin embedding and sectioning was also carried out by the Histopathology Unit, GOSH, who also performed Periodic acid-Schiff (PAS) and Haematoxylin & Eosin (H&E) staining were performed for phenotype analysis.

For cryo-preparation, 4% PFA-fixed kidneys were placed in 30% sucrose overnight at 4°C. Kidneys were then moved from 30% sucrose to 1:1 30% sucrose:OCT embedding matrix (Fisher) for 30 minutes on a shaker to gradually remove all sucrose from the sections, and then into 100% OCT. Kidneys were moulded in OCT on dry ice with ethanol to snap freeze the sections. Tissues were stored at -80°C. Serial sections of the kidneys were cut at 10µm on SuperFrost® Plus glass slides (VWR) using the cryostat and stored at 80°C until staining.

2.7.2 Urine protein analysis

Urinary albumin and creatinine levels were determined using the mouse albumin ELISA quantitation set (Bethyl Laboratories, E90-134) and R&D systems creatinine assay (KGE005) kits respectively. For Albumin ELISAs, mouse albumin serum of 0-500ng/ml through to Blank (1:2 dilution series) were used to set the standard curve and urine was

diluted between 1:1,000–20,000 due to differing concentrations of albumin in each sample. Absorbance was measured on a plate reader at 450nm and concentrations were analysed using the 4-parameter curve method. Creatinine assay standards were prepared from 0-20mg/dl (1:2 dilution series) and most urine samples were diluted 1:20. Absorbance was measured on a plate reader at 490nm and measured using a log/log curve fit. Concentrations of albumin and creatinine were multiplied by their dilution and units were converted to $\mu\text{g/ml}$ (albumin) and mg/ml (creatinine) in order to calculate a final ratio of albumin/creatinine ($\mu\text{g/mg}$). The results were analysed using Prism GraphPad 6.

Furthermore, albuminuria was determined by using Western blot analysis with the albumin antibody (Bethyl laboratories, E90-134; 1:1,000 dilution). Urine samples were diluted 1:100 and loaded 10 μl /lane. Urine samples were collected from *Cre-ER^{TM+/-};Wt1^{ff}* and *Cre-ER^{TM+/-};Wt1^{ff}* mice at D4, 5, 6, 8, and 12 P.I. to test for albumin.

2.7.3 Immunohistochemistry and immunofluorescence multi-labelling

2.7.3.1 Immunofluorescence on paraffin sections (IHC)

A list of antibodies used can be found in Table 2.7.

Sections were deparaffinised in Histo-Clear and rehydrated through a series of graded EtOH washes and then rinsed with H₂O. For antibody staining, microwave antigen retrieval was performed in citrate buffer (pH6) for 15 minutes on a high heat setting (Panasonic NN-S758WC, 950W max. output), followed by a 20 minute cooling period at room temperature (RT). Slides were incubated in blocking buffer (PBS + 15% BSA + Goat Serum) or Universal Blocking Reagent (DAKO) in a humidified chamber for one hour at RT to prevent drying of sections. Sections were probed with primary antibodies diluted in incubation buffer (PBS+30% BSA+Goat serum+ 0.1% Tween-20) or DAKO buffer overnight at 4°C. The following day, sections were washed three times in PBS for 10 minutes, and incubated with Alexa Fluor-conjugated secondary antibodies for one hour at RT. Slides were then washed in PBS, counterstained with DAPI (Sigma) and mounted using VECTASHIELD mounting medium (Vector laboratories H-1000).

2.7.3.2 Immunofluorescence on cryosections

Sections were brought to room temperature, washed in PBS and permeabilised in 0.5% Triton X-100 (Sigma) for 5 minutes, followed by 3x5 minute PBS washes. Sections were

incubated in blocking buffer (10% goat serum (Sigma), 1% BSA (Sigma), 0.1% Triton X-100, PBS) in a humidified chamber for one hour, then incubated in primary antibody diluted in blocking buffer overnight at 4°C. The following day, slides were washed in PBS 3x5minutes and incubated with Alexa Fluor-conjugated secondary antibodies for one hour at RT. Slides were then washed in PBS, counterstained with DAPI and mounted with coverslips using VECTASHIELD mounting medium.

2.7.3.3 Cellular immunofluorescence

For all cellular immunostaining, approximately 1×10^5 podocytes were seeded on Matrigel-coated (Corning 354234) chamber slides (Millipore Cat no. PEZGS0816) in RPMI (supplemented with 10% FBS, 1% ITS, 1% P/S).

Cells were fixed in 4% PFA for 15 minutes at room temperature, washed three times in PBS and incubated in blocking solution (10% goat serum (Sigma), 1% bovine serum albumin (BSA, Sigma-Aldrich), 0.1% Triton X-100, PBS) for one hour at RT. Cells were then probed with the selected primary antibodies diluted in blocking solution overnight at 4°C. A day later, cells were washed twice in PBS and probed with Alexa Fluor-conjugated secondary antibodies for one hour at RT. Slides were then washed in PBS, counterstained with DAPI and mounted with coverslips using VECTASHIELD mounting medium.

Electron Microscopy (EM) and imaging were performed at the Histopathology Unit, GOSH.

Table 2.7. Antibodies for IHC, ICC, IFC

| Antibody | Isotype | Species reactive | Dilution | Use | Company |
|-----------------------------------|-------------------|-------------------------|-------------------|-----------------|---|
| <i>B-Actin (13E5)</i> | Rabbit mAB IgG | H, M, R, Mk, Pg, B | 1:1,000 | Western | Cell Signalling |
| <i>CD13 (553370)</i> | Rat IgG2a | M | 1:100 | IHC | BD Biosciences |
| <i>NICD1(Val1744)</i> | Rabbit mAB | H, M, R, Mk | 1:50 | IHC | Cell Signalling |
| <i>Notch1 (D1E11)</i> | Rabbit mAB | H, M, R | 1:1,000 | Western | Cell Signalling |
| <i>Cleaved Notch2 (Ala1734)</i> | Rabbit | H, M, R | 1:150 | IHC | Thermo Fisher |
| <i>Cleaved Notch2 (07-1234)</i> | Rabbit | H, M | 1:200, 1:1,000 | IHC, Western | Millipore |
| <i>Jagged 1(C20)</i> | Goat | H, M, R | 1:100 | IHC | Santa Cruz |
| <i>Jagged 1 (H114)</i> | Rabbit | H, M | 1:1,000 | Western | Santa Cruz |
| <i>Podoplanin (811)</i> | Hamster mAB | M | 1:100 | IHC | Novus Biologicals |
| <i>Hes1</i> | Rabbit | M | 1:1000 | IHC | Gift-Professor Ryoichiro Kageyama, Kyoto university |
| <i>Synaptopodin (GD14)</i> | Mouse IgG1 | H, M, R, GP, B | Diluent | IHC | OriGene CAT no. BM5086 |
| <i>Podocin (P0372)</i> | Rabbit | H, M, R | 1:100 | IHC | Sigma Aldrich |
| <i>LTL biotinylated (B1325)</i> | | | 1:100 | IHC | Vector laboratories |
| <i>Cleaved caspase-3 (Asp175)</i> | Rabbit | H, M, R, Mk | 1:400 | IHC | Cell Signalling |
| <i>Slug (C19G7)</i> | Rabbit | H, M | 1:1,000 | Western | Cell Signalling |
| <i>Delta-like1 (HMD1-5)</i> | Hamster | M | 1:1,000 | Western | ThermoFisher |
| <i>WT1 (C-19)</i> | Rabbit | H, M, R | 1:250 | IHC | Santa Cruz |
| <i>POFUT1 (PA5-31357)</i> | Rabbit | H, M | 1:1,000 | Western | Invitrogen |

| Antibody | Isotype | Species reactive | Dilution | Use | Company |
|----------------------------------|---|------------------|--------------|--------------|---|
| <i>PSMAD2</i> (D27F4) | Rabbit mAB | H, M, R, Mk | 1:100 | IHC | Cell Signalling |
| <i>Nestin</i> (NB100-1604) | Chicken | H, M, R | 1:100 | IHC | Novus Biologicals |
| <i>Mash1/Ascl1</i> (556604) | Mouse IgG1 | M, R | 1:100, 1:100 | IHC, Western | BD Pharmingen |
| <i>Mash1/Ascl1</i> | Rabbit | M | 1:1,000 | IHC | Gift – Dr Jane Johnson, UT Southwestern |
| <i>Nephrin</i> (20R-NP002) | Guinea Pig | H, M | 1:50 | IHC | Fitzgerald |
| <i>Alexa Fluor 488, 594, 680</i> | Goat/sheep anti-Rabbit/Mouse/Guinea pig/chicken IgG (H+L) | M | 1:10,000 | IHC | ThermoFisher |

2.8 Apoptosis Assays

2.8.1 Cleaved caspase 3 analysis

Cleaved caspase-3 antibody staining was carried out on cryosections using the same method as described in section 2.7.3.2.

2.8.2 DeadEnd Fluorometric TUNEL assay

Cells were fixed in 4% PFA for 15 minutes at RT and washed three times in PBS. The DeadEnd Fluorometric TUNEL (Terminal deoxynucleotidyl transferase dUTP nick-end labelling) assay (Promega G3250 I) was used to assess apoptosis in the podocytes at different stages post-tamoxifen induction. Following fixation, cells were permeabilised with 0.2% Triton X-100 in PBS for 5 minutes, washed in PBS for 5 minutes and equilibrated in Equilibration TdT Buffer for 5-10 minutes at RT. rTdT [Terminal Deoxynucleotidyl Transferase, recombinant enzyme] incubation buffer (45µl Equilibration buffer + 5µl Nucleotide mix + 1µl rTdT enzyme) was then added to the cells

for one hour at 37°C. To ensure even distribution of the buffer, the slides were covered with plastic cover slips. Plastic coverslips were removed by immersing the slides in 2XSSC (Saline-sodium citrate: 3M NaCl, 0.3M trisodium citrate pH7.0) for 15 minutes at RT. Slides were then washed twice in PBS at RT. VECTASHIELD with DAPI mounting medium (Vector Laboratories H-1200) was added to stain the nuclei and slides were mounted. For double staining with antibodies, cells were blocked following rTdT incubation and probed with the desired antibody for one hour at RT or overnight at 4°C. The next day, cells were washed twice in PBS and probed with Alexa Fluor-conjugated secondary antibodies for one hour at RT. Slides were then washed in PBS and mounted as previously described.

2.8.3 Caspase 3/7 immunostaining

Podocytes were incubated in 5µM Cell Event caspase 3-7 green detection reagent Green (prepared in complete RPMI - Life Technologies, C10423) for 30 minutes at 37°C. Cells were then fixed with 4% PFA, for 15 minutes at RT, washed in PBS, counterstained with DAPI and mounted with VECTASHIELD mounting medium. Caspase 3/7- and DAPI- positive cells were quantified in 10 different fields for each sample.

2.8.4 Annexin V staining

Following podocyte isolation and culture of six days, cells were collected and analysed at the FACS facility, Moorfields Eye Hospital. The samples were spun down at 320xg for 5 minutes and washed with Annexin V Binding Buffer (ThermoFisher Scientific, 88-8103-74). The cells were then stained with Annexin V-PE-Cy7 (ThermoFisher) for 30 minutes on ice, in the dark. Following incubation, the samples were washed again and re-suspended in the Annexin V Binding Buffer. Samples were stained with SYTOX Blue at a final concentration of 0.3 mM (Thermo Fisher Scientific, Cat. No. S34857). Before cell acquisition, the cells were filtered through a 35mm cell strainer, preventing cellular aggregation during sample acquisition. The cells (control and mutant) were acquired using a 5-laser BD LSRFortessa X-20 Analyser, equipped with 355nm (UV), 405nm (violet), 488nm (blue), 561nm (yellow) and 640nm (red) lasers.

2.8.5 Fluorescence microscopy

All cellular and tissue sections were imaged in the laboratory using a Zeiss upright microscope with an AxioCam MRm camera and UV lamp. Confocal imaging was also performed using a Zeiss LSM-710 system with an upright DM6000 compound

microscope and images were processed with Zen software suite. Z stacks were acquired at 0.5 μ m intervals and converted to single planes by maximum projection with Fiji software.

All images were processed using ImageJ/Fiji.

2.9 Western blotting

Protein extraction

2x10⁵ podocytes were seeded in 100mm Matrigel-coated dishes overnight and lysed the following day with RIPA lysis buffer (50 mM Tris–HCL [pH 7.5], 150 mM NaCl, 0.5% Triton X-100, 0.5% sodium deoxycholate, 0.1% sodium dodecyl sulphate), supplemented with phosphatase and protease inhibitors (Sodium orthovanadate and protease inhibitor cocktail, Sigma P8340) for one hour on ice. Lysis was completed by shearing through a 26-gauge syringe needle and samples were spun at 10,000xg for one minute at 4°C. The supernatant was collected and protein concentration was measured using the BCA protein assay kit (Thermo Scientific, 23225) where absorbance at 562nm was measured on a plate reader and concentrations were calculated using the standard curve log/log curve fit.

Western Blot Analysis

Samples were denatured with 10% β -Mercaptoethanol (Sigma) in 4X Laemmli sample buffer at 95°C for 10 minutes. 15 μ g protein was loaded per lane. Primary and immortalized podocyte lysates were run on 4–15% SDS-PAGE gradient gels (Bio-Rad Laboratories). Prepared 10X Running buffer (30g Tris base, 144g glycine, 10g SDS, 1L H₂O, [pH 8.3]) was diluted to 1X Running buffer for sample running and separation. All gels were transferred onto polyvinylidene fluoride (PVDF, Bio-Rad) membranes using 1X Transfer buffer (Diluted from 10X Transfer; 30 g Tris, 144g glycine, 1L H₂O), blocked in 5% non-fat milk in PBS+ 0.5% Tween-20 before being probed with primary antibodies (overnight at 4°C) and secondary antibodies (one hour at RT) in blocking buffer (2.5% non-fat milk in PBS+ 0.5% Tween-20). Blots were developed with Pierce ECL Western Blotting Substrate (Thermo Scientific; 32106) and images were collected by film.

2.10 Glomerular RNA sequencing

Mouse glomeruli were isolated at day 4 post-tamoxifen induction and RNA was extracted using the QIAGEN RNeasy mini kit (74104) for whole transcriptome sequencing. Samples were processed by UCL Genomics, where pair end reads were produced using the Illumina TruSeq stranded assay. BAM files were generated and analysed using the Strand NGS 2.5 software. This software uses DESeq algorithm, incorporating additional downstream analysis including Gene Ontology (GO) and pathway analysis. A Mann-Whitney test was performed to analyse differential gene expression with a 2-fold change and p value of <0.5 to filter genes. GO and pathway analysis were used to understand the function and relationship between the identified genes of interest.

2.11 Podocyte shRNA experiments

Transformations and plasmid purifications

shRNA GIPZ hairpin plasmids (provided by UCL Cancer Institute) were obtained as bacterial agar stab cultures. The stab cultures were streaked onto a Lysogeny broth (LB) agar plate (with 100µg/ml ampicillin) under sterile conditions and incubated at 37°C overnight. The following day, colonies from each shRNA plasmid were picked and inoculated in 3ml LB with 100µg/ml ampicillin in 15ml falcon tubes. These were incubated at 37°C overnight in a shaking incubator (300rpm). The bacterial cells were then harvested and the plasmids were purified using the Qiagen miniprep kit (Qiagen 27104) according to the manufacturer's protocol. Purified plasmids were sent off to the Cambridge Source Bioscience facility for Sanger sequencing using the GIPZ sequencing primer (5' - GCATTAAAGCAGCGTATC - 3') and analysed by Sequencher. Plasmids were used to knock down Manic Fringe (GE Dharmacon V3LMM_20363) and Rbpsuh (GE Dharmacon V3LMM_437682) genes from D6 P.I. *Cre-ER^{TM+/-};Wt1^{fl/fl}* primary podocytes, and non-silencing vectors (RHS4346) were used as controls.

For *Nphs2;rtTA* podocyte transfection, Tet-O-Hes1 plasmids [Addgene 6154, (Cassady et al., 2014)] and control GFP only plasmids were purchased and grown using Stbl3 chemically-competent cells (Thermo Fisher C737303). Colonies were grown on LB agar plates as mentioned above and plasmids were purified using the Qiagen miniprep kit.

shRNA transient transfections

On the day before transfection, 1×10^5 cells/well were seeded in 6-well plates in RPMI medium (15% FBS, 1% P/S, 1% I/T/S) to allow between 70-90% confluency at the time of transfection. Cells were *Cre-ERTM+/+*; *Wt1^{ff}* mutants at D6 post-tamoxifen induction. Transfection was carried out using the Lipofectamine 2000 protocol (ThermoFisher, 11668019). On the day of transfection, 4 μ g plasmid was diluted in 250 μ l Opti-MEM and mixed gently. 10 μ l Lipofectamine 2000 was diluted in 250 μ l Opti-MEM and incubated for 5 minutes. The diluted plasmid and diluted Lipofectamine 2000 were then combined, mixed and incubated at RT for 20 minutes. 500 μ l of the mixture was then added to each well containing the medium and cells and gently mixed by rocking (according to the manufacturer's protocol). Cells were then incubated at 37°C, 5% CO₂ and RNA was extracted after 24, 48, 72 and 96 hours post-transfection. RNA was collected using the Qiagen RNeasy Micro Kit to examine gene expression using real-time qPCR (sections 2.5 and 2.6).

Primary transgenic murine *Nphs2;rtTA* podocytes were transfected with Tet-O-Hes1 plasmid or control-GFP only plasmid with Lipofectamine 3000 kit (Thermo Fisher Scientific, L3000001). Cells were transfected at 70% confluency. After 24 hours, both Tet-O-Hes1- and control plasmid-transfected cells were treated with Doxycycline [2 and 4 μ g/ml] for 72 and 96 hours. RNA was extracted according to the manufacturer's instructions using the Qiagen microRNA extraction kit. Protein was extracted as per section 2.9.

2.12 Statistical analysis

GraphPad Prism V.7 (GraphPad Prism Software, USA) was used to perform statistical analyses. Depending on the availability of the mice, between 3-10 mice per experimental group were used for each analysis. For qRT-PCR analysis, the average of duplicate reactions was used as the value of that sample. Normally distributed data was expressed as means \pm SD (Standard deviations) or SEM (Standard error of the means) relative to the specified controls; non-normally distributed data was reported as medians with respective interquartile ranges (IQR). A two-tailed, unpaired student's t-test or Mann-Whitney test were used for statistical analysis between two groups and the Bonferroni correction and two-way ANOVA tests were used when more than two groups were compared. Values were regarded as significant if $p < 0.05$ was calculated; error bars represent SEM, SD or IQR.

Chapter 3 - Podocyte Notch activation coincides with the onset of *Wt1* Glomerulopathy

3.1 Introduction

Notch is a highly conserved pathway that mediates cell-to-cell signalling during organogenesis and is essential during podocyte development (Cheng et al., 2003, Piscione et al., 2004, Cheng and Kopan, 2005, Chen and Al-Awqati, 2005). Podocytes are terminally differentiated visceral epithelial cells crucial for glomerular permselectivity (Pavenstadt et al., 2003, Reiser et al., 2000, Fukasawa et al., 2009) and mutations in podocyte genes can result in various events including EMT, apoptosis, podocyte dedifferentiation and proliferation (Niranjan et al., 2008, Waters et al., 2008). As previously mentioned, the *WT1* gene is key not only to podocyte development but also essential for podocyte homeostasis throughout adult kidney life (Guo et al., 2002, Kreidberg et al., 1993, Kreidberg, 2010, Dong et al., 2015a). Thus, the rationale for this study was that manipulating *WT1* would allow further investigation of pathways secondary to podocyte injury. In order to examine the molecular mechanisms and pathways underlying *WT1* glomerulopathy, a transgenic mouse line was established whereby *Wt1* could be deleted and any glomerular phenotype examined. Temporal deletion of *Wt1* was investigated using a ubiquitously expressed Cre-driver mouse line crossed to mice with a conditional floxed allele of *Wt1*, which allowed ubiquitous deletion including in podocytes following tamoxifen induction.

The importance of the Notch pathway during kidney development is established in kidney-related diseases including GS (Cheng and Kopan, 2005, Piscione et al., 2004). Notch was shown to be essential at the early stages of podocyte development but detrimental during podocyte differentiation and in mature podocytes (Waters et al., 2008, Niranjan et al., 2008). Waters *et al.* reported that when cleaved *Notch1* was activated in the developing podocytes, podocyte proliferation with DMS resulted (Waters et al., 2008); Niranjan *et al.* reported that activating Notch at the capillary loop stage led to podocyte apoptosis with FSGS (Niranjan et al., 2008) as well as a reduction in podocyte markers, including *Wt1*.

In view of this existing data supporting interaction between *WT1* and *NOTCH*, I tested the following hypothesis:

Temporal deletion of *Wt1* activates the Notch pathway and induces EMT and podocyte apoptosis.

3.2 Results

3.2.1 *Wt1* deletion leads to glomerulosclerosis (GS)

To establish a transgenic mouse line of *Wt1* glomerulopathy, Cre-inducible mice carrying the *Wt1* exon 1 floxed gene were tamoxifen-induced to delete *Wt1* and a glomerular phenotype was examined.

3.2.1.1 Temporal *Wt1* deletion is observed in *Cre-ER^{TM+/-};Wt1^{ff}* mutants post-tamoxifen

Tamoxifen induction in *Cre-ER^{TM+/-};Wt1^{ff}* transgenic mice has previously been reported to result in *Wt1* deletion and GS at day 7 P.I. (post-induction) (Chau et al., 2011). In this project, earlier time-points of *Wt1* deletion were explored to investigate the molecular mechanisms prior to and during the manifestation of GS. Day 4 P.I. was the earliest stage examined, allowing 3 days of tamoxifen to facilitate *Wt1* deletion. Animals were very sick, showing signs of oedema at D12 P.I. This was therefore the latest time-point to examine due to humane reasons.

Genetic deletion of *Wt1* was supported by immunohistochemical findings with WT1 protein expression significantly downregulated in *Cre-ER^{TM+/-};Wt1^{ff}* mutants compared to *Cre-ER^{TM-/-};Wt1^{ff}* controls at day 4 P.I. (Figure 3.1A, A'), day 5 P.I. (Figure 3.1B, B') and absent by day 12 P.I. (Figure 3.1C, C'). Only non-specific autofluorescence was seen in figure 3.1C' that did not co-localise with Dapi. *Wt1* deletion was also validated on a molecular level through PCR at D4 and D5 P.I., where the recombination of *Cre-LoxP* spanning exon 1 was detected post-tamoxifen induction. An amplicon size of 400bp was observed, presenting the deletion of exon 1, only seen in *Cre-ER^{TM+/-};Wt1^{ff}* mutants compared to *Cre-ER^{TM-/-};Wt1^{ff}* controls, where no recombination was observed (Figure 3.1D, E). The floxed *Wt1* amplicon was faintly present in the mutant, but evidently less than the *Cre-ER^{TM-/-};Wt1^{ff}* control at all time-points. Moreover, real-time qPCR analysis at D12 P.I. demonstrated a highly significant reduction in *Wt1* gene expression in the *Cre-ER^{TM+/-};Wt1^{ff}* mutants compared to *Cre-ER^{TM-/-};Wt1^{ff}* controls (Figure 3.1F).

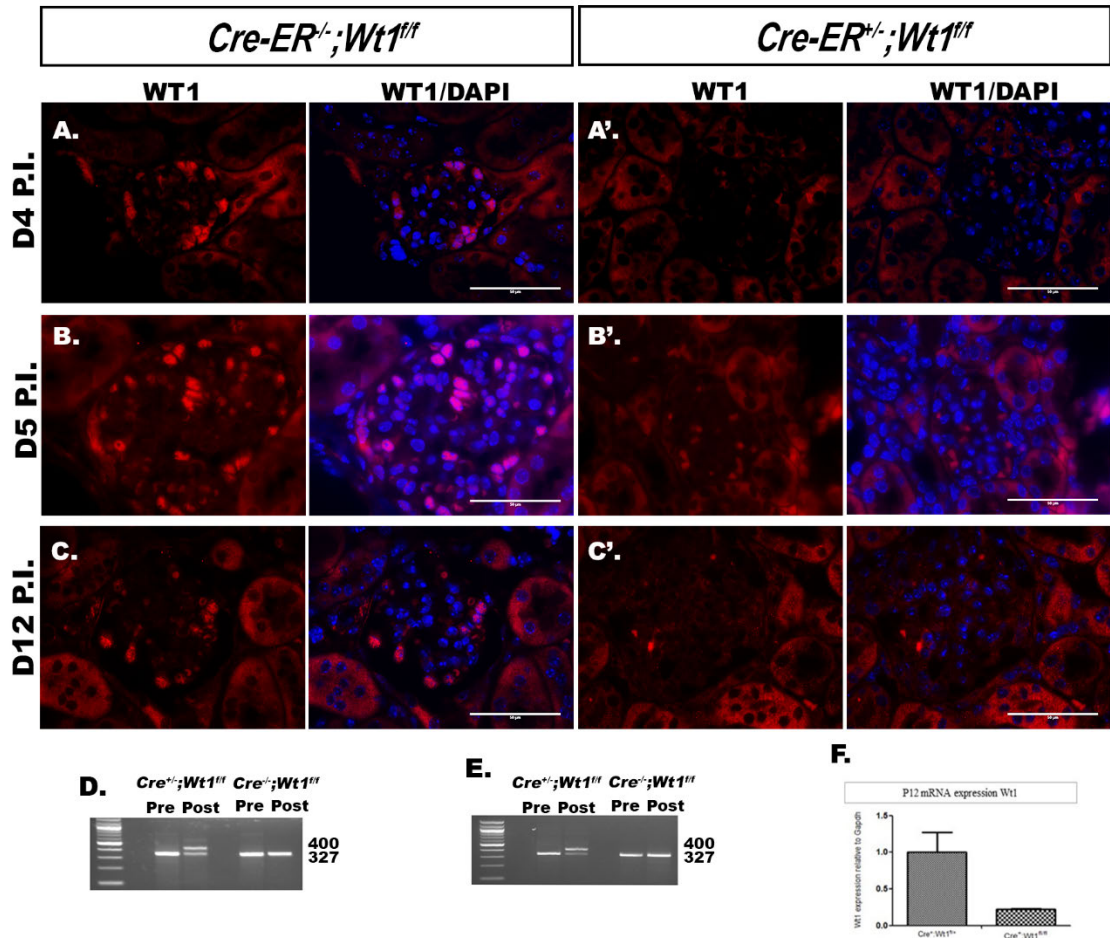


Figure 3.1. Temporal *Wt1* deletion in *Cre-ER^{TM+/-};Wt1^{ff}* mutants.

Illustrative images of WT1 protein in glomeruli following immunofluorescence labelling with WT1 antibody of *Cre-ER^{TM+/-};Wt1^{ff}* control mouse kidney tissue sections, n=6 vs. *Cre-ERT^{+/+};Wt1^{ff}* mutants, n=6 (scale bars, 50µm). counterstained with DAPI. **(A, A')** D4 P.I. controls show WT1 protein expression (red arrows) **(A)** compared to mutants, where there's reduced WT1 protein expression **(A')**. **(B, B')** D5 P.I. micrographs highlighting WT1 protein expression in controls as indicated by arrows **(B)** vs. mutants, where no WT1 protein is observed **(B')**. **(C, C')** Representative micrographs of glomeruli following immunofluorescent labelling of podocytes with WT1 in D12 P.I. sections. WT1 protein is present in controls (red arrows) **(C)** vs. mutants, where WT1 is absent **(C')**. **(D)** DNA expression of *Wt1* post-tamoxifen induction following PCR analysis at D4 P.I.; Recombination is seen in the mutants vs. controls. **(E)** PCR analysis of *Wt1* genotyping post-tamoxifen induction at D5 P.I. in mutants vs. controls. The quantity of the *Wt1* amplicon is reduced and recombination is shown in the mutant. **(F)** Quantitative real-time qPCR showing mRNA expression of *Wt1* relative to *Gapdh* at D12 P.I., where *Wt1* expression is reduced in the mutant vs. control (n=6 vs n=6 for each time-point). Analysed by Livak, $\Delta\Delta$ CT method. (Asfahani et al., 2018)

3.2.1.2 Early manifestation of GS is evident at day 5 post-tamoxifen induction in *Cre-ER^{TM+/-};Wt1^{ff}* mutants

To begin to address the underlying mechanisms and pathways following *Wt1* deletion, it was important to confirm a phenotype of *Cre-ER^{TM+/-};Wt1^{ff}* mutants in comparison to *Cre-ER^{TM-/-};Wt1^{ff}* and *Cre-ER^{TM+/-};Wt1^{f/+}* controls post-tamoxifen induction. This was achieved through PAS staining on paraffin-embedded kidney sections to assess the temporal induction of GS post-tamoxifen induction. *Cre-ER^{TM-/-};Wt1^{ff}* and heterozygote *Cre-ER^{TM+/-};Wt1^{f/+}* controls did not exhibit any GS at any time-point (Figure 3.2A-D, Figure 3.3A-F). To categorise glomerular morphology, the severity of GS was assessed based on the proportion of glomeruli analysed by extent of intra-GS (Score 0, <25% of glomerulus sclerosed; Score 1: 25-50% sclerosed, score 2: 50-75% sclerosed glomerulus, Score 3: >75% sclerosed glomerulus) in transgenic mice.

At D4 P.I., some mutant glomeruli exhibited early segmental GS with higher urinary albumin/creatinine (UA/UC) ratios, however these were not statistically significant ($p=0.21$) between mutants and controls (Figure 3.2A, A'). At D5 P.I., the proportion of mutant glomeruli exhibiting segmental GS was significantly higher than the controls (>50% GS, \geq score 2, $p<0.05$), (Figure 3.2B). UA/UC ratio was significantly increased in the mutants compared to the controls ($*p=0.01$) (Figure 3.2B'). By D6 P.I., hyaline-filled tubules were observed in the mutant kidneys with more extensive GS associated with significant albuminuria relative to the controls (Figure 3.2C, C'). Global GS was evident by D12 P.I. in the mutants with a significant increase in albuminuria compared to the controls ($***p<0.0001$ GS, $*p=0.04$ urine albumin/creatinine ratio) (Figure 3.2D, D'). Temporal induction of albuminuria in mutant mice from D4 to D12 P.I. was seen by Western blot analysis, where no albumin was present in the controls (Figure 3.2E). Due to limited availability of the mice, mouse numbers varied for each time-point.

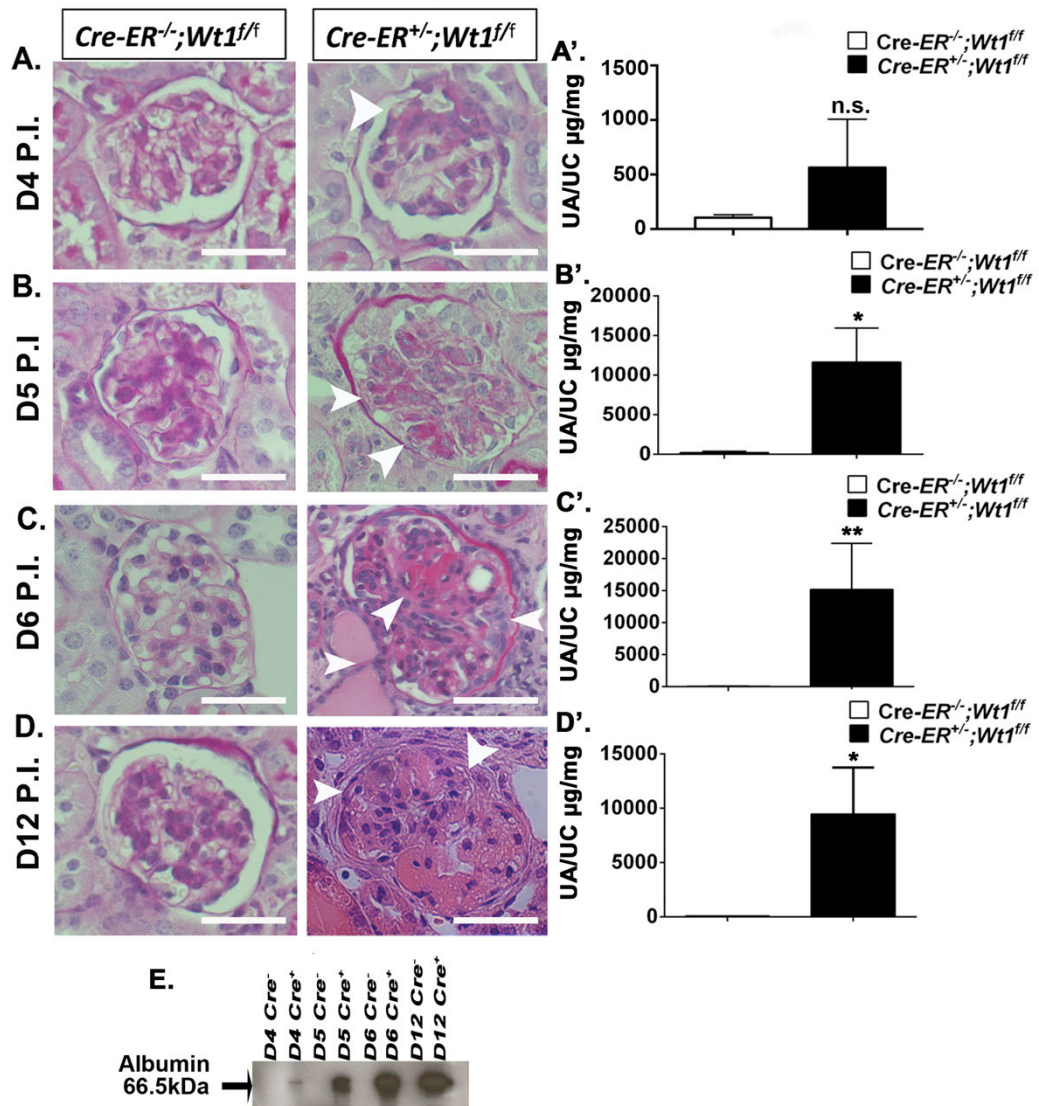


Figure 3.2. Temporal increase of GS in *Cre-ER^{TM+/-};Wt1^{ff}* mutants post-tamoxifen induction

(A) Glomeruli of *Cre-ER^{TM+/-};Wt1^{ff}* transgenic mutant mice are morphologically similar to their controls, at D4 P.I. (A') Quantitative graph displaying mean urine albumin/creatinine ratio ($\mu\text{g}/\text{mg}$) at D4 P.I. controls vs. mutants (n=14 vs n=10); 104.4 ± 25.71 vs. 563.5 ± 443 , $p=0.21$, Student t-test. (B) At D5 P.I., mutant mice reveal segmental GS compared to control mice. (B') Graph showing mean urine albumin/creatinine ratio ($\mu\text{g}/\text{mg}$) at D5 P.I. in controls vs. mutants (n=14 vs n=14); 217 ± 157.5 vs. 11654 ± 4304 , $*p=0.01$, Student t-test. (C) More extensive GS is evident at D6 P.I. in mutants with hyaline filled tubules vs. control mice. (C') Graph presenting mean urine albumin/creatinine ratio ($\mu\text{g}/\text{mg}$) at D6 P.I. in controls vs. mutants (n=5 vs n=6); 79.8 ± 29.8 vs. 15202 ± 7210 , $**p=0.004$, Student t-test. (D) Mutant mice glomeruli exhibit global GS at D12 P.I., with hyaline-filled tubules and pyknotic podocyte nuclei. (D') Graph showing mean urine albumin/creatinine ratio ($\mu\text{g}/\text{mg}$) at D12 P.I. controls vs. mutants (n=7 vs. n=7); 76.8 ± 13.9 vs. 9469 ± 4279 , $*p=0.04$, Student t-test (E). Western blot analysis from D4, D5 and D6 D12 P.I. reveals increased albumin levels in the mutants vs. controls. (Scale bars=50 μm). (Asfahani et al., 2018)

Heterozygotes (*Cre-ER^{TM+/-};Wt1^{ff/+}*) analysed at D4 (Figure 3.3A, A'), D8 (Figure 3.3B, B') and D12 P.I. (Figure 3.3C, C') were no different to *Cre-ER^{TM+/-};Wt1^{ff}* controls. WT1

was observed in the glomeruli of these mice (Figure 3.3A, B, C). A normal phenotype was seen at all time-points (Figure 3.3A', B', C') with no hyaline tubules or GS.

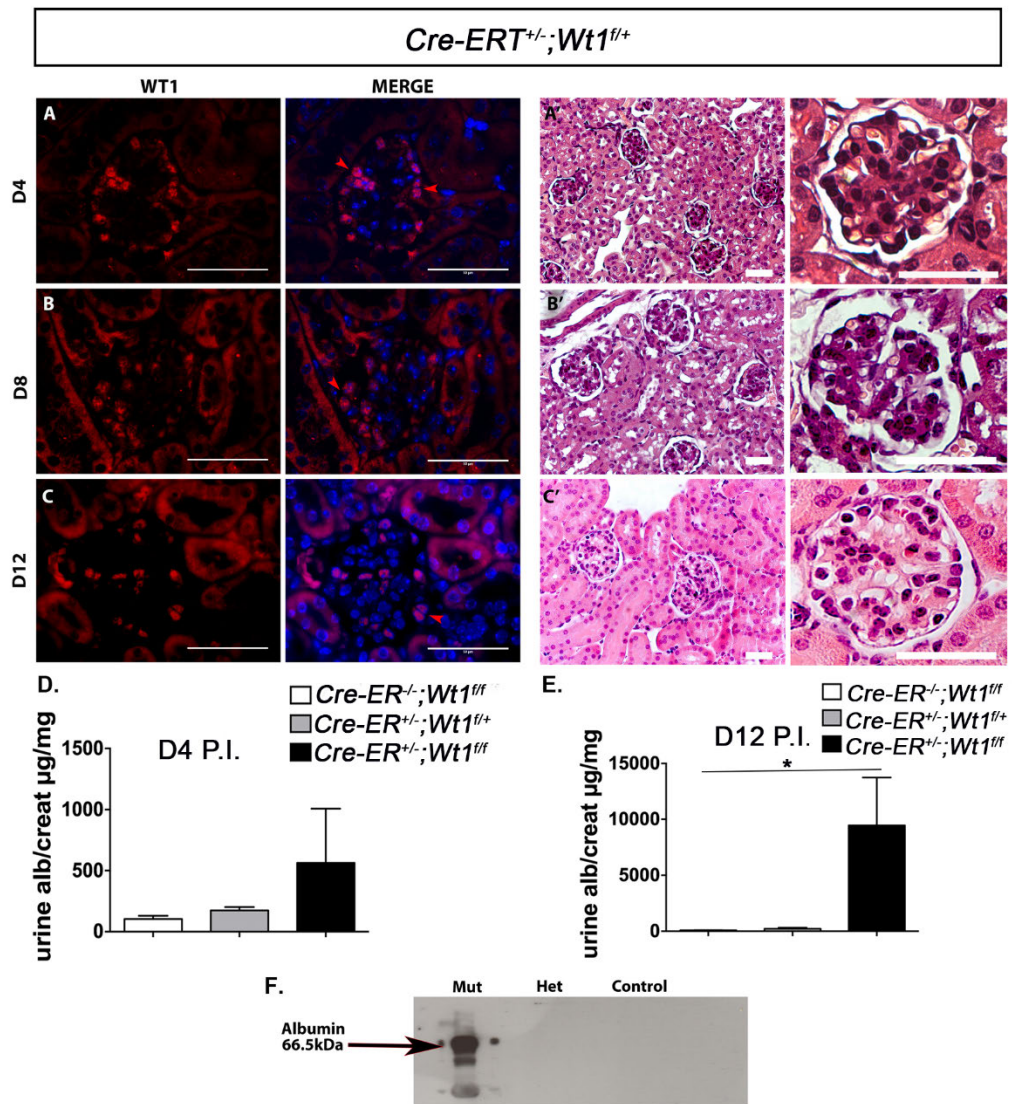


Figure 3.3. WT1 is expressed *Cre-ER^{TM+/-};Wt1^{fl/+}* hets transgenic mice post-tamoxifen induction

Representative micrographs of murine glomeruli labelling podocytes with immunofluorescent anti-WT1 antibody in D4 (A), D8 (B), D12 P.I. (C) *Cre-ER^{TM+/-};Wt1^{fl/+}* heterozygotes P.I. reveal WT1 expression (Red arrow), Scale bar 50µm. (A'-B') H&E stained glomeruli at D4, D8 and D12 P.I., Scale bar 25µm. (A') No histological abnormalities exhibited at D4 P.I. (B') D8 P.I.; intact glomeruli (C') D12 P.I.; healthy glomeruli with no hyaline material in tubules (D) Graph presenting mean urine albumin/creatinine ratio (µg/mg) in D4 P.I. controls vs. heterozygotes vs. mutants (n=14 vs. n=8 vs. n=10); 104.4±25.7 vs. 174.9±27.0 vs. 563.5±443.9, p=0.21, Student t-test. (E) Graph displaying mean urine albumin/creatinine ratio (µg/mg) in D12 P.I. controls vs. heterozygotes vs. mutants (n=8 vs. n=3 vs. n=7); 76.8±13.9 vs. 223.5±93.8 vs. 9469±4279 (p=0.21, mutants vs controls), (*p=0.05, mutants vs hets), student t-test. (F) Immunoblot analysis of *Cre-ER^{TM+/-};Wt1^{fl/fl}*, *Cre-ER^{TM+/-};Wt1^{fl/+}* and *Cre-ER^{TM+/-};Wt1^{fl/fl}* urine samples at D8 P.I. probed with anti-albumin [MW of albumin, 66.5kDa]. (Asfahani et al., 2018)

The manifestation of GS was first observed at D5 P.I. with a significant increase in proteinuria in the mutants compared to the controls. This temporal model of GS allowed us to further explore the fundamental mechanisms and pathways, which may be associated with *Wt1* glomerulopathy at the early and late stages of the disease; proteinuria and global GS.

3.2.1.3 Podocyte FP effacement prior to the manifestation of GS

Podocyte FP effacement was evident at D4 P.I. in *Cre-ER^{TM+/-};Wt1^{ff}* mutants compared to controls (Figure 3.4A, B).

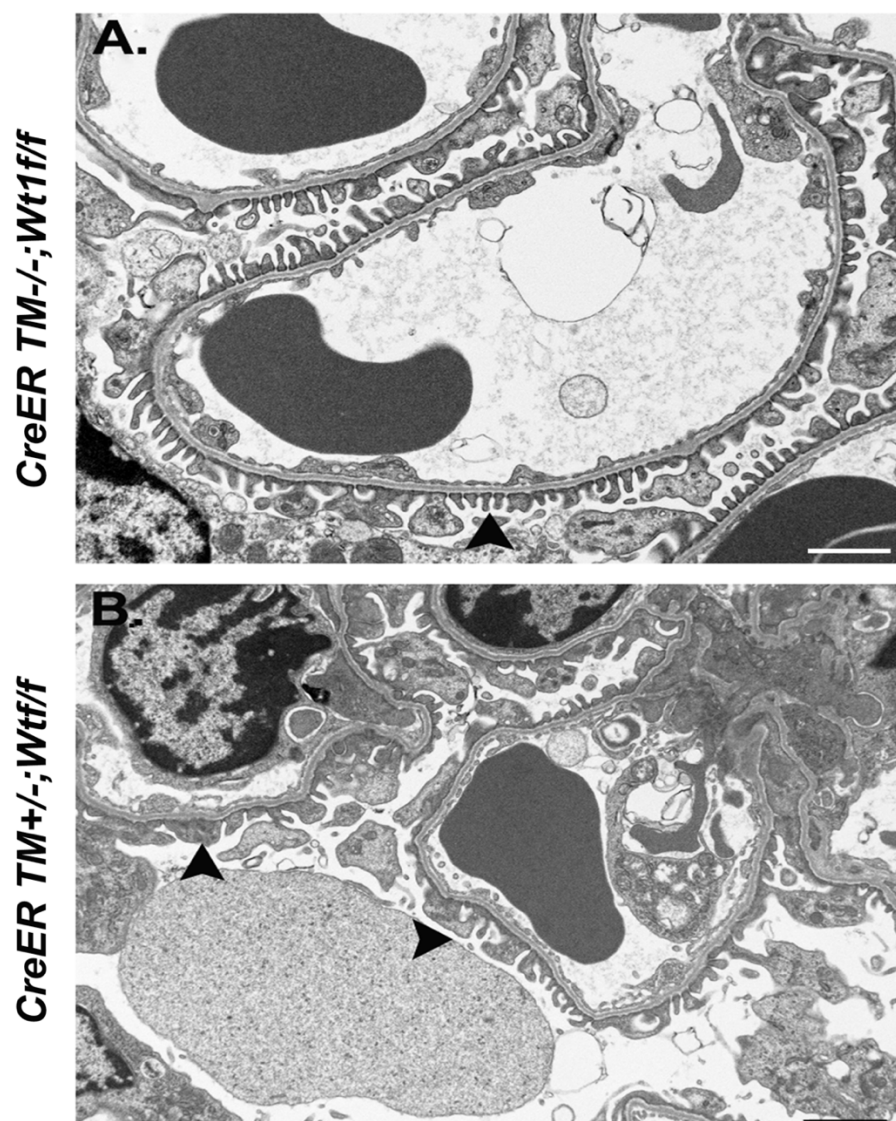


Figure 3.4. FP effacement at D4 P.I. in *Cre-ER^{TM+/-};Wt1^{ff}* transgenic mice

Electron micrographs exhibiting focal FP effacement in *Cre-ER^{TM+/-};Wt1^{ff}* mutants (**B**) at D4 P.I. compared to control mice (**A**). (Asfahani et al., 2018)

Interestingly, PAS staining revealed no morphological difference between both controls and the mutants at this time-point (Figure 3.2A); however, albumin/creatinine ratio was higher in the mutants, although not significant compared to the controls (Figure 3.2A'). TEM highlights the early stages of glomerular disease, prior to GS, indicating that the deletion of *Wt1* at an early time creates defects in the normal charge barrier, causing a leak of larger proteins, including albumin into the urine. This could be an indication of MCD, rather than FSGS or DMS, where the glomeruli show noticeable phenotypes.

3.2.1.4 Tubulointerstitial disease is evident by D12 P.I.

GS can lead to tubulointerstitial disease, causing tubular atrophy and fibrosis or inflammation of the interstitium, resulting in reduced renal function. Tubulointerstitial fibrosis is associated with an increased build-up of fibroblasts in the tubules expressing α -smooth muscle actin (α -SMA) and can lead to CKD.

In order to confirm tubulointerstitial fibrosis in the *Wt1*-deleted mutants, glomeruli were marked with vascular α -SMA and the tubule marker LTL at D12 P.I. due to the high levels of proteinuria and GS at this time-point. Mutant mice showed evidence of the disease with increased vascular α -SMA expression within the glomeruli and peritubular cells (Figure 3.5A bottom panel, B bottom panel, green arrows). Control mice, on the other hand displayed insignificant levels of α -SMA within the kidney interstitium and glomeruli (Figure 3.5A top panel, B top panel). Thus, in addition to GS, SMA protein expression suggested that there was a progression towards CKD, a leading cause of ESRD.

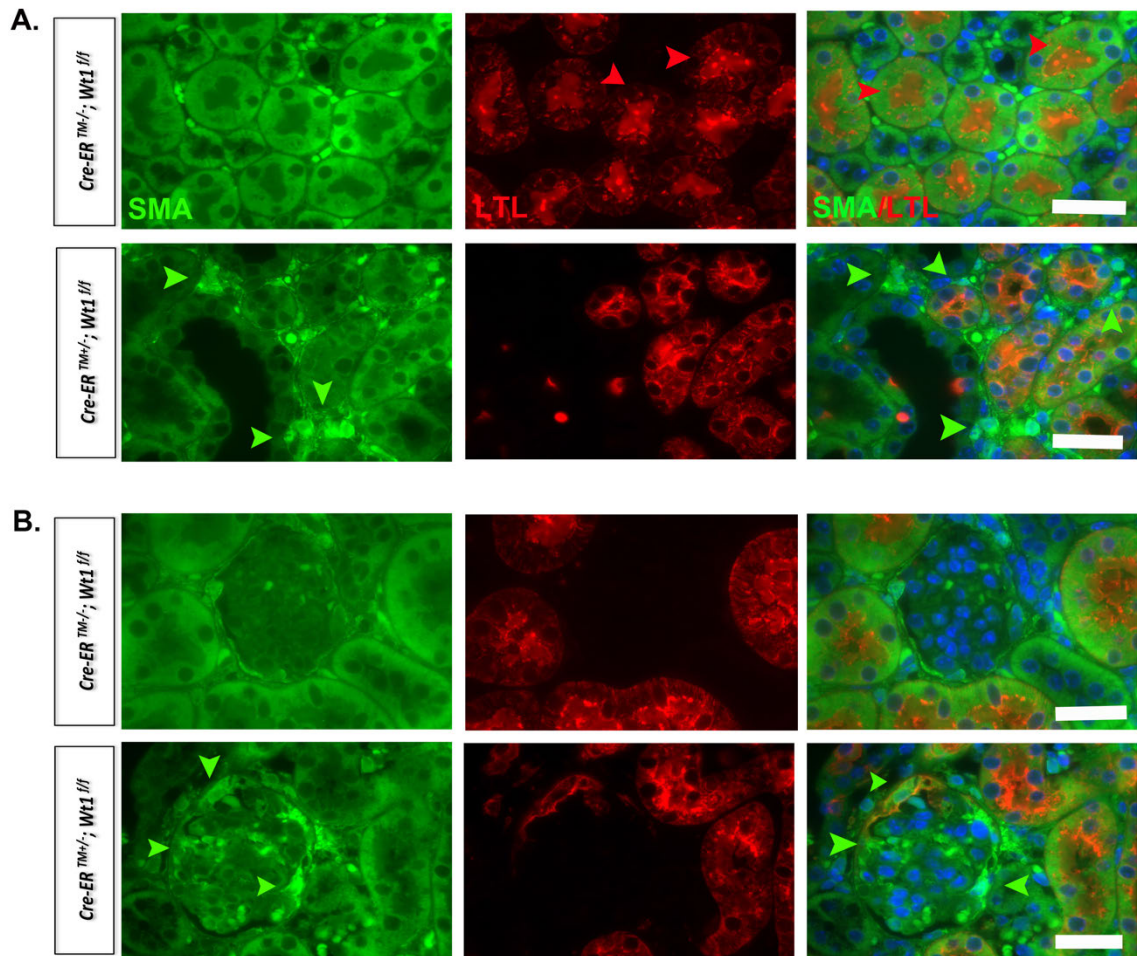


Figure 3.5. Vascular SMA expressed in *Cre-ERTM^{-/-};Wt1^{fl/fl}* mutants

(A-B) Representative micrographs of double immunofluorescent labelled glomeruli and tubules of transgenic mouse kidney tissue sections at D12 P.I.; anti- α smooth muscle actin (Alexa Fluor 488-conjugated) and Lotus tetragonolobus, LTL (Alexa Fluor 594-conjugated). tissues were counterstained with DAPI (scale bars, 50 μ m). (A) α -smooth muscle actin expansion is expressed in tubulointerstitial compartment in mutants (Green arrows, SMA) (A, bottom panel) vs. controls (red arrows, LTL) (A, top panel). SMA is not expressed within LTL-tubules of controls (A, top panel: merge) vs. mutants (A, bottom panel: merge, green arrows) (B) High power images of glomeruli and tubulointerstitium. α -SMA expression (green arrows) is stimulated in peritubular cells and in the glomerulus in the mutants (B, bottom panel) that is not seen in control *Cre-ERTM^{-/-};Wt1^{fl/fl}* transgenic mice (B, bottom panel). SMA is not expressed within LTL-tubules of controls (B, top panel: merge) vs. mutants (B, bottom panel: merge, green arrows). Scale bars 50 μ m. (Asfahani et al., 2018)

3.2.1.5 Podocin is detected within the tubular lumens of *Cre-ER^{TM+/-};Wt1^{ff}* mutants

Due to the evidence of albuminuria and GS in the tamoxifen-induced *Cre-ER^{TM+/-};Wt1^{ff}* mutants, further investigation was carried out to determine whether podocyte depletion was taking place outside of the GBM. Under extreme stress, podocytes are in danger of detaching from the GBM causing disruption, and eventually leading to proteinuria (Kriz et al., 2013). TEM revealed that podocyte FP effacement was occurring as early as D4 P.I. in the tamoxifen-induced mutants (Figure 3.4), which explained proteinuria at this time-point. This evidence drove us to investigate podocyte detachment further.

Podocin is important for the glomerular SD and absence of this protein can lead to albuminuria and NS (Mollet et al., 2009). Following immunohistochemical findings of tamoxifen-induced D8 *Cre-ER^{TM-/-};Wt1^{ff}* controls and *Cre-ER^{TM+/-};Wt1^{ff}* mutants, Podocin was seen in the glomeruli of the controls with little expression in the tubules (Figure 3.6A-F).

Podocin staining of glomeruli in controls was weak (Figure 3.6E), but was completely absent from mutant glomeruli (Figure 3.6H, I). In the mutants, Podocin was seen in the kidney tubular lumen (Figure 3.6K, L), further supporting FP effacement and podocyte injury in the mutants, with podocyte detachment leading to GS. Research on animal models of progressive GS have reported that podocytes are undergoing apoptosis (Hara et al., 1998, Niranjana et al., 2008). GS, proteinuria and podocyte detachment led us to investigate the mechanisms of podocyte injury, namely apoptosis.

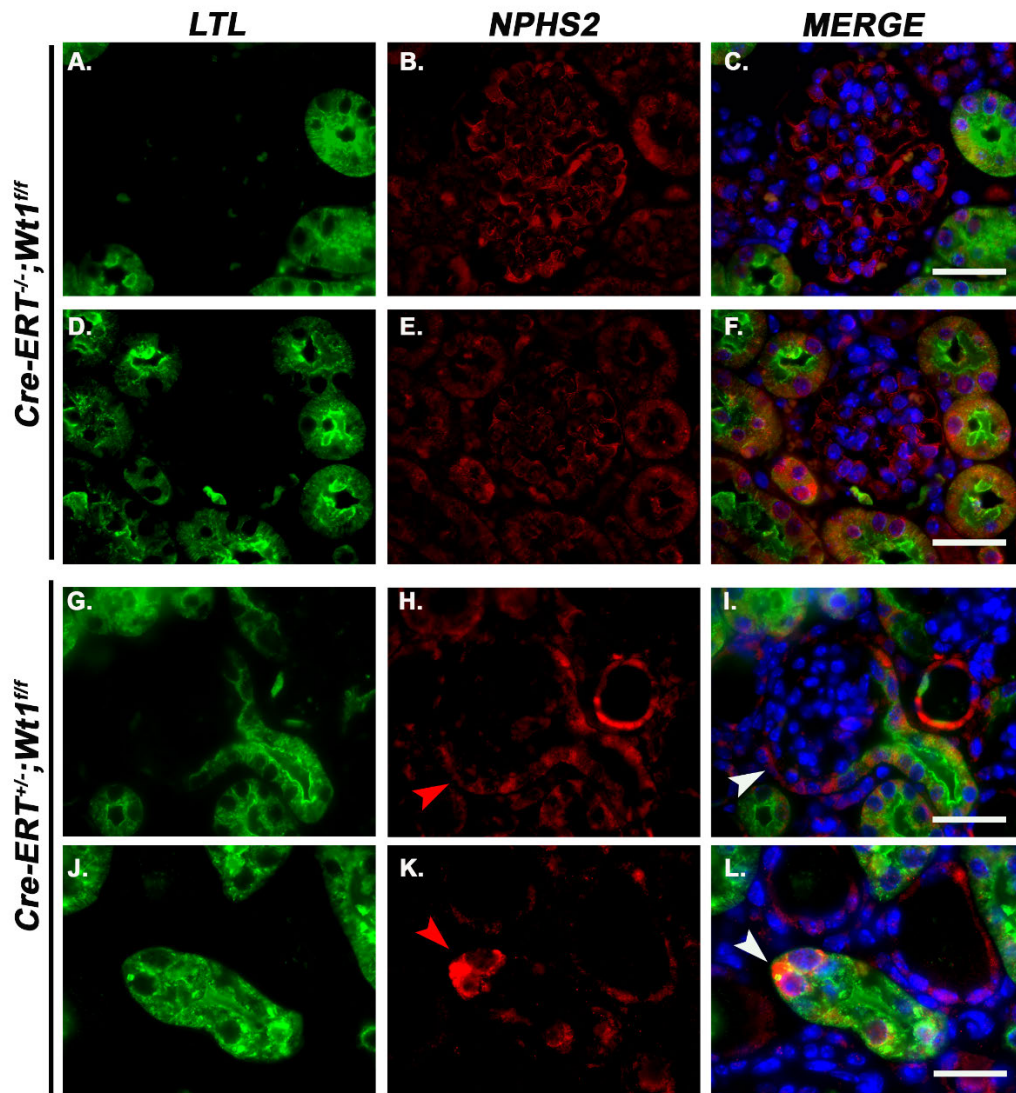


Figure 3.6. Podocin-positive cells in kidney tubules of D8 P.I $Cre-ER^{TM+/-};Wt1^{ff}$ mutants

Representative micrographs of kidney tubules and glomeruli in $Cre-ER^{TM-/-};Wt1^{ff}$ controls (**A-F**) vs. $Cre-ER^{TM+/-};Wt1^{ff}$ mutants (**G-L**), marked with the tubule marker, biotinylated *Lotus tetragonolobus* lectin (LTL, Alexa Fluor 488) and podocin (NPHS2, Alexa Fluor 594). $Cre-ER^{TM-/-};Wt1^{ff}$ controls exhibit low NPHS2 protein in the tubules, whilst NPHS2 is seen in the glomeruli, although faint (**B, C, E, F**). $Cre-ER^{TM+/-};Wt1^{ff}$ mutants show loss of NPHS2 protein in the glomerulus and NPHS2 is seen in the tubules, indicated by red arrows (**H, K, Alexa Fluor 594**) and white arrows (**I, L, merged**). Scale bar 25 μ m.

3.2.2 Apoptosis is evident in $Cre-ER^{TM+/-};Wt1^{ff}$ mutants

Due to the terminally differentiated nature of the podocytes, loss or injury of these cells can lead to GS. Although cell death can occur in three different forms: apoptosis, autophagy, and necrosis (Galluzzi et al., 2018, Elmore, 2007), given the evidence that apoptosis is a key mechanism in the pathogenesis of GS (Niranjan et al., 2008), this was an important mechanism to investigate following *Wt1* deletion. Apoptosis is recognised by a compression of nuclei, along with cell shrinkage, plasma membrane blebbing and

cell detachment (Brauchle et al., 2014). Initial histological investigation of the glomeruli of *Wt1* deleted mice led us to believe that podocyte apoptosis may be taking place in the mutant transgenic mice.

One of the key components of apoptosis are the activated proteases, caspase-3 and caspase-6, which are the hallmark of apoptosis, triggering the “death cascade” (Crowley and Waterhouse, 2016). Caspases are usually inactive under normal conditions, however, become activated once cleaved. Upstream caspases, including caspase-8 and caspase-9 are the main components of triggering caspase-3 activation. In these experiments, cleaved caspase-3 was a major marker in detecting apoptosis at different time-points following *Wt1* deletion.

Additional apoptosis markers were explored with TUNEL assay to detect DNA fragmentation in the podocytes. Real-time qPCR was used to identify apoptotic genes expressed in the podocytes of the mutants compared with controls, and flow cytometry to detect Annexin V-positive podocytes in D8 P.I. mutants compared with controls. Annexin V staining detects translocated phosphatidylserine, identifying early actions of apoptosis. Together, these experiments enabled us to confirm podocyte apoptosis in the *Wt1*-deleted mice.

3.2.2.1 Cleaved caspase-3 and caspase-3/7 protein expression support apoptosis in mutant podocytes from D4 P.I.

At D4 P.I., cleaved caspase-3 protein was observed *in vivo* within the mutant glomeruli but quantitatively, was not significantly different compared to the controls, $p=0.06$ (Figure 3.7A, A', D). However, cleaved caspase-3/DAPI-positive cell numbers were significantly higher in the mutants by D5 P.I. compared to the controls, coinciding with the early manifestation of GS, $***p<0.0001$ (Figure 3.7B, B', E). Moreover, a significant increase of cleaved caspase-3/DAPI-positive cells was observed by D8 P.I., where severe GS was detected by PAS, $***p<0.0001$ (Figure 3.7C, C', F). Cleaved caspase-3 protein, however, was not colocalised with DAPI in all places. DAPI was evidently more condensed and pyknotic in the mutants in comparison to the controls, highlighting degeneration of the nuclei at this time-point. Podoplanin protein expression was severely reduced in the mutants at D8 P.I. compared to the controls, indicating a loss of glomerular architecture (Figure 3.7C), supporting the PAS histology analysis at D6 and D12 P.I.

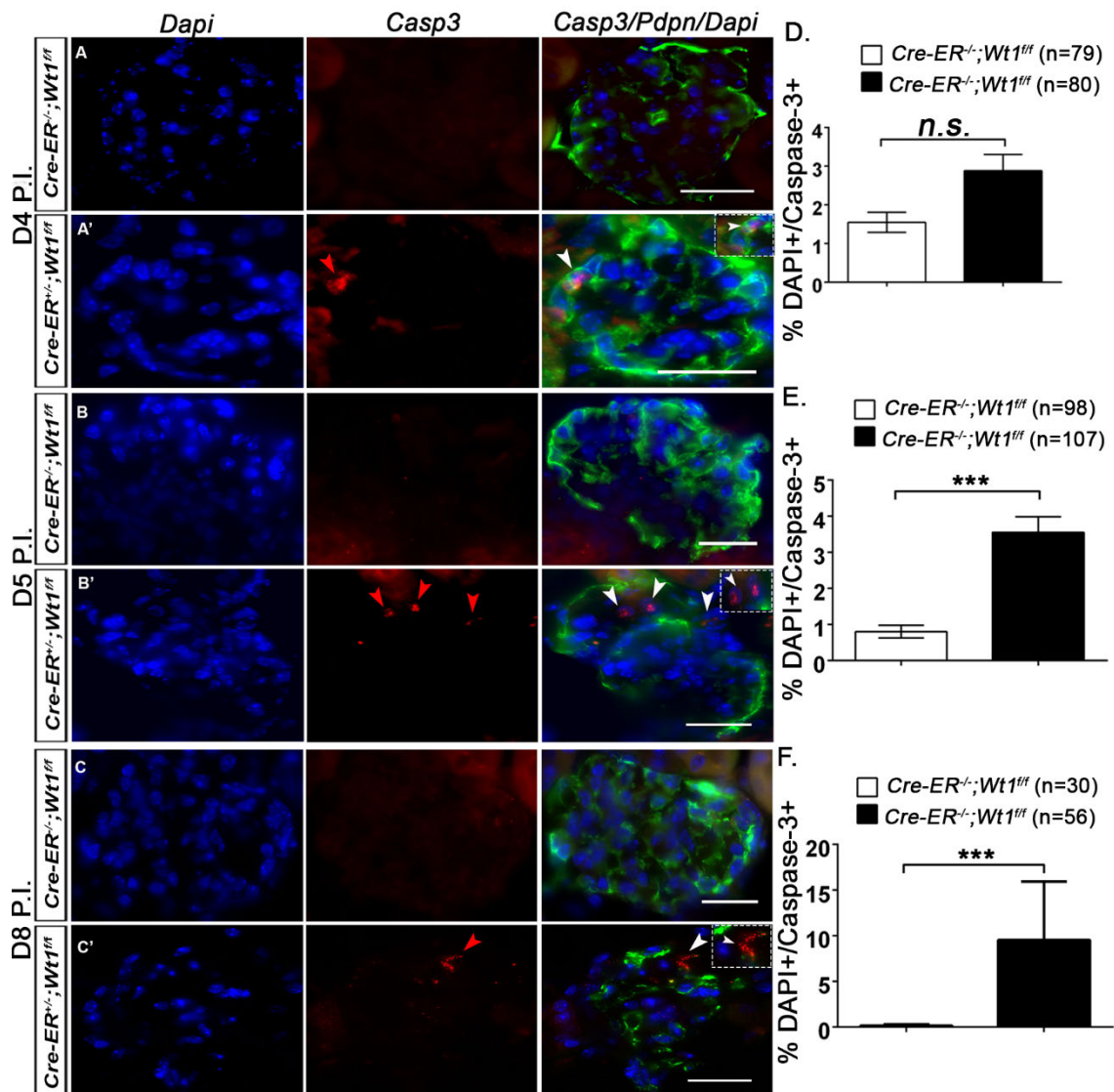


Figure 3.7. Temporal increase in podocyte apoptosis in *Cre-ER^{TM/+}; Wt1^{ff}* mutants

(A-F) Double immunofluorescence labelling of mouse of glomeruli; anti-cleaved caspase-3 (Casp-3) (Alexa Fluor 594–conjugated secondary antibody) and anti-Podoplanin (Pdpn) (Alexa Fluor 488–conjugated secondary antibody) at day 4, 5 and 8 P.I. counterstained with DAPI. Casp-3 (red arrows) and Podoplanin-positive cells observed in DAPI-positive cells in mutant glomeruli (inset, white arrows) (**A'**, **B'**, **C'**) and not in control glomeruli (**A**, **B**, **C**). Scale bars 25 μ m. **(D)** Graph mean percentage of DAPI-positive, Casp-3–positive cells per glomerulus at D4 PI in control and mutant mice. Bars represent mean and error bars specify the SEM. The number of DAPI-positive, Casp-3–positive glomerular cells were increased in mutant vs. control mice at D4 PI: Controls vs. mutants (n=79 vs. n=80 glomeruli from n=3 per genotype); $1.6 \pm 0.3\%$ vs. $3.0 \pm 0.4\%$, $p=0.06$, not significant (NS). Student's t-test. **(E)** Graph mean percentage of DAPI-positive, cleaved caspase-3–positive, Podoplanin-positive cells per glomerulus at D5 PI in control and mutant mice: controls vs. mutants (n=98 vs. n=107 glomeruli from n=3 per genotype); $0.8 \pm 0.2\%$ versus $3.6 \pm 0.4\%$, $***p < 0.0001$, Student's t-test. **(F)** Graph mean percentage of DAPI-positive, Casp-3–positive, Podoplanin-positive cells per glomerulus at D8 PI in control and mutant mice: controls vs. mutants (n=30 vs. n=56 glomeruli from n=3 per genotype); $0.1 \pm 0.1\%$ vs. $9.5 \pm 6.4\%$, $***p = 0.0005$, Student's t-test. (Asfahani et al., 2018)

In addition to this staining, D6 P.I. cellular immunostaining of cleaved caspase-3/7/DAPI positivity was also assessed and quantified in primary podocyte cultures (Figure 3.8). We observed increased cleaved caspase-3/7 positivity in the mutant podocytes (Figure 3.8B) compared to the controls (Figure 3.8A), providing further evidence of podocyte apoptosis in early *Wt1* glomerulopathy.

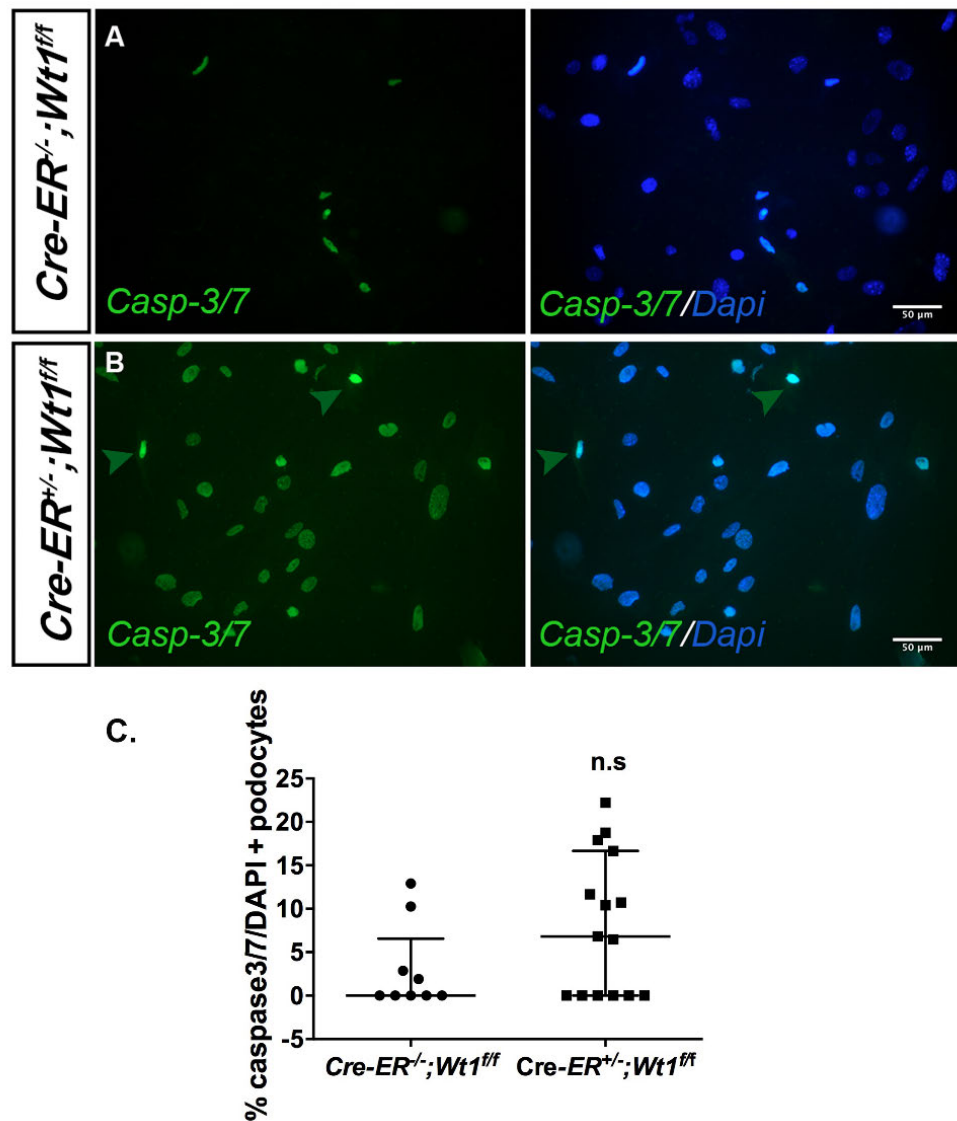


Figure 3.8. Cleaved-caspase-3/7 is activated in primary *Cre-ER^{TM+/-};Wt1^{f/f}* podocytes

(A-B) Representative micrographs of D6 P.I. primary podocytes (cultured for 6 days) showing immunofluorescent labelling of anti-cleaved caspase-3/7 (Alexa Fluor 488-conjugated secondary antibody, green arrows) in control (A) and mutant mice (B). Dot plot showing the median number of cleaved caspase-3/7- positive podocytes in mutants vs. controls (C). Bars denote the median per group. Error bars symbolise the interquartile ranges (IQR). Median percentage of DAPI-positive, cleaved caspase 3/7-positive podocytes in controls (n=9) vs. mutants (n=15): 0 (IQR: 0, 6.56) % vs. 6.8 (IQR: 0, 16.7) % $p=0.19$ (n.s.), Mann-Whitney test. (n=number cells counted/sample). (Asfahani et al., 2018)

3.2.2.2 TUNEL expression coincides with the early manifestation of GS

Apoptosis was further assessed using *in vitro* TUNEL analysis in D6 P.I. primary podocytes, and TUNEL-positive podocytes were apparent in the mutants (Figure 3.9D-G) compared to the controls (Figure 3.9A-C). Quantification of TUNEL/DAPI-positive cells was significantly higher in the mutants vs. controls, $*p=0.04$ (Figure 3.9H).

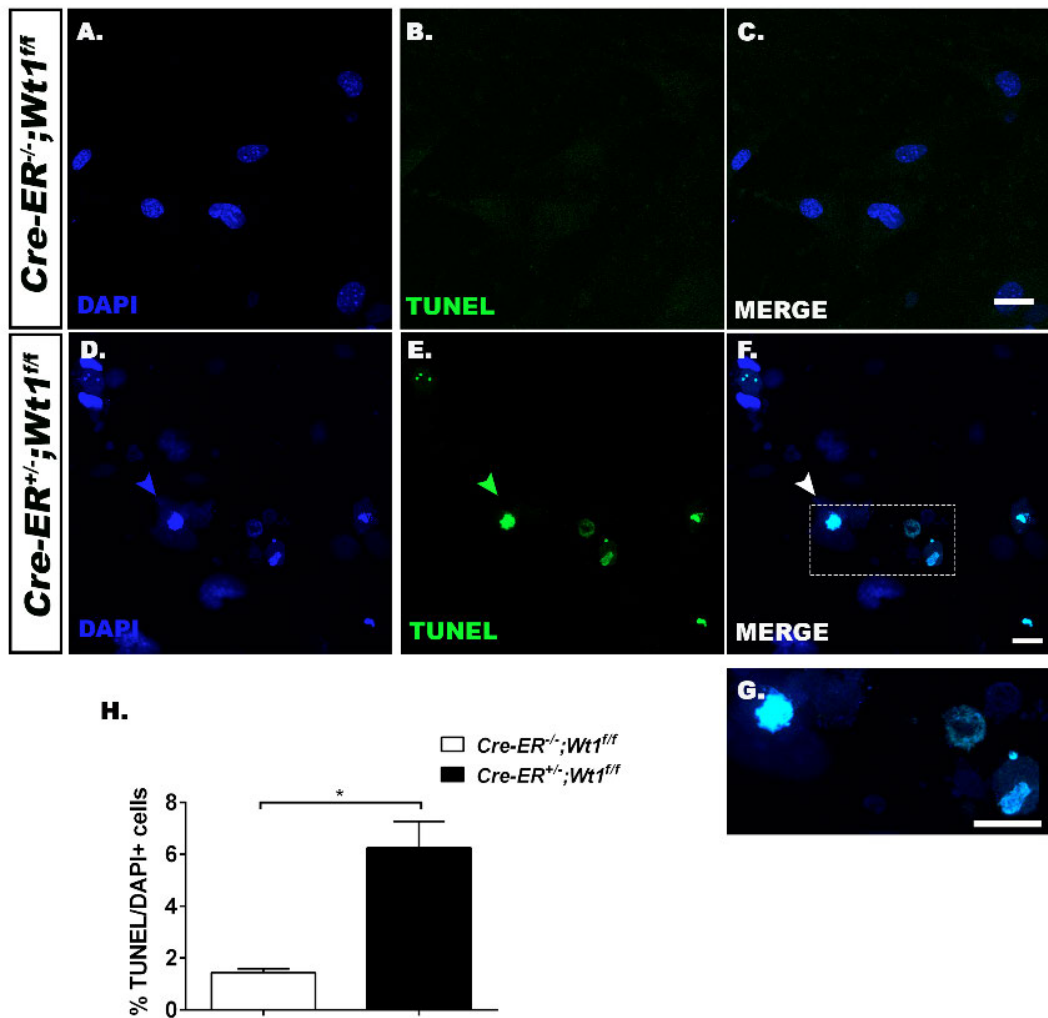


Figure 3.9. TUNEL-positive primary podocytes in D6 P.I. $Cre-ER^{TM+/-};Wt1^{ff}$ mutants

D6 P.I. Labelling of terminal deoxynucleotidyl transferase dUTP nick end-labelling (TUNEL)-positive primary podocytes (Alexa Fluor 488-conjugated secondary antibody, green arrows) isolated from control and mutant mice (A-G) Sections counterstained with DAPI. (G) Higher-power image displaying cell nucleus expressing TUNEL-positive signal. (H) Graph of apoptotic cells showing the proportion of TUNEL-DAPI-positive podocytes at D6 P.I. *in vitro*. Bars represent the mean, and error bars denote the SEM. $Cre-ER^{TM+/-};Wt1^{ff}$ (n=2 samples, number of cells quantified per sample) versus $Cre-ER^{TM+/-};Wt1^{ff}$ (n=2 samples, number of cells quantified per primary podocyte line per mouse); $1.4\pm 0.2\%$ versus $6.3\pm 1.0\%$, $*p=0.04$, Student t-test. Scale bar 25 μ m. (Asfahani et al., 2018)

Moreover, TUNEL-positive mutant podocytes were detected *in vivo* in D5 P.I. glomeruli (Figure 3.10A'), but not in controls (Figure 3.10A). There was a significant increase TUNEL/DAPI-positive cells in the mutants vs. controls, $**p < 0.0001$ (Figure 3.10B). *In vivo* TUNEL analysis was further analysed at D12 P.I., where there were obvious TUNEL-positive podocytes in the mutants (Figure 3.11B, C, D) compared to the controls (Figure 3.11A). The increase in significance by D12 P.I. correlated with its phenotype of global GS and proteinuria, supporting apoptosis as a mechanism linked to the development of GS and potentially secondary tubulointerstitial fibrosis.

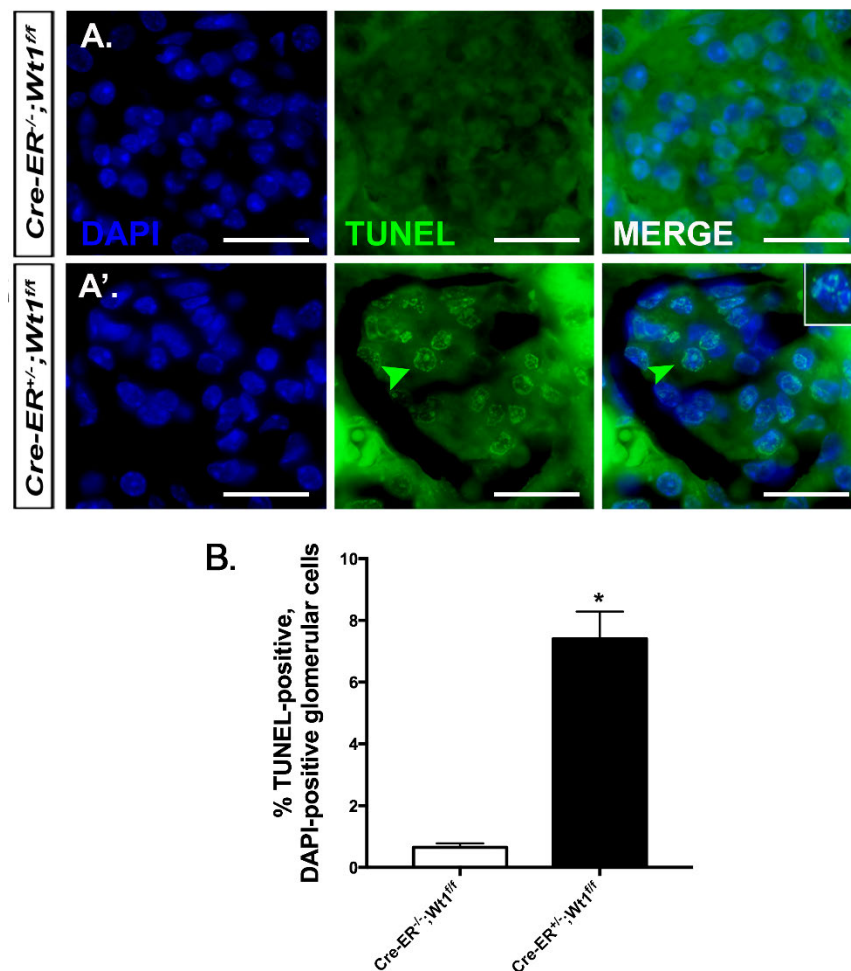


Figure 3.10. TUNEL-positive glomeruli in D5 P.I. of *Cre-ER^{TM+/-};Wt1^{ff}* mutants

Representative images of D5 P.I. cryosections, TUNEL-positive and DAPI-positive cells [inset] in *Cre-ER^{TM+/-};Wt1^{ff}* mutants (A') compared to *Cre-ER^{TM-/-};Wt1^{ff}* controls (A). Scalebar, 50µm. (B). Graph demonstrating increased proportion of median number of TUNEL-positive podocytes in *Cre-ER^{TM-/-};Wt1^{ff}* controls (n=2, 30 glomeruli counted/sample) vs *Cre-ER^{TM+/-};Wt1^{ff}* mutants (n=3, 30 glomeruli counted/sample). Bars display the median of each group. Error bars represent interquartile ranges, $**p < 0.0001$, Mann-Whitney test. (Asfahani et al., 2018)

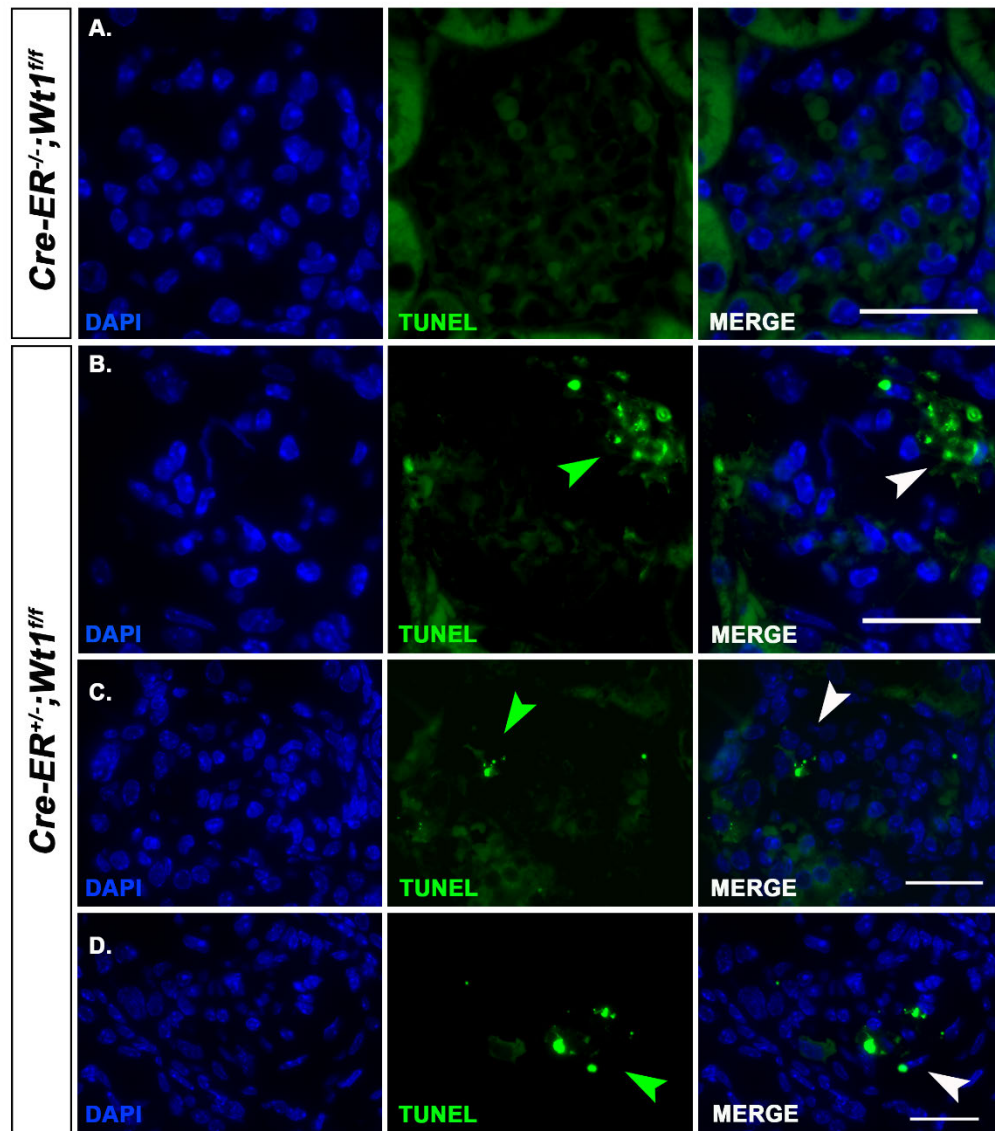


Figure 3.11. TUNEL-positive cells in $Cre-ER^{TM+/-};Wt1^{ff}$ glomeruli at D12 P.I.

(A-D) D12 P.I. micrographs of glomeruli of transgenic mouse kidney tissue sections marked with TUNEL (Green arrows) and counterstained with DAPI (Scale bars, 25 μ m). **(A)** In the glomerulus of $Cre-ER^{TM-/-};Wt1^{ff}$ controls, no TUNEL-positive cells are detected. **(B-D)** D12 P.I. $Cre-ER^{TM+/-};Wt1^{ff}$ mutants exhibit TUNEL/DAPI-positive cells in the glomeruli. (Asfahani et al., 2018)

3.2.2.3 Early and late apoptosis is evident in the late stages of GS

In vitro detection of apoptosis was also investigated along with cell necrosis through Annexin V/SYTOX Blue staining of D8 P.I. podocytes. Annexin V is a marker of early apoptosis and it identifies changes in the plasma membrane due to membrane externalisation of phosphatidylserine (Crowley et al., 2016). It is a useful assay to detect the development of apoptosis but it cannot identify which cells are undergoing late apoptosis or are early necrotic cells. For this reason, double staining of Annexin

V/SYTOX Blue was carried out to determine which cells were apoptotic and which were necrotic.

Annexin V/SYTOX Blue positive (late apoptotic/necrotic, Figure 3.12A, C) and Annexin V/SYTOX Blue negative (early apoptosis, Figure 3.12B, D) expression were higher in the primary mutant podocytes than the control podocytes, but not significantly so. The increase in Annexin V expression in the mutants vs. controls at D8 supported the previous findings of increased cleaved caspase-3 expression at this time-point, but at a less significant level.

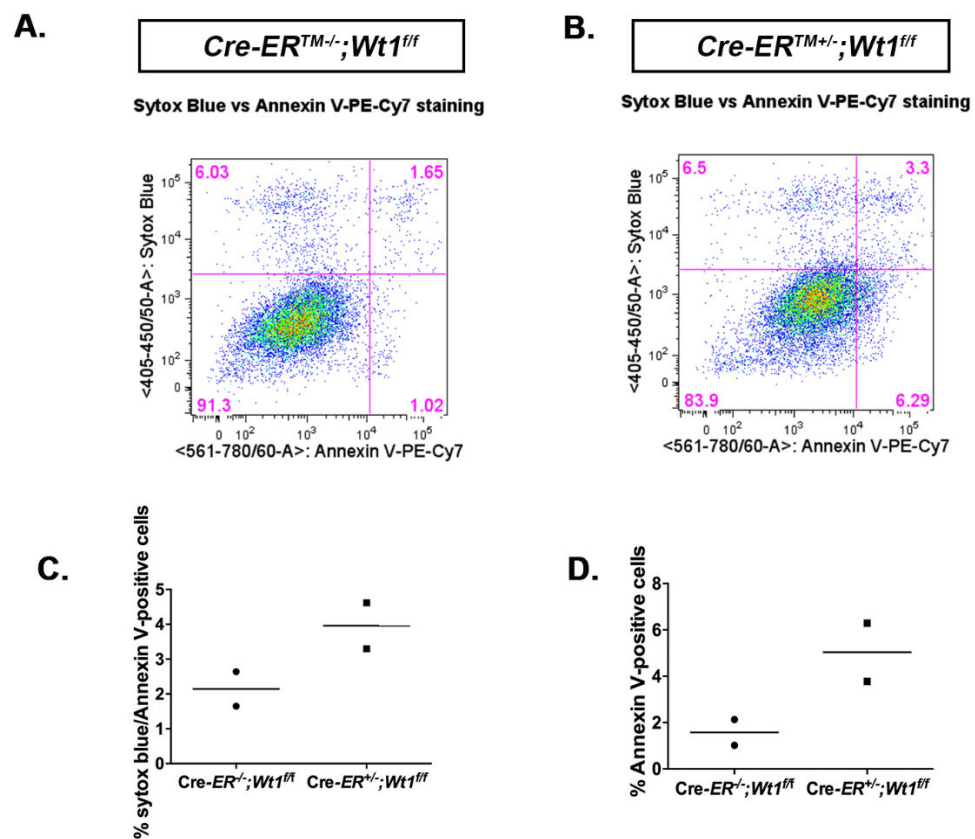


Figure 3.12. Apoptosis is increased at D8 P.I. in *Cre-ERTM^{+/-};Wt1^{fl/fl}* mutant podocytes

(A, B) Flow cytometry analysis of primary podocytes from Day 8 P.I. *Cre-ERTM^{-/-};Wt1^{fl/fl}* control and *Cre-ERTM^{+/-};Wt1^{fl/fl}* mutant transgenic mice. The abscissa and ordinate represent the fluorescence intensity of Annexin V Cy7 and SYTOX Blue, respectively. (C) Dot plot showing podocyte cell death. Bars display the median percentages of Annexin V–positive/SYTOX Blue–positive (late apoptotic/necrotic) podocytes. *Cre-ERTM^{-/-};Wt1^{fl/fl}* controls (n=2) vs. *Cre-ERTM^{+/-};Wt1^{fl/fl}* mutants (n=2): 2.1% versus 3.9%, $p=0.33$ (n.s). (D) Dot plot showing median percentages of Annexin V-positive cells (early apoptosis); 1.6% versus 5.0%, $p=0.33$ (n.s). Mann-Whitney test. (Asfahani et al., 2018)

3.2.2.4 Increased apoptotic gene transcript levels in the mutants

In addition to the detection of apoptosis on a protein level, further markers of apoptosis were investigated on an RNA level, including *Bcl2* and *Bax*. Both genes are regulators of apoptosis, involved in either inducing or inhibiting the pathway (Hardwick and Soane, 2013); *Bcl2* is anti-apoptotic, inhibiting cell death and promoting cell survival, whilst *Bax* is pro-apoptotic, and both are involved in the intrinsic apoptosis pathway, affecting the mitochondria.

Real-time qPCR data revealed an increase in apoptosis in the mutants compared to controls. Expression of apoptosis-related genes was carried out on D4, D5, and D6 P.I. glomerular isolates. The trend of the anti-apoptotic marker, *Bcl2*, was not significant in the mutants compared to the controls at D4 and D5 P.I. (Figure 3.13A). The pro-apoptotic marker, *Bax*, was also increased in the mutants at these time-points, but failed to reach statistical significance (Figure 3.13B). Interestingly, both *Bcl2* and *Bax* were slightly increased in the mutants vs controls at these time-points (D4 and D5 P.I.), suggesting that the apoptotic pathway may be activated. *Bcl2* transcript levels were at approximately equivalent levels in both the mutants and controls at both time-points; however, *Bax* transcript levels had increased by D5 P.I. in the mutants. This corroborated my findings of the activation of apoptosis using cleaved caspase-3 and TUNEL at D5 P.I. By D6 P.I. on the other hand, the anti-apoptotic transcript, *Bcl2* was lower in the mutants compared to the controls, but again failed to reach statistical significance (Figure 3.13A). This correlates with my earlier findings of increased TUNEL and caspase-3 expression. While this was the case, *Bax* transcript levels were lower in the mutants vs. controls at D6 P.I., however were not significant (Figure 3.13B). D6 P.I. sample numbers were less than D4 and D5 P.I., thus may be impacting the final result. It is also important to note that this experiment was done in the early stages of the project, where RNA transcripts were analysed from glomerular isolates that were not cultured. These isolates were not only podocytes, but were also mesangial and endothelial cells. *Bcl2* and *Bax2* transcript levels would have therefore been analysed from a heterogenous population. This may explain the lower expression of *Bax* transcript levels in the mutants in comparison to other apoptosis assay markers, such as cleaved caspase-3 and TUNEL, as the latter experiments (figures presented earlier) were focused on podocyte cells undergoing apoptosis. Moreover, limited sample numbers for real-time qPCR may also be impacting our final results.

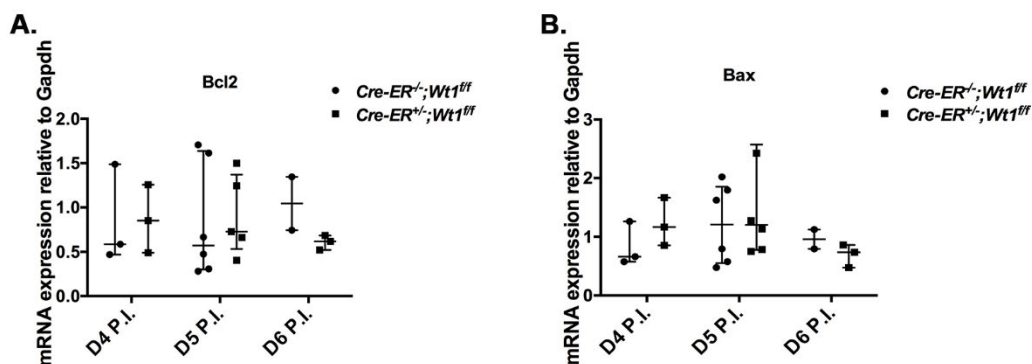


Figure 3.13. Podocyte apoptosis in pre-proteinuric and GS *Cre-ER^{TM+/-};Wt1^{ff}* mutants.

Representative dot plot analyses showing the median mRNA levels of apoptosis at D4, 5 and 6 P.I. Error bars represent IQR. **(A) Bcl2**; D4 P.I. *Cre-ER^{TM-/-};Wt1^{ff}* controls (n=3) vs. *Cre-ER^{TM+/-};Wt1^{ff}* mutants (n=3), 0.6 (IQR: 0.5, 1.5) vs. 0.9 (IQR: 0.5, 1.3), $p=0.9$; D5 P.I. *Cre-ER^{TM-/-};Wt1^{ff}* controls (n=6) vs. *Cre-ER^{TM+/-};Wt1^{ff}* mutants (n=5), 0.6 (IQR: 0.3, 1.6) vs. 0.7 (IQR: 0.5, 1.4), $p=0.77$; D6 P.I. *Cre-ER^{TM-/-};Wt1^{ff}* controls (n=2) vs. *Cre-ER^{TM+/-};Wt1^{ff}* mutants (n=3), 1.0 (IQR: 0.7, 1.3) vs. 0.6 (IQR: 0.5, 0.7), $p=0.2$ **(B) Bax**; D4 P.I. *Cre-ER^{TM-/-};Wt1^{ff}* controls (n=3) vs. *Cre-ER^{TM+/-};Wt1^{ff}* mutants (n=3), 0.7 (IQR: 0.6, 1.3) vs. 1.2 (IQR: 0.9, 1.7), $p=0.4$; D5 P.I. *Cre-ER^{TM-/-};Wt1^{ff}* controls (n=6) vs. *Cre-ER^{TM+/-};Wt1^{ff}* mutants (n=6), 1.2 (IQR: 0.6, 1.9) vs. 1.2 (IQR: 0.8, 2.6), $p=0.6$; D6 P.I. *Cre-ER^{TM-/-};Wt1^{ff}* controls (n=2 mice) vs. *Cre-ER^{TM+/-};Wt1^{ff}* mutants (n=3 mice), 1.0 (IQR: 0.8, 1.1) vs. 0.7 (IQR: 0.5, 0.9), $p=0.4$. Mann-Whitney test. (n= number of mice).

3.2.3 Podocyte Notch activation precedes GS in *Cre-ER^{TM+/-};Wt1^{ff}* mutants

As previously mentioned, the Notch pathway is highly relevant during the early stages of kidney development and is activated following glomerular injury (Niranjan et al., 2009, Cheng and Kopan, 2005, Barak et al., 2012, Sirin and Susztak, 2012, Barisoni, 2008). Studies revealed that ectopically inducing cleaved *Notch1* during the late stages of kidney development resulted in DMS and FSGS with reduced expression of podocyte markers, including *Wt1*, *Nphs1*, *Nphs2* as well as increased podocyte apoptosis and dedifferentiation (Niranjan et al., 2008, Waters et al., 2008). Thus, we postulated that deleting *Wt1* would trigger the Notch signalling pathway in the mutants, causing GS.

3.2.3.1 Notch components are activated following *Wt1* deletion

Cleaved NOTCH1 is a transmembrane protein involved in the Notch pathway, which is cleaved following γ -secretase activation post-ligand binding (Jorissen and De Strooper, 2010). As stated previously, the Notch pathway consists of 2 ligand family members including the Dll and Jag families. Upon binding with the Notch receptors, the Notch cell signalling pathway is activated, cleaving the intercellular domains of the Notch receptors,

thus finally activating the downstream transcription factors, including *HES1* and *HEYL*, which are important for organogenesis and tissue patterning (Kopan and Ilagan, 2009, Bray, 2006, Bray, 2016, Hori et al., 2013).

After detecting increased podocyte apoptosis in *Cre-ER^{TM+/-};Wt1^{ff}* transgenic mice, we postulated that podocyte Notch activation may be a factor in early *Wt1* glomerulopathy. The Notch pathway was analysed using real-time qPCR at D4 and D5 P.I. (Figure 3.14). At D4 P.I., the bHLH transcription factor, *Hes6*, was significantly reduced in the mutants compared to controls ($*p=0.03$) (Figure 3.14A, Appendix B [figure B.1 A-S, individual dot plots]). *Hes6* has been shown to promote neuronal differentiation by negatively regulating *Hes1* activity (Gratton et al., 2003, Carvalho et al., 2015).

The current data shows that *Hes1* transcript was increased in D4 P.I. mutants, however, this was not significant ($p=0.53$) (Figure 3.14A). There was an increase in *HeyL* transcript levels, however the increase was not significant (Figure 3.14A). Interestingly, the β 3-N-acetylglucosaminyltransferase, *Lfng*, was significantly lower in the mutants compared to the controls at this time-point ($**p=0.008$) (Figure 3.14A). *Lfng* has been reported to inhibit Notch1 activity from Jag1 and enhance its activity from Dll1 by modifying Notch1 EGF6 and 36 (Kakuda and Haltiwanger, 2017). At D4 P.I, Notch signalling was activated by showing increased transcript levels of bHLH transcription factors *Hes1*, *Hes3*, *Hes5*, *Hey1*, *Hey2*, *HeyL* in the mutants, although these were not significant (Figure 3.14A). Notch signalling was indeed activated at D4 P.I., however, sample sizes were quite low ($n=5$ /group) due to the availability of mice.

At D5 P.I., bHLH transcription factors, *Hes3* ($*p=0.01$) and *Hey1* ($*p=0.03$) were significantly lower in the mutants compared to controls (Figure 3.14B, Appendix B [figure B.2 A-R, individual dot plots]). *Dll4* transcript levels were reduced in the mutants compared to the controls, however, these were not significantly different (Figure 3.14B). There was an outlier in the control group, showing a reduction in *Dll4* mRNA levels. *Mfng* transcript levels were increased in mutant podocytes, however, not significantly ($p=0.45$, Figure 3.14B). Although *Mfng* was not significantly increased in the mutants, we were keen to explore whether there was a link between increased *Mfng* transcript and Notch activity in our mice. Manic Fringe is a β 3-N-acetylglucosaminyltransferase that facilitates NECD glycosylation during signal transduction (Kakuda and Haltiwanger, 2017). Sample numbers for *Neur* were not equal between control and mutants due to availability of the samples. Due to apoptosis being significantly increased at D6 P.I., we were specifically interested in analysing the Notch pathway at this time-point. Individual dot plots for the genes at D4, D5 and D6 P.I. are shown in Appendix B.

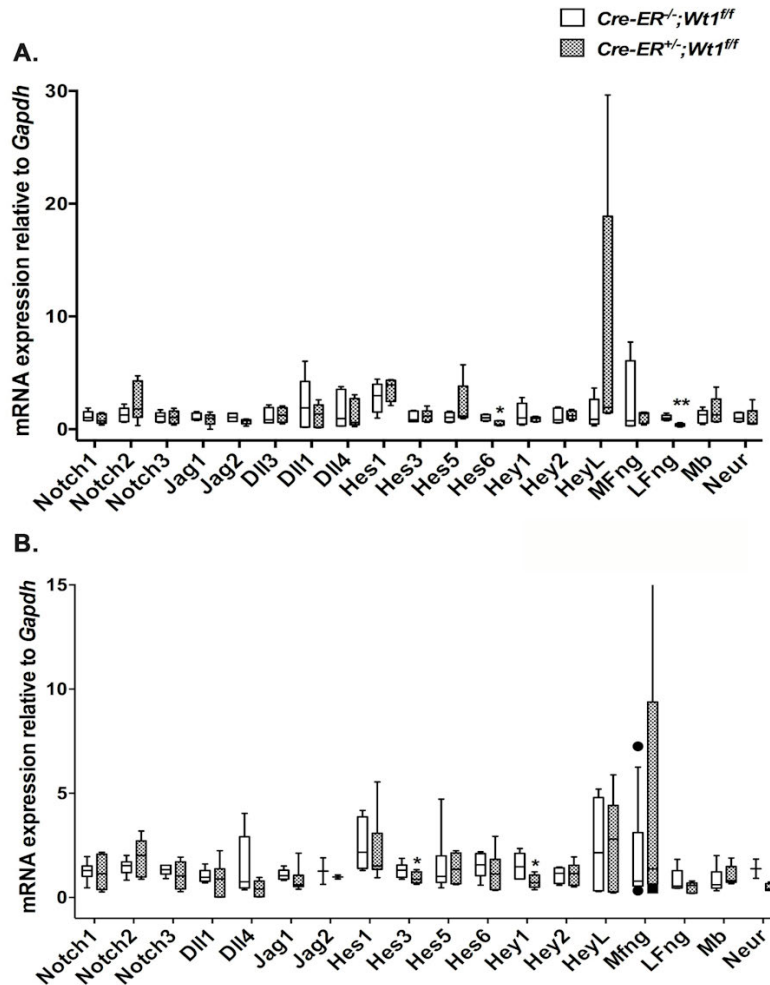


Figure 3.14. Podocyte Notch pathway gene expression in pre-proteinuric *Cre-ERTM+/-;Wt1^{flf}* primary podocytes

(A) Notch pathway transcripts in D4 P.I. *Cre-ERTM+/-;Wt1^{flf}* mutants compared to *Cre-ERTM-/-;Wt1^{flf}* controls. Box and whisker plots showing relative mRNA levels of Notch pathway components in primary podocytes of *Cre-ERTM+/-;Wt1^{flf}* vs. *Cre-ERTM-/-;Wt1^{flf}*. Horizontal lines within the box show medians. The boundaries of the box nearest zero mark the 25% percentile, the boundaries farthest from zero mark the 75% percentile (IQR). Whiskers indicate outliers outside the 10% and 90% percentiles. *Notch1* (n=5 vs n=5): 1.1 (IQR: 0.8, 1.6) vs. 0.8 (IQR: 0.5, 1.4), $p=0.53$; *Notch2* (n=5 vs. n=5): 1.3 (IQR: 0.7, 1.9) vs. 1.8 (IQR: 1.1, 4.3), $p=0.31$; *Notch3* (n=5 vs. n=5): 1.2 (IQR: 0.7, 1.5) vs. 1 (IQR: 0.5, 1.6), $p=0.94$; *Jag1* (n=5 vs. n=5): 1 (IQR: 0.8, 1.4) vs. 1 (IQR: 0.5, 1.3), $p=0.94$; *Jag2* (n=5 vs. n=5): 1 (IQR: 0.7, 1.4) vs. 0.8 (IQR: 0.5, 0.8), $p=0.22$; *Dll3* (n=5 vs. n=5): 0.8 (IQR: 0.6, 1.9) vs. 1.2 (IQR: 0.6, 1.9), $p>0.99$; *Dll1*(n=5 vs. n=5): 1.9 (IQR: 0.2, 4.2) vs. 1.3 (IQR: 0.2, 2.2), $p=0.67$; *Dll4* (n=5 vs. n=5): 0.9 (IQR: 0.3, 3.5) vs. 0.6 (IQR: 0.4, 2.7), $p=0.67$; *Hes1* (n=5 vs. n=5): 3 (IQR: 1.5, 4) vs. 4 (IQR: 2.5, 4.3), $p=0.53$; *Hes3* (n=5 vs. n=5), 0.8 (IQR: 0.7, 1.6) vs. 1.2 (IQR: 0.7, 1.6), $p=0.94$; *Hes5* (n=5 vs. n=5), 1.1 (IQR: 0.7, 1.5) vs. 1.2 (IQR: 1, 3.8), $p=0.31$; *Hes6*, (n=5 vs. n=5), 1 (IQR: 0.8, 1.3) vs. 0.4 (IQR: 0.4, 0.8), $*p=0.03$; *Hey1*, (n=5 vs. n=5), 1 (IQR: 0.5, 2.3) vs. 1 (IQR: 0.7, 1.1), $p=0.94$; *Hey2*, (n=5 vs. n=5), 0.8 (IQR: 0.6, 1.9) vs. 1.2 (IQR: 0.9, 1.6), $p=0.8$; *HeyL*, (n=5 vs. n=5), 0.9 (IQR: 0.5, 2.7) vs. 1.9 (IQR: 1.5, 18.9), $p=0.15$; *Mfng*, (n=4 vs. n=5), 0.8 (IQR: 0.3, 6.1) vs. 1.4 (IQR: 0.5, 1.5), $p=0.68$; *Lfng* (n=5 vs. n=5),

1 (IQR: 0.8, 1.2) vs. 0.4 (IQR:0.3, 0.5), $**p=0.008$; Mb (n=5 vs. n=5), 1.3 (IQR: 0.6, 1.7) vs. 1.3 (IQR: 0.7, 2.7), $p=0.8$; Neur (n=5 vs. n=5), 1 (IQR: 0.7, 1.5) vs. 0.5 (IQR: 0.5, 1.6), $p=0.22$. Mann-Whitney U test. **(B)** Notch pathway transcripts in D5 P.I. *Cre-ER^{TM+/-};Wt1^{fl/fl}* mutants compared to *Cre-ER^{TM+/-};Wt1^{fl/fl}* controls. Box and whisker plots showing relative mRNA levels of Notch pathway components in primary podocytes of *Cre-ER^{TM+/-};Wt1^{fl/fl}* vs. *Cre-ER^{TM+/-};Wt1^{fl/fl}*. Horizontal lines within the box show medians. The boundaries of the box nearest zero mark the 25% percentile, the boundaries farthest from zero mark the 75% percentile (IQR). Whiskers indicate outliers outside the 10% and 90% percentiles. *Notch1* (n=6 vs n=6), 1.3(IQR:1, 1.5) vs. 1.1(IQR: 0.4,2.1), $p>0.99$; *Notch2* (n=6 vs. n=6), 1.5 (IQR: 1.2, 1.7) vs. 2 (IQR: 1, 2.7), $p=0.33$; *Notch3* (n=6 vs. n=7), 1.3(IQR: 1.1, 1.5) vs. 1 (IQR:0.4, 1.7) $p=0.36$; *Dll1* (n=6 vs. n=8), 1 (IQR: 0.8, 1.3) vs. 0.9 (IQR: 0.03, 1.4), $p=0.84$; *Dll4* (n=6 vs. n=7), 0.8 (IQR: 0.5, 2.9) vs. 0.4 (IQR: 0.04, 0.8), $p=0.18$; *Jag1* (n=6 vs. n=8), 1.1 (IQR: 0.9, 1.3) vs. 0.6 (IQR: 0.5, 1.1), $p=0.08$; *Jag2* (n=2 vs. n=2), 1.3 (IQR: 0.6, 1.9) vs. 1 (IQR: 0.9, 1.1), $p>0.99$; *Hes1* (n=7 vs. n=8), 2.2 (IQR: 1.4, 3.9) vs. 1.5 (IQR: 1.4, 3.1), $p=0.39$; *Hes3* (n=9 vs. n=11), 1.3 (IQR: 0.9, 1.5) vs. 0.8 (IQR: 0.6, 1.2), $*p=0.01$; *Hes5* (n=6 vs. n=7), 1 (IQR: 0.7, 2) vs. 1.4 (IQR: 0.7, 2.1), $p=0.7$; *Hes6*, (n=8 vs. n=8), 1.6 (IQR: 1, 2.1) vs. 1.1 (IQR: 0.4, 1.8), $p=0.41$; *Hey1*, (n=6 vs. n=8), 1.5 (IQR: 0.9, 2.1) vs. 0.7 (IQR: 0.5, 1.1), $*p=0.03$; *Hey2*, (n=6 vs. n=8), 1.2 (IQR: 0.7, 1.4) vs. 1.2 (IQR: 0.6, 1.5), $p>0.99$; *HeyL*, (n=6 vs. n=7), 2.2 (IQR: 0.3, 4.8) vs. 2.8 (IQR: 0.3, 4.4), $p=0.8$; *Mfng*, (n=12 vs. n=10), 0.8 (IQR: 0.6, 3.1) vs. 1.4 (IQR: 0.6, 9.4), $p=0.45$; *Lfng* (n=6 vs. n=8), 0.6 (IQR: 0.5, 1.3) vs. 0.6 (IQR:0.2, 0.7), $p=0.49$; *Mb* (n=6 vs. n=5), 0.6 (IQR: 0.4, 1.2) vs. 0.8 (IQR: 0.7, 1.5), $p=0.33$; *Neur* (n=2 vs. n=4), 1.4 (IQR: 0.9, 1.8) vs. 0.4 (IQR: 0.3, 0.7), $p=0.13$. Mann-Whitney U test. Individual dot plots are shown in Appendix B.

Double immunofluorescence labelling at D4 P.I. between the controls and mutants (Figure 3.15A-H) showed increased cleaved Notch1 (Val1744) protein expression in the mutant nuclei of Nestin-positive podocytes, with a loss of podocyte glomerular architecture (Figure 3.15E-H). We observed no cleaved Notch1 (Val1744) protein in the podocyte nuclei of the controls, labelled with the podocyte marker, synaptopodin (Synpo) at D5 P.I. (Figure 3.15I-L). In the mutants, however, cleaved Notch1 protein was seen in the podocytes (Figure 3.15M-P). Podocyte markers, Podoplanin at D4 P.I, and Synaptopodin at D5 P.I. were used due to the lack of availability of one or the other during the experiment.

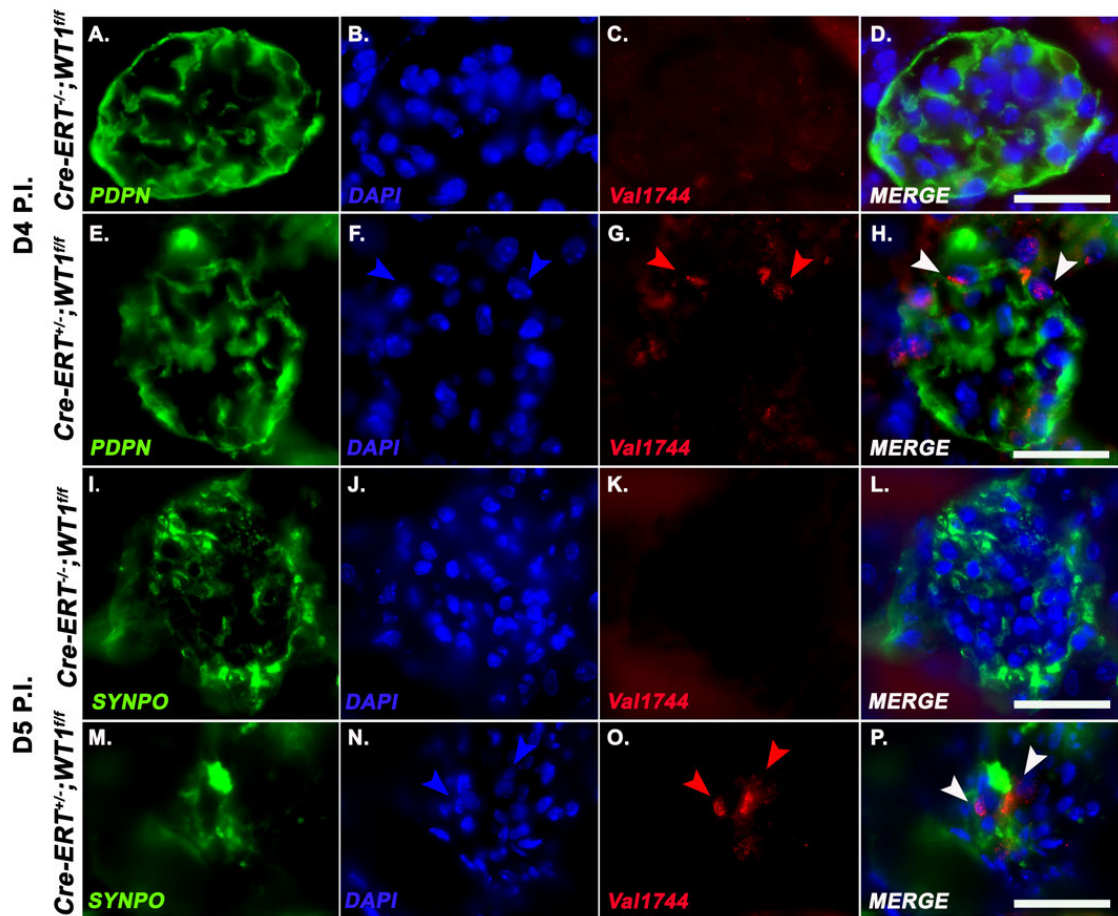


Figure 3.15. Activated cleaved Notch1 at the early onset of disease in *Cre-ER^{TM+/-};Wt1^{fl/fl}* mutants

Representative micrographs of glomeruli in D4 P.I., stained with the glomerular marker, podoplanin (PDPN, Alexa Fluor 488, green), and cleaved notch 1 (Val1744, Alexa Fluor 594, red), counterstained with the nuclear marker, DAPI (**A-H**) NICD protein expression is not evident in the control *Cre-ER^{TM-/-};Wt1^{fl/fl}* mice (**C, D**) in comparison to the *Cre-ER^{TM+/-};Wt1^{fl/fl}* mutants, where NICD appears to be expressed in the podocytes, indicated by red and white arrows (**G, H**) Representative micrographs of mouse glomeruli at D5 P.I. stained with the podocyte marker, Synaptopodin (SYNPO, Alexa Fluor 488, green) and NICD (Alexa Fluor 594, red), counterstained with DAPI (**I-P**). Control *Cre-ER^{TM-/-};Wt1^{fl/fl}* mice display no NICD protein in the glomerulus (**K, L**) compared to *Cre-ER^{TM+/-};Wt1^{fl/fl}* mutants, where NICD protein expression is revealed in the podocytes, indicated by red and white arrows (**O, P**). Scale bar, 25 μ m.

Next, we examined the Notch pathway at the onset of GS, D6 P.I. Concomitant with early GS and albuminuria, Notch transcripts, *Notch1*, *Hes1*, *3*, *5* and *Hey2* were increased in primary mutant podocyte lysates compared to controls (Figure 3.16A, Appendix B [Figure B.3 A-R, individual dot plots]). *FoxC2* transcript was repressed in the mutants, with increased *Nrarp* expression (Figure 3.16A). Notch regulated ankyrin repeat protein (NRARP) is a downstream effector of Notch signalling (Zhang et al., 2017). Earlier studies showed that *Nrarp* is regulated by Notch signalling and is highly expressed in mouse tissues where *Notch1* is expressed (Krebs et al., 2001). Our data reveals a

significant increase in *Notch1* (* $p=0.04$), *Nrarp* (** $p=0.0087$), *Hes5* (** $p=0.005$), and *Hey3* (* $p=0.03$) transcripts in the mutants. This data suggests that the increased *Nrarp* transcript is regulated by Notch activity. Repression of *FoxC2* coincides with the upregulation of the Notch components and onset of GS in the mutants (Figure 3.16A).

Immunofluorescence labelling at D6 P.I. validated these results, where cleaved Notch1 protein (Val1744) was seen in the mutant podocytes compared to controls (Figure 3.16B). Western blot analysis further validated this data, where Notch1 protein was increased in primary mutant podocyte lysates relative to controls (Figure 3.16C). Supporting activation of a pathogenic Notch signal was further observed in increased podocyte *Mfng* transcript (Figure 3.16A). Pofut1 protein was also observed in primary mutant podocytes at D6 P.I. (Figure 3.16D). Fucosylation of the extracellular domain of the Notch protein is mediated by Pofut1, an O-fucosyltransferase 1 enzyme (Rana and Haltiwanger, 2011).

A role for ligand-dependent activation of podocyte *Notch1* was suggested by the observation of a striking upregulation of *Jag1* in the parietal epithelium of mutants compared to controls (Figure 3.17 A, B). Mutant glomeruli fragments revealed *Jag1* expression in foci of Podocin-positive cells (Figure 3.17a, b, insets). At D6 P.I., *Jag1* protein expression was evident in the primary mutant lysates compared to controls (Figure 3.17C). Increased transcript levels of *Mfng*, as well as increased *Jag1* and Pofut1 protein expression in the mutants led us to hypothesis that *Jag1* may be activating Notch1 signalling via *Mfng* and Pofut1 modification in our disease model. These data support a role for the potentiation of *Notch1* signalling in early *Wt1* glomerulopathy.

To further validate Notch activation following *Wt1* deletion, immortalised podocytes of DDS and FS patients were analysed. DDS patients carried C1096T mutations in *WT1*, (p.Arg366Cys) and FS patients carried mutations at intron 9 of *WT1*, affecting the ratio of +/-KTS. There was an increase in transcript levels of Notch pathway components, *NOTCH1*, *NOTCH2*, *HES1*, *HEYL*, *JAG1* (Figure 3.18A). PCR data showed no *WT1* amplicon in the DDS and FS patients compared to the control sample, where *WT1* was expressed (Figure 3.18B). While this corroborates our *in vivo* findings, patient sample numbers were very low. Therefore, increasing sample sizes will provide us with a more accurate result.

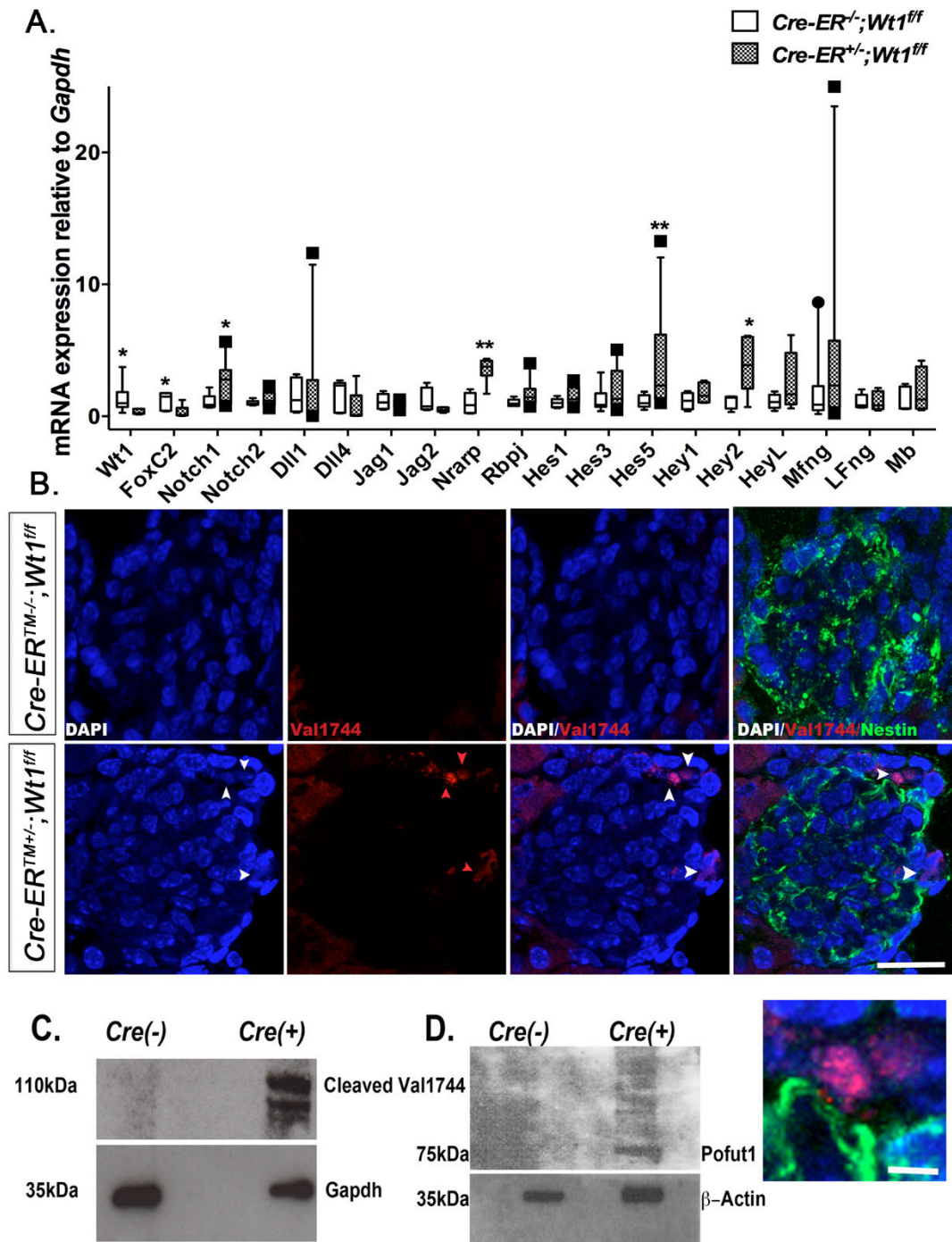


Figure 3.16. Notch activation coincides with onset of GS in $Cre-ER^{TM+/-};Wt1^{ff}$ mutants

(A) At D6 P.I.; Box and whisker plots showing relative mRNA levels of Notch pathway components in primary podocytes of mutants vs controls. Horizontal lines within the box show medians. The boundaries of the box nearest zero mark the 25% percentile, the boundaries farthest from zero mark the 75% percentile. Whiskers indicate outliers outside the 10% and 90% percentiles. $Cre-ER^{TM-/-};Wt1^{ff}$ vs. $Cre-ER^{TM+/-};wt1^{ff}$: *Wt1* (n=6 vs. n=6), 1 (IQR: 0.7, 1.8) vs. 0.2 (IQR: 0.2, 0.6), * $p=0.02$; *FoxC2* (n=5 vs. n=6), 1.5 (IQR: 0.4, 1.7) vs. 0.1 (IQR: 0.1, 0.7), * $p=0.03$; *Notch1* (n=6 vs. n=11), 0.9(IQR:0.7, 1.5) vs. 2.9(IQR: 0.9, 3.5), * $p=0.036$; *Notch2* (n=6 vs. n=10), 0.9 (IQR: 0.9, 1.2) vs. 1.2 (IQR: 0.8, 1.8), $p=0.41$; *Dll1* (n=6 vs. n=10), 1.2 (IQR: 0.4, 2.9) vs. 0.3 (IQR: 0.1, 2.8), $p=0.3$; *Dll4* (n=5 vs. n=5), 2.3 (IQR: 0.3, 2.5) vs. 0.1 (IQR: 0.04, 1.6), $p=0.15$; *Jag1* (n=6 vs. n=10), 1.1 (IQR: 0.6, 1.7) vs. 0.9 (IQR: 0.7, 1.2), $p=0.71$; *Jag2* (n=5 vs. n=5), 0.8 (IQR: 0.5, 2.2) vs. 0.5

(IQR: 0.4, 0.7), $p=0.15$; *Nrarp* (n=5 vs. n=5), 0.8 (IQR: 0.3, 1.8) vs. 3.8 (IQR: 3.1, 4.2), $**p=0.0087$; *Rbpj* (n=7 vs. n=10), 1 (IQR: 0.8, 1.3) vs. 1.5 (IQR: 1, 2.1), $p=0.05$; *Hes1* (n=6 vs. n=11), 1 (IQR: 0.7, 1.3) vs. 1.3 (IQR: 1, 2.2), $p=0.12$; *Hes3* (n=6 vs. n=11), 0.9 (IQR: 0.7, 1.7) vs. 1.3 (IQR: 0.9, 3.4), $p=0.17$; *Hes5* (n=6 vs. n=11), 0.9 (IQR: 0.7, 1.4) vs. 2.3 (IQR: 1.3, 6.2), $**p=0.005$; *Hey1*, (n=4 vs. n=5), 1.2 (IQR: 0.5, 1.8) vs. 2 (IQR: 1.2, 2.6), $p=0.29$; *Hey2*, (n=4 vs. n=5), 1.4 (IQR: 0.6, 1.5) vs. 3.9 (IQR: 2.1, 6), $*p=0.03$; *HeyL*, (n=5 vs. n=5), 1.1 (IQR: 0.6, 1.6) vs. 1.7 (IQR: 0.9, 4.8), $p=0.31$; *Mfng*, (n=9 vs. n=10), 0.9 (IQR: 0.5, 2.3) vs. 2.3 (IQR: 0.7, 5.7), $p=0.21$; *Lfng* (n=5 vs. n=5), 0.8 (IQR: 0.7, 1.6) vs. 0.8 (IQR: 0.5, 1.9), $p=0.8$; *Mb* (n=5 vs. n=5), 0.6 (IQR: 0.6, 2.3) vs. 1.3 (IQR: 0.6, 3.8), $p=0.53$. Mann-Whitney U test. Individual dot plots are shown in Appendix B. **(B)** Representative image of D6 P.I. glomeruli following double immunofluorescence labelling of mouse kidney sections with anti-cleaved Notch1 (Val1744, Alexa Fluor 594-conjugated secondary antibody) and anti-Nestin (demarcates podocytes, Alexa Fluor 488-conjugated secondary antibody) in *Cre-ERTM^{-/-};Wt1^{fl/fl}* (controls) and *Cre-ERTM^{+/-};Wt1^{fl/fl}* (mutants) counterstained with DAPI. Arrows indicate positive Cleaved Notch1 nuclear staining in mutant glomeruli within Nestin-positive cells, which are not detected in control glomeruli. Scale bar 50 μm . Inset display high power image of same cell, scale bar 10 μm . **(C, D)** western blot images of protein derived from primary podocytes isolated from mutant and control mice. Immunoblots show that **(C)** cleaved Notch1 [Val1744] and Pofut1 **(D)** are expressed at D6 P.I. in mutant podocytes and not in controls (Asfahani et al., 2018).

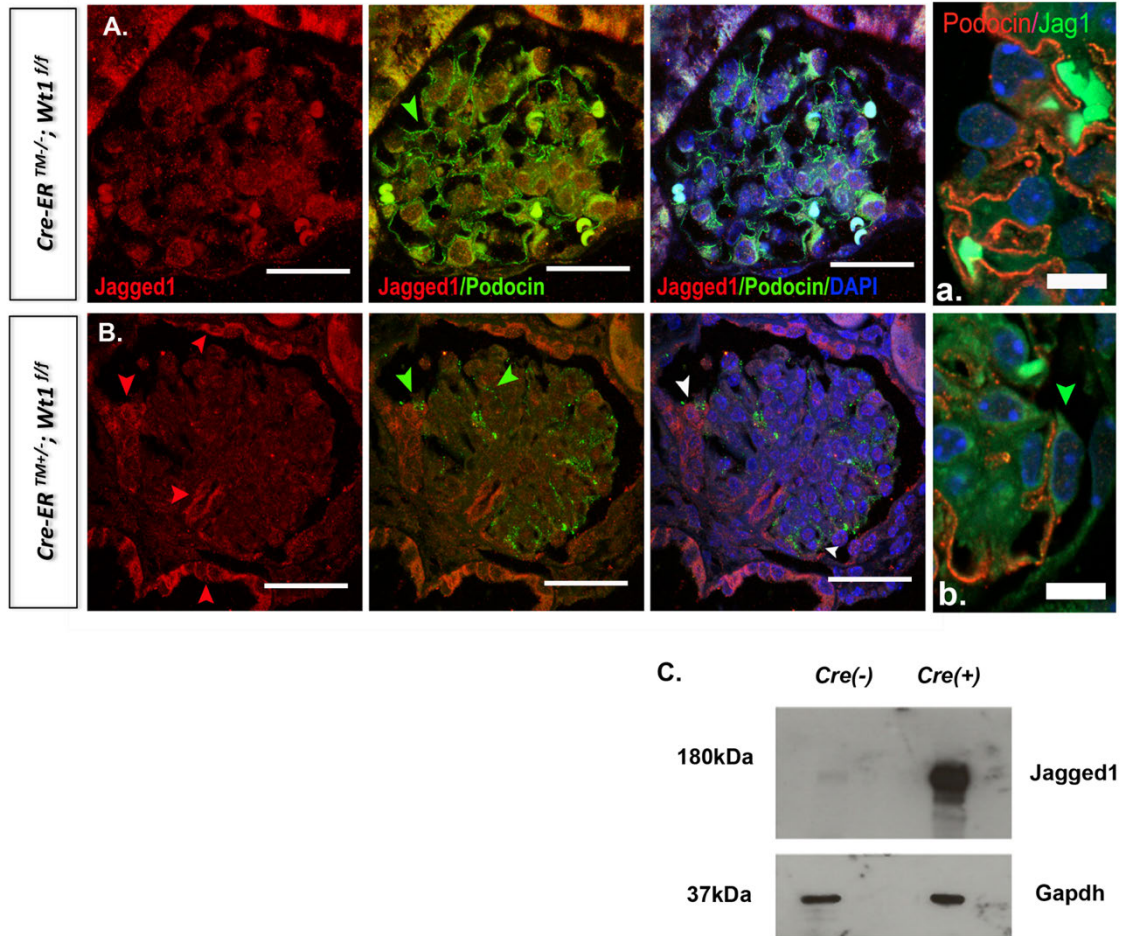


Figure 3.17. JAGGED 1 is expressed in *Cre-ERTM^{-/-};Wt1^{fl/fl}* glomeruli at disease onset

Representative images showing glomeruli double immunofluorescence labelled with anti-JA1 (Alexa Fluor 594–conjugated secondary antibody) and anti-Podocin (demarcates podocytes; Alexa Fluor 488–conjugated secondary antibody) in D6 P.I. mouse kidney sections of *Cre-ERTM^{-/-};Wt1^{fl/fl}* (control) and *Cre-ERTM^{-/-};Wt1^{fl/fl}* (mutant) mice. Sections are counterstained with DAPI. Positive Jagged1 staining in the parietal epithelium (red arrows), areas of podocyte adhesion (on the surface of Podocin-positive podocytes, green arrows, [B]; white arrows in merged image) to Bowman’s capsule and in the glomerular stalk of mutant glomeruli that are not evident in control glomeruli. Scale bar 50µm. **(A, B)** Higher-power views showing perimembranous expression of Jagged1 (green) in Podocin-positive podocytes (red) in controls **(a)** compared to mutants **(b)**. **(C)** Western blot analyses of protein derived from primary podocytes isolated from mutants and control mice. Jagged1 is shown to be increased at D6 P.I. in mutant podocytes but not in controls.

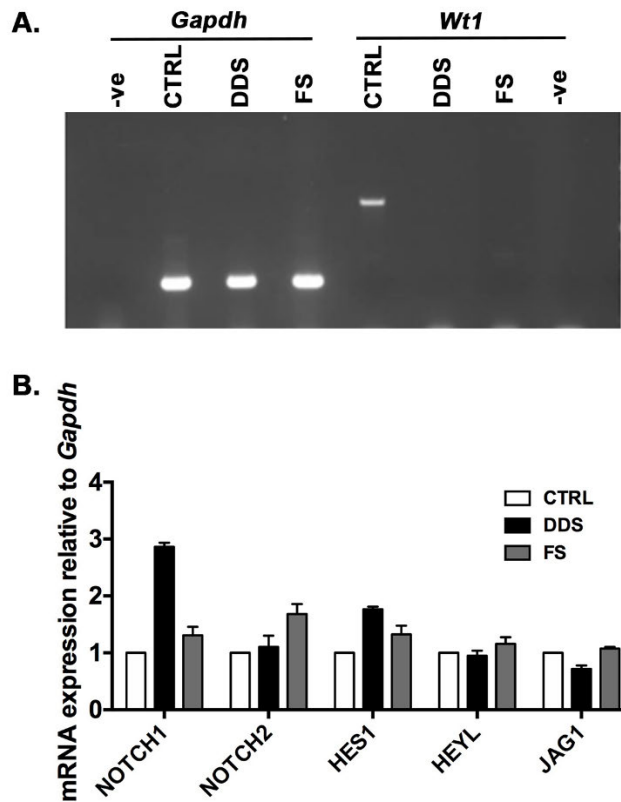


Figure 3.18. Increased Notch pathway transcripts in primary mutant *WT1* podocytes

(A) *WT1* is absent in patients carrying *WT1* mutations compared to control DNA. *GAPDH* expression is equal amongst all groups. **(B)** Relative transcript levels of the Notch pathway in controls lacking *WT1* mutations vs. DDS (exon 8 C1096T mutation) and FS (intron 9 splice site mutation) patients. Bars represent the median, error bars represent the IQR; Ctrl (n=3) vs. DDS (n=3): *NOTCH1*, 1 ± 0 (IQR: 1, 1) vs. 2.9 (IQR: 2.5, 2.9), $p=0.1$; *NOTCH2*, 1 ± 0 (IQR: 1, 1) vs. 1.1 (IQR: 1.1, 1.3), $p=0.1$; *HES1*, 1 (IQR: 1, 1) vs. 1.8 (IQR: 1.1, 1.8), $p=0.1$, *HEYL*, 1 (IQR: 1, 1) vs. 0.9 (IQR: 0.6, 1), $p=0.7$; *JAG1*, 1 (IQR: 1, 1) vs. 0.7 (IQR: 0.7, 0.8), $p=0.1$. Ctrl (n=3) vs. FS (n=3): *NOTCH1*, 1 (IQR: 1, 1) vs. 1.3 (IQR: 1.2, 1.5), $p=0.1$; *NOTCH2*, 1 (IQR: 1, 1) vs. 1.7 (IQR: 1.3, 1.9), $p=0.1$, *HES1*, 1 (IQR: 1, 1) vs. 1.3 (IQR: 1.3, 1.5), $p=0.1$, *HEYL*, 1 (IQR: 1, 1) vs. 1.2 (IQR: 1, 1.3), $p=0.1$, *JAG1*, 1 (IQR: 1, 1) vs. 1.1 (IQR: 0.9, 1.1), $p=0.7$. DDS (n=3) vs. FS (n=3): *NOTCH1*, $p=0.1$; *NOTCH2*, $p=0.2$; *HES1*, $p=0.7$; *HEYL*, $p=0.1$; *JAG1*, $p=0.1$. Mann-Whitney U test. DDS, Denys-Drash syndrome; FS, Frasier syndrome

3.2.3.2 *HES1* is apparent at the onset of GS and is associated with podocyte EMT

We next investigated the activation of *Hes* and *Hey* in early disease. Immunofluorescence revealed expression of *Hes1* in Synaptopodin-positive podocytes at the onset of GS in mutants compared with controls (Figure 3.19A, B). *Hes1*-positive glomerular epithelial cells exhibited *Hes1* protein distinctive from *Hes1*-positive LTL-positive tubules, indicating Notch activation specifically in the podocytes (Figure 3.19B, B'). *Hes1* protein was also revealed as clusters in the Synaptopodin-positive podocytes

compared to PECAM-positive glomerular endothelial cells of the mutants (Figure 3.19 D, D'). Hes1 was absent in the Synaptopodin-positive cells of controls (Figure 3.19C).

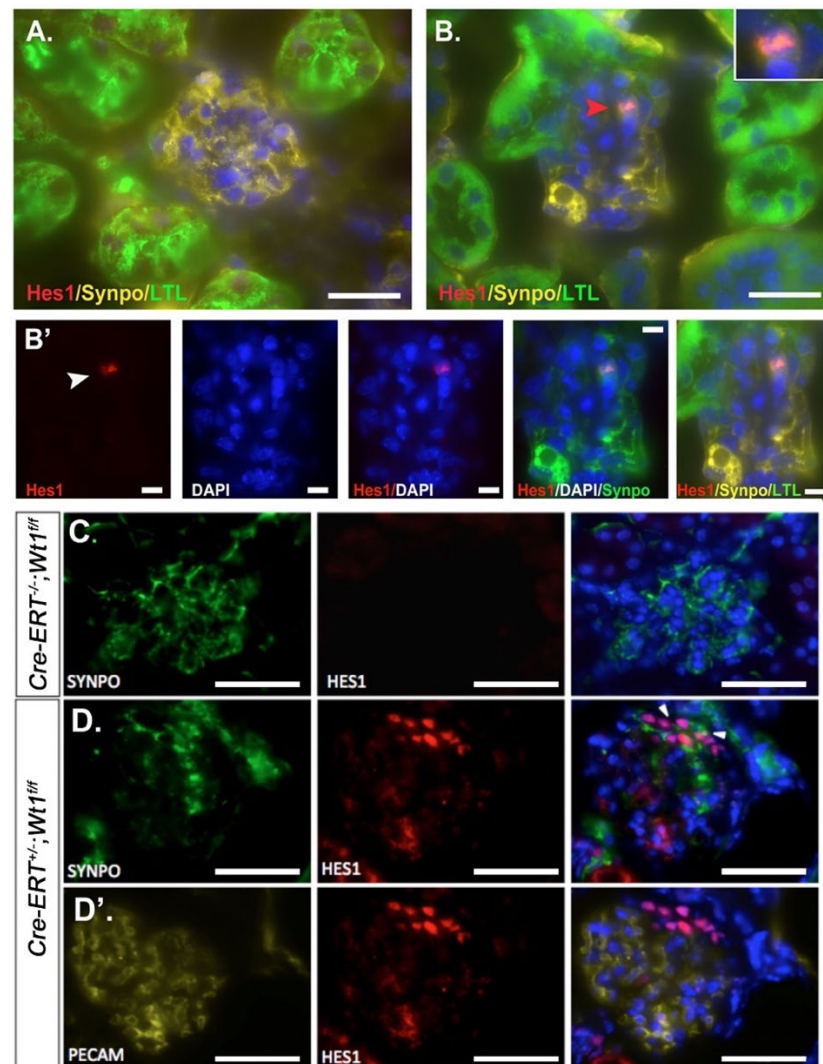


Figure 3.19. Podocyte Hes1 expression coincides with onset of GS in $Cre-ER^{TM+/-};Wt1^{ff}$ mutants

(A, B, B') D5 P.I. glomeruli following double immunofluorescence labelling of mouse kidney sections with anti-Hes1 (Alexa Fluor 594–conjugated secondary antibody), anti-Synaptopodin (SYNPO, demarcates podocytes (Alexa Fluor 647–conjugated secondary), and LTL, demarcates tubules (Alexa Fluor 488–conjugated secondary antibody) of $Cre-ER^{TM-/-};Wt1^{ff}$ (control) and $Cre-ER^{TM+/-};Wt1^{ff}$ (mutant) transgenic mice. Sections are counterstained with DAPI. Scale bar, 50 μ m. **(B, B')** Hes1-positive, SYNPO-positive glomerular epithelial cells were observed in regions distinct from LTL-positive tubules in the mutants. Scale bar, 50 μ m. **(B')** 10 μ m. **(C, D, D')** Segmental clusters of nuclear Hes1 expression in Synpo-positive, PECAM-negative podocytes detected in glomeruli of the mutants and not in the control glomeruli. Scale bar, 50 μ m. (Asfahani et al., 2018)

Due to HES1's association with EMT (Wang et al., 2015), we tested whether there was an upregulation of *Snail* and *Slug* mRNAs in D6 P.I. mutant podocytes compared to

controls (Figure 3.20A). Both EMT transcript levels were significantly increased in the mutants compared to controls, suggesting a role for *Hes1* inducing EMT gene expression. To examine this, primary podocytes were isolated from *Nphs2;rtTA* mice, cultured, and transfected with constructs expressing either Tet-O-*Hes1* or GFP. *Hes1* was not detected in untreated Tet-O-*Hes1* nor doxycycline-treated GFP transfected *Nphs2;rtTA* podocytes (Figure 3.20B). Dose-dependent doxycycline treatment led to an increase in podocyte *Hes1* mRNA and protein expression (Figure 3.20B, C, Figure 3.21). Induction of *Hes1* expression led to a 3-fold upregulation of *Snail* and *Slug* mRNAs compared to untreated TetO-*Hes1* transfected and doxycycline-treated GFP transfected *Nphs2;rtTA* podocytes (Figure 3.20C). Thus, the induction of *Hes1* in podocytes could facilitate manifestation of GS by controlling expression of EMT genes in podocytes.

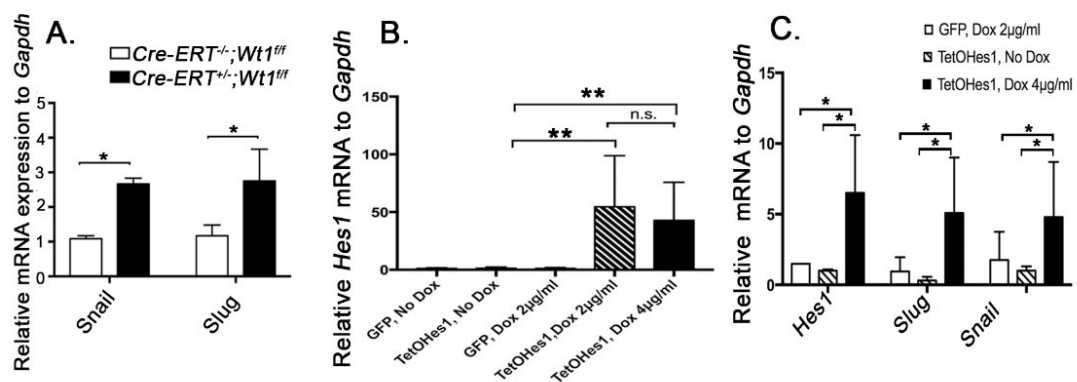


Figure 3.20. Upregulation of podocyte EMT genes in *TetOHes1*-induced podocytes

(A) Graph at D6 P.I. showing an upregulation of podocyte *Snail* and *Slug* EMT transcripts. Median *Snail* mRNA expression at D6 PI in control vs mutant mice: 1.1 (interquartile range [IQR]: 0.9, 1.2) vs. 2.7 (IQR:1.8, 2.8), $*p=0.045$, Mann-Whitney. Median *Slug* mRNA expression at D6 PI in control vs. mutant mice: 1.2 (IQR: 0.6, 1.5) vs. 2.8 (IQR: 1.4, 3.7), $*p= 0.03$, Mann-Whitney. **(B)** *Hes1* mRNA expression is increased in doxycycline-treated primary *Nphs2;rtTA* podocytes transduced with TetO*Hes1* plasmid vs. untreated TetO*Hes1* and treated green fluorescence protein (GFP)-transduced primary *Nphs2;rtTA* podocytes. Mean *Hes1* mRNA expression relative to *Gapdh* (\pm SD): untreated control (GFP) vs. untreated TetO*Hes1* vs. treated control (doxycycline 2 μ g/ml) vs. treated TetO*Hes1* (2 μ g/ml) vs. treated TetO*Hes1* (4 μ g/ml): 1.15 \pm 0.66 vs. 1.26 \pm 1.13 vs. 1.21 \pm 0.88 vs. 54.56 \pm 44.24 ($**p<0.004$) vs. 42.78 \pm 33.07 ($**p<0.008$). No significant difference in dose-response was observed, $p=.045$ (n.s.). **(C)** EMT genes, *Snail* and *Slug* are upregulated in doxycycline-treated primary *Nphs2;rtTA* podocytes transduced with TetO*Hes1* plasmid vs. untreated TetO*Hes1* and treated GFP-transduced primary *Nphs2;rtTA* podocytes. Untreated control (GFP) vs. untreated TetO*Hes1* vs. treated TetO*Hes1* (4 μ g/ml): mean *Snail* mRNA expression relative to *Gapdh* (\pm SD): 1.76 \pm 2.1 vs. 1.01 \pm 0.31 vs. 4.82 \pm 3.94, $*p< 0.05$. Mean *Slug* mRNA expression relative to *Gapdh* (\pm SD): 0.95 \pm 1.12 vs. 0.31 \pm 0.26 vs. 5.10 \pm 0.3, $*p<0.05$. (Asfahani et al., 2018)

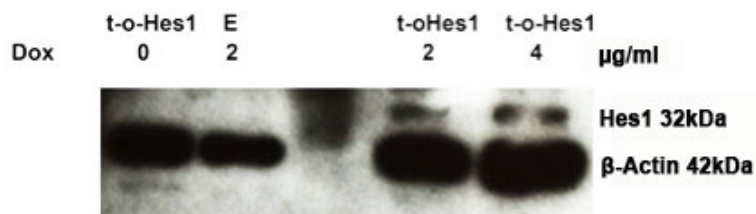


Figure 3.21. Hes1 is increased post-doxycycline treatment in *Nphs2;rtTA*-transduced podocytes

Western blot analysis showing a representative image of protein lysates from doxycycline-treated primary *Nphs2;rtTA* podocytes transduced with *TetoHes1* (t-o-Hes1) and GFP plasmids. Increased Hes1 protein expression was detected following a dose increase of doxycycline in the *tetoHes1* transduced podocytes. No Hes1 protein expression was observed in GFP-transduced *Nphs2;rtTA* podocyte lysates post-doxycycline treatment (Asfahani et al., 2018).

In addition to analysis of Notch activation in *Wt1* glomerulopathy in mice, we examined biopsy samples from an FSGS patient with the mutation *WT1c.1390G>T*. JAGGED1 protein was detected in cells with focal NEPHRIN staining in the patient but was predominantly in the parietal epithelium (Figure 3.22A, bottom panel). The control samples, which were non-diseased time-zero renal transplant biopsies, showed JAGGED1 expression in regions distal to NEPHRIN suggesting that there was endothelial JAGGED1 expression (Figure 3.22A, top panel). JAGGED1 was not observed in the control parietal epithelium to the extent that was seen in the mutant *WT1* patient tissue. The bHLH transcription factor, HES1 was also examined by immunofluorescence staining on the patient tissue and was detected in the podocytes (Figure 3.22B, bottom panel) compared to the control biopsy tissue (Figure 3.22B, top panel).

The data above has highlighted an increase in the Notch pathway components in *Wt1* glomerulopathy in both murine and patient samples, supporting a role for Notch activation in human *WT1*-mediated glomerular disease. A recent study has shown that both *Jag1* and *Notch2* are associated with kidney fibrosis in mouse models of folic-acid (FA)-induced nephropathy, UUO and apolipoprotein L1 (APOL1)-associated kidney disease (Huang et al., 2018). Similarly, our immunohistochemistry and Western blot findings show that *Jag1* may be playing a role in the activation of Notch1 in *Wt1* glomerulopathy.

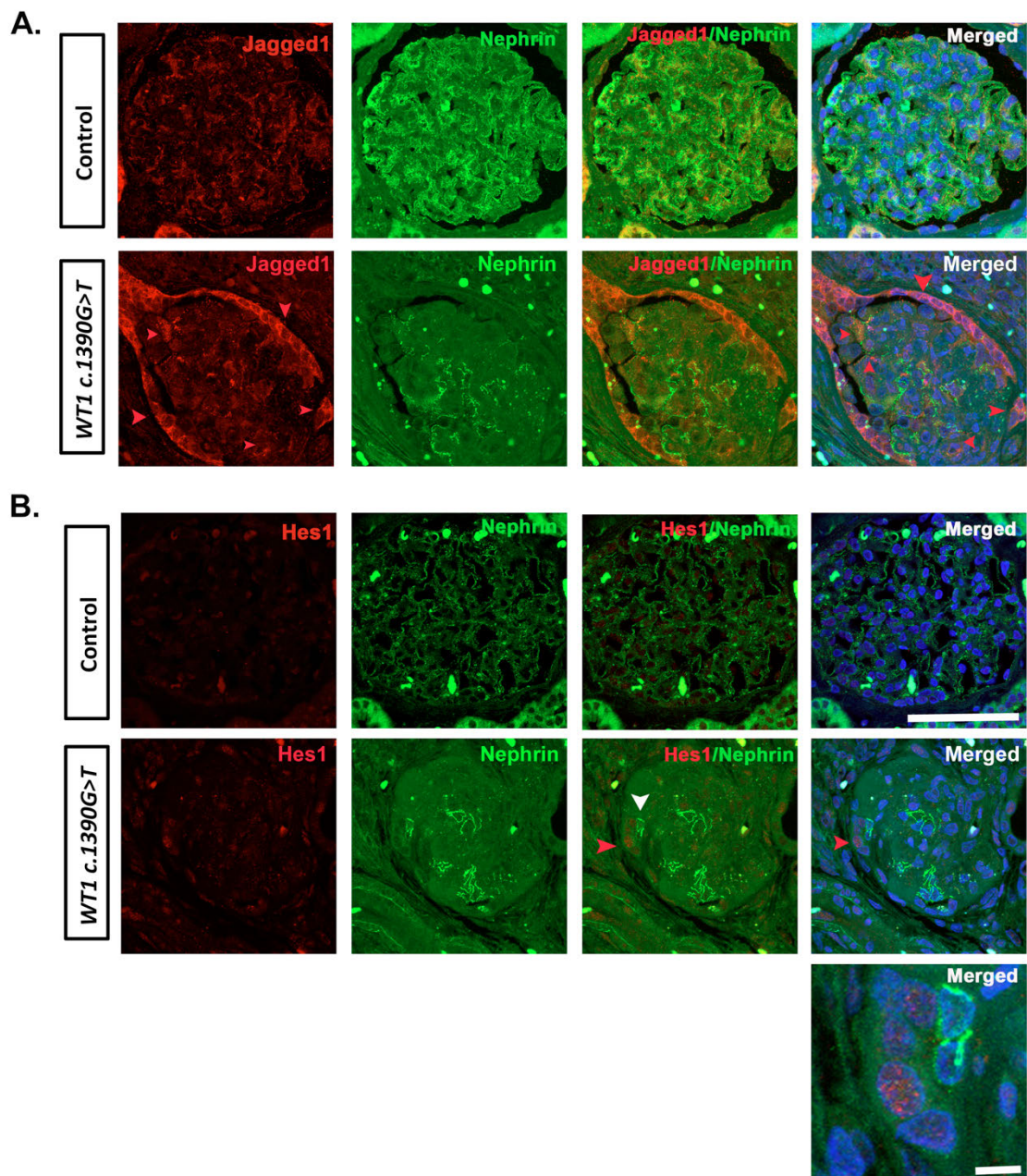


Figure 3.22. JAGGED1 and HES1 are expressed in *WT1 c.1390G>T* (p.Asp464Asn) human glomeruli

(A, B) Representative micrographs of glomeruli following double immunofluorescence labelling of human kidney sections from control (time-zero renal allograft biopsy) and *WT1 c.1390G>T* mutant patient with anti-JAGGED1 (A) or anti-HES1 (B) antibodies (Alexa Fluor 594) and anti-Nephrin antibody (demarcates podocyte slit diaphragm, Alexa Fluor 488). (A) JAGGED1 is upregulated in parietal epithelium of *WT1 c.1390G>T* glomeruli vs. controls (red arrows) and is also expressed in a linear pattern associated with focal NEPHRIN staining in podocytes. JAGGED1 expression is also detected in the endothelium of time-zero allograft glomeruli, which do not exhibit GS. Scale bars, 50 μ m. (B) Increased HES1 expression is observed in nuclei of cells adjacent to NEPHRIN-positive podocytes of *WT1 c.1390G>T* glomeruli with advanced GS. Scale bars, 50 μ m (Asfahani et al., 2018).

3.2.4 Notch inhibition ameliorates disease severity in *Wt1* glomerulopathy

Finding that there was an activation of the Notch pathway in early disease, we next determined the consequences of γ -secretase inhibition in *Cre-ER^{TM+/-};Wt1^{ff}* mutant mice to inhibit Notch during disease manifestation. Mice were given an intraperitoneal injection of the γ -secretase inhibitor, GSI-IX (DAPT), at late D4 P.I. and a second dose was given 16 hours later (D5 P.I.). Mice were then sacrificed at least 8 hours following the second treatment. Paraffin-embedded PAS-stained tissue sections were examined using a light microscope to score the severity of GS in the GSI-IX-treated vs. vehicle (DMSO only)-treated mutants, treated at the same time. Hyaline-filled tubules were observed in the vehicle-treated mutants, showing evidence of proteinaceous material in the tissues. Sclerotic glomeruli with mesangial proliferation were also evident in the vehicle-treated mutants (Figure 3.23B), whilst these features were not exhibited in the GSI-IX-treated mutants (Figure 3.23C). GS was significantly higher in the vehicle-treated mutant glomeruli compared to the GSI-IX-treated mutants ($**p=0.008$) (Figure 3.23D).

The hypothesis that podocyte Notch activation is likely a ligand-dependent event is supported by the efficacy of GSI inhibition in manifestation of early glomerulopathy. GSI-IX-treated mutants showed improved urine albumin/creatinine ratio in contrast to the vehicle-treated mutants ($*p=0.02$) (Figure 3.23F). Notch transcript levels were reduced post-GSI treatment compared to the vehicle-treated mutants (Figure 3.23E). *Wt1* transcript levels and protein expression were verified by real-time qPCR and immunofluorescence in both GSI-IX- and vehicle-treated mutants to confirm whether any alteration of *Wt1* expression was observed following treatment (Figure 3.24). There was no significant difference of *Wt1* transcript levels between the vehicle- and the GSI-IX-treated mutant mice (Figure 3.24B) as well as no difference in WT1 protein expression. *Cre-ER^{TM-/-};Wt1^{ff}* controls were used for comparison of *Wt1* levels post-tamoxifen induction, and it was evident that *Wt1* expression was reduced in the mutants vs. *Cre-ER^{TM+/-};Wt1^{ff}* controls on an mRNA and protein level. To examine urine albumin levels further, Western blot analysis revealed absence of albuminuria in the GSI-IX-treated mice compared to vehicle-treated mutants at D5 P.I. (Figure 3.23G).

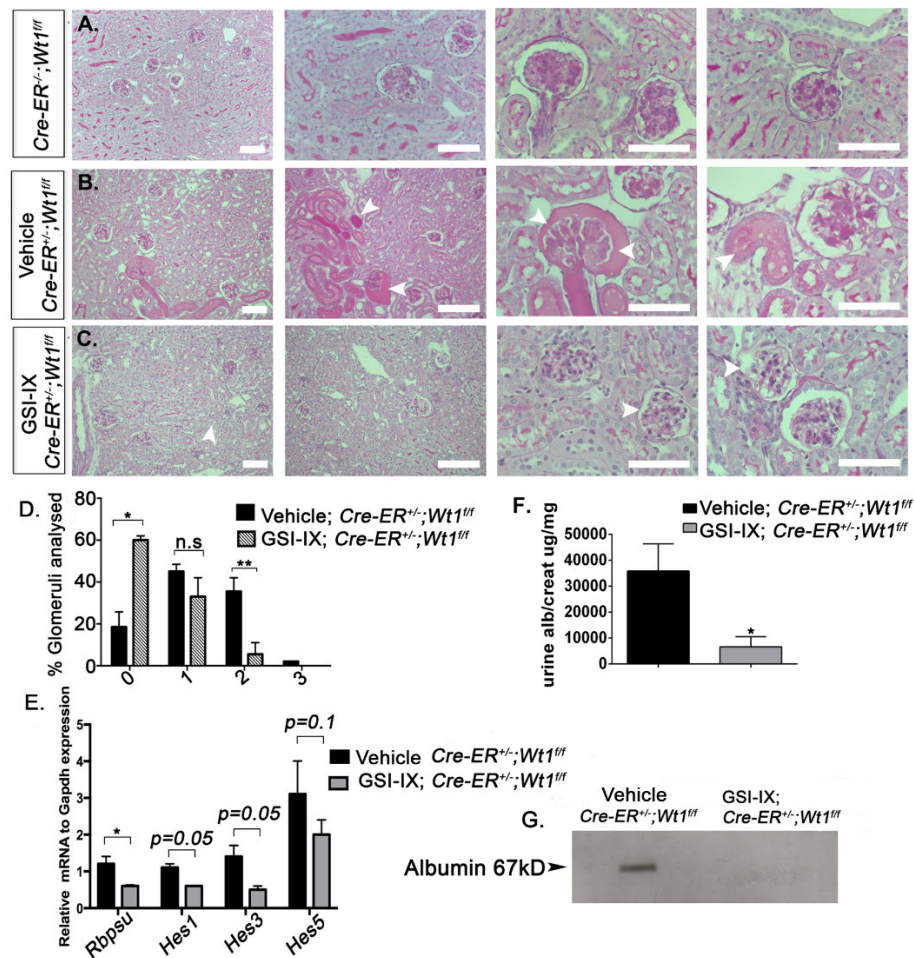


Figure 3.23. γ -secretase inhibition of Notch ameliorates early *Wt1* glomerulopathy

(A) PAS-stained sections of D5 P.I. *Cre-ER^{TM+/-};Wt1^{ff}* mutants. (B) Vehicle-treated *Cre-ER^{TM+/-};Wt1^{ff}* mutants. (C) GSI-IX-treated *Cre-ER^{TM+/-};Wt1^{ff}* mutants. Scale bar, 50 μ m. (A, B) GS with hyaline material in the tubules in mutants and vehicle-treated mice. (C) Glomeruli of GSI-IX-treated mutants present lower levels of GS vs. vehicle-treated mutants. (D) Graph showing proportion in glomeruli per genotype with different levels of GS (score 0: <25% sclerosis; score 1: 25%–50% sclerosis; score 2: 50%–75% sclerosis; score 3: >75% sclerosis). Bars show mean percentage of scores, error bars show SEMs. Normal glomerular morphology was present in a higher proportion of GSI-IX-treated *Cre-ER^{TM+/-};Wt1^{ff}* transgenic mice (n=52 glomeruli, n=5 mice) compared with vehicle-treated *Cre-ER^{TM+/-};Wt1^{ff}* (mutants) at D5 P.I. (n=52 glomeruli, n=4 mice): vehicle-treated *Cre-ER^{TM+/-};Wt1^{ff}* vs. GSI-IX-treated *Cre-ER^{TM+/-};Wt1^{ff}* transgenic mice: score 0: 18.09% vs. 59.10%, * p <0.02, Student's t-test; score 2: 39.5% vs. 8.3%, * p <0.008, Student's t-test. (E) Graph showing reduced mean relative *Rbpsuh*, *HES1*, *Hes3*, and *HES5* mRNA expression from cultured podocytes from GSI-IX-untreated vs. untreated mutant mice: *Rbpsuh*, 1.2±0.2 vs. 0.6±0.03, * p =0.01; *Hes1*, 1.1±0.1 vs. 0.6±0.01, p =0.05; *Hes3*, 1.4±0.3 vs. 0.5±0.1, p =0.05; *Hes5*: 3.1±0.9 vs. 2.0±0.4, P =0.1. Bars represent means and error bars represent SEMs. (F) Graph illustrating median urine albumin-creatinine ratio in vehicle-treated vs. GSI-IX-treated mutant mice. Bars represent the median of each group. Error bars represent the interquartile ranges (IQRs): *Cre-ER^{TM+/-};Wt1^{ff}* vs. GSI-IX-treated *Cre-ER^{TM+/-};Wt1^{ff}* mice: 35,836 (IQR: 21,304, 46,371) vs. 6,657 (IQR: 1,337, 10,565), * p =0.02, Mann-Whitney test. (G) Western blot analysis reveals albumin in urine samples of vehicle-treated vs. GSI-IX-treated mutant mice (MW albumin, 66.5 kDa), n=3 mice/group (Asfahani et al., 2018).

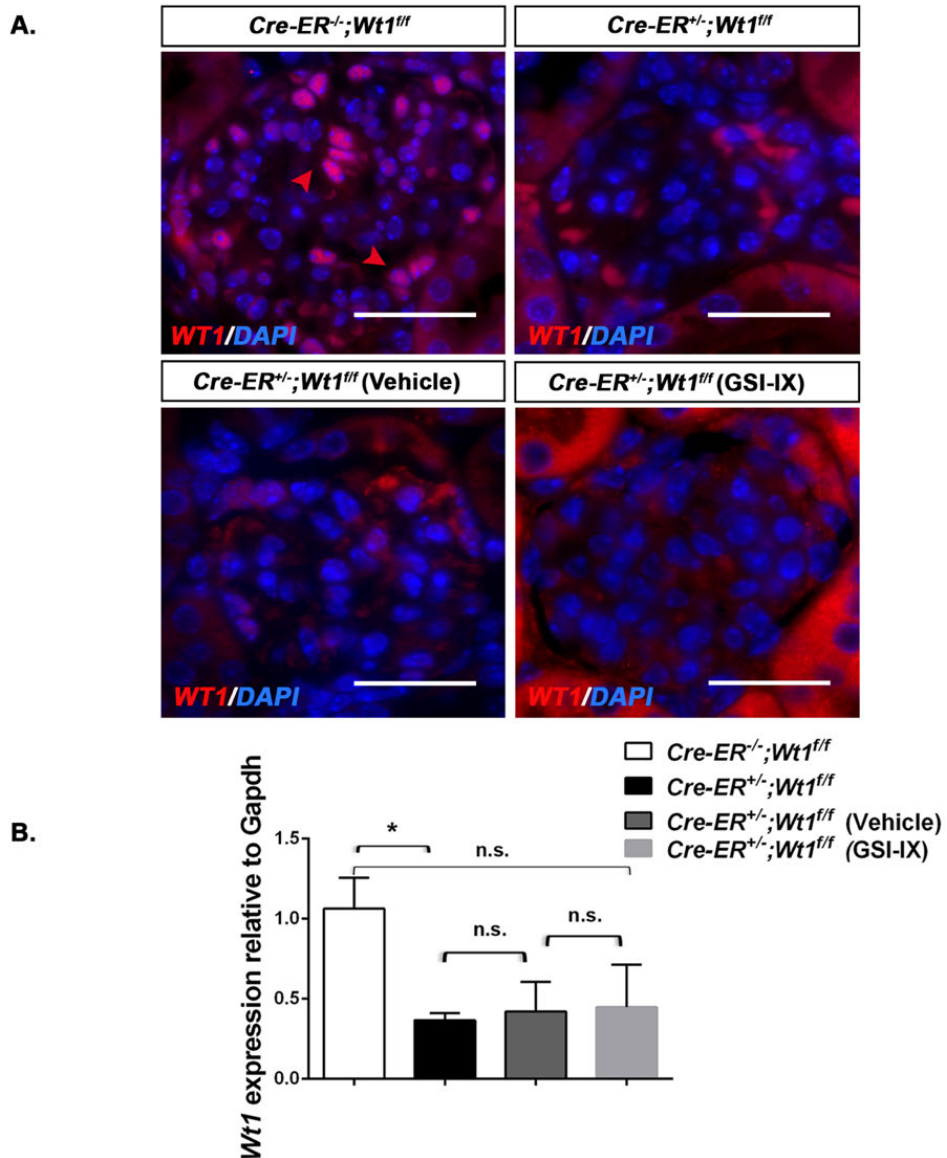


Figure 3.24. *Wt1* transcript and protein levels are comparable in *Cre-ER^{TM+/-};Wt1^{f/f}* mutants post- γ -secretase inhibition and vehicle treatment

(A) Representative images of glomeruli following immunofluorescence labelling of kidney sections: *Cre-ER^{TM-/-};Wt1^{f/f}* (control), *Cre-ER^{TM+/-};Wt1^{f/f}* (mutant), vehicle-treated *Cre-ER^{TM+/-};Wt1^{f/f}* and GSI-IX-treated *Cre-ER^{TM+/-};Wt1^{f/f}* transgenic mice with anti-WT1 (Alexa Fluor 594-conjugated secondary antibody). WT1 is evident in control and reduced in the mutants. **(B)** Quantitative graph illustrating relative transcript levels of *Wt1* in primary podocytes of *Cre-ER^{TM-/-};Wt1^{f/f}* (control), *Cre-ER^{TM+/-};Wt1^{f/f}* (mutant), vehicle-treated *Cre-ER^{TM+/-};Wt1^{f/f}* and GSI-IX treated *Cre-ER^{TM+/-};Wt1^{f/f}* transgenic mice. Bars signify the mean, error bars denote the standard error of the mean, (SEM). *Cre-ER^{TM-/-};Wt1^{f/f}* vs. *Cre-ER^{TM+/-};Wt1^{f/f}*: 1.1 ± 0.2 vs. 0.4 ± 0.4 , $*p=0.03$; *Cre-ER^{TM-/-};Wt1^{f/f}* vs. vehicle-treated *Cre-ER^{TM+/-};Wt1^{f/f}* mice: 1.1 ± 0.2 vs. 0.4 ± 0.2 , $p=0.07$; vehicle-treated *Cre-ER^{TM+/-};Wt1^{f/f}* vs. GSI-IX treated *Cre-ER^{TM+/-};Wt1^{f/f}*: 0.4 ± 0.2 vs. 0.4 ± 0.3 , $p=0.93$, Student t-test, $n=6$ mice/group (Asfahani et al., 2018).

We next tested the effects of GSI-IX treatment in established disease by inhibiting γ -secretase at D7 P.I. in *Cre-ERTM+/-;Wt1^{ff}* mutant mice. Mice were treated with the compound twice and late D8 P.I. kidney histology analysed by PAS staining using a light microscope (n=2 mice) following tissue harvest. There was no significant difference in the severity of GS or albumin levels between the GSI-IX- and vehicle-treated mutants at this time-point (Figure 3.25A, E). In fact, a scoring of 3 for GS was relatively high in both groups (Figure 3.25C). Albumin/creatinine levels were lower in the GSI-IX-treated mutants; however, the difference did not reach statistical significance (Figure 3.25D). Furthermore, immunofluorescence revealed no difference in tubulointerstitial expression of vascular smooth muscle actin between both groups (Figure 3.25B).

These data illustrate that the activation of Notch in podocytes occurs in early *Wt1* glomerulopathy. Additional mice need to be analysed to further establish the effect of GSI-inhibition at later time-points.

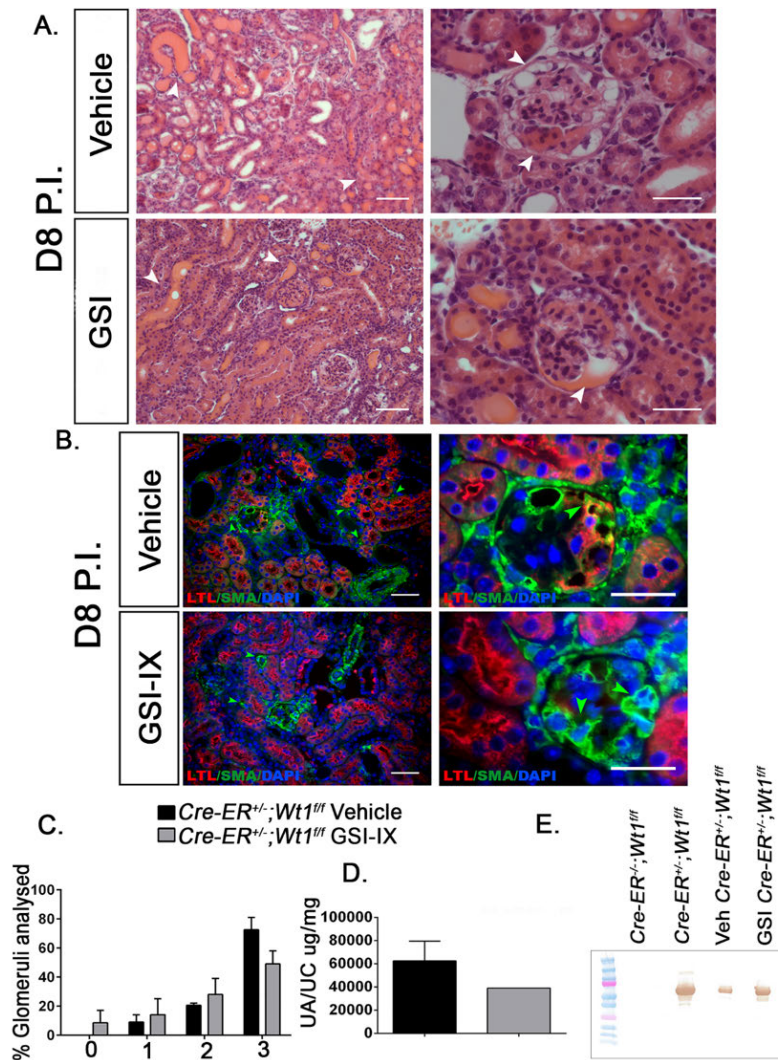


Figure 3.25. γ -secretase inhibition in *Cre-ER^{TM+/-};Wt1^{ff}* at D8 P.I. does not rescue GS

(A) Representative images of H&E stained kidney sections of GSI-IX-treated *Cre-ER^{TM+/-};Wt1^{ff}* and vehicle (DMSO)-treated *Cre-ER^{TM+/-};Wt1^{ff}* mutant mice treated at D8 P.I. Global GS with hyaline material in the tubules is observed in vehicle-treated mice (**top panel**). A lower power image of glomeruli and tubules is presented in the top left, with hyaline material in the tubules (indicated by white arrows, Scale bar 50 μ m); A high-power image of the glomerulus is shown in the top right panel exhibiting global glomerulosclerosis (indicated by white arrows, scale bar 25 μ m). The same level of GS is displayed in glomeruli of GSI-IX treated mice (**bottom panel**) and vehicle-treated mice, with global GS. Bottom left image shows a lower power image of the glomeruli and tubules, with hyaline-filled tubules (indicated by white arrows, Scale bar 50 μ m); Bottom right panel displays a high-power image of the glomerulus, with severe glomerulosclerosis (indicated by white arrows, Scale bar 25 μ m). **(B)** Merged images of kidney sections following double immunofluorescence labelling of vehicle- and GSI-IX-treated *Cre-ER^{TM+/-};Wt1^{ff}* kidney tissue sections with α -SMA (Alexa Fluor 488-conjugated secondary antibody) and LTL (Alexa Fluor 594-conjugated secondary antibody) (scale bars, 50 μ m). Top panel represents lower power image (left) of the tubules and glomeruli in vehicle-treated mutants, highlighting α -SMA between the tubules (green arrows), indicating tubulointerstitial disease; higher power (right) shows α -

SMA- positive staining in dilated capillary loop (green arrow). Bottom panel; low power image (left) of the tubules and glomeruli in GSI-IX-treated mutants, showing α -SMA in peritubular interstitium (green arrows); higher power (right) images highlights the glomerulus with α -SMA expression within the glomerular tuft (green arrows). **(C)** Graph illustrating semi-quantitative GS scoring (Score 0-3, 0, < 25%, 1, 25-50%, 2, 50-75%, 3, >75% sclerosis). Vehicle-treated mutants (n=62 glomeruli, n=2 mice) vs. GSI-IX-treated mutants (n=66 glomeruli, n=2 mice): Bars symbolise the mean of each group, error bars display the standard error of the mean (SEM). Score 0: 0% vs. 8.5 \pm 8.5% ($p=0.42$); Score 1: 9 \pm 5% vs. 28.5 \pm 3.5% ($p=0.09$); Score 2: 20.5 \pm 1.5% vs. 28 \pm 11% ($p=0.57$); Score 3: 72.5 \pm 8.5% vs. 49 \pm 9% ($p=0.20$) Student t-test. **(D)** Quantitative graph showing mean urine albumin/creatinine ratio in vehicle- (n=3) vs. GSI-IX-treated (n=1) *Cre-ER^{TM+/-};Wt1^{ff}* transgenic mice. Bars represent the mean; error bars represent the standard error of the mean (SEM). **(E)** Albuminuria is detected by Western blot analysis in D8 P.I., *Cre-ER^{TM+/-};Wt1^{ff}* (mutant), vehicle-treated *Cre-ER^{TM+/-};Wt1^{ff}* and GSI-IX treated *Cre-ER^{TM+/-};Wt1^{ff}* transgenic mice but not in *Cre-ER^{TM-/-};Wt1^{ff}* control mice [MW of albumin, 66.5kDa] (Asfahani et al., 2018).

3.2.5 Podocyte epithelial-mesenchymal transition (EMT) in *Cre-ER^{TM+/-};Wt1^{ff}* mutants at the onset of *Wt1* glomerulopathy

As previously mentioned, the Notch pathway consists of ligand binding, which is affected by the glycosyltransferases; Manic, Lunatic and Radical Fringe, located in the Golgi (Okajima et al., 2003, Bray, 2006, Kakuda and Haltiwanger, 2017). The Fringes bind to the EGF domains of the extracellular domain of the Notch receptors, affecting which ligands the Notch receptors bind to prior to the activation of the Notch pathway (Kopan and Ilagan, 2009, Taylor et al., 2014, Kakuda and Haltiwanger, 2017). Studies have shown that when Fringe proteins bind to different parts of the EGF domains of the receptors, the affinity of binding with either the Dll or Jag families gets influenced (Kakuda and Haltiwanger, 2017).

As *Mfng* and *Rbpj* transcript levels were upregulated at D6 P.I. (Figure 3.26A, C), we sought to determine the influence of knockdown of both transcripts on podocyte EMT and apoptotic gene expression. Although both *Mfng* and *Rbpj* levels were reduced following knockdown, with repression of the Notch bHLH transcripts, there was no sign of a significant decrease of the EMT genes, *Snail* and *Slug*, nor a significant upregulation of podocyte-specific transcripts including *Nphs1* and *Nphs2* (Figure 3.26). Sample numbers were very low (n=2 mice/group), therefore we could not draw final conclusions for this data. Podocytes that were transfected were the only available D6 P.I. cells. This was due to slow growth, apoptosis, and the viability of the primary mutant podocytes. In

future, higher sample numbers of podocytes that show increased transcript levels of the BHLH transcription factors would be selected.

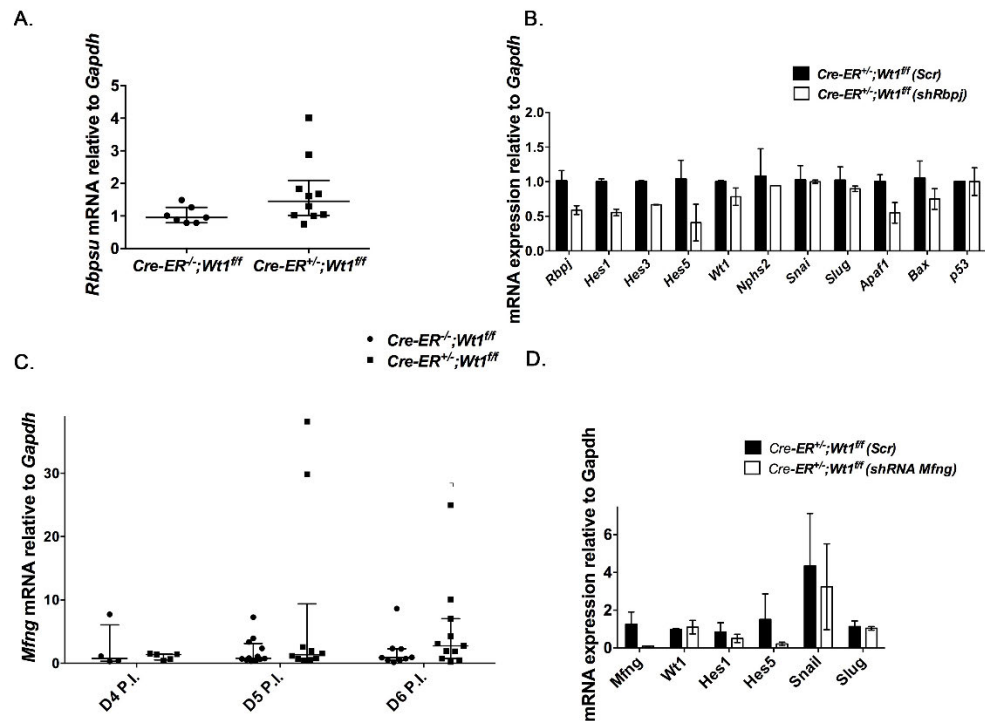


Figure 3.26. *Mfng/Rbpj* shRNA knockdown in *Cre-ERTM+/-;Wt1ff* podocytes repress Notch BHLH transcripts

(A) Dot plot analysis showing the median relative transcript mRNA levels of *Rbpj* (canonical Notch target) in D6 P.I. primary podocytes of *Cre-ERTM+/-;Wt1ff* controls cultured for 6 days (n=7) vs. *Cre-ERTM+/-;Wt1ff* mutants (n=10). Error bars represent the interquartile range (IQR). *Rbpsuh* expression is increased in D6 P.I. *Cre-ERTM+/-;Wt1ff* vs. *Cre*-negative controls: 0.95 (IQR: 0.79, 1.27) vs. 1.45 (IQR: 1.01, 2.09), $p=0.05$. Mann-Whitney test. **(B)** Relative transcript levels of *Rbpj*, Notch bHLH components, *Hes1*, 3 and 5, *Snai*, *Slug* (markers of EMT), podocyte-specific transcripts *Wt1*, *Nphs1* and *Nphs2* and apoptosis components, *Apaf1*, *Bax* and *p53* following 48 hours of *Rbpj* shRNA knockdown. Bars represent the median, error bars represent the IQR. Scrambled shRNA (SCR) *Cre-ERTM+/-;Wt1ff* mutants (n=2), vs. shRNA *Rbpj*-*Cre-ERTM+/-;Wt1ff* mutants (n=2); *Rbpj*, 1.0 (IQR: 0.9, 1.2) vs. 0.6 (IQR: 0.5, 0.7), $p=0.33$; *Hes1*, 1.0 (1, 1) vs. 0.6 (IQR: 0.5, 0.6), $p=0.33$; *Hes3*, 1.0 (IQR: 1, 1) vs. 0.7 (IQR: 0.7, 0.7), $p=0.33$; *Hes5*, 1.0 (IQR: 0.8, 1.3) vs. 0.4 (IQR: 0.1, 0.7), $p=0.33$; *Wt1*, 1.0 (IQR: 1,1) vs. 0.8 (0.7, 0.9), $p=0.33$; *Snai*, 1.0 (IQR: 0.8, 1.2) vs. 1.0 (IQR: 1, 1), $p>0.99$; *Slug*, 1.0 (IQR: 0.8, 1.2) vs. 0.9 (IQR: 0.9, 0.9), $p>0.99$; *Apaf1*, 1.0 (IQR: 0.9, 1.1) vs. 0.71 (IQR: 0.5, 0.9), $p=0.67$; *Bax*, 1.1 (IQR: 0.7, 1.4) vs. 0.8 (IQR: 0.6, 1), $p=0.67$; *p53*, 1.0 (IQR: 1, 1) vs. 0.7 (IQR: 0.5, 0.9), $p=0.33$. Mann Whitney U test. **(C)** Representative dot plot analysis showing the median relative transcript mRNA levels of Manic Fringe in *Cre-ERTM+/-;Wt1ff* controls vs. *Cre-ERTM+/-;Wt1ff* mutants at D4, D5 and D6 P.I. Error bars represent the IQR. D4: *Mfng*: 0.8 (IQR: 0.3, 6.1) vs. 1.4 (IQR: 0.5, 1.5), $p=0.68$; D5 *Mfng*: 0.8 (IQR: 0.6, 3.1) vs. 1.4 (IQR: 0.6, 9.4), $p=0.45$; D6: *Mfng*: 0.9 (IQR: 0.5, 2.3) vs. 2.8 (IQR: 0.8, 7), $p=0.15$. Mann Whitney U test. **(D)** Relative transcript levels of *Mfng*, Notch bHLH components, *Hes1*, 3 and 5, *Snai*, *Slug* (markers of EMT) and podocyte-specific transcript *Wt1* following 48

hours of *Mfng* shRNA knockdown. Scrambled shRNA transfected (*Scr*) *Cre-ERT^{+/+};Wt1^{fl/fl}* (n=2) vs. Manic Fringe shRNA (*ShMfng*) transfected *Cre-ERT^{TM+/+};Wt1^{fl/fl}* (n=2). Bars display the median, error bars present the IQR, *Mfng* expression is reduced following shRNA knockdown. *Scr* vs. *ShMfng*: *Mfng*: 1.3 (IQR: 0.6, 1.9) vs. 0.1 (IQR: 0.1, 0.1), $p=0.33$. *Wt1* transcript levels are equal in both groups post-transfection, 1.0 (IQR: 0.9, 1) vs. 1.1 (IQR: 0.7, 1.5), $p>0.99$; *Hes1*: 0.8 (IQR: 0.4, 1.3) vs. 0.5 (IQR: 0.3, 0.7), $p=0.67$; *Hes5*: 1.5 (IQR: 0.1, 2.9) vs. 0.2 (IQR: 0.1, 0.3), $p=0.67$; EMT marker, *Snail* is reduced: 4.4 (IQR: 1.6, 7.1) vs. 3.2 (IQR: 0.9, 5.5), $p=0.67$; *Slug*: 1.1 (IQR: 0.8, 1.4) vs. 1.0 (IQR: 0.9, 1.1), $p>0.99$. Analysed by Mann Whitney U test.

3.3 Discussion

This project demonstrates that our inducible model of *Wt1* deletion shows activation of the Notch pathway in the pathogenesis of *Wt1* glomerulopathy. A temporal rise in urine albumin/creatinine urine levels was seen in our mutants with FP effacement and development of GS. PAS staining of tissue sections revealed FSGS as early as D5 P.I. in our mutants. All together, these results support the view of podocyte apoptosis contributing to the development of *Wt1* glomerulopathy. Likewise, tubulointerstitial disease was evident at D12 P.I., which may be a result of glomerular injury and podocyte apoptosis. This corroborates earlier findings of podocyte apoptosis leading to GS (Niranjan et al., 2008). Thus, investigating podocyte apoptosis was an obvious mechanism to pursue in our inducible model of *Wt1* deletion.

Due to the terminally differentiated nature of podocytes, previous studies have shown that apoptosis of these cells contributes to disorders that lead to ESRD, including FS, DDS, NS and diabetic nephropathy (DN) (Wang et al., 2014, Niranjan et al., 2008). Loss of podocytes and tubular injury have been linked to podocyte apoptosis (Chang et al., 2012) leading to FSGS and DMS (Shankland, 2006). An earlier study introduced high doses of Diphtheria toxin (dT) in a rat model, which led to a reduced number of podocytes and FSGS. This work demonstrated the importance of podocytes in glomerular selectivity and maintenance (Wharram et al., 2005). Here, we present data from numerous apoptosis assays to validate this mechanism in our inducible model. Podocyte apoptosis occurs as early as D4 P.I. in the mutants, before GS is evident. Apoptosis is significantly increased in the mutants at D5-D12 P.I. and is associated with increased albuminuria and the progression of GS.

Temporal Wt1 deletion leads to proteinuria and GS

Despite the accumulated research of *Wt1* being vital during the early stages of kidney development, it has not been studied in depth in the mouse adult kidneys. Various

studies have shown that *Wt1* mutations in mice can lead to aberrant kidney morphogenesis, kidney failure, and embryonic lethality (Davies et al., 2004, Kreidberg et al., 1993, Hammes et al., 2001). *Wt1* deletion in *Cre*-inducible adult mice results in glomerulopathy with tubule casts and FP effacement (Chau et al., 2011). While detailed analysis of temporal *Wt1* deletion has been performed by Chau and colleagues, their main focus was to examine multiple organs affected by *Wt1* deletion, and the tissues analysed were no later than D10 P.I. (Chau et al., 2011). This therefore provided us with a great platform to investigate different stages of NS, including pre-proteinuric, proteinuric and GS following temporal deletion of *Wt1*.

Our findings demonstrate a key role for *Wt1* in maintaining kidney homeostasis and podocyte morphology in adult kidneys. *Cre-ERT^{TM+/-};Wt1^{ff}* mutants showed FP effacement as early as D4 P.I., with proteinuria at D5 P.I. Glomeruli of D6-D12 P.I. mutants presented with either FSGS or DMS, with severe proteinuria and tubulointerstitial fibrosis. There was progressive loss of *Wt1* in the mutants following tamoxifen induction, which was supported by DNA and protein findings. The temporal loss of *Wt1* is associated with the progression of GS and proteinuria, supporting earlier connections of *Wt1* with renal disorders (Gessler et al., 1990, Orloff et al., 2005).

Numerous mutations of *WT1*, including missense, nonsense and splice site-mutations have been variously associated with DDS, FS, and SRNS, leading to ESRD (Orloff et al., 2005, Benetti et al., 2010, Hall et al., 2015, Ruf et al., 2004, Topaloglu et al., 1999). The majority of the mutations lie within exon 8 and 9, which have been linked to DDS and FS, mainly due to the disruption of the KTS isoforms (Patek et al., 1999, Barbaux et al., 1997, Barbosa et al., 1999, Saylam and Simon, 2003, Hashimoto et al., 2016). Additionally, deletion of this gene has given rise to glomerulopathies linked to DDS, FS and SRNS. Our data illustrates that time-point analysis following *Wt1* deletion in adult kidneys show a striking deterioration of the glomerulus and proteinuria, with rapid progression towards GS, as early as day 5 P.I.

Podocyte architecture was altered in the *Cre-ERT^{TM+/-};Wt1^{ff}* mutants at D4 P.I., where FP effacement was seen. *Wt1* has been reported to be a master regulator of numerous genes associated with podocyte integrity. Target genes include, *Itga3*, which is associated with podocyte adherence to the GBM (Dong et al., 2015b). Mutations in *Itga3* have been linked to FP effacement and proteinuria. *Wt1* has been reported to bind to the proximal promoters of *Nphs1*, *Nphs2* and *Magi2* DNA, regulating their expression within the kidney (Lefebvre et al., 2015). Injury to the SD can lead to proteinuria (Grahammer et al., 2013, Dong et al., 2015b). The polarity and cytoskeleton of the podocytes are

regulated by WT1 where it binds the *cis*-regulatory elements of genes specific to cytoskeletal features of the podocytes (Kann et al., 2015b, Dong et al., 2015b). Therefore, direct target genes of WT1 are necessary for the integrity of podocyte architecture and maintaining an intact GFB.

Human FSGS and DMS can be caused by mutations in podocyte-specific genes, including, *WT1*, *NPHS1*, *NPHS2*, *LAMB2*, *PAX2*, which lead to SRNS and ESRD (Chen and Liapis, 2015, Lipska et al., 2014). Clinical research has demonstrated the importance of podocyte-specific genes in maintaining podocyte integrity (Chen and Liapis, 2015, Kaverina et al., 2017). Here, we show that *Wt1* deletion leads to FSGS and DMS in the mutants from D5 to D12 P.I. Expansion of the mesangial space was observed in the glomeruli at D6, D8 and D12 P.I. with fragmented podocyte nuclei in the mutants compared to the controls. Hypercellularity and basement membrane thickening was detected, possibly due to the increase in protein components following podocyte injury as well as the proliferation of endothelial and mesenchymal cells. Extensive hyaline material was also noted in the tubules and was associated with tubular dilatation. Hyalinosis is a result of capillary wall injury, leading to plasma protein leakage in the filtration system, resulting from podocyte injury. Glomerular global scarring was seen at D12 P.I., with thickening of the capillary walls, where podocyte and parietal epithelial cells were on some occasions, confluent. This may be due to podocytes re-entering the cell cycle in order to adhere to the denuded glomeruli (Wiggins et al., 2005). However, due to the nature of the terminally differentiated podocytes, their lack of proliferation contributed to the manifestation of GS. As a result, hypercellular glomeruli with collapsing lesions were observed with proliferation of endothelial and mesangial cells, and basement membrane thickening.

Wt1 deletion led to podocyte depletion, GS and tubulointerstitial fibrosis by D12 P.I., showing α SMA protein in the mutants' tubules and glomeruli. The development of GS initiates with an adhesion of the tuft and Bowman's capsule, eventually affecting the parietal epithelial membrane and glomerulotubular junction. This leads to the obstruction of the urinary opening. Due to the reduced filtrate release, tubules no longer function appropriately and degenerate (Kaissling et al., 2013). This disease progression was revealed from D4 to D12 P.I. in *Wt1* mutants. Proteinuria and FP effacement were signs of podocyte injury at D4 P.I., and global GS and tubulointerstitial fibrosis developed by D12 P.I. Apoptosis was explored as an important mechanism underlying podocyte loss.

Podocyte apoptosis is a mechanism of podocyte injury in *Wt1* glomerulopathy

Podocyte apoptosis has been reported to instigate the pathogenesis of GS and DN (Niranjan et al., 2008, Susztak et al., 2006, Li et al., 2013). By performing a number of different apoptosis assays in our inducible model, we show that podocyte apoptosis plays a key role in GS following *Wt1* deletion. Cleaved caspase-3 protein is a common tool to detect apoptosis and is activated by the upstream caspases 8 and 9 (Barrett et al., 2001). Cleaved caspase-3 protein was observed as early as D4 P.I. in the adult *Cre-ER^{TM+/-};Wt1^{ff}* mutants, before GS was detected. This protein was significantly increased in the mutants showing GS. TUNEL analysis and Annexin V staining were also used to validate podocyte apoptosis in the mutants. Whilst there was an increase in Annexin V in the mutants compared to controls, sample sizes were very low (n=2/group). This was due to the low survival of podocytes at D8 P.I., when GS was already evident. In addition, mRNA transcripts for the pro-apoptotic marker, *Bax* and anti-apoptotic marker, *Bcl2* were tested on D4, 5 and 6 P.I. Interestingly, *Bax*, was reduced in the mutants at D6 P.I. vs. controls in comparison to D4 and D5 P.I., however this was not statistically significant. *Bcl2* was also reduced in the mutants at this time point, with no significance compared to the controls. It was difficult to draw conclusions from these data due to the low sample number analysed (n=3 at D6 P.I.). These results demonstrate that a loss of *Wt1* in mature podocytes leads to podocyte apoptosis.

Previous work has shown that ectopic induction of the Notch pathway in developing and mature podocytes can induce FSGS and DMS, with an associated activation of apoptosis (Niranjan et al., 2008, Waters et al., 2008). Following this theory, the current project demonstrated both FSGS and DMS following *Wt1* deletion, with an activation of apoptosis. The next question in this project was to determine whether the Notch pathway was mediating podocyte apoptosis.

The Notch pathway plays a role in the pathogenesis of *Wt1* glomerulopathy

The Notch pathway is activated in early proximal nephron development, and the inhibition of Notch signalling during development affects proximal tubule formation (Cheng et al., 2003). During terminal podocyte differentiation, the Notch components, including the bHLH transcription factors, *Hes/Hey* are progressively downregulated (Piscione et al., 2004, Chen and Al-Awqati, 2005). Here, we demonstrate that Notch signalling is activated in our mutants following *Wt1* deletion. Prior to GS, cleaved Notch 1 and Hes1 proteins are seen in the podocytes of the mutants post-*Wt1* deletion. At the

onset of GS, there is an upregulation of the canonical Notch targets, as well as *Notch1* and *Nrarp*, its transcriptional target gene (Krebs et al., 2001).

Vertebrate podocyte differentiation has been shown to be regulated by a transcriptional network of *wt1*, *foxC1/C2*, and *rbpj* (O'Brien et al., 2011, White et al., 2010). WT1-binding regions have also been found to target FOX transcription factor binding motifs, further supporting their coordinating relationship in podocyte regulation (Lefebvre et al., 2015, Kann et al., 2015b). In zebrafish, podocyte depletion has been linked to double knockdown of either *wt1a/rbpj* or *wt1a/foxc1a*, highlighting the significance of interaction between these genes in regulating podocyte differentiation (O'Brien et al., 2011). Our model of *Wt1* glomerulopathy shows reduced *FoxC2* transcript levels and an increase in Notch signalling at the onset of GS. We postulate that *FoxC2* is repressing the Notch bHLH genes, including *Hey2*, due to their increased transcript levels in the mutants. Supporting this, a previous study demonstrated that FOXC2 targeted HEY2 in endothelial cells (Hayashi and Kume, 2008). Further studies showed that WT1 was able to inhibit NICD1 from activating a synthetic Notch reporter controlled by *Rbpj* sites (O'Brien et al., 2011), suggesting that both *WT1* and *Foxc1/2* can antagonise the Notch pathway in mature podocytes. Based on our current findings, podocyte-specific gene expression may be rescued following restoration of *FoxC2* levels in the adult *Cre-ER^{TM+/-};Wt1^{ff}* mutants, which may in turn inhibit Notch bHLH gene expression.

The current data shows that the canonical Notch target, *Hey1*, is also increased in the mutants at the onset of GS. Co-immunoprecipitation studies revealed an interaction among WT1, RPB1 and FOXC2 proteins and a combination of these genes induce *Hey1* expression (O'Brien et al., 2011). In xenopus, *xwt1* knockdown leads to reduced *xhrt1* expression (*Hey1* orthologue) in the developing glomus (glomerulus of the pronephric kidney in Xenopus), but not in the late glomus, proposing a role for *xwt1* mediating *xhrt1* expression in early glomerulogenesis (Taelman et al., 2006). Subsequent investigations revealed that WT1 regulates *HeyL* expression in pre-tubular aggregates as well as binds to the *HeyL* promoter (Hartwig et al., 2010). Together, these findings support a role for WT1 and FOXC1/2 modulating Notch targets during nephrogenesis.

Our model of *Wt1* glomerulopathy shows an upregulation of the EMT genes, *Snail* and *Slug* at the onset of GS. This data proposes that the loss of *Wt1* in mature podocytes activates Notch signalling, which may mediate podocyte EMT and apoptosis. Increased *Hes1* transcript levels were accompanied by increased *Snail* and *Slug* at the onset of GS. *Hes1* has been reported to induce EMT in various cancers (Thiery and Sleeman, 2006). To further validate *Hes1*-mediated EMT in our model of *Wt1* glomerulopathy,

Nphs2;rtTA primary podocytes were induced to overexpress *HES1*. This led to an upregulation of the EMT markers, *Snail* and *Slug*, suggesting that Notch was triggering genes promoting EMT in our model of *Wt1* glomerulopathy. Further evidence of Notch being associated with both podocyte apoptosis and EMT has been demonstrated in earlier studies where the conditional deletion of *Notch1* in DN abrogated GS with a reduced expression of *Snail1* mRNA and protein (Sweetwyne et al., 2015).

An earlier study demonstrated that podocytes transduced with *Notch1* ICD inhibits apoptosis following pifithrin- α treatment, proposing that *Notch1* may be inducing podocyte apoptosis via the p53 pathway (Niranjan et al., 2008). In the current study, it is possible that p53 may be playing a role in mediating podocyte apoptosis in the pathogenesis of *Wt1* glomerulopathy. An interesting way to investigate this would be to conditionally-inactivate *Notch1* in podocytes of the adult *Cre-ER^{TM+/-};Wt1^{ff}* mice. In our model of *Wt1* glomerulopathy, Notch inhibition was carried out using a γ -secretase inhibitor at different stages of the disease. The inhibition of Notch at D4 and D5 P.I. showed decreased severity of GS and albuminuria. However, Notch inhibition at D7 and D8 P.I. failed to rescue the disease, and albuminuria was not reduced. Early intervention of γ -secretase inhibition reveals the importance of the Notch pathway at the initiation and during early manifestation of disease.

Podocyte Notch activation post-*Wt1* deletion may also be mediated by Hippo signalling activation. Hippo signalling has been shown to be a transcriptional target of Notch ligands in human epidermal stem cells (Totaro et al., 2017). An earlier study exposed TEAD transcription motifs (Hippo signalling effectors) within WT1 ChIP sequencing peaks (Kann et al., 2015b). Therefore, *Wt1* deletion in mature podocytes may also induce Notch activation through regulating Hippo components.

Notch glycosylation is evident post-Wt1 deletion

The current data reveals that Jag1 and Pofut1 are expressed at the onset of GS, supporting ligand-dependant Notch activation in podocytes at disease manifestation. The Notch pathway is activated by o-glycosylation of the extracellular domains of the Notch ligands and receptors (Stanley and Okajima, 2010). Pofut1, is an O-fucosyltransferase 1 enzyme that mediates fucosylation of the Notch ECD. Pofut1 has been reported to regulate cell surface expression of Notch1 (Okajima et al., 2003). Manic Fringe, a β 3-N-acetylglucosaminyltransferase, that mediates glycosylation of the Notch ECD, was also increased in our *Cre-ER^{TM+/-};Wt1^{ff}* mutants. Studies have argued that Dll1 activation of the Notch pathway is mainly influenced by Fringe-mediated NOTCH1

glycosylation (Kakuda and Haltiwanger, 2017). The current study, however, has demonstrated jagged1 expression in the *Cre-ER^{TM/+};Wt1^{ff}* mutants as well as in human biopsies of *WT1*-glomerular disease, followed by an activation of Manic Fringe. It would therefore be interesting to examine the relationship between Fringe proteins and Notch ligands, namely, Mfng and Jag1 in the context of podocyte injury.

One avenue to explore would be to study Notch1 EGF domains and its activation through the Fringe proteins in the context of podocyte injury. Earlier research has already shown that Notch1 can be activated or inhibited by Fringe modifications on specific EGF domains (Kakuda and Haltiwanger, 2017). Mutations in specific EGF domains of Notch receptors can reduce Delta-1 mediated Notch signalling from all Fringes. Mfng and Lfng modify similar EGF domains of Notch1, while Rfng modifies a portion, thus enhancing Notch activation through both ligands (Kakuda and Haltiwanger, 2017). Knowing that Fringe modification can impact Notch signalling, exploring and manipulating Fringe expression in injured podocytes will allow us to appreciate Notch glycosylation in the context of podocyte injury.

Previous work in *Drosophila* explored EGF8 in Notch 2 and showed that Dll1/Jag1-mediated Notch2 activation can occur without EGF8 modification, indicating that the Notch orthologues and their EGF repeats show differences in where Fringe modification occurs (Yamamoto et al., 2012). Fringe modification causes conformational changes in NOTCH1, exposing its EGF repeats to POFUT1, thus becoming more modified by O-fucosylation and inducing Notch proteolytic activation. The absence of Fringe therefore decreases Notch modification. An example of Pofut1 modification occurs in EGF26 following Fringe elongation, where NOTCH1 conformational changes exposes its EGF domain and allows POFUT1 to bind to it (Kakuda and Haltiwanger, 2017).

Studying alternative Notch receptors could further illuminate the role of Notch glycosylation. Fringe glycosylation also occurs in Notch2, stimulating Dll1/Jag1-mediated Notch activity or Jag1-induced Notch inhibition by Lfng and Mfng. Although Notch1 and Notch2 are structurally parallel with their 36 EGF repeats, their chemical requirements for activation vary. Studies have reported that Notch2 is more prone to ligand mediated activation than Notch1, perhaps due to the distinct conformational changes in their NRR to expose the S2 site for proteolytic cleavage (Stephenson and Avis, 2012).

Notch ligands exhibited in early disease progression

In the current study, the Notch ligand *Jag1* was expressed in both podocytes and parietal epithelium at the early stages of GS in the *WT1* deleted mouse, observations supported by evidence from earlier studies (Niranjan et al., 2008, Murea et al., 2010). In contrast, the *Dll1* ligand showed no quantitative difference between the *Cre-ERT^{M+/-};Wt1^{ff}* mutants and controls at any time point. During kidney development, *Jag1* and *Dll1* expression overlaps within the middle portion of the S-shaped body. Moreover, their loss in *Cre;Dll1^{ff};Jag1^{ff}* mouse mutants leads to a significant decrease in glomeruli and proximal tubules (Liu et al., 2013), highlighting their importance in mediating Notch activation during renal development. *Jag1* plays a role in determining podocyte fate induction; *Dll1* replacement by a *Jag1* allele rescues *WT1*-positive podocytes (Liu et al., 2013). Furthermore, Niranjan *et al.* showed that in podocyte injury, *Jag1* was upregulated following TGF- β 1 treatment, suggesting a role for *Jag1* in podocyte fate (Niranjan et al., 2008). A more recent study using genome-wide expression analysis in human tubular epithelial cells has shown that *JAG1* and *NOTCH2* are increased in kidney fibrosis (Huang et al., 2018). Mouse models of nephropathy corroborated these findings, showing higher levels of *Jag1* and *Notch2* in renal fibrosis (Huang et al., 2018). Given that there is an increase in podocyte expression of Notch1 and *Jag1* in our mutants, future work could focus on conditionally deleting each of these in adult *Cre-ERT^{M+/-};Wt1^{ff}* transgenic mice. Subsequent evaluation of disease manifestation might help identify which ligand and receptor pair are responsible for the manifestation of GS in *Wt1* glomerulopathy.

In summary, upregulation of specific Notch components and EMT genes together with reduced *FoxC2* expression correlated with the onset of GS in *Cre-ERT^{M+/-};Wt1^{ff}* transgenic mice. In addition, induced HES1 podocyte expression lead to increased expression of the EMT markers, *Snail* and *Slug*, supporting a role for HES1 in regulating podocyte EMT. Downregulation of *FoxC2* expression led to the activation of Notch signalling. These data support the hypothesis that *Wt1* deletion in podocytes results in apoptosis that contributes to the initiation of glomerular fibrosis. This is supported by the observation that early pharmacological inhibition of the Notch pathway reduced albuminuria and GS severity.

Nonetheless, *WT1* is a complex gene with multiple roles within the podocyte. As such, to explore further its mechanisms of action including its relationship to Notch signalling and programmed cell death in glomerular fibrosis in more detail, further study of

transgenic mice, for example with *Wt1* point mutations relating to human disease would help explore further mechanisms involved.

Chapter 4 - *Ascl1* expression precedes podocyte Notch activation in *Wt1* glomerulopathy

4.1 Introduction

RNA sequencing of glomerular isolates in *Wt1*-deleted mutants at D4 P.I. indicated that mRNA expression of another downstream effector of the Notch signalling pathway, achaete-scute complex homologue-1 (*ASCL1*) is increased. Thus, to complement investigation of Notch pathway activation in murine *WT1* mediated glomerulopathy, the role of *ASCL1* in podocyte differentiation and *WT1* glomerulopathy was examined further. The aim was to build on existing experimental evidence that *ASCL1* upregulation may precede Notch pathway activation and consequently play an important part in the pathogenesis of GS in murine *Wt1* glomerulopathy.

ASCL1 has a key role in Notch signalling during neuronal differentiation and proliferation (Kageyama et al., 2005, Vasconcelos and Castro, 2014), further supporting evidence that it may also mediate podocyte differentiation. *Ascl1* both regulates and is regulated by, the Notch signalling pathway (Figure 4.1).

Ascl1 stimulates neuronal differentiation by directly activating the Notch ligand, *Dll1*, eventually leading to the activation of the transcriptional repressors, *Hes1* and *Hes5* (Borromeo et al., 2014, Raposo et al., 2015). These repressors inhibit proneural gene expression by binding to their promoters, thereby repressing neuronal differentiation (Kageyama et al., 2005). This process prevents all progenitors from simultaneously differentiating, guaranteeing that a suitable number are sustained during embryonic development (Vasconcelos and Castro, 2014).

ASCL1, the proneural bHLH TF

ASCL1, also known as Mammalian achaete-scute complex homologue-1 (*Mash1*), is a class II proneural basic-helix-loop-helix transcription factor mainly known for its key role in initiating neurogenesis (Guillemot et al., 1993). *ASCL1* binds to E-box motif (5'-CANNTG-3') and dimerises with other bHLH proteins to activate transcription (Nakada et al., 2004).

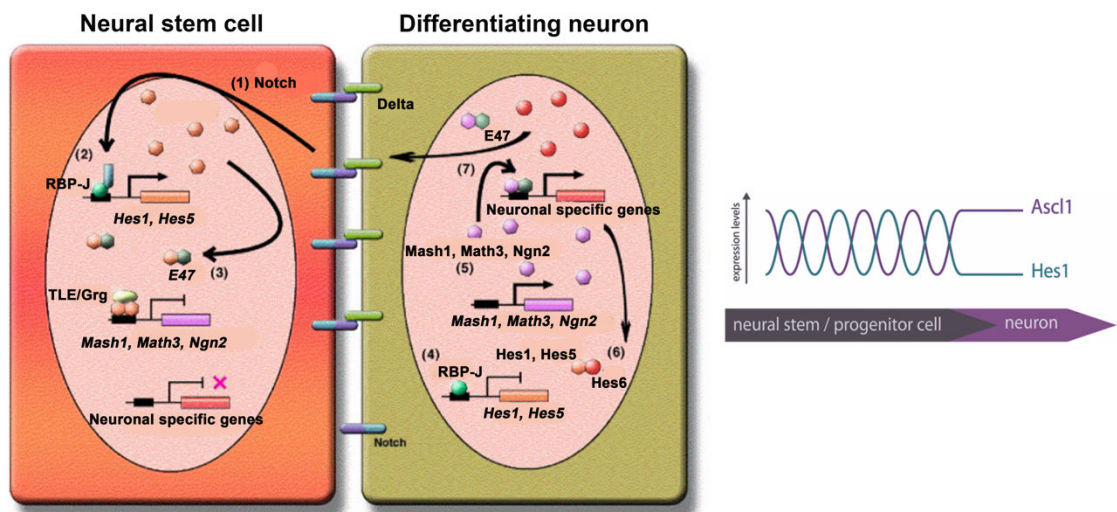


Figure 4.1. Interplay between *Ascl1* and Notch signalling during neurogenesis

Neuronal differentiation is controlled by the activator-type and repressor-type bHLH transcription factors. **(1)** In a neural stem cell, Delta-Notch binding triggers Notch signalling. **(2)** NICD is cleaved and translocates to the nucleus, where it co-binds with Rbpj, activating *Hes1* and *Hes5* expression. **(3)** These genes inhibit the activity the activator genes (*Ascl1* [*Mash1*], *Math3*, *Ngn2*) by sequestering E47, a bHLH transcription factor. Transcription of the activator genes is also inhibited due to *Hes1* and *Hes5* binding to their promoters and employing the corepressor TLE/Grg. **(4)** in the differentiating neuron, Notch signalling is downregulated, and the repressor-type TFs *Hes1* and *Hes5* expression is inhibited by RBPJ. **(5)** Expression of the activator-type bHLH TFs is triggered. **(6)** The activator-type bHLH TFs activate *Hes6* expression, which represses *Hes1* activity. **(7)** Other specific neuronal genes are stimulated by the activator type bHLH TFs, including the Delta ligand, which induces Notch activity in neighbouring cells (lateral induction). Right image displays modes of *Ascl1* expression in neural stem cells; The oscillation between *Ascl1* and *Hes1* occurs within a 2-3 hour period, where their modes of expression are out of phase. *Hes1* expression is terminated following neuronal differentiation, while *Ascl1* expression becomes sustained. Adapted from (Kageyama et al., 2005, Vasconcelos and Castro, 2014).

ASCL1 has multiple roles in sequentially triggering target genes in the progenitors of differentiating and proliferating neurons (Raposo et al., 2015), which not only induce cell cycle exit, but promote proliferation in specific cell contexts (Castro et al., 2011, Wilkinson et al., 2013). Its dual role during neurogenesis, including the proliferation of neural progenitor cells (NPCs), is controlled by other genes including *Hes1*, the downstream Notch target, which represses *Ascl1*, thus regulating neuronal proliferation (Dhanesh et al., 2016, Shimojo et al., 2008). Proliferation and differentiation of NPCs depend on *Ascl1*'s expression being either transient or sustained (Imayoshi et al., 2013, Urban et al., 2016).

ASCL1 has been identified to regulate genes associated with podocyte differentiation, including, *Lmx1b* (Borromeo et al., 2014) and *Wnt1* (Burghardt et al., 2013). ASCL1 represses *Wnt1* in the spinal cord during early dorsal ventral patterning (Augustine et al., 1995, Lee and Jessell, 1999, Herzlinger et al., 1994).

ASCL1 mediates Notch signalling

Experiments in chick retinal progenitors support an association between *Ascl1* and *Dll* genes (Nelson et al., 2009) in that co-expression increased *Dll* gene expression and Notch signalling in retinal progenitors. During neuronal differentiation, *Dll1*, *Dll4*, and *Ascl1* demonstrate similar expression patterns. Overexpression of *Ascl1* potentiates Notch signalling by inducing *Dll1* and *Dll4* gene expression (Nelson and Reh, 2008). ASCL1 binds DLL1 through the former's E-box domain (Castro et al., 2006). *Ascl1* binds to a specific enhancer of *Dll4* during ventral spinal cord development, activating *Dll4* expression (Bertrand et al., 2002, Misra et al., 2014). Similarly, *Dll3* expression is mainly reliant on *Ascl1*, which binds to *Dll3*'s E box subdomain during neurogenesis (Henke et al., 2009).

Both *Rbpj* and *Ascl1* have been shown to interact transcriptionally in the ventral telencephalon of *Drosophila*, mainly promoting proliferation (Nellesen et al., 1999, Castro et al., 2011).

Murine in vivo studies associated with Ascl1 and the Notch pathway

Ascl1 activates Notch signalling through *Dll* and *Jag* induction (Castro et al., 2006). Both, *Dll1* and 3 have been found to be expressed in the mouse ventral telencephalon. Mutant *Ascl1* embryos revealed a loss of both *Dll* genes, highlighting *Ascl1*'s importance in Notch ligand expression (Casarosa et al., 1999). Research in *Ascl1*-deficient mouse retina also showed a significant reduction in *Dll1* expression (Nelson et al., 2009). Expression of the murine *Hes5* gene was reduced following Notch signalling disruption in the *Ascl1* mutants, further confirming the relevance of *Ascl1* in Notch signalling (Casarosa et al., 1999).

Previous findings have reported that *Ascl1* is able to convert astrocytes to neurons *in vivo*; one study discovered that stroke and attenuated Notch signalling in mice led to *Ascl1* expression in striatal astrocytes and transdifferentiation into neurons (Magnusson et al., 2014). The combination of *Ascl1* overexpression and Notch inhibition has been

revealed to be a potential treatment in glioblastomas, where *Ascl1* expression can reduce cancer cell proliferation and encourage cell cycle exit (Park et al., 2017).

The relationship between the proneural bHLH repressors and Ascl1

The bHLH *Hes1* has been shown to play a role in repressing *Ascl1* either transcriptionally or through protein-protein interaction during neural stem cell differentiation (Kageyama et al., 2005). Both repressor bHLH HES1 and activator-type bHLH (ASCL1) work together to promote fate determination in a subset of cells, while others remain as neural cells (Shimojo et al., 2008).

Since a definitive role for ASCL1 in nephrogenesis has not been established, in order to elucidate its contribution to the early mechanisms of Notch induction in *Wt1* glomerulopathy, glomerular RNA from mice at day 4 post Tamoxifen induction was sequenced (n=3/group). Interestingly, *Ascl1* transcript was increased in the mutants compared to controls, suggesting a role for *Ascl1* in the manifestation of GS. Gene expression analysis was performed for several genes, listed in Appendix A.

Our qPCR and Western blot data presented in this chapter, demonstrate increased *Ascl1* RNA and protein expression in our *Cre-ER^{TM+/-};Wt1^{ff}* mutants compared to *Cre-ER^{TM+/-};WT1^{ff}* controls in D4 and D5 P.I. primary podocytes. Furthermore, tissue IHC at D4, 5 and 12 P.I. reveal ASCL1 protein in the podocytes. ASCL1 expression during nephrogenesis has not been published to date, therefore its expression pattern was analysed by IHC during early and late glomerulogenesis. Finally, *Ascl1* gene expression was induced in differentiating and mature podocytes *in vivo* to examine whether an increase in *Ascl1* induces Notch signalling and GS.

4.2 Results

4.2.1 *Ascl1* is upregulated in D4 P.I. *Cre-ER^{TM+/-};Wt1^{ff}* mutant glomeruli

Following *Wt1* deletion at D4 P.I., RNA data showed an upregulation of *Ascl1* in the mutants compared to the controls (Figure 4.2A). This was further validated through real-time qPCR, demonstrating an increase in the *Cre-ER^{TM+/-};Wt1^{ff}* mutants compared to *Cre-ER^{TM+/-};WT1^{ff}* controls at D4 P.I., but this failed to reach statistical significance (Figure 4.2B). Studies have reported that *Ascl1* and *Hes1* expression patterns oscillate in neurogenesis (Vasconcelos and Castro, 2014). Here, we show that there is a fluctuation in *Ascl1* mRNA levels from D4-D6 P.I. in the mutants. Transcript levels of *Ascl1* were

reduced in the mutants at D5 P.I., followed by an increase in mRNA levels at D6 P.I., but this failed to reach statistical significance (Figure 4.2B).

ASCL1 protein levels were examined using Western blot analysis (Figure 4.2C) and immunostaining (Figure 4.2D-I') to validate *Ascl1* increase in the mutants. Western blot analysis demonstrated an increase in ASCL1 protein levels at D4 P.I. in the mutant vs. control (Figure 4.2C).

Furthermore, immunostaining at D4 P.I. revealed ASCL1 nuclear expression within the podocytes of the mutants (Figure 4.2E, F, inset F'), whilst the controls did not display any ASCL1 protein within the glomerulus (Figure 4.2D). At D5 P.I., ASCL1 was also detected in the mutants, namely in the podocytes and possibly in the PECs (Figure 4.2H, I, inset, H', I') compared to the control, where it was faintly identified (Figure 4.2G). Insets illustrate ASCL1 expression in the nucleus (Figure 4.2F', H', I').

Genes significant for podocyte biology were also shown to be up or downregulated following *Wt1* deletion at D4 P.I. *Wifi1*, *Nphs1*, *Nphs2*, *Kirrel2*, *Lmx1b* were all decreased in the mutants at D4 P.I. (Figure 4.2A), supporting previous studies of glomerular disease where reduced expression of these genes was demonstrated (Boute et al., 2000, Koziell et al., 2002, Caridi et al., 2005, Ihalmo et al., 2007, Boyer et al., 2013, Woroniecki and Kopp, 2007).

Wnt3a, a member of the Wnt signalling pathway, involved in cell fate and patterning during embryogenesis, was increased in the mutants compared to the controls. Studies have shown that sustained activation of Wnt signalling can lead to renal fibrosis and chronic kidney disease. High glucose in mice has been reported to impair podocyte integrity by inducing *Wnt3a* and suppressing podocyte-specific genes, *Nphs1* and *Nphs2* (Wang et al., 2018). Here, we show that *Nphs1* and *Nphs2* are downregulated in the mutants, with increased *Wnt3a* expression, suggesting a role for the *Wnt* pathway in *Wt1* glomerulopathy. Intriguingly, the Notch components, *Notch2*, *Hes1*, *Hes5*, *Dll1*, *Dll4*, *Jag1* and *Lfng* showed no difference between the mutants and the controls. Real-time qPCR at D4 P.I., however, showed *Lfng* to be significantly decreased in the mutants compared to the controls (Figure 3.14A).

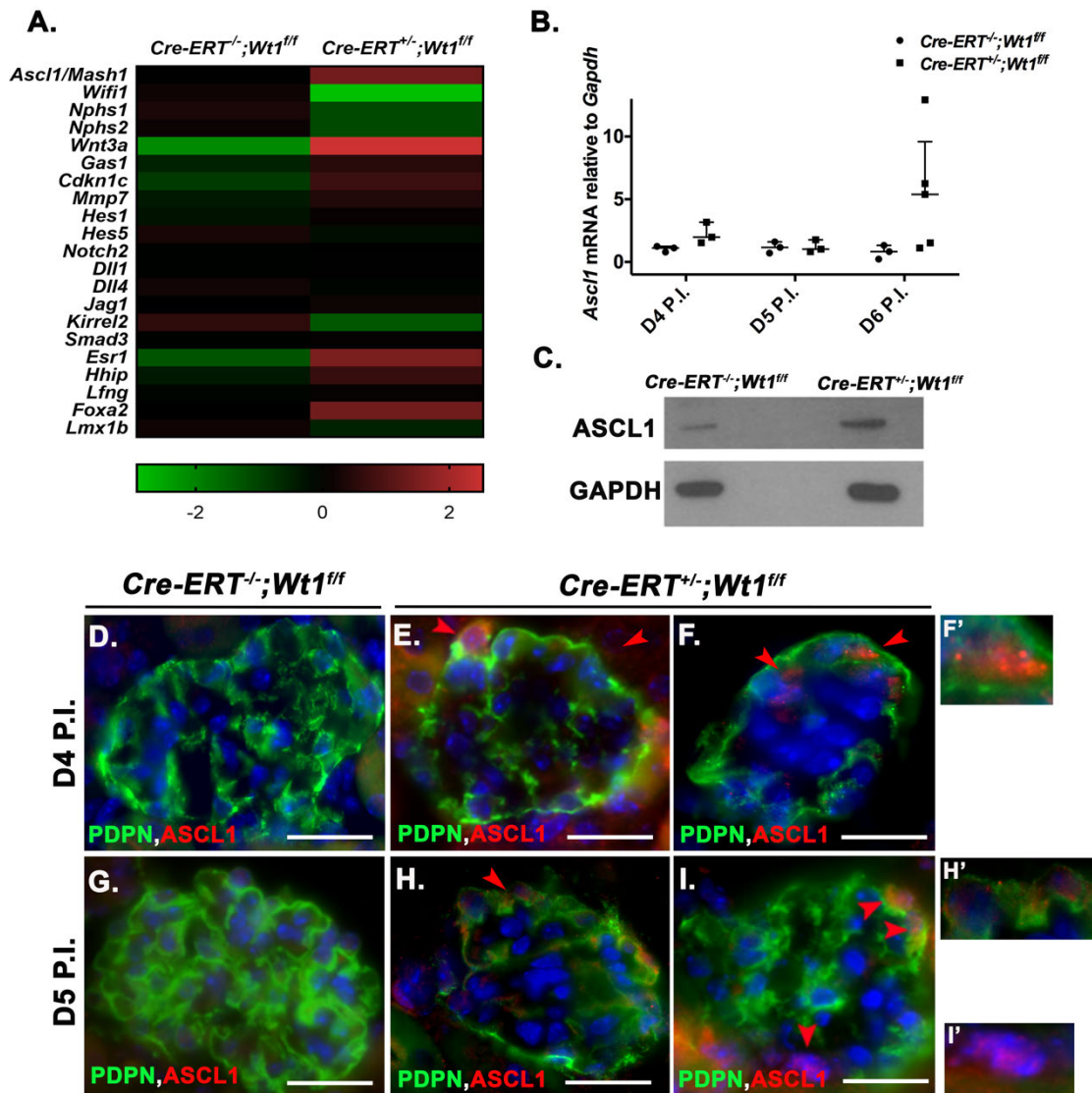


Figure 4.2. Upregulation of *Ascl1* mRNA and protein in D4 P.I. *Cre-ERT^{TM+/-};Wt1^{ff}* mutant glomeruli

(A) Heatmap demonstrating differential gene expression of genes in *Cre-ERT^{TM+/-};Wt1^{ff}* controls (n=3) vs. *Cre-ERT^{TM+/-};Wt1^{ff}* mutants (n=3) with a 2.0-fold change; *Ascl1*, -0.02 vs. 1.39; *Wif1*, 0.18 vs. -2.93; *Nphs1*, 0.31 vs. -1.12; *Nphs2*, 0.15 vs. -1.12; *Wnt3a*, -2.11 vs. 2.53; *Gas1*, -0.52 vs. 0.48; *Cdkn1c*, -0.90 vs. 0.72; *Mmp7*, -0.40 vs. 0.41; *Hes1*, -0.29 vs. 0.09; *Hes5*, 0.275 vs. -0.20; *Notch2*, -0.03 vs. 0; *Dll1*, -0.04 vs. 0.01; *Jag1*, -0.01 vs. 0.16; *Kirrel2*, 0.54 vs. -1.32; *Smad3*, -0.03 vs. 0.06; *Esr1*, -1.29 vs. 1.50; *Hhip*, -0.37 vs. 0.68; *Lfng*, -0.08 vs. 0.07; *Foxa2*, 0 vs. 1.37; *Lmx1b*; 0.20 vs. -0.52. **(B)** Dot plot showing relative transcript levels of *Ascl1* in *Cre-ERT^{TM+/-};Wt1^{ff}* controls (n=3) vs. *Cre-ERT^{TM+/-};Wt1^{ff}* mutants (n=3) representing the median and error bars IQR, D4 P.I., 1.1 (IQR: 0.8, 1.2) vs. 2 (IQR: 1.5, 3.2), $p=0.1$; D5 P.I., 1.2 (IQR: 0.7, 1.6) vs. 1 (IQR: 0.8, 1.8), $p=0.9$; D6 P.I., 0.8 (IQR: 0.2, 1.3) vs. 5.4 (IQR: 1.3, 9.6), $p=0.07$. Mann Whitney U test. **(C)** Representative image of Western blot analysis of protein derived primary podocytes isolated from controls vs. mutant mice. Immunoblot reveals increased ASCL1 expression in the mutants at D4 P.I., with weaker expression of the protein in the controls. **(D-I')** Shown are representative micrographs of double immunofluorescence labelled glomeruli marked with podoplanin (Alexa

Fluor 488) and ASCL1 (Alexa Fluor 594), counterstained with DAPI at D4 P.I. (**D-F'**) and D5 P.I. (**G-I'**) controls vs. mutants. ASCL1 is not present in D4 controls (**D**), however co-nuclear expression of ASCL1 is revealed in the mutants, within the podocytes (**E, F, red arrows**). Inset shows a higher power view of ASCL1 nuclear expression in D4 P.I. mutants (**F'**). ASCL1 protein is not seen in D5 P.I. controls (**G**), however it is present in the podocytes of D5 P.I. mutants (**H, I, red arrows**), with insets showing higher power images of ASCL1 positive cells (**H', I'**). Scalebar 25 μ m.

It is important to note that the RNA sequencing data presented here were analysed from glomerular isolates. Glomerular isolates included a heterogenous population of podocytes, endothelial and mesangial cells. This may have resulted in the difference in expression levels between RNA sequencing and real-time qPCR. RNA sequencing was also performed on only 3 mice/group, whereas the qPCR data was analysed on a larger number of mice, giving us a more accurate conclusion. *Esr1* (Estrogen Receptor 1) was also increased in the mutants, and has been known to be expressed in pathological processes, such as breast cancer (Martin et al., 2017). The Forkhead Box A2 (*Foxa2*) was upregulated in the mutants, a transcription factor associated with embryonic development as well as regulating gene expression in differentiated tissues. Interestingly, *Lmx1b* has been shown to interact with genes including *Foxa2* during neurogenesis (Nakatani et al., 2010) and *Foxa2* plays a specific role in the differentiation of dopaminergic neurones (Domanskyi et al., 2014). The downregulation of *Lmx1b* may have had an effect on *Foxa2* expression.

Hes1 and *Ascl1* mRNA levels were compared from D4 to D6 P.I. in the mutants (Figure 4.3). Expression levels of *Ascl1* oscillated at D4 (Figure 4.3A, B), D5 (Figure 4.3A, C) and D6 P.I. (Figure 4.3A, D). *Hes1* mRNA levels were lower than *Ascl1* at D6 P.I., however remained higher in the mutants compared to controls (Figure 3.16A). Studies have shown an association between *Ascl1* and *Hes1* in neurogenesis (Vasconcelos and Castro, 2014). The data here shows that Notch activation at disease onset may be due to an interaction between *Ascl1* and *Hes1* expression, regulating Notch signalling. Reduced levels of *Hes1* are associated with increased levels of *Ascl1*. At D4 P.I., *Hes1* mRNA is higher than *Ascl1*. Levels of both transcripts are almost equal at D5 P.I., with their expression levels switching by D6 P.I.

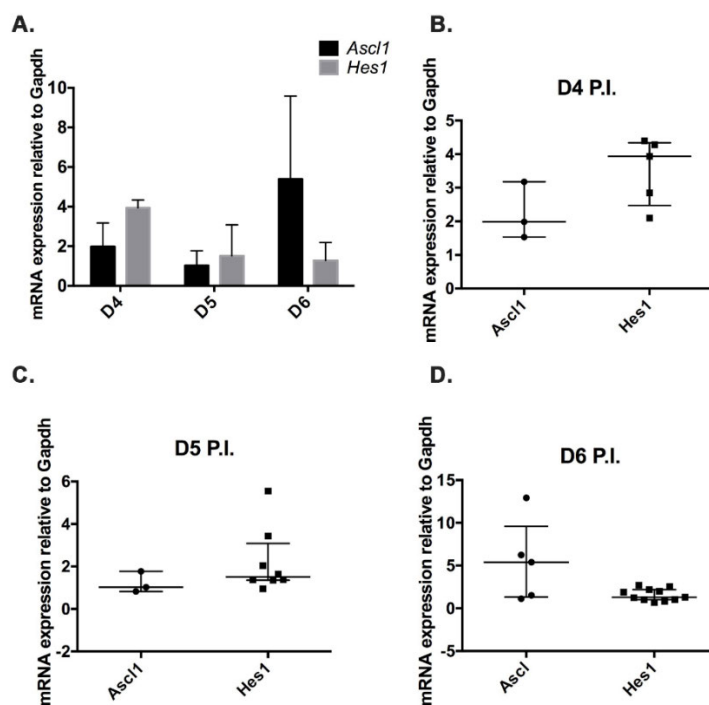


Figure 4.3. *Ascl1* and *Hes1* mRNA levels oscillate in *Cre-ER^{TM+/-};Wt1^{fl/fl}* mutants from D4 to D6 P.I.

(A) Graph showing relative transcript levels of *Ascl1* vs. *Hes1* in *Cre-ER^{TM+/-};Wt1^{fl/fl}* mutants at D4 (n=3 vs n=5), D5 (n=3 vs n=8) and D6 P.I. (n=5 vs n=11). Bars represent the median, error bars represent IQR. D4 P.I., 2 (IQR: 1.5, 3.2) vs 4 (IQR: 2.5, 4.3), $p=0.14$; D5 P.I., 1 (IQR: 0.8, 1.8) vs 1.5 (IQR: 1.4, 3), $p=0.24$; D6 P.I., 5 (IQR: 1.3, 9.6) vs 1.3 (IQR: 1, 2.2), $p=0.09$ (ns). Analysed by Mann-Whitney. **(B)** Dot plot analysis showing the median relative transcript levels of *Ascl1* vs *Hes1* at D4 P.I. **(C)** Dot plot analysis of *Ascl1* vs *Hes1* at D5 P.I. **(D)** Dot plot analysis of *Ascl1* vs *Hes1* at D6 P.I. Bars represent the IQR.

4.2.2 Glomerular ASCL1 and HES1 protein in patient *WT1* glomerulopathies

Since *Ascl1* was increased in the mouse mutants vs. controls, its expression pattern was examined in human kidney biopsies from patients with DDS caused by mutations of *WT1*: R390X and R362X. Findings were compared with time-zero renal allograft biopsies of normal kidneys as controls. The oscillatory relationship between the transcription factors, *Hes1* and *Ascl1* described during neurogenesis was examined in association in human *WT1* mutations. Immunostaining revealed higher expression of HES1 in both *WT1* R390X and *WT1* R362X compared with controls (Figure 4.4A-C). Additionally, upregulation of nuclear ASCL1 expression was evident in both *WT1* mutant biopsies compared with controls (Figure 4.4D-F), where only low, non-nuclear expression of the protein was observed. HES1 protein expression was detected at higher levels than ASCL1 in the human mutants, supporting a role of the Notch pathway in glomerular injury.

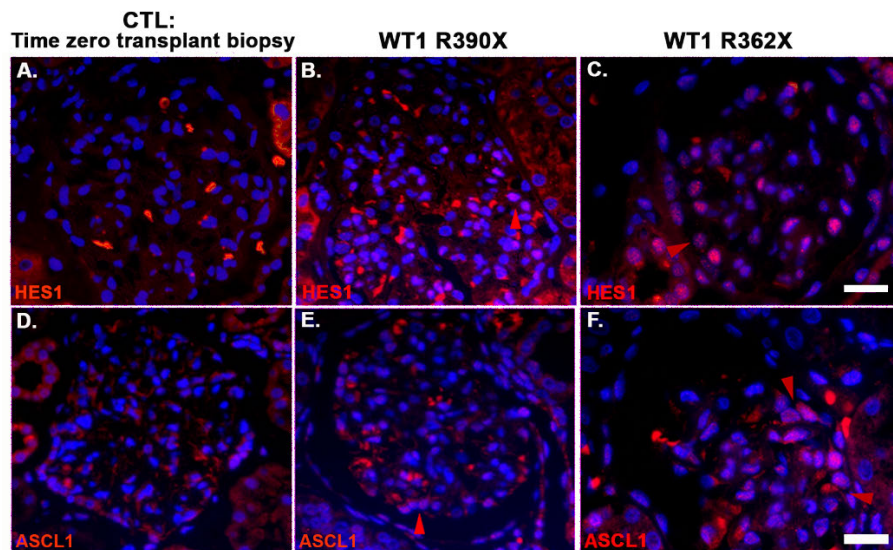


Figure 4.4. ASCL1 and HES1 are expressed in *WT1* glomeruli

(A-F) Representative micrographs of immunofluorescence labelling with HES1 (Alexa Fluor 594) and ASCL1 (Alexa Fluor 594) in patient glomeruli. Control biopsies (time-zero renal allografts) reveal no glomerular HES1 expression (A) compared to patients carrying *WT1* mutations (B, C, red arrows), with increased expression of the protein in both glomeruli. Control biopsies display low glomerular ASCL1 protein expression (D) but are increased in the patients of *WT1* mutations (E, F, red arrows). Scalebar 25 μ m.

4.2.3 TUNEL is not detected in all ASCL1-positive cells in late GS

ASCL1 was upregulated in both murine and human samples with *WT1* mutations. In view of the role of Notch/ASCL1 signalling in apoptosis, this was examined in ASCL1-positive cells. TUNEL analysis was used to identify cell apoptosis along with ASCL1 immunostaining in both *Cre-ERTM^{-/-};Wt1^{fl/fl}* controls vs. *Cre-ERTM^{+/-};Wt1^{fl/fl}* mutants at D12 P.I. (Figure 4.5A-L). Only one ASCL1-positive cell was also TUNEL-positive in the *Cre-ERTM^{+/-};Wt1^{fl/fl}* mutants (Figure 4.5E-L), suggesting that podocyte apoptosis is not associated with ASCL1.

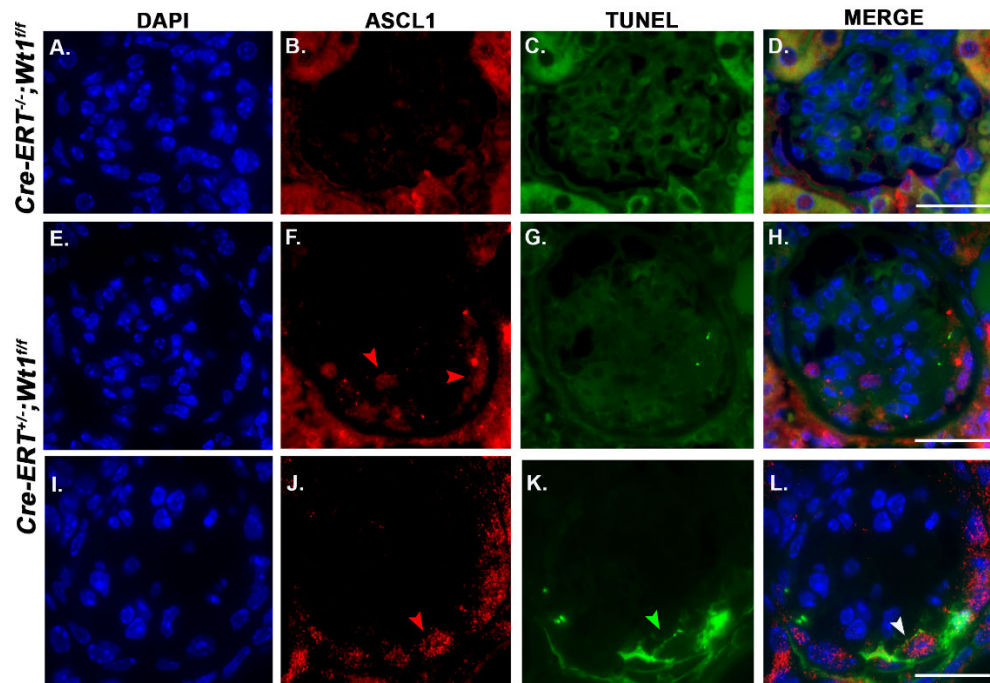


Figure 4.5. ASCL1 protein is expressed in D12 P.I. *Cre-ERT^{TM+/-};Wt1^{fl}* glomeruli

Representative micrographs of immunofluorescence labelled glomeruli with Ascl1 (Alexa Fluor 594) and apoptosis detection by TUNEL assay reveals no ASCL1 or TUNEL positive cells in the *Cre-ERT^{TM+/-};Wt1^{fl}* controls (A-D). D12 *Cre-ERT^{TM+/-};Wt1^{fl}* mutants (E-L); ASCL1-positive cells (F), with no TUNEL (G, H), ASCL1-positive cells (J) and TUNEL-positive cells (K,L). Scalebar, 25 μ m. (n=3 mice)

4.2.4 Patterns of ASCL1 expression during glomerulogenesis

Initial data indicated that ASCL1 was upregulated in the mutants and in patients with *WT1* mutations. In view of its participation in neurogenesis and the similarities with nephrogenesis regarding Notch signalling, a role for ASCL1 in nephrogenesis was examined. Mouse kidneys were collected at E17.5 and P7, and ASCL1 protein was analysed at different stages to identify its expression pattern during nephrogenesis (Figure 4.6, Figure 4.7). Embryonic kidneys isolated at E17.5 were immunostained with ASCL1, co-stained with LAMB2 to mark the podocytes, CD31, to mark the endothelial cells, and DESMIN, to mark the mesangial cells (Figure 4.6). ASCL1 demonstrated a perinuclear expression pattern in the mid-S-shaped body (Figure 4.6A-C) with expression sustained into the capillary loop stage, primarily in podocyte progenitors (Figure 4.6J-L), as well as mesangial cells (Figure 4.6G-I). ASCL1 expression was absent in endothelial cells (Figure 4.6D-F).

P7 kidneys were also isolated to examine the role of ASCL1 in late glomerulogenesis (Figure 4.7). Interestingly, its expression pattern had changed from being perinuclear to

being nuclear at the capillary loop stage. Cells were also co-stained with podoplanin to mark the developing glomerulus. Clusters of ASCL1-positive cells were mainly podocyte-specific, suggesting a role for ASCL1 during podocyte differentiation (Figure 4.7A-F).

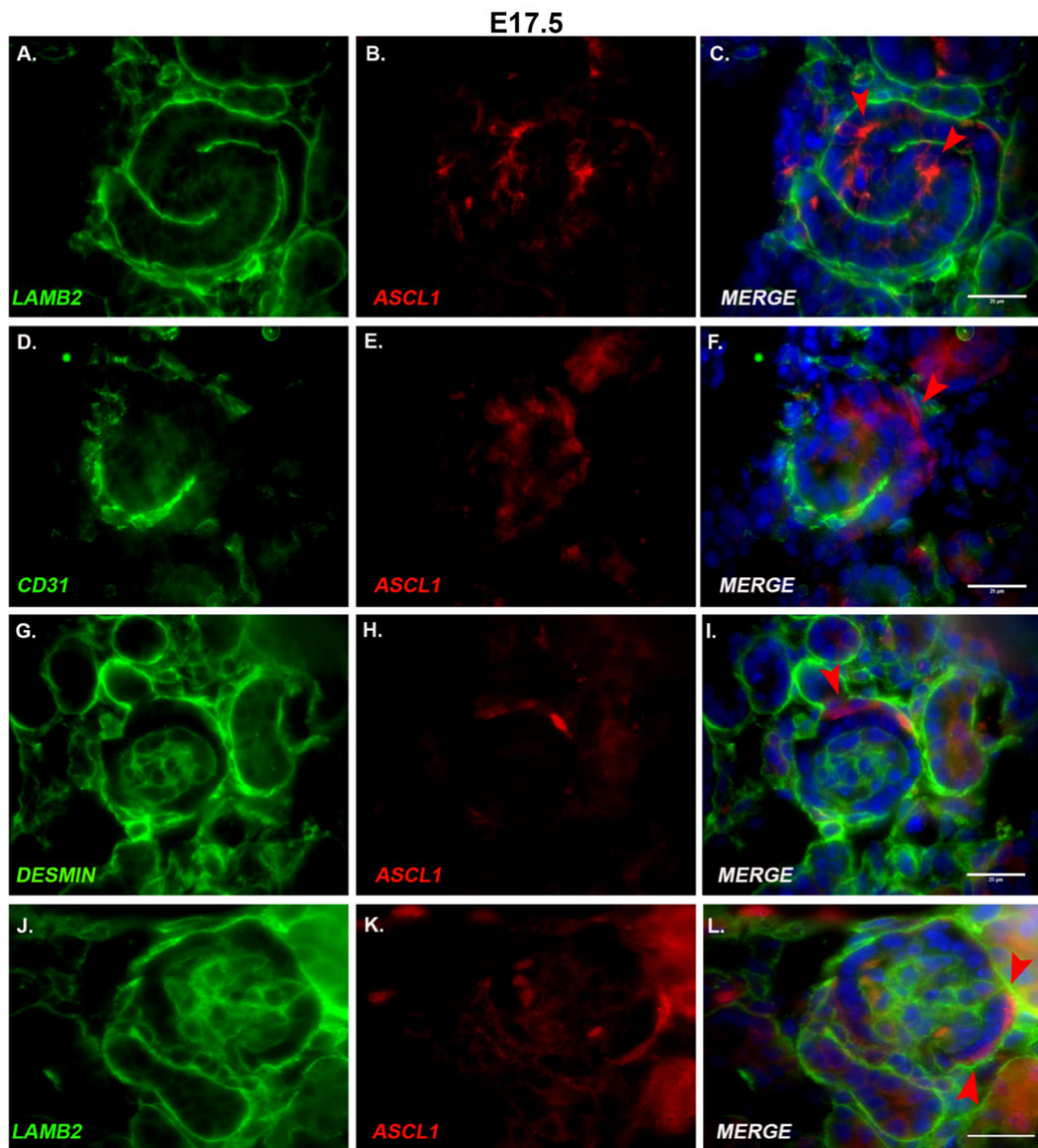


Figure 4.6. ASCL1 protein expression during early glomerulogenesis

(A-L) Shown are representative micrographs of double immunofluorescence labelled glomeruli highlighting ASCL1 expression (Alexa Fluor 594), Lamb2 (podocyte marker, Alexa Fluor 488), CD31 (endothelial marker, Alexa Fluor 488), Desmin (mesangial marker, Alexa Fluor 488) at E17.5. ASCL1 protein is expressed in the middle segment of the S-shaped body, marked with Lamb2 (B, C) The comma-shaped body exhibits increased ASCL1 protein expression, showing a perinuclear pattern of expression (F, I, L, red arrows). Scalebar 25µm.

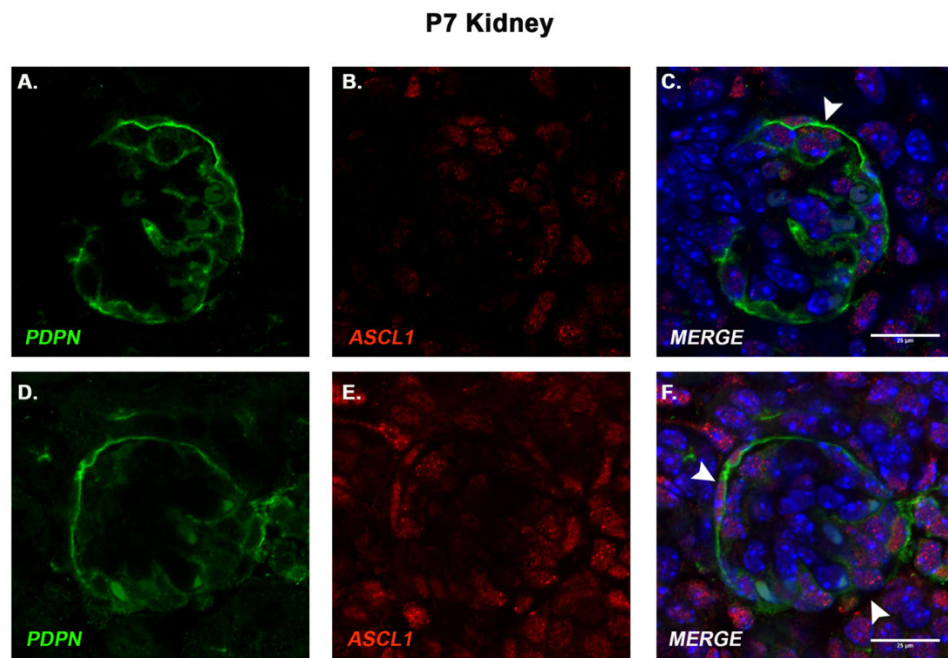


Figure 4.7. ASCL1 protein expression during late glomerulogenesis

(A-F) Representative micrographs of double immunofluorescence labelled glomeruli demonstrating ASCL1 protein expression in the differentiating capillary loops of the glomerulus. Three different representative images of the same stage reveal an abundant expression of the protein during this stage of development, predominantly in the podocytes, as indicated by the white arrows **(C, F, I)**. Scalebar, 25 μ m.

4.2.5 Doxycycline-induced *Ascl1* expression in *TetOAscl1;NPHS2;rtTA* mice

Initial data demonstrated upregulation of ASCL1 in *Wt1* glomerulopathy and during nephrogenesis. The next aim was to determine whether cell-specific overexpression of ASCL1 might result in a glomerular phenotype. Mice carrying the reverse tetracycline receptor (rtTA) under the control of the human Podocin promoter (*NPHS2*) were crossed with transgenic mice carrying the tetracycline-responsive element with the *Ascl1* gene under the mCherry reporter (*TetOAscl1*). Overexpression of *Ascl1* was induced in the podocytes following administration of doxycycline. *Ascl1* upregulation was analysed in 3-week-old mice following 2 weeks of 2mg/ml doxycycline in 5% sucrose water. Primary podocytes were then cultured and treated with 4 μ g/ml doxycycline for another four days.

To confirm overexpression, *mCherry* reporter gene was tested using fresh cryosections to determine the presence of *Ascl1* (Figure 4.8A-G). Additionally, glomerular RNA was collected from these kidney tissues and analysed by real-time qPCR to validate upregulation of *Ascl1* compared with no-doxycycline treated *TetOAscl1;NPHS2;rtTA* mice (Figure 4.8H). Podocytes were also isolated from fresh kidneys of doxycycline- vs.

no-doxycycline-treated mice, cultured and fixed to confirm *mCherry* presence (Figure 4.8I-Q).

Cryosections of the kidney revealed mCherry expression in glomeruli of the doxycycline-treated *TetOAscl1;rtTA;NPHS2* mice (Figure 4.8E-G) compared to the non-treated *TetOAscl1;rtTA;NPHS2* mice, where mCherry expression was absent (Figure 4.8A-D). In support of these findings, real-time qPCR confirmed a significant increase in *Ascl1* expression in the doxycycline-treated *TetOAscl1;rtTA;NPHS2* mutants vs. *TetOAscl1;rtTA;NPHS2* controls (** $p=0.0063$), where *Ascl1* expression was undetectable (Figure 4.8H). In addition, primary podocyte cells confirmed the upregulation of *Ascl1*, where there was clear detection of *mCherry* reporter expression (Figure 4.8I-Q).

These results confirmed that the *TetOAscl1;rtTA;NPHS2* system resulted in upregulation of *Ascl1* in the doxycycline-treated mice compared with negative controls. Following validation of *Ascl1* overexpression model, urine was collected for measurement of urine protein levels and mice sacrificed in order to ascertain the glomerular phenotype.

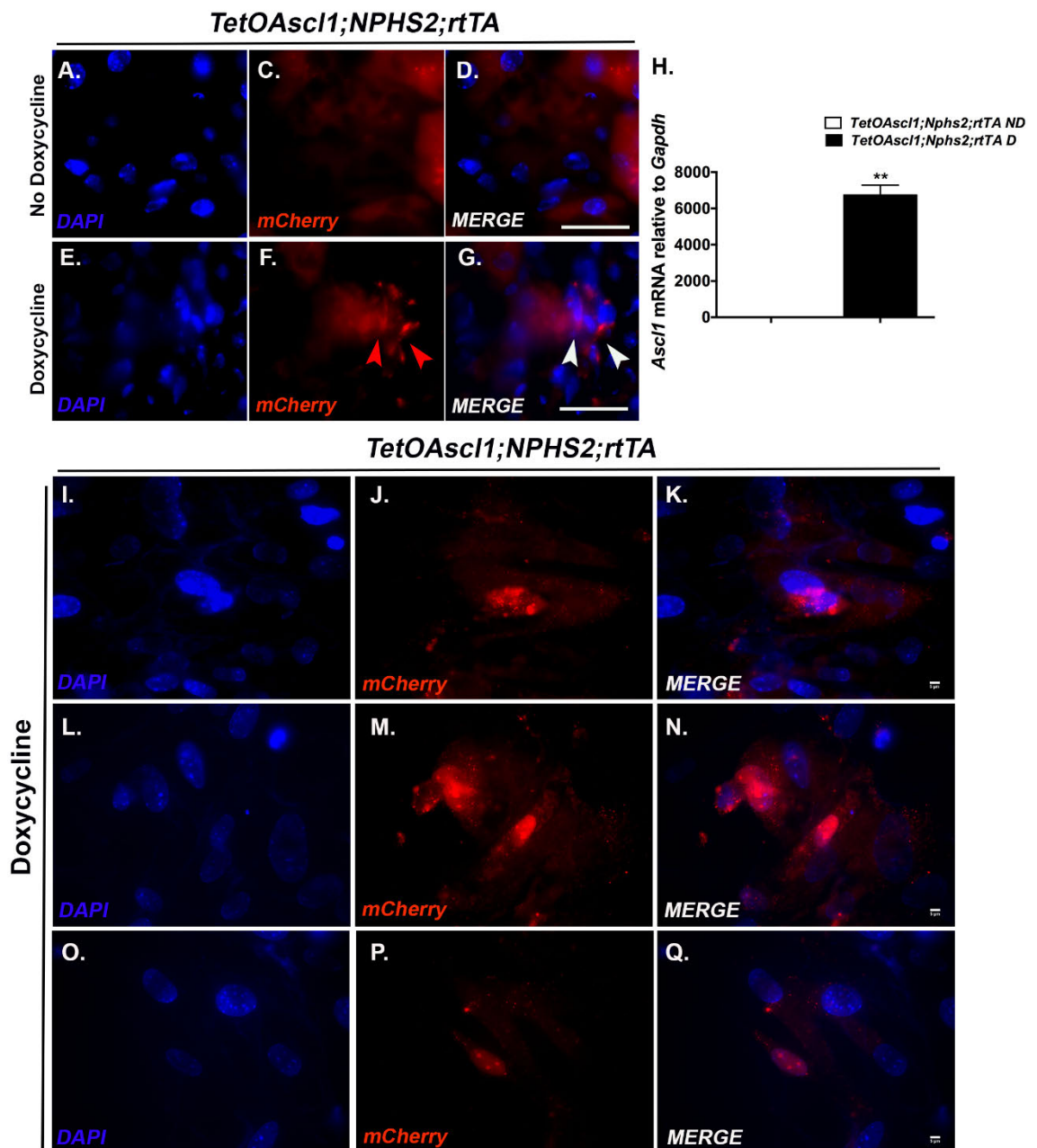


Figure 4.8. Upregulation of Ascl1 mRNA and protein in doxycycline-induced *TetOAscl1;NPHS2rtTA* primary podocytes

(A-I) Shown are representative micrographs of mouse kidney cryosections highlighting mCherry expression in the podocytes **(F, G)** post-doxycycline treatment, indicating an increase in Ascl1 expression (Scalebar, 25 μ m). Relative transcript levels showing the mean expression of Ascl1 in doxycycline-treated (D) vs. non-treated (ND) *TetO:Ascl1;NPHS2;rtTA* transgenic mice **(H)** Ascl1 transcript levels are significantly increased post-doxycycline treatment; mean \pm SEM non-treated (n=2) vs. treated (n=2), 1.02 \pm 0.19 vs. 6745 \pm 539.5, ***p*=0.0063. Representative images showing mCherry expression in doxycycline-treated *TetO:Ascl1;NPHS2;rtTA* transgenic mice of primary podocytes **(I-Q)** ASCL1 protein expression is revealed in the podocytes via mCherry in the doxycycline treated cells. Scalebar, 10 μ m.

4.2.5.1 Increased doxycycline dosage in *TetOAsc1;NPHS2;rtTA* mice does not lead to glomerulopathy

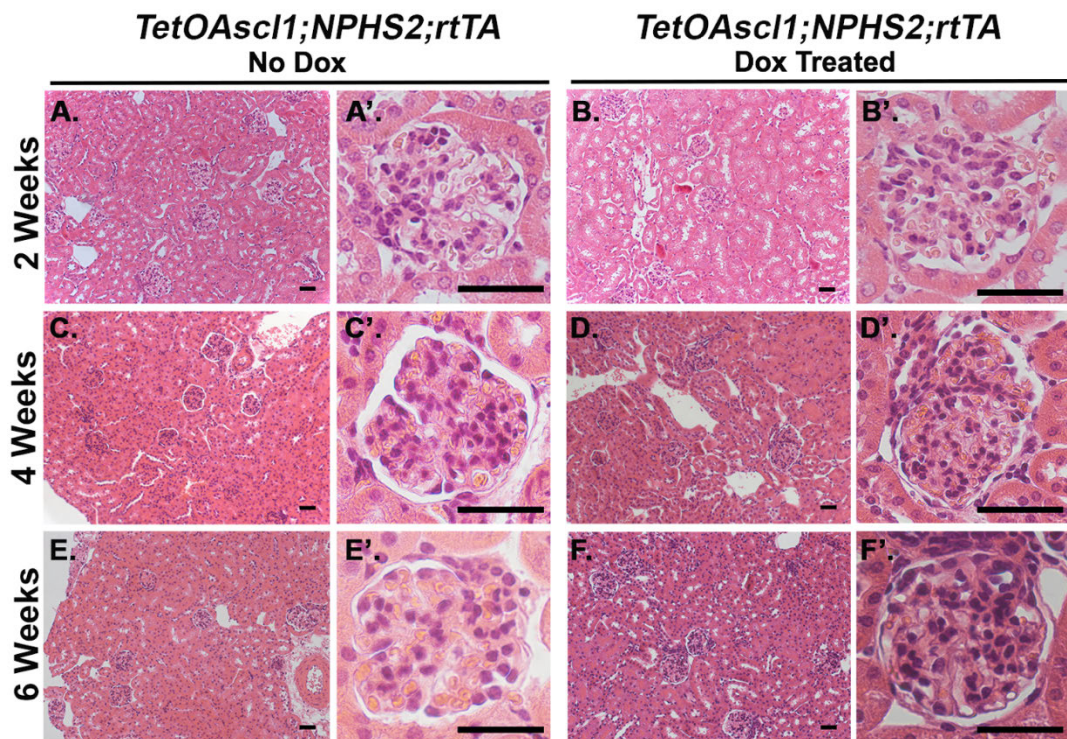
Administration of 2mg/ml doxycycline in *TetOAsc1;rtTA;NPHS2* mutants resulted in a significant increase of *Asc1*. However, this did not result in a phenotype as urine protein levels and glomerular phenotypes remained normal. The doxycycline dosage was therefore increased to 4-5g/day in chow in three-week-old mice, and urine protein loss measured on alternate days. Histological analysis by H&E to establish whether a glomerular phenotype was present was performed on kidneys collected at 2, 4 and 6 weeks post-doxycycline and histological analysis by H&E was performed (Figure 4.9).

At 2 weeks post-doxycycline, there was no glomerular or tubular phenotype present in either treated mice or non-treated controls (Figure 4.9B, B') in comparison to the non-treated controls (Figure 4.9A, A'). Glomeruli were intact with a normal number of cells and no red cells, or proteinaceous or hyaline material observed in the tubules. At four weeks, the glomeruli remained normal with no evidence of GS or tubulointerstitial abnormalities (Figure 4.9D, D') compared to their non-treated controls (Figure 4.9C, C'). Cryosections of kidneys, 6 weeks post-doxycycline, showed no evidence of GS nor tubule interstitial fibrosis with hyaline material (Figure 4.9F, F'). Higher magnification of the glomerulus showed a normal mesangial matrix with no hypo- nor hypercellularity. Tubules contained no hyaline material (Figure 4.9F') compared to the non-treated controls, where both groups were indistinguishable (Figure 4.9E, E').

Urine was collected every other day and was analysed for proteinuria following doxycycline treatment (Figure 4.9G). Four different groups were analysed, including the mutant group, doxycycline-treated *TetOAsc1;rtTA;NPHS2* vs. three control groups; no-doxycycline-treated *TetOAsc1;rtTA;NPHS2*, doxycycline-treated *TetOAsc1*, and doxycycline-treated *rtTA;NPHS2* mice. Urine was collected up to 11 days and tested using urine reagent strips to measure protein levels. We were unable to collect urine at later time-points as the metabolic cages were not available in the following weeks. Protein levels did not reach above 1+, which was considered normal and all groups were comparable, including the mutants, where all mice had either 0 or 1+ protein in their urine. Protein levels did not increase in the days post-doxycycline and remained similar to the control groups, showing no indication of proteinuria (Figure 4.9G).

At 6 weeks of doxycycline administration, both histology and urine-protein analysis remained normal. This indicated that in contrast to *Wt1*-deleted mutants, overexpression of *Asc1* did not result in a renal phenotype. Therefore, although there was an increase

in *Ascl1* in *Wt1*-glomerulopathy, this might simply be secondary or compensated by Hes/other Notch pathway members.



G.

| Proteinuria level | Mutant | | | | Controls | | | | | | | | | | | |
|-------------------|---------------------------|---------|---------|----------|------------------------------|---------|---------|----------|-----------------|---------|---------|----------|-----------------|---------|---------|----------|
| | TetOAscl1;NPHS2rtTA (DOX) | | | | TetOAscl1;NPHS2rtTA (No DOX) | | | | TetOAscl1 (DOX) | | | | NPHS2rtTA (DOX) | | | |
| | D5 Post | D7 Post | D9 Post | D11 Post | D5 Post | D7 Post | D9 Post | D11 Post | D5 Post | D7 Post | D9 Post | D11 Post | D5 Post | D7 Post | D9 Post | D11 Post |
| 0 | 3 | 4 | 4 | 3 | 2 | 2 | 3 | 4 | 1 | 1 | 2 | | | 1 | 1 | |
| 1+ | 4 | 3 | 3 | 4 | 2 | 2 | 1 | | | 2 | 1 | 1 | 1 | 4 | 4 | |
| 2+ | | | | | | | | | | | | | | | | |

Figure 4.9. Doxycycline-induced *TetO:Ascl1;NPHS2;rtTA* exhibit normal glomerular morphology

Shown are representative H&E sections of *TetO:Ascl1;NPHS2;rtTA* mice after 2, 4 and 6 weeks of non-doxycycline (**A-E'**) and doxycycline (**B-F'**) treatment. Low power images of non-treated mice reveal no abnormality in the tubules and glomeruli (**A,C,E**). Higher power images show intact glomeruli with a normal number of cells (**A', C', E'**). Low power image of the kidney after 2 weeks of doxycycline treatment exhibited no phenotype in the interstitium which remained normal after 4 and 6 weeks of doxycycline treatment in the *TetO:Ascl1;NPHS2;rtTA* mice (**B, D, F**). Higher power images of the glomerulus at these time points revealed healthy glomeruli (**B', D', F'**). Scalebar 25 μ m. Table demonstrating levels of proteinuria in doxycycline-treated *TetO:Ascl1;NPHS2;rtTA* mice vs. controls; non-doxycycline-treated *TetO:Ascl1;NPHS2;rtTA*, doxycycline-treated *TetOAscl1* and doxycycline-treated *NPHS2;rtTA* mice (**G**) Levels of urine protein remain consistent amongst mutants and controls throughout the treatment.

4.3 Discussion

This chapter has investigated a role for *Ascl1* in *Wt1* glomerulopathy and nephrogenesis. RNA and protein analysis showed that levels of *Ascl1* are indeed increased at D4, D5 and D6 P.I. mutants compared to the controls. *Ascl1* function has been studied in neurogenesis and has been shown to play a role in cell cycle promotion and termination (Castro et al., 2011, Ge et al., 2006). In this study, we explored the role of ASCL1 in early and late nephrogenesis. Interestingly, the expression patterns of ASCL1 transformed from perinuclear to nuclear from early to late nephrogenesis. This is suggestive of a role in Notch signalling mediated transcriptional activation.

The effect of *Ascl1* overexpression on differentiating podocytes was examined by crossing transgenic mice carrying the dox-inducible *podocin-rtTA* with transgenic mice carrying *TetO-Ascl1* under the mCherry reporter. Following 6 weeks of doxycycline treatment, mice did not show any histological renal phenotype nor evidence of proteinuria. These results suggest that *Ascl1* does not participate in podocyte injury following *Wt1* deletion and its upregulation may only be relevant to regulation of Notch pathway signalling.

***Ascl1* mRNA levels oscillate from D4 to D6 P.I. *Cre-ER^{TM+/-};Wt1^{ff}* mutants**

Ascl1 transcript levels were increased in the *Cre-ER^{TM+/-};Wt1^{ff}* mutants compared to controls at D4 and D6 P.I. Transcript levels of *Ascl1* oscillated at each time-point, showing reduced *Ascl1* mRNA levels at D5 P.I. in the mutants. Previous research has highlighted the role of *Ascl1* during different stages of neurogenesis, where its expression patterns oscillate with the Notch bHLH transcription factor, *Hes1* (Vasconcelos and Castro, 2014). The proneural transcription factors, including *Ascl1*, play a crucial role in both proliferation and complete differentiation of neuronal development, with the assistance of specific genes, including *Hes1* of the Notch pathway. Genetic ablation of *Ascl1* results in decreased neuron generation (Casarosa et al., 1999, Horton et al., 1999), whilst overexpression of *Ascl1* induces cell cycle exit and complete neuronal differentiation (Castro et al., 2006, Berninger et al., 2007, Geoffroy et al., 2009), highlighting its importance in regulating vertebrate neurogenesis.

Our data shows that increased *Ascl1* mRNA expression at D6 P.I. is accompanied by reduced levels of *Hes1* in the mutants which to some extent mirrors the oscillatory expression pattern seen in neurogenesis. *Hes1* levels were higher in the mutants compared to controls at each time-point. *Ascl1* oscillations depend on *Hes1* oscillations

in neurogenesis, regulating active or quiescent neural stem cells. The oscillation between *Hes1* and *Ascl1* levels in our model may suggest that both genes interact to regulate the Notch pathway in podocytes. The expression of podocyte ASCL1 was further validated through Western blot analysis at D4 P.I., showing a clear increase of the protein in the *Cre-ERT^{M+/-};Wt1^{ff}* mutants. By immunofluorescence, ASCL1 protein was nuclear and mainly restricted to podocytes, indicating that ASCL1 may be activated in *Wt1* glomerulopathy, and may interact with HES1 during Notch activation.

Earlier findings have proposed that *Wt1* acts upstream of *Ascl1* during olfactory neuron development. *Wt1* KTS^{-/-} mouse mutants had reduced *Ascl1* and severely impaired neural retina, with thinner retinas and fewer cells (Wagner et al., 2005). *Hes1* and *Wt1* are the two main transcription factors regulating *Ascl1* during embryonic olfactory development. *Hes1* and *Hes5* are its downstream targets and their expression prevents premature differentiation of neurons (Cau et al., 2000, Nicolay et al., 2006), whilst *Wt1* is upstream (Wagner et al., 2005). Although little is known about the molecular control of *Ascl1* expression, earlier research (Wagner et al., 2005) and work presented in this chapter suggest that *Wt1* deletion may increase *Ascl1* mRNA levels in *Wt1* glomerulopathy. Furthermore, *Hes1* and *Hes5* expression are affected following *Wt1* deletion, which may be a consequence of *Ascl1* overexpression, manipulating the expression levels of the canonical Notch targets. One way to further examine this would be to investigate the Notch pathway following *Ascl1* overexpression in the *TetOAscl1;rtTA;NPHS2* mutants.

The specific expression patterns of both ASCL1 and HES1 in the podocytes corroborated our findings of increased mRNA levels of both bHLH transcription factors in podocyte injury and onset of GS. Patients with R390X and R362X *WT1* mutations also showed ASCL1 overexpression in their glomeruli compared to control biopsies. HES1 was also overexpressed in the glomeruli of the patients. Both of our *WT1* patient samples carry a mutation lacking three of the four zinc fingers in which the KTS isoforms are present, leading to DDS. Here, we show that *WT1* mutations and deletion result in increased ASCL1 expression with glomerular injury, suggesting that WT1 may be controlling ASCL1 activity. By contrast, *Wt1* +KTS mutations in mice have shown reduced *Ascl1* expression during olfactory development (Wagner et al., 2002). By studying -KTS/+KTS isoforms, we could further explore the relationship between *Wt1* and *Ascl1* in podocyte development and injury.

Ascl1-positive podocytes do not undergo apoptosis in late GS

Since apoptosis is a major mechanism following podocyte injury (Chapter 3.2.2), the aim was to investigate whether *Ascl1* participated in inducing cell death. Apoptosis was detected by TUNEL analysis in D12 P.I. mutants, where a very small number of ASCL1-positive cells were observed. TUNEL was not detected in the majority of ASCL1-positive podocytes. This suggests that podocyte apoptosis is not activated by increased ASCL1 expression. Conversely, *Ascl1* mRNA has been associated with apoptosis in the adult rat brain (Kolobov et al., 2012). While research has focused on ASCL1 contributing to apoptosis in SCLC and the brain, no work has explored its role in the pathogenesis of podocyte injury and apoptosis. The preliminary data presented here shows that there is an upregulation of *Ascl1* in our D4 to D6 P.I. mutants, however, this does not contribute to apoptosis or the progression of GS.

Ascl1 is expressed during podocyte differentiation

The current data shows that *Ascl1* is increased in our model of *Wt1* glomerulopathy. Given its oscillatory role with *Hes1* in neurogenesis and the role of the Notch pathway during nephrogenesis, we sought to investigate whether *Ascl1* plays a role during nephrogenesis.

Results revealed that in murine E17.5, ASCL1 was present in the middle region of the S-shaped body during glomerulogenesis, similar to components of the Notch pathway, namely HES1 and HES5 (Piscione et al., 2004). ASCL1 displayed a perinuclear pattern of expression at this time-point, rather than nuclear, indicating that it may be playing several roles during nephrogenesis, as it does in neurogenesis (Garcez et al., 2015, Britz et al., 2006, Pacary et al., 2011, Liu et al., 2017). One of its major roles in neurogenesis is during mitotic spindle assembly, which may explain its specific pattern of expression in the S-shaped body, as ASCL1 is detected at each end of the nucleus, indicating that mitosis may be occurring at that point in time.

At post-embryonic stage, P7, ASCL1 was detected in the nuclei of the capillary loops, further emphasising its numerous roles during development. At this time-point, ASCL1 was mainly detected within the podocytes and within the same regions as the Notch components, suggesting an association between *Ascl1* and the Notch pathway during nephrogenesis.

ASCL1 has been shown to play certain roles with the Notch pathway during neuronal differentiation. One study demonstrated its interaction with specific E-box sites within the *Dll3* promoter *in vitro* during neural tube development (Henke et al., 2009). Furthermore, *in situ* hybridisation revealed its expression within the developing mouse hypothalamus along with *Dll1*, *Hes5* and *Hey1*, where its pattern of expression overlapped with both *Dll1* and *Hes5* (Guillemot et al., 1993). Its relationship with the *Dll* genes was further revealed in chick retinal progenitors, where it was co-expressed in *Dll* progenitors of differentiating neurons and its presence was necessary for normal *Dll* gene expression (Nelson et al., 2009). Moreover, ASCL1 was discovered to regulate *Hes6* during neural differentiation (Nelson et al., 2009), adding to its importance in regulating the Notch pathway. Phosphorylation of ASCL1 serine residues regulate DNA binding, resulting in selection of transcriptional target genes with open chromatin, including *Dll1* (Guillemot and Hassan, 2017).

Together, these elements highlight ASCL1's importance and association with the Notch pathway during differentiation and its possible role with the Notch pathway during nephrogenesis. Since the Notch pathway plays a crucial role during early podocyte differentiation as well as being regulated by ASCL1 during neuronal development, ASCL1's expression patterns during glomerular development does not seem surprising. Perhaps, during podocyte development, ASCL1 regulates the Notch pathway to induce cell proliferation and differentiation, as part of glomerular morphogenesis. A more reliable method to explore *Ascl1* expression during podocyte differentiation would be by lineage tracing. An *Ascl1*-GFP mouse line can be analysed at different stages of development, such as E13.5, E15.5, E18.5 and P7.

Overexpression of Ascl1 in the podocytes does not induce podocyte injury

The upregulation of *Ascl1* in *Wt1* deleted *Cre-ERTM+/-;Wt1^{fl/fl}* mutants encouraged us to explore whether ectopic expression of *Ascl1* in murine podocytes would induce podocyte injury manifested as GS. Overexpression of *Ascl1* was validated by real-time qPCR as well as *mCherry* reporter gene expression in kidney cryosections and podocyte cells. Although *Ascl1* RNA expression was increased at D4 P.I. in the mutants compared to the controls, overexpression up until 6 weeks in the *TetoAscl1;rtTA;NPHS2* system did not reveal any signs podocyte injury, including proteinuria and GS. Previous studies revealed that ectopically induced *Notch1* in the developing and differentiated podocytes resulted in GS and podocyte apoptosis (Waters et al., 2008, Niranjana et al., 2008), thus suggesting that *Ascl1* is not the main inducer of podocyte injury in *Wt1* glomerulopathy. Although it may have a role in regulating the Notch pathway, there are other possible

upstream players that may influence the Notch pathway to stimulate podocyte injury and GS. Furthermore, while *Ascl1* overexpression was confirmed in this mouse model, 6 weeks of doxycycline may have not been enough time to induce injury. In future, extending doxycycline treatment for a longer period of time, or challenging the mice with toxic agents could result in a diseased phenotype and allow us to further understand *Ascl1* expression patterns in the podocyte injury further.

Overall, this chapter has demonstrated an increase in *Ascl1* in our model of *Wt1* glomerulopathy. Increased levels of *Ascl1* mRNA is associated with reduced levels of *Hes1*, the canonical target of the Notch pathway. The oscillation between both genes suggests that *Ascl1* and the Notch pathway may be regulating each other in the context of podocyte injury to rescue disease. This correlates with our findings of ASCL1 being expressed in the middle region of the S shaped body in early nephrogenesis, similar to the Notch components, HES1 and HES5. Overexpression of *Ascl1* in transgenic mice does not induce podocyte apoptosis or GS, suggesting that it may be activated to rescue disease as a result of podocyte injury. To further investigate the role of *Ascl1* in nephrogenesis, future experiments could focus on analysing an *Ascl1*-GFP mouse line at different stages of nephrogenesis. RNA studies, including *in situ hybridisation* could be used to highlight the association between *Ascl1* and the Notch pathway during nephrogenesis. To conclude, *Ascl1* may be a participant in regulating Notch signalling activity during glomerulogenesis and podocyte injury.

Chapter 5 - Discussion and Future Directions

5.1 Overall Discussion

5.1.1 Utility of inducible models to study mechanisms underlying disease onset

Data presented in this thesis has demonstrated a novel role for Jag1-mediated Notch activation in *Wt1* glomerulopathy, with semi-quantitative evidence of GS in an inducible model of mature podocyte injury.

Podocyte apoptosis is evident in the early proteinuric stages, accompanied by FP effacement. Increased levels of albuminuria correlate with the loss of podocytes following *Wt1* deletion. GS is evident at later stages of *Wt1* deletion with increased expression of mesenchymal markers, including *Snail* and *Slug*, highlighting an EMT in the primary mutant podocytes.

Previous studies demonstrated that ectopically activating Notch in developing and mature podocytes leads to podocyte injury associated with podocyte apoptosis and dedifferentiation, as well as DMS and FSGS histological phenotypes (Waters et al., 2008, Niranjan et al., 2008), and this also correlated with *WT1* mutations (Chernin et al., 2010, Lipska et al., 2014). Our model revealed an upregulation of several Notch components in primary podocytes following *Wt1* deletion, including the Notch bHLH transcription factors, *Notch1* and *Nrarp* (Krebs et al., 2001). Primary mutant podocytes also revealed an upregulation of JAGGED1 and POFUT1, suggesting a ligand-dependent mechanism of podocyte Notch activation at the progression of disease. Additionally, HES1 induction in *Nphs2;rtTA* primary podocytes increased *Snail* and *Slug* expression, further supporting the role of Notch stimulating EMT.

γ -secretase inhibitors administered prior to disease onset prevented GS and albuminuria, proposing a role for Notch-mediated activation of podocyte apoptosis and EMT in *Wt1* glomerulopathy. In support of this, earlier findings demonstrated podocyte Notch activation in human biopsies of glomerular injury and in models of GS (Niranjan et al., 2008, Murea et al., 2010, Sweetwyne et al., 2015, Morimoto et al., 2016). Increased expression of the canonical Notch targets, including *Hes1*, *Hes3*, *Hes5*, *Hey1*, *Hey2* and *HeyL* were demonstrated in STZ- and PAN-induced models of GS (Niranjan et al., 2008). Increased Notch activity has been found to promote podocyte apoptosis, and in turn podocyte apoptosis has been shown to induce FSGS pathogenesis. Apoptotic genes

including *Trp53* and *Apaf1*, as well as positive TUNEL staining, have been detected in murine models of induced Notch1 ICD in mature podocytes (Niranjan et al., 2008). Podocyte apoptosis is inhibited following pifithrin- α induction in the *Notch1* ICD-induced models, suggesting a role for the p53 pathway in Notch-mediated apoptosis (Niranjan et al., 2008). The role of p53 mediated apoptosis might to be involved in the pathogenesis of GS in our *Wt1* glomerulopathy model. Further evidence of Notch-induced podocyte apoptosis has been provided by conditionally deleting podocyte *Rbpj* in mice with DN, where podocyte apoptosis was decreased (Niranjan et al., 2008). Given that *Notch1* deletion has been associated with abrogating GS in models of DN, as well as downregulating *Snail1*, an EMT marker (Sweetwyne et al., 2015), it would be noteworthy to explore whether conditional *Notch1* deletion would reduce podocyte apoptosis and EMT in our model. Conditional inactivation of *Notch1* and its canonical targets in early and late *Wt1* glomerulopathy will allow us to further delineate Notch's role in disease pathogenesis.

Notch bHLH transcription factors, *Hes/Hey* genes are downregulated following terminal podocyte differentiation (Piscione et al., 2004) and podocyte differentiation has been found to be regulated by a transcriptional network of genes, including *Wt1*, *Foxc1/c2*, and *Rbpj* (O'Brien et al., 2011, White et al., 2010). Binding motifs of FOX have been linked with WT1 binding regions, supporting their synchronised relationship in podocyte regulation (Lefebvre et al., 2015, Kann et al., 2015b). Podocyte numbers are seen to be reduced in zebrafish following double knockdown of *wt1a/rbpj* or *wt1a/foxc1a* compared to single knockdown of any of the three genes, supporting a collaborating network between the genes in regulating podocyte specification (O'Brien et al., 2011). Moreover, an interaction between WT1, FoxC2 and RBPJ has been reported on a protein level, and HEY1 expression can be triggered through the combination of WT1, NICD and FOXC1/2 (O'Brien et al., 2011). *Wt1* regulates expression of the *Hey1* orthologue, *XHRT*, in *Xenopus*, in early glomus development (Taelman et al., 2006) as well as modulating *HeyL* expression during murine metanephric development in pre-tubular aggregates, by binding to its promoter (Hartwig et al., 2010). Collectively, these studies highlight the relevance of *Wt1* and *Foxc1/2* in regulating Notch transcriptional targets during nephrogenesis.

As highlighted above, normal mature podocytes no longer express Notch components. *Wt1* deletion in our model led to an upregulation of the Notch pathway markers, *Notch1*, *Nrarp*, *Hey1*, *HeyL*, *Hes1*, *Hes3* and *Hes5*. These changes are reminiscent of earlier findings in zebrafish that *Wt1* and *Foxc1a* repress NICD1's ability to activate a synthetic Notch reporter driven by *Rbpj* sites (O'Brien et al., 2011), proposing a role for WT1 and

FOXC1/2 to antagonise Notch signalling. Our data also reveals downregulation of *Foxc2* expression following *Wt1* deletion, with increased Notch transcript expression at the onset of GS and proteinuria. Our current findings demonstrate an increase in *Hey2* transcript expression concurrent with a downregulation of *Foxc2* in the mature podocytes, advocating a role for *FoxC2* in inhibiting *Hey2* expression, as well as other Notch components, in differentiated podocytes. Earlier studies in endothelial cells revealed that *Hey2* is a transcriptional target of *FoxC2* (Hayashi and Kume, 2008), which correlates with our current findings. Therefore, restoring *FoxC2* quantities in the adult *Cre-ER^{TM+/-};Wt1^{ff}* mutants may suppress Notch bHLH gene activity, and restore podocyte-specific gene expression. Alternatively, Hippo signalling may be another pathway mediating Notch activity in *Wt1* glomerulopathy. Hippo signalling has been found to target Notch components (Totaro et al., 2017), as well as being a target of *Wt1* during podocyte specification (Kann et al., 2015b). This can be explored by knocking down or overexpressing Hippo signalling components in our model of *Wt1* glomerulopathy.

Notch glycosylation is necessary for the activation of Notch signalling through the binding of Notch receptors and ligands (Chung et al., 2017). Our data revealed increased expression of the O-fucosyltransferase POFUT1 in the *Cre-ER^{TM+/-};Wt1^{ff}* mutant podocytes, as well as *Mfng*, which facilitates Notch ECD glycosylation (Bruckner et al., 2000, Kakuda and Haltiwanger, 2017). Typically, Fringe glycosylation of *Notch1* activates Notch signalling through the Dll1 ligand. A more recent study showed *Notch2* and *Jag1* play a role in kidney fibrosis. Our data reveals increased expression of *Jag1* and Manic Fringe in our *Cre-ER^{TM+/-};Wt1^{ff}* mutants as well as in human samples of WT1-mutated GS, with increased Notch activity. This data suggests that *Mfng* and *Jag1* contribute to Notch signalling activation in our model of *Wt1* glomerulopathy.

JAG1 protein was increased in our mutant podocytes in the early stages of disease, which correlates with earlier reports showing *Jag1* in GS (Niranjan et al., 2008, Murea et al., 2010). *Dll1* expression, on the other hand, showed no difference between the mutants and the controls at this time point. Both ligands overlap in the middle region of the S-shaped body during kidney development, and murine models showing double deletion of both ligands results in reduced numbers of proximal tubules and glomeruli, highlighting Notch's importance in proximal nephron development (Liu et al., 2013). Moreover, the *Jag1* allele has been shown to rescue some WT1-positive podocytes in *Dll1-null* mice, highlighting its potential role in podocyte fate induction (Liu et al., 2013). Therefore, deletion of *Jag1* in adult *Cre-ER^{TM+/-};Wt1^{ff}* mice will allow us to further analyse targets of disease manifestation.

The proneural transcription factor *Ascl1* was also increased in the *Cre-ER^{TM+/-};Wt1^{fl/fl}* mutants at the early stages of disease. Several studies have highlighted the role of *Ascl1* and an overlapping relationship with the Notch pathway in neurogenesis. Intriguingly, *Ascl1* plays a role in the maintenance of *Hes1* oscillations in neural stem cells (Vasconcelos and Castro, 2014), correlating with our model showing oscillating *Ascl1* and *Hes1* mRNA levels during early stages of the disease. Our data demonstrates Notch signalling is potentially activated through *Jag1* binding, proposing a role for *Ascl1*-mediated Jagged Notch activation. Former investigations revealed that *Wt1* expression is upstream of *Ascl1* during olfactory development (Wagner et al., 2005), highlighting a link between both genes during neurogenesis. The deletion of *Wt1* in our adult mice may result in *Ascl1* overexpression in the podocytes, contributing to aberrant Notch activation. These findings are consistent with patient biopsies of *WT1* mutations (namely in R390X and R362X mutations), where ASCL1 protein expression was increased, further supporting the theory of *WT1* deletions/mutations altering *Ascl1* expression patterns. Our model shows that *Ascl1* may contribute to the temporal gene expression of *Hes1* in podocyte injury.

5.1.2 Utility of primary podocyte culture

The isolation of primary podocytes has proven to be a valuable tool in investigating the mechanisms and pathways associated with podocyte injury. To confirm that our cells were purely podocytes, cells were stained with the podocyte-specific antibody, Nestin. Having utilised this method, we were able to specifically explore podocyte genes and podocyte-related disease.

5.1.3 Limitations

Despite achieving the overall goals of the project, technical challenges were encountered along the way. RNA sequencing was achieved through glomerular isolation. This work was undertaken at an early stage of the project; thus, the analysis was based on a heterogenous population including podocytes, mesangial and endothelial cells. Primary podocyte isolation was then utilised, which will allow future RNA sequencing analysis to be achieved with pure podocytes. Furthermore, due to the injury to the cells, their viability and ability to survive in culture was limited, thus restricting us from carrying out later experiments on the cells. With this in mind, genetic rescue experiments were limited due to the low viability of the primary cells.

5.2 Future work

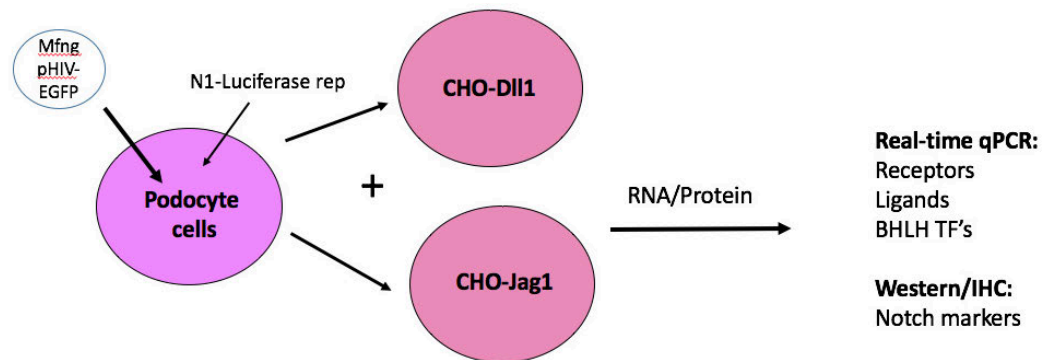
5.2.1 Pharmacological inhibition of Notch to prevent late stages of disease

GSI-IX treatment reduced Notch activity in adult *Cre-ER^{TM+/-};Wt1^{ff}* mice at D4-D5 P.I., preventing GS and reducing albuminuria. While prophylactic treatment prevented onset of disease progression, GSI-IX treatment did not rescue disease at the later stages (D7-D8 P.I.). Increasing the sample size, this would validate existing findings with regards to rescuing a disease phenotype using GSI-IX. It would also be worth treating mutant mice at D6 P.I., where there is onset of disease. Gastrointestinal toxicity has been reported to be a major side-effect of GSI-IX (Barten et al., 2006). It has also been shown to alter lymphocyte development (Wong et al., 2004). Alternative compounds inhibiting Notch activity include SAHM1, which interferes with the *Notch1* transactivation complex, repressing its downstream targets. Previous reports have shown that SAHM1 specifically represses Notch signalling in human T-ALL (T-cell acute lymphoblastic leukaemia) cells and a mouse model of NOTCH1-driven T-ALL, with no toxic effects in comparison to DAPT (Moellering et al., 2009). This therefore will be a valuable avenue to pursue by exploring its effects on *Wt1* glomerulopathy.

5.2.2 Investigating Fringe and ligand-mediated Notch signalling in podocytes

Our data reveals an upregulation of Notch signalling with increased Manic Fringe and JAG1 expression in the mutants compared to the controls. Elucidating the effects of Manic Fringe on JAG1-mediated Notch1 signalling would be an interesting avenue to explore. One way of approaching this would be to overexpress Manic Fringe by transfecting it into immortalised podocytes co-transfected with a Notch1 luciferase reporter construct. These would then be co-cultured with DLL1 or JAG1 expressing CHO cells in order to reveal which ligand induces Notch1 activity. An experimental design to overexpress Manic Fringe in immortalised podocytes is illustrated in Figure 5.1. Past studies have utilised this method in order to determine ligand-mediated Notch signalling in other cells/species (Yang et al., 2005, Ilagan et al., 2011, Chen et al., 2001). Luciferase assays would reveal Notch signalling and upregulation of its downstream bHLH targets, including *HES* and *HEY* would be explored through protein and transcript analysis. This approach may highlight which ligand is potentiating Notch activity by Manic Fringe, or if in fact other Fringes are participants. Furthermore, by using shRNA knockdown of Manic Fringe in the mutant podocytes to inhibit Notch activity, EMT and podocyte apoptosis may be prevented. Preliminary data (Figure 3.26) using sh*Mfng* has already shown evidence of target knockdown, as well as reduced Notch activity through its bHLH TFs.

Additionally, EMT genes *Snail* and *Slug* were downregulated (Figure 3.26). Despite there being a decrease in the above markers, p values were not significant, and differential gene expression between scrambled and *Mfng* shRNA were also not significant. Increasing sample numbers (n=10) would allow us to produce a more significant and accurate result. Additionally, knockdown of other acetylglucosaminyltransferases may also be necessary to further dissect the role of Fringe-mediated Notch signalling in the context of podocyte injury.



Does overexpressed *Mfng* activate Notch in podocytes?

Figure 5.1. Experimental design for Manic Fringe overexpression in podocytes

5.2.3 Strategies to investigate transcriptional networks

Ascl1 expression and the Notch pathway oscillate during neurogenesis (Vasconcelos and Castro, 2014); future experiments examining *Ascl1*'s temporal and spatial role alongside the Notch components and *Wt1* during nephrogenesis will allow us to appreciate their relationship further. Our data revealed that ASCL1 protein is expressed during glomerulogenesis (4.2.4); Additional experiments analysing ASCL1 protein expression, in conjunction with *in situ* hybridisation of Notch components and *Wt1*, will allow further appreciation of ASCL1's role in early kidney development. During nephrogenesis, the Notch transcription factors are known to become downregulated (Barak et al., 2012, Asanuma et al., 2017), suggesting a role for Notch in podocyte fate specification. Utilising a transgenic mouse in which the *Ascl1* locus carries a GFP element would allow us to further explore the spatial and temporal expression of the gene during nephrogenesis at E13.5, E15.5, E18.5 and P7, where Notch expression is downregulated. Another approach would be to cross *CreTM-Wt1* mice with *Ascl1*-GFP mice, induce with tamoxifen, and harvest the kidneys at D4 post-tamoxifen (only proteinuria is detected), D5 (early GS), D6 and D7 P.I. (established GS with significant albuminuria). Primary podocytes would be isolated and the *Ascl1*-GFP positive podocytes sorted from the *Ascl1*-GFP-negative podocytes. RNA would be extracted from

both and differential Notch pathway expression investigated in both groups by real-time qPCR. This would allow us to understand the relationship between *Wt1* and *Ascl1*. Furthermore, analysing podocyte differentiation in *Ascl1*^{-/-} null mice (from Professor Francois Guillemot), would allow us to further validate whether *Ascl1* has a significant role during podocyte development. We know that *Dll1* is expressed in the proximal domain of the RV during nephrogenesis (Kopan et al., 2007, O'Brien and McMahon, 2014) and ASCL1 binds to the enhancer of *Dll1* during neurogenesis, triggering its transcription (Nelson and Reh, 2008, Nelson et al., 2009). Thus, it would be of interest to examine their association during nephrogenesis. *Ascl1* expression would be examined in the glomeruli, S-shaped bodies and the tubules in *Ascl1*-null mice versus wild-types.

Examination of *Ascl1*'s promoter sequence revealed conserved binding sites for *Wt1* (Figure 5.2). Additionally, the Notch bHLH protein, *HeyL* is a direct transcriptional target of *Wt1* (Hartwig et al., 2010) and conserved binding sites for *Wt1* have been revealed in the Notch bHLH protein, *Hes1* (Figure 5.2). Studies have highlighted a transcriptional complex between *WT1* and *ASCL1* (Wagner et al., 2005, Kang et al., 2014) as well as *Hes1/Ascl1* (Vasconcelos and Castro, 2014). Therefore, ChIPSeq of ASCL1 and WT1 as well as Notch components in the context of podocyte injury would be an interesting avenue to explore.

Wt1, *FoxC* and Notch signalling collaborate transcriptionally during podocyte differentiation (O'Brien et al., 2011, Kann et al., 2015b). In this project, *FoxC2* transcript was downregulated following *Wt1* deletion, with increased expression of the Notch bHLH TF, *Hey2*, at the onset of GS. By overexpressing *FoxC2* *in vivo* and *in vitro* in models of GS through a podocyte-specific *tetO;rtTA* system, we can examine whether podocyte-specific markers are upregulated, with reduced Notch signalling. RNA and ChIPSeq analysis of cells overexpressing *FoxC2* could further confirm the relationship between *FoxC2/Notch/Wt1* in models of GS.

WT1-Ascl1 promoter



WT1-Hes1 promoter

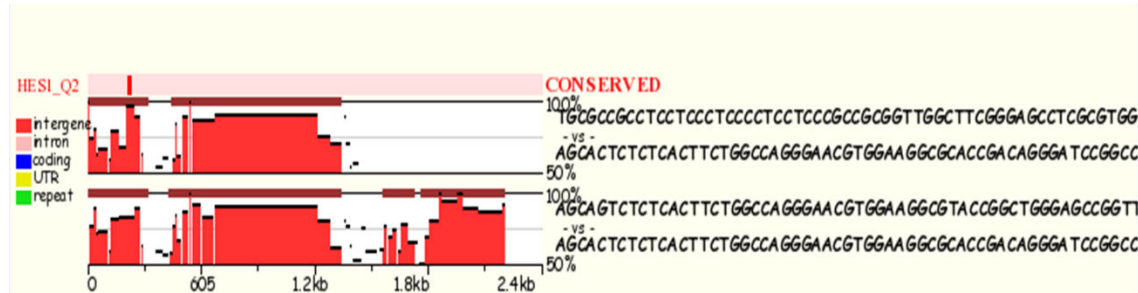


Figure 5.2. Binding domains within the *WT1* promoter for Notch bHLH genes

(% of ECR [evolutionary conserved regions])

5.2.4 Genetic rescue strategies

While GSI-IX treatment has been a mode of inhibiting the Notch pathway post-tamoxifen induction, toxic side-effects have been reported (Barten et al., 2006). An alternative method would be to genetically inhibit the Notch pathway by repressing the activation of its components, namely *Rbpj*, *Hes1* and *Notch1* in the *Cre-ER^{TM+/-};Wt1^{ff}* mouse line. Gene editing these Notch components has been achieved in the past using several mouse models of disease (Niranjan et al., 2008, Imayoshi et al., 2008, Yang et al., 2004b). With this approach, adult *Cre-ER^{T-/-};Wt1^{ff}* controls (group 1) vs. *Cre-ER^{TM+/-};Wt1^{ff}* mutants (group 2) vs. *Cre-ER^{TM+/-};Wt1^{ff};Rbpj^{ff}* or *Hes1^{ff}* or *Notch1^{ff}* rescue mice (group 3) mice could be analysed at different time-points to examine whether the genetic inhibition of Notch signalling prevents disease manifestation (Figure 5.3). The aim would be to knockout *Wt1* and the Notch targets through tamoxifen induction in all groups, then compare and examine them at each stage of disease by histological and urine analysis. By removing *Rbpj*, *Hes* or *Notch1*, we aim to rescue glomerulopathy, which would be confirmed through mRNA and protein analysis of Notch and podocyte components, including the bHLH transcription factors, *Hes* and *Hey*, and podocyte markers *Nphs1*, *Nphs2*. Furthermore, the antagonising relationship of *FoxC* on Notch signalling could be further validated in these systems by analysing *FoxC* expression following Notch signalling knockout. Podocyte apoptosis, proliferation, and EMT would be examined in all groups to confirm whether deleting Notch components ameliorates glomerular disease and podocyte injury.

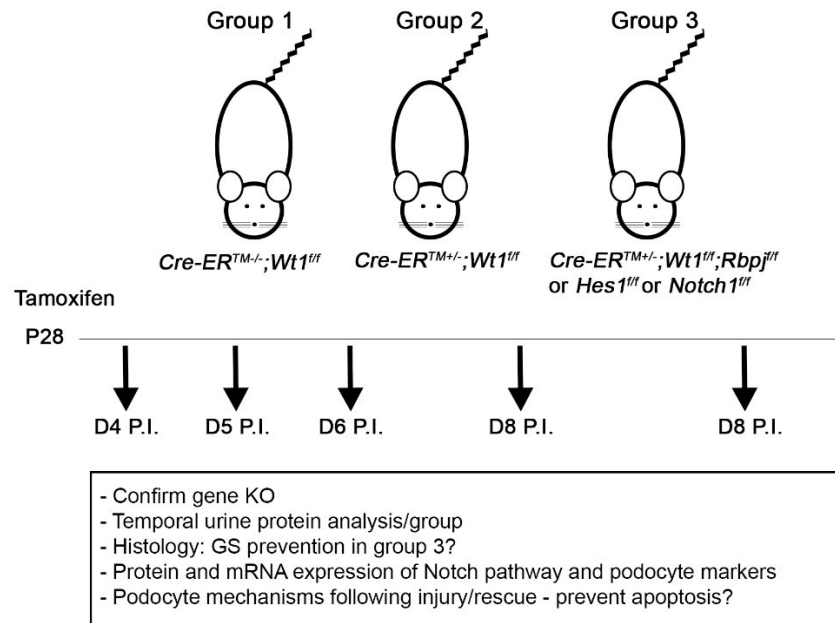


Figure 5.3. Experimental strategy to genetically inhibit Notch target genes in *Wt1* glomerulopathy

Another avenue to explore would be to validate the role of the canonical Notch targets, *Hes1* and *Hes5* in podocyte apoptosis *in vivo*. Recently, Ohtsukas's group overexpressed *Hes1* and *Hes5* in podocytes of *Nestin-rtTA;TetO^{Hes1}* or *Hes5* transgenic mice through doxycycline treatment to study neurogenesis and gliogenesis in neocortical development (Bansod et al., 2017). This would be a good model to examine whether these genes do indeed play a role in promoting podocyte apoptosis, as well as EMT upregulation in GS. Furthermore, this model will allow us to investigate other mechanisms involved in bHLH-induced podocyte injury.

5.2.5 Transgenic *Wt1*^{R394W} mutant mice

While ubiquitous *Wt1* deletion revealed GS with induced Notch signalling and apoptosis, examining models of SRNS with specific *WT1* point mutations would be a valuable route to pursue. GS accounts for 5-10% of ESRD with a recurrence of 30-60% in renal allografts (Saran et al., 2015). Genetically-mediated SRNS develops in approximately 70% of infants within the first 3 months, and 50% of children between 4 and 12 months (Rheault and Gbadegesin, 2016). *WT1* mutations contribute to about 3% of paediatric SRNS, where no treatments are currently available (Rheault and Gbadegesin, 2016, Lipska et al., 2014). The missense mutation *WT1* R394W, known to be a C-to-T transition, results in the substitution of tryptophan to arginine at amino acid 34 (R394W), disrupting zinc finger 3, and deleting the KTS insert and zinc finger 4 (Gao et al., 2004).

R394W mutations affect *WT1* DNA binding, and DDS (Lipska et al., 2014). GS presents in *Wt1^{r394w/+}* heterozygous mice by 4 months postnatally (Gao et al., 2004), providing a useful model to further examine the pathogenic role of Notch activation in *Wt1* glomerulopathy. Our data also revealed an activation of Notch in patient biopsies with de novo heterozygous *WT1* mutations associated with DMS (Figure 3.22), a phenotype also manifested in the *Wt1^{r394w/+}* transgenic mice. This represents an opportunity to investigate Notch signalling in *WT1* glomerulopathy further by confirming a histological phenotype and proteinuria. Immunohistochemistry analysis of the TGF- β pathway, including Smad2/3 activation as well as markers of EMT, would be analysed to assess the development of tubulointerstitial disease. Furthermore, temporal analysis of Notch activation would be examined at different ages in kidney sections.

5.2.6 Notch pathway analysis in other murine models of GS

WT1 mutations account for around 2-3% of SRNS, whereas mutations in other podocyte-specific genes, account for around 27-30% of SRNS (Jain et al., 2014). Our data supports Notch as a key player in GS linked to *WT1* abnormalities. *WT1* is known to act as a “master controller” of gene transcription within the podocyte, regulating many other podocyte genes linked to podocytopathy. Therefore, by conditionally deleting other key podocyte genes with tamoxifen, we would be able to explore the pathogenic mechanisms mediated by Notch signalling in other monogenic types of SRNS.

5.3 Summary

In summary, *Wt1* deletion in adult podocytes leads to podocyte apoptosis at the very early stages of GS. Notch signalling and EMT components are upregulated at the onset of disease. Induced podocyte HES1 expression results in increased *Snail* and *Slug* expression, advocating a role for HES1 in podocyte EMT. Early pharmacological inhibition of the Notch pathway reduces the severity of GS and albuminuria. Our data illustrates a possibility for repressed *FoxC2* expression to be mediating Notch activity. Due to *WT1*'s intricate biological structure and roles, examining mouse models of *Wt1* point mutations will provide unique tools to decipher the underlying transcriptional and post-transcriptional mechanisms involved in *WT1* GS.

References

Abkhezr, M. & Dryer, S. E. 2014. Angiotensin II and canonical transient receptor potential-6 activation stimulate release of a signal transducer and activator of transcription 3-activating factor from mouse podocytes. *Mol Pharmacol*, 86, 150-8.

Abrahamson, D. R. & St John, P. L. 1993. Laminin distribution in developing glomerular basement membranes. *Kidney Int*, 43, 73-8.

Acar, M., Jafar-Nejad, H., Takeuchi, H., Rajan, A., Ibrani, D., Rana, N. A., Pan, H., Haltiwanger, R. S. & Bellen, H. J. 2008. Rumi is a CAP10 domain glycosyltransferase that modifies Notch and is required for Notch signaling. *Cell*, 132, 247-58.

Adam, M. G., Berger, C., Feldner, A., Yang, W. J., Wustehube-Lausch, J., Herberich, S. E., Pinder, M., Gesierich, S., Hammes, H. P., Augustin, H. G. & Fischer, A. 2013. Synoptojanin-2 binding protein stabilizes the Notch ligands DLL1 and DLL4 and inhibits sprouting angiogenesis. *Circ Res*, 113, 1206-18.

Armstrong, J. F., Pritchard-Jones, K., Bickmore, W. A., Hastie, N. D. & Bard, J. B. 1993. The expression of the Wilms' tumour gene, WT1, in the developing mammalian embryo. *Mech Dev*, 40, 85-97.

Asanuma, K. 2015. The role of podocyte injury in chronic kidney disease. *Nihon Rinsho Meneki Gakkai Kaishi*, 38, 26-36.

Asanuma, K., Oliva Trejo, J. A. & Tanaka, E. 2017. The role of Notch signaling in kidney podocytes. *Clin Exp Nephrol*, 21, 1-6.

Asfahani, R. I., Tahoun, M. M., Miller-Hodges, E. V., Bellerby, J., Virasami, A. K., Sampson, R. D., Moulding, D., Sebire, N. J., Hohenstein, P., Scambler, P. J. & Waters, A. M. 2018. Activation of podocyte Notch mediates early Wt1 glomerulopathy. *Kidney Int*, 93, 903-920.

Augustine, K. A., Liu, E. T. & Sadler, T. W. 1995. Interactions of Wnt-1 and Wnt-3a are essential for neural tube patterning. *Teratology*, 51, 107-19.

Bahiense-Oliveira, M., Saldanha, L. B., Mota, E. L., Penna, D. O., Barros, R. T. & Romao-Junior, J. E. 2004. Primary glomerular diseases in Brazil (1979-1999): is the frequency of focal and segmental glomerulosclerosis increasing? *Clin Nephrol*, 61, 90-7.

- Bai, X., Geng, J., Li, X., Yang, F. & Tian, J. 2014. VEGF-A inhibition ameliorates podocyte apoptosis via repression of activating protein 1 in diabetes. *Am J Nephrol*, 40, 523-34.
- Bansod, S., Kageyama, R. & Ohtsuka, T. 2017. Hes5 regulates the transition timing of neurogenesis and gliogenesis in mammalian neocortical development. *Development*, 144, 3156-3167.
- Barak, H., Surendran, K. & Boyle, S. C. 2012. The role of Notch signaling in kidney development and disease. *Adv Exp Med Biol*, 727, 99-113.
- Barboux, S., Niaudet, P., Gubler, M. C., Grunfeld, J. P., Jaubert, F., Kuttann, F., Fekete, C. N., Souleyreau-Therville, N., Thibaud, E., Fellous, M. & Mcelreavey, K. 1997. Donor splice-site mutations in WT1 are responsible for Frasier syndrome. *Nat Genet*, 17, 467-70.
- Barbosa, A. S., Hadjiathanasiou, C. G., Theodoridis, C., Papathanasiou, A., Tar, A., Merksz, M., Gyorvari, B., Sultan, C., Dumas, R., Jaubert, F., Niaudet, P., Moreira-Filho, C. A., Cotinot, C. & Fellous, M. 1999. The same mutation affecting the splicing of WT1 gene is present on Frasier syndrome patients with or without Wilms' tumor. *Hum Mutat*, 13, 146-53.
- Bardeesy, N. & Pelletier, J. 1998. Overlapping RNA and DNA binding domains of the wt1 tumor suppressor gene product. *Nucleic Acids Res*, 26, 1784-92.
- Barisoni, L. 2008. Notch signaling: a common pathway of injury in podocytopathies? *J Am Soc Nephrol*, 19, 1045-6.
- Barisoni, L., Kriz, W., Mundel, P. & D'agati, V. 1999. The dysregulated podocyte phenotype: a novel concept in the pathogenesis of collapsing idiopathic focal segmental glomerulosclerosis and HIV-associated nephropathy. *J Am Soc Nephrol*, 10, 51-61.
- Barisoni, L., Mokrzycki, M., Sablay, L., Nagata, M., Yamase, H. & Mundel, P. 2000. Podocyte cell cycle regulation and proliferation in collapsing glomerulopathies. *Kidney Int*, 58, 137-43.
- Baron, M. 2012. Endocytic routes to Notch activation. *Semin Cell Dev Biol*, 23, 437-42.
- Barrett, K. L., Willingham, J. M., Garvin, A. J. & Willingham, M. C. 2001. Advances in cytochemical methods for detection of apoptosis. *J Histochem Cytochem*, 49, 821-32.

- Barten, D. M., Meredith, J. E., Jr., Zaczek, R., Houston, J. G. & Albright, C. F. 2006. Gamma-secretase inhibitors for Alzheimer's disease: balancing efficacy and toxicity. *Drugs R D*, 7, 87-97.
- Benetti, E., Caridi, G., Malavventura, C., Dagnino, M., Leonardi, E., Artifoni, L., Ghiggeri, G. M., Tosatto, S. C. & Murer, L. 2010. A novel WT1 gene mutation in a three-generation family with progressive isolated focal segmental glomerulosclerosis. *Clin J Am Soc Nephrol*, 5, 698-702.
- Berninger, B., Guillemot, F. & Gotz, M. 2007. Directing neurotransmitter identity of neurones derived from expanded adult neural stem cells. *Eur J Neurosci*, 25, 2581-90.
- Berry, R. L., Ozdemir, D. D., Aronow, B., Lindstrom, N. O., Dudnakova, T., Thornburn, A., Perry, P., Baldock, R., Armit, C., Joshi, A., Jeanpierre, C., Shan, J., Vainio, S., Baily, J., Brownstein, D., Davies, J., Hastie, N. D. & Hohenstein, P. 2015. Deducing the stage of origin of Wilms' tumours from a developmental series of Wt1-mutant mice. *Dis Model Mech*, 8, 903-17.
- Bertrand, N., Castro, D. S. & Guillemot, F. 2002. Proneural genes and the specification of neural cell types. *Nat Rev Neurosci*, 3, 517-30.
- Bharathavikru, R., Dudnakova, T., Aitken, S., Slight, J., Artibani, M., Hohenstein, P., Tollervey, D. & Hastie, N. 2017. Transcription factor Wilms' tumor 1 regulates developmental RNAs through 3' UTR interaction. *Genes Dev*, 31, 347-352.
- Bi, J., Chase, S. E., Pellenz, C. D., Kurihara, H., Fanning, A. S. & Krendel, M. 2013. Myosin 1e is a component of the glomerular slit diaphragm complex that regulates actin reorganization during cell-cell contact formation in podocytes. *Am J Physiol Renal Physiol*, 305, F532-44.
- Bielesz, B., Sirin, Y., Si, H., Niranjan, T., Gruenwald, A., Ahn, S., Kato, H., Pullman, J., Gessler, M., Haase, V. H. & Susztak, K. 2010. Epithelial Notch signaling regulates interstitial fibrosis development in the kidneys of mice and humans. *J Clin Invest*, 120, 4040-54.
- Bielinska, E., Matiakowska, K. & Haus, O. 2017. Heterogeneity of human WT1 gene. *Postepy Hig Med Dosw (Online)*, 71, 595-601.
- Bierzynska, A., Soderquest, K. & Koziell, A. 2014. Genes and podocytes - new insights into mechanisms of podocytopathy. *Front Endocrinol (Lausanne)*, 5, 226.

- Borggrefe, T. & Liefke, R. 2012. Fine-tuning of the intracellular canonical Notch signaling pathway. *Cell Cycle*, 11, 264-76.
- Borromeo, M. D., Meredith, D. M., Castro, D. S., Chang, J. C., Tung, K. C., Guillemot, F. & Johnson, J. E. 2014. A transcription factor network specifying inhibitory versus excitatory neurons in the dorsal spinal cord. *Development*, 141, 2803-12.
- Bouchard, M., Souabni, A. & Busslinger, M. 2004. Tissue-specific expression of cre recombinase from the Pax8 locus. *Genesis*, 38, 105-9.
- Boute, N., Gribouval, O., Roselli, S., Benessy, F., Lee, H., Fuchshuber, A., Dahan, K., Gubler, M. C., Niaudet, P. & Antignac, C. 2000. NPHS2, encoding the glomerular protein podocin, is mutated in autosomal recessive steroid-resistant nephrotic syndrome. *Nat Genet*, 24, 349-54.
- Boyer, O., Woerner, S., Yang, F., Oakeley, E. J., Linghu, B., Gribouval, O., Tete, M. J., Duca, J. S., Klickstein, L., Damask, A. J., Szustakowski, J. D., Heibel, F., Maignon, M., Baudouin, V., Chantrel, F., Champigneulle, J., Martin, L., Nitschke, P., Gubler, M. C., Johnson, K. J., Chibout, S. D. & Antignac, C. 2013. LMX1B mutations cause hereditary FSGS without extrarenal involvement. *J Am Soc Nephrol*, 24, 1216-22.
- Braden, G. L., Mulhern, J. G., O'shea, M. H., Nash, S. V., Ucci, A. A., Jr. & Germain, M. J. 2000. Changing incidence of glomerular diseases in adults. *Am J Kidney Dis*, 35, 878-83.
- Brauchle, E., Thude, S., Brucker, S. Y. & Schenke-Layland, K. 2014. Cell death stages in single apoptotic and necrotic cells monitored by Raman microspectroscopy. *Sci Rep*, 4, 4698.
- Bray, S. J. 2006. Notch signalling: a simple pathway becomes complex. *Nat Rev Mol Cell Biol*, 7, 678-89.
- Bray, S. J. 2016. Notch signalling in context. *Nat Rev Mol Cell Biol*, 17, 722-735.
- Britz, O., Mattar, P., Nguyen, L., Langevin, L. M., Zimmer, C., Alam, S., Guillemot, F. & Schuurmans, C. 2006. A role for proneural genes in the maturation of cortical progenitor cells. *Cereb Cortex*, 16 Suppl 1, i138-51.
- Brown, K. W. & Malik, K. T. 2001. The molecular biology of Wilms tumour. *Expert Rev Mol Med*, 2001, 1-16.

- Bruckner, K., Perez, L., Clausen, H. & Cohen, S. 2000. Glycosyltransferase activity of Fringe modulates Notch-Delta interactions. *Nature*, 406, 411-5.
- Brunskill, E. W., Georgas, K., Rumballe, B., Little, M. H. & Potter, S. S. 2011. Defining the molecular character of the developing and adult kidney podocyte. *PLoS One*, 6, e24640.
- Burghardt, T., Kastner, J., Suleiman, H., Rivera-Milla, E., Stepanova, N., Lottaz, C., Kubitzka, M., Boger, C. A., Schmidt, S., Gorski, M., De Vries, U., Schmidt, H., Hertting, I., Kopp, J., Rascle, A., Moser, M., Heid, I. M., Warth, R., Spang, R., Wegener, J., Mierke, C. T., Englert, C. & Witzgall, R. 2013. LMX1B is essential for the maintenance of differentiated podocytes in adult kidneys. *J Am Soc Nephrol*, 24, 1830-48.
- Call, K. M., Glaser, T., Ito, C. Y., Buckler, A. J., Pelletier, J., Haber, D. A., Rose, E. A., Kral, A., Yeger, H., Lewis, W. H. & Et Al. 1990. Isolation and characterization of a zinc finger polypeptide gene at the human chromosome 11 Wilms' tumor locus. *Cell*, 60, 509-20.
- Caricasole, A., Duarte, A., Larsson, S. H., Hastie, N. D., Little, M., Holmes, G., Todorov, I. & Ward, A. 1996. RNA binding by the Wilms tumor suppressor zinc finger proteins. *Proc Natl Acad Sci U S A*, 93, 7562-6.
- Caridi, G., Perfumo, F. & Ghiggeri, G. M. 2005. NPHS2 (Podocin) mutations in nephrotic syndrome. Clinical spectrum and fine mechanisms. *Pediatr Res*, 57, 54R-61R.
- Carroll, T. J., Park, J. S., Hayashi, S., Majumdar, A. & McMahon, A. P. 2005. Wnt9b plays a central role in the regulation of mesenchymal to epithelial transitions underlying organogenesis of the mammalian urogenital system. *Dev Cell*, 9, 283-92.
- Carroll, T. J. & Vize, P. D. 1996. Wilms' tumor suppressor gene is involved in the development of disparate kidney forms: evidence from expression in the *Xenopus* pronephros. *Dev Dyn*, 206, 131-8.
- Carvalho, F. L., Marchionni, L., Gupta, A., Kummangal, B. A., Schaeffer, E. M., Ross, A. E. & Berman, D. M. 2015. HES6 promotes prostate cancer aggressiveness independently of Notch signalling. *J Cell Mol Med*, 19, 1624-36.
- Casarosa, S., Fode, C. & Guillemot, F. 1999. Mash1 regulates neurogenesis in the ventral telencephalon. *Development*, 126, 525-34.

Cassady, J. P., D'alessio, A. C., Sarkar, S., Dani, V. S., Fan, Z. P., Ganz, K., Roessler, R., Sur, M., Young, R. A. & Jaenisch, R. 2014. Direct lineage conversion of adult mouse liver cells and B lymphocytes to neural stem cells. *Stem Cell Reports*, 3, 948-56.

Castro, D. S., Martynoga, B., Parras, C., Ramesh, V., Pacary, E., Johnston, C., Drechsel, D., Lebel-Potter, M., Garcia, L. G., Hunt, C., Dolle, D., Bithell, A., Ettwiller, L., Buckley, N. & Guillemot, F. 2011. A novel function of the proneural factor *Ascl1* in progenitor proliferation identified by genome-wide characterization of its targets. *Genes Dev*, 25, 930-45.

Castro, D. S., Skowronska-Krawczyk, D., Armant, O., Donaldson, I. J., Parras, C., Hunt, C., Critchley, J. A., Nguyen, L., Gossler, A., Gottgens, B., Matter, J. M. & Guillemot, F. 2006. Proneural bHLH and Brn proteins coregulate a neurogenic program through cooperative binding to a conserved DNA motif. *Dev Cell*, 11, 831-44.

Cau, E., Gradwohl, G., Casarosa, S., Kageyama, R. & Guillemot, F. 2000. Hes genes regulate sequential stages of neurogenesis in the olfactory epithelium. *Development*, 127, 2323-32.

Chang, A. M., Ohse, T., Krofft, R. D., Wu, J. S., Eddy, A. A., Pippin, J. W. & Shankland, S. J. 2012. Albumin-induced apoptosis of glomerular parietal epithelial cells is modulated by extracellular signal-regulated kinase 1/2. *Nephrol Dial Transplant*, 27, 1330-43.

Charlton, J. & Pritchard-Jones, K. 2016. WT1 Mutation in Childhood Cancer. *Methods Mol Biol*, 1467, 1-14.

Chase, S. E., Encina, C. V., Stolzenburg, L. R., Tatum, A. H., Holzman, L. B. & Krendel, M. 2012. Podocyte-specific knockout of myosin 1e disrupts glomerular filtration. *Am J Physiol Renal Physiol*, 303, F1099-106.

Chau, Y. Y., Brownstein, D., Mjoseng, H., Lee, W. C., Buza-Vidas, N., Nerlov, C., Jacobsen, S. E., Perry, P., Berry, R., Thornburn, A., Sexton, D., Morton, N., Hohenstein, P., Freyer, E., Samuel, K., Van't Hof, R. & Hastie, N. 2011. Acute multiple organ failure in adult mice deleted for the developmental regulator *Wt1*. *PLoS Genet*, 7, e1002404.

Chen, H., Lun, Y., Ovchinnikov, D., Kokubo, H., Oberg, K. C., Pepicelli, C. V., Gan, L., Lee, B. & Johnson, R. L. 1998. Limb and kidney defects in *Lmx1b* mutant mice suggest an involvement of *LMX1B* in human nail patella syndrome. *Nat Genet*, 19, 51-5.

- Chen, J., Moloney, D. J. & Stanley, P. 2001. Fringe modulation of Jagged1-induced Notch signaling requires the action of beta 4galactosyltransferase-1. *Proc Natl Acad Sci U S A*, 98, 13716-21.
- Chen, L. & Al-Awqati, Q. 2005. Segmental expression of Notch and Hairy genes in nephrogenesis. *Am J Physiol Renal Physiol*, 288, F939-52.
- Chen, Y. M. & Liapis, H. 2015. Focal segmental glomerulosclerosis: molecular genetics and targeted therapies. *BMC Nephrol*, 16, 101.
- Cheng, H. T., Kim, M., Valerius, M. T., Surendran, K., Schuster-Gossler, K., Gossler, A., McMahon, A. P. & Kopan, R. 2007. Notch2, but not Notch1, is required for proximal fate acquisition in the mammalian nephron. *Development*, 134, 801-11.
- Cheng, H. T. & Kopan, R. 2005. The role of Notch signaling in specification of podocyte and proximal tubules within the developing mouse kidney. *Kidney Int*, 68, 1951-2.
- Cheng, H. T., Miner, J. H., Lin, M., Tansey, M. G., Roth, K. & Kopan, R. 2003. Gamma-secretase activity is dispensable for mesenchyme-to-epithelium transition but required for podocyte and proximal tubule formation in developing mouse kidney. *Development*, 130, 5031-42.
- Chernin, G., Vega-Warner, V., Schoeb, D. S., Heeringa, S. F., Ovunc, B., Saisawat, P., Cleper, R., Ozaltin, F., Hildebrandt, F. & Members of The, G. P. N. S. G. 2010. Genotype/phenotype correlation in nephrotic syndrome caused by WT1 mutations. *Clin J Am Soc Nephrol*, 5, 1655-62.
- Chou, C. W., Lin, J., Jiang, Y. J. & Liu, Y. W. 2017. Aberrant Global and Jagged-Mediated Notch Signaling Disrupts Segregation Between wt1-Expressing and Steroidogenic Tissues in Zebrafish. *Endocrinology*, 158, 4206-4217.
- Chugh, S. S. 2007. Transcriptional regulation of podocyte disease. *Transl Res*, 149, 237-42.
- Chung, E., Deacon, P. & Park, J. S. 2017. Notch is required for the formation of all nephron segments and primes nephron progenitors for differentiation. *Development*.
- Ciani, L., Patel, A., Allen, N. D. & Ffrench-Constant, C. 2003. Mice lacking the giant protocadherin mFAT1 exhibit renal slit junction abnormalities and a partially penetrant cyclopia and anophthalmia phenotype. *Mol Cell Biol*, 23, 3575-82.

- Conlon, R. A., Reaume, A. G. & Rossant, J. 1995. Notch1 is required for the coordinate segmentation of somites. *Development*, 121, 1533-45.
- Costantini, F. & Kopan, R. 2010. Patterning a complex organ: branching morphogenesis and nephron segmentation in kidney development. *Dev Cell*, 18, 698-712.
- Crowley, L. C., Marfell, B. J., Scott, A. P. & Waterhouse, N. J. 2016. Quantitation of Apoptosis and Necrosis by Annexin V Binding, Propidium Iodide Uptake, and Flow Cytometry. *Cold Spring Harb Protoc*, 2016.
- Crowley, L. C. & Waterhouse, N. J. 2016. Detecting Cleaved Caspase-3 in Apoptotic Cells by Flow Cytometry. *Cold Spring Harb Protoc*, 2016, pdb prot087312.
- D'agati, V. D. 2008. The spectrum of focal segmental glomerulosclerosis: new insights. *Curr Opin Nephrol Hypertens*, 17, 271-81.
- D'agati, V. D., Fogo, A. B., Bruijn, J. A. & Jennette, J. C. 2004. Pathologic classification of focal segmental glomerulosclerosis: a working proposal. *Am J Kidney Dis*, 43, 368-82.
- D'souza, B., Meloty-Kapella, L. & Weinmaster, G. 2010. Canonical and non-canonical Notch ligands. *Curr Top Dev Biol*, 92, 73-129.
- Dandapani, S. V., Sugimoto, H., Matthews, B. D., Kolb, R. J., Sinha, S., Gerszten, R. E., Zhou, J., Ingber, D. E., Kalluri, R. & Pollak, M. R. 2007. Alpha-actinin-4 is required for normal podocyte adhesion. *J Biol Chem*, 282, 467-77.
- Datta, N., Lindfors, S., Miura, N., Saleem, M. A. & Lehtonen, S. 2016. Overexpression of transcription factor FOXC2 in cultured human podocytes upregulates injury markers and increases motility. *Exp Cell Res*, 340, 32-42.
- Dattilo, M., Penington, N. J. & Williams, K. 2008. Inhibition of TRPC5 channels by intracellular ATP. *Mol Pharmacol*, 73, 42-9.
- Davies, J. A., Lodomery, M., Hohenstein, P., Michael, L., Shafe, A., Spraggon, L. & Hastie, N. 2004. Development of an siRNA-based method for repressing specific genes in renal organ culture and its use to show that the Wt1 tumour suppressor is required for nephron differentiation. *Hum Mol Genet*, 13, 235-46.
- Dehbi, M., Ghahremani, M., Lechner, M., Dressler, G. & Pelletier, J. 1996. The paired-box transcription factor, PAX2, positively modulates expression of the Wilms' tumor suppressor gene (WT1). *Oncogene*, 13, 447-53.

- Delville, M., Sigdel, T. K., Wei, C., Li, J., Hsieh, S. C., Fornoni, A., Burke, G. W., Bruneval, P., Naesens, M., Jackson, A., Alachkar, N., Canaud, G., Legendre, C., Anglicheau, D., Reiser, J. & Sarwal, M. M. 2014. A circulating antibody panel for pretransplant prediction of FSGS recurrence after kidney transplantation. *Sci Transl Med*, 6, 256ra136.
- Dhanesh, S. B., Subashini, C. & James, J. 2016. Hes1: the maestro in neurogenesis. *Cell Mol Life Sci*, 73, 4019-42.
- Dimke, H., Maezawa, Y. & Quaggin, S. E. 2015. Crosstalk in glomerular injury and repair. *Curr Opin Nephrol Hypertens*, 24, 231-8.
- Disenza, M. T., He, S., Lee, T. H., Chu, L. L., Bolon, B., Goodyer, P., Eccles, M. & Pelletier, J. 2003. WT1 is a modifier of the Pax2 mutant phenotype: cooperation and interaction between WT1 and Pax2. *Oncogene*, 22, 8145-55.
- Domanskyi, A., Alter, H., Vogt, M. A., Gass, P. & Vinnikov, I. A. 2014. Transcription factors Foxa1 and Foxa2 are required for adult dopamine neurons maintenance. *Front Cell Neurosci*, 8, 275.
- Dong, L., Pietsch, S. & Englert, C. 2015a. Towards an understanding of kidney diseases associated with WT1 mutations. *Kidney Int*, 88, 684-90.
- Dong, L., Pietsch, S., Tan, Z., Perner, B., Sierig, R., Kruspe, D., Groth, M., Witzgall, R., Grone, H. J., Platzer, M. & Englert, C. 2015b. Integration of Cistromic and Transcriptomic Analyses Identifies Nphs2, Mafb, and Magi2 as Wilms' Tumor 1 Target Genes in Podocyte Differentiation and Maintenance. *J Am Soc Nephrol*, 26, 2118-28.
- Donoviel, D. B., Freed, D. D., Vogel, H., Potter, D. G., Hawkins, E., Barrish, J. P., Mathur, B. N., Turner, C. A., Geske, R., Montgomery, C. A., Starbuck, M., Brandt, M., Gupta, A., Ramirez-Solis, R., Zambrowicz, B. P. & Powell, D. R. 2001. Proteinuria and perinatal lethality in mice lacking NEPH1, a novel protein with homology to NEPHRIN. *Mol Cell Biol*, 21, 4829-36.
- Donoviel, D. B., Hadjantonakis, A. K., Ikeda, M., Zheng, H., Hyslop, P. S. & Bernstein, A. 1999. Mice lacking both presenilin genes exhibit early embryonic patterning defects. *Genes Dev*, 13, 2801-10.
- Dormoy, V., Jacqmin, D., Lang, H. & Massfelder, T. 2012. From development to cancer: lessons from the kidney to uncover new therapeutic targets. *Anticancer Res*, 32, 3609-17.

- Drash, A., Sherman, F., Hartmann, W. H. & Blizzard, R. M. 1970. A syndrome of pseudohermaphroditism, Wilms' tumor, hypertension, and degenerative renal disease. *J Pediatr*, 76, 585-93.
- Dressler, G. R., Wilkinson, J. E., Rothenpieler, U. W., Patterson, L. T., Williams-Simons, L. & Westphal, H. 1993. Deregulation of Pax-2 expression in transgenic mice generates severe kidney abnormalities. *Nature*, 362, 65-7.
- Dressler, G. R. & Woolf, A. S. 1999. Pax2 in development and renal disease. *Int J Dev Biol*, 43, 463-8.
- Dureau, P., Attie-Bitach, T., Salomon, R., Bettembourg, O., Amiel, J., Uteza, Y. & Dufier, J. L. 2001. Renal coloboma syndrome. *Ophthalmology*, 108, 1912-6.
- Dustin, M. L., Olszowy, M. W., Holdorf, A. D., Li, J., Bromley, S., Desai, N., Widder, P., Rosenberger, F., Van Der Merwe, P. A., Allen, P. M. & Shaw, A. S. 1998. A novel adaptor protein orchestrates receptor patterning and cytoskeletal polarity in T-cell contacts. *Cell*, 94, 667-77.
- Eccles, M. R. 1998. The role of PAX2 in normal and abnormal development of the urinary tract. *Pediatr Nephrol*, 12, 712-20.
- El Machhour, F., Keuylian, Z., Kavvadas, P., Dussaule, J. C. & Chatziantoniou, C. 2015. Activation of Notch3 in Glomeruli Promotes the Development of Rapidly Progressive Renal Disease. *J Am Soc Nephrol*, 26, 1561-75.
- Elmore, S. 2007. Apoptosis: a review of programmed cell death. *Toxicol Pathol*, 35, 495-516.
- Eremina, V., Baelde, H. J. & Quaggin, S. E. 2007. Role of the VEGF--a signaling pathway in the glomerulus: evidence for crosstalk between components of the glomerular filtration barrier. *Nephron Physiol*, 106, p32-7.
- Eremina, V. & Quaggin, S. E. 2004. The role of VEGF-A in glomerular development and function. *Curr Opin Nephrol Hypertens*, 13, 9-15.
- Eremina, V., Sood, M., Haigh, J., Nagy, A., Lajoie, G., Ferrara, N., Gerber, H. P., Kikkawa, Y., Miner, J. H. & Quaggin, S. E. 2003. Glomerular-specific alterations of VEGF-A expression lead to distinct congenital and acquired renal diseases. *J Clin Invest*, 111, 707-16.

Essafi, A., Webb, A., Berry, R. L., Slight, J., Burn, S. F., Spraggon, L., Velecela, V., Martinez-Estrada, O. M., Wiltshire, J. H., Roberts, S. G., Brownstein, D., Davies, J. A., Hastie, N. D. & Hohenstein, P. 2011. A wt1-controlled chromatin switching mechanism underpins tissue-specific wnt4 activation and repression. *Dev Cell*, 21, 559-74.

Ezaki, J., Hashimoto, K., Asano, T., Kanda, S., Akioka, Y., Hattori, M., Yamamoto, T. & Shibata, N. 2015. Gonadal tumor in Frasier syndrome: a review and classification. *Cancer Prev Res (Phila)*, 8, 271-6.

Fakhrudin, S., Alanazi, W. & Jackson, K. E. 2017. Diabetes-Induced Reactive Oxygen Species: Mechanism of Their Generation and Role in Renal Injury. *J Diabetes Res*, 2017, 8379327.

Fischbach, B. V., Trout, K. L., Lewis, J., Luis, C. A. & Sika, M. 2005. WAGR syndrome: a clinical review of 54 cases. *Pediatrics*, 116, 984-8.

Foster, R. R., Hole, R., Anderson, K., Satchell, S. C., Coward, R. J., Mathieson, P. W., Gillatt, D. A., Saleem, M. A., Bates, D. O. & Harper, S. J. 2003. Functional evidence that vascular endothelial growth factor may act as an autocrine factor on human podocytes. *Am J Physiol Renal Physiol*, 284, F1263-73.

Fryer, C. J., White, J. B. & Jones, K. A. 2004. Mastermind recruits CycC:CDK8 to phosphorylate the Notch ICD and coordinate activation with turnover. *Mol Cell*, 16, 509-20.

Fukasawa, H., Bornheimer, S., Kudlicka, K. & Farquhar, M. G. 2009. Slit diaphragms contain tight junction proteins. *J Am Soc Nephrol*, 20, 1491-503.

Gallon, L., Leventhal, J., Skaro, A., Kanwar, Y. & Alvarado, A. 2012. Resolution of recurrent focal segmental glomerulosclerosis after retransplantation. *N Engl J Med*, 366, 1648-9.

Galluzzi, L., Vitale, I., Aaronson, S. A., Abrams, J. M., Adam, D., Agostinis, P., Alnemri, E. S., Altucci, L., Amelio, I., Andrews, D. W., Annicchiarico-Petruzzelli, M., Antonov, A. V., Arama, E., Baehrecke, E. H., Barlev, N. A., Bazan, N. G., Bernassola, F., Bertrand, M. J. M., Bianchi, K., Blagosklonny, M. V., Blomgren, K., Borner, C., Boya, P., Brenner, C., Campanella, M., Candi, E., Carmona-Gutierrez, D., Cecconi, F., Chan, F. K., Chandel, N. S., Cheng, E. H., Chipuk, J. E., Cidlowski, J. A., Ciechanover, A., Cohen, G. M., Conrad, M., Cubillos-Ruiz, J. R., Czabotar, P. E., D'angiola, V., Dawson, T. M., Dawson, V. L., De Laurenzi, V., De Maria, R., Debatin, K. M., Deberardinis, R. J., Deshmukh, M., Di Daniele, N., Di Virgilio, F., Dixit, V. M., Dixon, S. J., Duckett, C. S.,

Dynlacht, B. D., El-Deiry, W. S., Elrod, J. W., Fimia, G. M., Fulda, S., Garcia-Saez, A. J., Garg, A. D., Garrido, C., Gavathiotis, E., Golstein, P., Gottlieb, E., Green, D. R., Greene, L. A., Gronemeyer, H., Gross, A., Hajnoczky, G., Hardwick, J. M., Harris, I. S., Hengartner, M. O., Hetz, C., Ichijo, H., Jaattela, M., Joseph, B., Jost, P. J., Juin, P. P., Kaiser, W. J., Karin, M., Kaufmann, T., Kepp, O., Kimchi, A., Kitsis, R. N., Klionsky, D. J., Knight, R. A., Kumar, S., Lee, S. W., Lemasters, J. J., Levine, B., Linkermann, A., Lipton, S. A., Lockshin, R. A., Lopez-Otin, C., Lowe, S. W., Luedde, T., Lugli, E., Macfarlane, M., Madeo, F., Malewicz, M., Malorni, W., Manic, G., et al. 2018. Molecular mechanisms of cell death: recommendations of the Nomenclature Committee on Cell Death 2018. *Cell Death Differ*, 25, 486-541.

Gao, F., Maiti, S., Sun, G., Ordonez, N. G., Udtha, M., Deng, J. M., Behringer, R. R. & Huff, V. 2004. The *Wt1*+/*R394W* mouse displays glomerulosclerosis and early-onset renal failure characteristic of human Denys-Drash syndrome. *Mol Cell Biol*, 24, 9899-910.

Gao, F., Yao, M., Cao, Y., Liu, S., Liu, Q. & Duan, H. 2016. Valsartan ameliorates podocyte loss in diabetic mice through the Notch pathway. *Int J Mol Med*, 37, 1328-36.

Gao, X., Chen, X., Taglienti, M., Rumballe, B., Little, M. H. & Kreidberg, J. A. 2005. Angioblast-mesenchyme induction of early kidney development is mediated by *Wt1* and *Vegfa*. *Development*, 132, 5437-49.

Garcez, P. P., Diaz-Alonso, J., Crespo-Enriquez, I., Castro, D., Bell, D. & Guillemot, F. 2015. *Cenpj*/CPAP regulates progenitor divisions and neuronal migration in the cerebral cortex downstream of *Ascl1*. *Nat Commun*, 6, 6474.

Ge, C. & Stanley, P. 2008. The O-fucose glycan in the ligand-binding domain of Notch1 regulates embryogenesis and T cell development. *Proc Natl Acad Sci U S A*, 105, 1539-44.

Ge, W., He, F., Kim, K. J., Bianchi, B., Coskun, V., Nguyen, L., Wu, X., Zhao, J., Heng, J. I., Martinowich, K., Tao, J., Wu, H., Castro, D., Sobeih, M. M., Corfas, G., Gleeson, J. G., Greenberg, M. E., Guillemot, F. & Sun, Y. E. 2006. Coupling of cell migration with neurogenesis by proneural bHLH factors. *Proc Natl Acad Sci U S A*, 103, 1319-24.

Gebeshuber, C. A., Kornauth, C., Dong, L., Sierig, R., Seibler, J., Reiss, M., Tauber, S., Bilban, M., Wang, S., Kain, R., Bohmig, G. A., Moeller, M. J., Grone, H. J., Englert, C., Martinez, J. & Kerjaschki, D. 2013. Focal segmental glomerulosclerosis is induced by microRNA-193a and its downregulation of *WT1*. *Nat Med*, 19, 481-7.

Gee, H. Y., Zhang, F., Ashraf, S., Kohl, S., Sadowski, C. E., Vega-Warner, V., Zhou, W., Lovric, S., Fang, H., Nettleton, M., Zhu, J. Y., Hoefele, J., Weber, L. T., Podracka, L., Boor, A., Fehrenbach, H., Innis, J. W., Washburn, J., Levy, S., Lifton, R. P., Otto, E. A., Han, Z. & Hildebrandt, F. 2015. KANK deficiency leads to podocyte dysfunction and nephrotic syndrome. *J Clin Invest*, 125, 2375-84.

Geoffroy, C. G., Critchley, J. A., Castro, D. S., Ramelli, S., Barraclough, C., Descombes, P., Guillemot, F. & Raineteau, O. 2009. Engineering of dominant active basic helix-loop-helix proteins that are resistant to negative regulation by postnatal central nervous system antineurogenic cues. *Stem Cells*, 27, 847-56.

Gerke, P., Huber, T. B., Sellin, L., Benzing, T. & Walz, G. 2003. Homodimerization and heterodimerization of the glomerular podocyte proteins nephrin and NEPH1. *J Am Soc Nephrol*, 14, 918-26.

Gessler, M., Poustka, A., Cavenee, W., Neve, R. L., Orkin, S. H. & Bruns, G. A. 1990. Homozygous deletion in Wilms tumours of a zinc-finger gene identified by chromosome jumping. *Nature*, 343, 774-8.

Ghiggeri, G. M., Gigante, M. & Di Donato, A. 2013. Constitutional Nephrin Deficiency in Conditionally Immortalized Human Podocytes Induced Epithelial-Mesenchymal Transition, Supported by beta-Catenin/NF-kappa B Activation: A Consequence of Cell Junction Impairment? *Int J Nephrol*, 2013, 457490.

Gordon, W. R., Vardar-Ulu, D., L'heureux, S., Ashworth, T., Malecki, M. J., Sanchez-Irizarry, C., McArthur, D. G., Histen, G., Mitchell, J. L., Aster, J. C. & Blacklow, S. C. 2009. Effects of S1 cleavage on the structure, surface export, and signaling activity of human Notch1 and Notch2. *PLoS One*, 4, e6613.

Grahammer, F., Schell, C. & Huber, T. B. 2013. The podocyte slit diaphragm--from a thin grey line to a complex signalling hub. *Nat Rev Nephrol*, 9, 587-98.

Gratton, M. O., Torban, E., Jasmin, S. B., Theriault, F. M., German, M. S. & Stifani, S. 2003. Hes6 promotes cortical neurogenesis and inhibits Hes1 transcription repression activity by multiple mechanisms. *Mol Cell Biol*, 23, 6922-35.

Greka, A. & Mundel, P. 2012. Cell biology and pathology of podocytes. *Annu Rev Physiol*, 74, 299-323.

Guillemot, F. & Hassan, B. A. 2017. Beyond proneural: emerging functions and regulations of proneural proteins. *Curr Opin Neurobiol*, 42, 93-101.

- Guillemot, F., Lo, L. C., Johnson, J. E., Auerbach, A., Anderson, D. J. & Joyner, A. L. 1993. Mammalian achaete-scute homolog 1 is required for the early development of olfactory and autonomic neurons. *Cell*, 75, 463-76.
- Guo, J. K., Menke, A. L., Gubler, M. C., Clarke, A. R., Harrison, D., Hammes, A., Hastie, N. D. & Schedl, A. 2002. WT1 is a key regulator of podocyte function: reduced expression levels cause crescentic glomerulonephritis and mesangial sclerosis. *Hum Mol Genet*, 11, 651-9.
- Hader, C., Marlier, A. & Cantley, L. 2010. Mesenchymal-epithelial transition in epithelial response to injury: the role of Foxc2. *Oncogene*, 29, 1031-40.
- Haldin, C. E., Nijjar, S., Masse, K., Barnett, M. W. & Jones, E. A. 2003. Isolation and growth factor inducibility of the *Xenopus laevis* Lmx1b gene. *Int J Dev Biol*, 47, 253-62.
- Hall, G., Gbadegesin, R. A., Lavin, P., Wu, G., Liu, Y., Oh, E. C., Wang, L., Spurney, R. F., Eckel, J., Lindsey, T., Homstad, A., Malone, A. F., Phelan, P. J., Shaw, A., Howell, D. N., Conlon, P. J., Katsanis, N. & Winn, M. P. 2015. A novel missense mutation of Wilms' Tumor 1 causes autosomal dominant FSGS. *J Am Soc Nephrol*, 26, 831-43.
- Hammes, A., Guo, J. K., Lutsch, G., Leheste, J. R., Landrock, D., Ziegler, U., Gubler, M. C. & Schedl, A. 2001. Two splice variants of the Wilms' tumor 1 gene have distinct functions during sex determination and nephron formation. *Cell*, 106, 319-29.
- Hara, M., Yanagihara, T., Itoh, M., Matsuno, M. & Kihara, I. 1998. Immunohistochemical and urinary markers of podocyte injury. *Pediatr Nephrol*, 12, 43-8.
- Hardwick, J. M. & Soane, L. 2013. Multiple functions of BCL-2 family proteins. *Cold Spring Harb Perspect Biol*, 5.
- Harshman, L. A. & Brophy, P. D. 2012. PAX2 in human kidney malformations and disease. *Pediatr Nephrol*, 27, 1265-75.
- Hartwig, S., Ho, J., Pandey, P., Macisaac, K., Taglienti, M., Xiang, M., Alterovitz, G., Ramoni, M., Fraenkel, E. & Kreidberg, J. A. 2010. Genomic characterization of Wilms' tumor suppressor 1 targets in nephron progenitor cells during kidney development. *Development*, 137, 1189-203.
- Hashimoto, H., Zhang, X., Zheng, Y., Wilson, G. G. & Cheng, X. 2016. Denys-Drash syndrome associated WT1 glutamine 369 mutants have altered sequence-preferences and altered responses to epigenetic modifications. *Nucleic Acids Res*, 44, 10165-10176.

Hastie, N. D. 2001. Life, sex, and WT1 isoforms--three amino acids can make all the difference. *Cell*, 106, 391-4.

Hastie, N. D. 2017. Wilms' tumour 1 (WT1) in development, homeostasis and disease. *Development*, 144, 2862-2872.

Hayashi, H. & Kume, T. 2008. Foxc transcription factors directly regulate Dll4 and Hey2 expression by interacting with the VEGF-Notch signaling pathways in endothelial cells. *PLoS One*, 3, e2401.

He, B., Ebarasi, L., Zhao, Z., Guo, J., Ojala, J. R., Hultenby, K., De Val, S., Betsholtz, C. & Tryggvason, K. 2014. Lmx1b and FoxC combinatorially regulate podocin expression in podocytes. *J Am Soc Nephrol*, 25, 2764-77.

Henke, R. M., Meredith, D. M., Borromeo, M. D., Savage, T. K. & Johnson, J. E. 2009. Ascl1 and Neurog2 form novel complexes and regulate Delta-like3 (Dll3) expression in the neural tube. *Dev Biol*, 328, 529-40.

Herreman, A., Hartmann, D., Annaert, W., Saftig, P., Craessaerts, K., Serneels, L., Umans, L., Schrijvers, V., Checler, F., Vanderstichele, H., Baekelandt, V., Dressel, R., Cupers, P., Huylebroeck, D., Zwijsen, A., Van Leuven, F. & De Strooper, B. 1999. Presenilin 2 deficiency causes a mild pulmonary phenotype and no changes in amyloid precursor protein processing but enhances the embryonic lethal phenotype of presenilin 1 deficiency. *Proc Natl Acad Sci U S A*, 96, 11872-7.

Herzlinger, D., Qiao, J., Cohen, D., Ramakrishna, N. & Brown, A. M. 1994. Induction of kidney epithelial morphogenesis by cells expressing Wnt-1. *Dev Biol*, 166, 815-8.

Hinkes, B., Wiggins, R. C., Gbadegesin, R., Vlangos, C. N., Seelow, D., Nurnberg, G., Garg, P., Verma, R., Chaib, H., Hoskins, B. E., Ashraf, S., Becker, C., Hennies, H. C., Goyal, M., Wharram, B. L., Schachter, A. D., Mudumana, S., Drummond, I., Kerjaschki, D., Waldherr, R., Dietrich, A., Ozaltin, F., Bakkaloglu, A., Cleper, R., Basel-Vanagaite, L., Pohl, M., Griebel, M., Tsygin, A. N., Soyulu, A., Muller, D., Sorli, C. S., Bunney, T. D., Katan, M., Liu, J., Attanasio, M., O'toole J, F., Hasselbacher, K., Mucha, B., Otto, E. A., Airik, R., Kispert, A., Kelley, G. G., Smrcka, A. V., Gudermann, T., Holzman, L. B., Nurnberg, P. & Hildebrandt, F. 2006. Positional cloning uncovers mutations in PLCE1 responsible for a nephrotic syndrome variant that may be reversible. *Nat Genet*, 38, 1397-405.

Hohenstein, P. & Hastie, N. D. 2006. The many facets of the Wilms' tumour gene, WT1. *Hum Mol Genet*, 15 Spec No 2, R196-201.

- Holthofer, H., Ahola, H., Solin, M. L., Wang, S., Palmen, T., Luimula, P., Miettinen, A. & Kerjaschki, D. 1999. Nephrin localizes at the podocyte filtration slit area and is characteristically spliced in the human kidney. *Am J Pathol*, 155, 1681-7.
- Holzman, L. B., St John, P. L., Kovari, I. A., Verma, R., Holthofer, H. & Abrahamson, D. R. 1999. Nephrin localizes to the slit pore of the glomerular epithelial cell. *Kidney Int*, 56, 1481-91.
- Hori, K., Sen, A. & Artavanis-Tsakonas, S. 2013. Notch signaling at a glance. *J Cell Sci*, 126, 2135-40.
- Hori, K., Sen, A., Kirchhausen, T. & Artavanis-Tsakonas, S. 2012. Regulation of ligand-independent Notch signal through intracellular trafficking. *Commun Integr Biol*, 5, 374-6.
- Horton, S., Meredith, A., Richardson, J. A. & Johnson, J. E. 1999. Correct coordination of neuronal differentiation events in ventral forebrain requires the bHLH factor MASH1. *Mol Cell Neurosci*, 14, 355-69.
- Hoshi, S., Shu, Y., Yoshida, F., Inagaki, T., Sonoda, J., Watanabe, T., Nomoto, K. & Nagata, M. 2002. Podocyte injury promotes progressive nephropathy in Zucker diabetic fatty rats. *Lab Invest*, 82, 25-35.
- Hostetter, T. H. 2001. Prevention of end-stage renal disease due to type 2 diabetes. *N Engl J Med*, 345, 910-2.
- Hu, Q., Gao, F., Tian, W., Ruteshouser, E. C., Wang, Y., Lazar, A., Stewart, J., Strong, L. C., Behringer, R. R. & Huff, V. 2011. Wt1 ablation and Igf2 upregulation in mice result in Wilms tumors with elevated ERK1/2 phosphorylation. *J Clin Invest*, 121, 174-83.
- Huang, S., Park, J., Qiu, C., Chung, K. W., Li, S. Y., Sirin, Y., Han, S. H., Taylor, V., Zimmer-Strobl, U. & Susztak, K. 2018. Jagged1/Notch2 controls kidney fibrosis via Tfm-mediated metabolic reprogramming. *PLoS Biol*, 16, e2005233.
- Huber, T. B., Hartleben, B., Kim, J., Schmidts, M., Schermer, B., Keil, A., Egger, L., Lecha, R. L., Borner, C., Pavenstadt, H., Shaw, A. S., Walz, G. & Benzing, T. 2003a. Nephrin and CD2AP associate with phosphoinositide 3-OH kinase and stimulate AKT-dependent signaling. *Mol Cell Biol*, 23, 4917-28.
- Huber, T. B., Simons, M., Hartleben, B., Sernetz, L., Schmidts, M., Gundlach, E., Saleem, M. A., Walz, G. & Benzing, T. 2003b. Molecular basis of the functional podocin-nephrin complex: mutations in the NPHS2 gene disrupt nephrin targeting to lipid raft microdomains. *Hum Mol Genet*, 12, 3397-405.

Hudson, B. G., Kalluri, R., Gunwar, S., Weber, M., Ballester, F., Hudson, J. K., Noelken, M. E., Sarras, M., Richardson, W. R., Saus, J. & Et Al. 1992. The pathogenesis of Alport syndrome involves type IV collagen molecules containing the alpha 3(IV) chain: evidence from anti-GBM nephritis after renal transplantation. *Kidney Int*, 42, 179-87.

Hynes, R. O. 2002. A reevaluation of integrins as regulators of angiogenesis. *Nat Med*, 8, 918-21.

Ihalmo, P., Schmid, H., Rastaldi, M. P., Mattinzoli, D., Langham, R. G., Luimula, P., Kilpikari, R., Lassila, M., Gilbert, R. E., Kerjaschki, D., Kretzler, M. & Holthofer, H. 2007. Expression of filtrin in human glomerular diseases. *Nephrol Dial Transplant*, 22, 1903-9.

Iijima, K., Someya, T., Ito, S., Nozu, K., Nakanishi, K., Matsuoka, K., Ohashi, H., Nagata, M., Kamei, K. & Sasaki, S. 2012. Focal segmental glomerulosclerosis in patients with complete deletion of one WT1 allele. *Pediatrics*, 129, e1621-5.

Ilagan, M. X., Lim, S., Fulbright, M., Piwnica-Worms, D. & Kopan, R. 2011. Real-time imaging of notch activation with a luciferase complementation-based reporter. *Sci Signal*, 4, rs7.

Imaki, J., Onodera, H., Tsuchiya, K., Imaki, T., Mochizuki, T., Mishima, T., Yamashita, K., Yoshida, K. & Sakai, M. 2000. Developmental expression of maf-1 messenger ribonucleic acids in rat kidney by in situ hybridization histochemistry. *Biochem Biophys Res Commun*, 272, 777-82.

Imayoshi, I., Isomura, A., Harima, Y., Kawaguchi, K., Kori, H., Miyachi, H., Fujiwara, T., Ishidate, F. & Kageyama, R. 2013. Oscillatory control of factors determining multipotency and fate in mouse neural progenitors. *Science*, 342, 1203-8.

Imayoshi, I., Shimogori, T., Ohtsuka, T. & Kageyama, R. 2008. Hes genes and neurogenin regulate non-neural versus neural fate specification in the dorsal telencephalic midline. *Development*, 135, 2531-41.

Inoue, T., Yaoita, E., Kurihara, H., Shimizu, F., Sakai, T., Kobayashi, T., Ohshiro, K., Kawachi, H., Okada, H., Suzuki, H., Kihara, I. & Yamamoto, T. 2001. FAT is a component of glomerular slit diaphragms. *Kidney Int*, 59, 1003-12.

Ishibashi, S. & Yasuda, K. 2001. Distinct roles of maf genes during *Xenopus* lens development. *Mech Dev*, 101, 155-66.

- Itoh, M., Nakadate, K., Horibata, Y., Matsusaka, T., Xu, J., Hunziker, W. & Sugimoto, H. 2014. The structural and functional organization of the podocyte filtration slits is regulated by Tjp1/ZO-1. *PLoS One*, 9, e106621.
- Jain, V., Feehally, J., Jones, G., Robertson, L., Nair, D. & Vasudevan, P. 2014. Steroid-resistant nephrotic syndrome with mutations in NPHS2 (podocin): report from a three-generation family. *Clin Kidney J*, 7, 303-5.
- Jefferson, J. A., Alpers, C. E. & Shankland, S. J. 2011. Podocyte biology for the bedside. *Am J Kidney Dis*, 58, 835-45.
- Jefferson, J. A. & Shankland, S. J. 2007. Familial nephrotic syndrome: PLCE1 enters the fray. *Nephrol Dial Transplant*, 22, 1849-52.
- Jefferson, J. A., Shankland, S. J. & Pichler, R. H. 2008. Proteinuria in diabetic kidney disease: a mechanistic viewpoint. *Kidney Int*, 74, 22-36.
- Jeong, H. W., Jeon, U. S., Koo, B. K., Kim, W. Y., Im, S. K., Shin, J., Cho, Y., Kim, J. & Kong, Y. Y. 2009. Inactivation of Notch signaling in the renal collecting duct causes nephrogenic diabetes insipidus in mice. *J Clin Invest*, 119, 3290-300.
- Jia, J., Ding, G., Zhu, J., Chen, C., Liang, W., Franki, N. & Singhal, P. C. 2008. Angiotensin II infusion induces nephrin expression changes and podocyte apoptosis. *Am J Nephrol*, 28, 500-7.
- Johns, D. W., Carey, R. M., Gomez, R. A., Lynch, K., Inagami, T., Saye, J., Geary, K., Farnsworth, D. E. & Peach, M. J. 1987. Isolation of renin-rich rat kidney cells. *Hypertension*, 10, 488-96.
- Jorissen, E. & De Strooper, B. 2010. Gamma-secretase and the intramembrane proteolysis of Notch. *Curr Top Dev Biol*, 92, 201-30.
- Kageyama, R., Ohtsuka, T., Hatakeyama, J. & Ohsawa, R. 2005. Roles of bHLH genes in neural stem cell differentiation. *Exp Cell Res*, 306, 343-8.
- Kaissling, B., Lehir, M. & Kriz, W. 2013. Renal epithelial injury and fibrosis. *Biochim Biophys Acta*, 1832, 931-9.
- Kakuda, S. & Haltiwanger, R. S. 2017. Deciphering the Fringe-Mediated Notch Code: Identification of Activating and Inhibiting Sites Allowing Discrimination between Ligands. *Dev Cell*, 40, 193-201.

Kang, H. J., Park, J. H., Chen, W., Kang, S. I., Moroz, K., Ladanyi, M. & Lee, S. B. 2014. EWS-WT1 oncoprotein activates neuronal reprogramming factor ASCL1 and promotes neural differentiation. *Cancer Res*, 74, 4526-35.

Kann, M., Bae, E., Lenz, M. O., Li, L., Trannguyen, B., Schumacher, V. A., Taglienti, M. E., Bordeianou, L., Hartwig, S., Rinschen, M. M., Schermer, B., Benzing, T., Fan, C. M. & Kreidberg, J. A. 2015a. WT1 targets Gas1 to maintain nephron progenitor cells by modulating FGF signals. *Development*, 142, 1254-66.

Kann, M., Ettou, S., Jung, Y. L., Lenz, M. O., Taglienti, M. E., Park, P. J., Schermer, B., Benzing, T. & Kreidberg, J. A. 2015b. Genome-Wide Analysis of Wilms' Tumor 1-Controlled Gene Expression in Podocytes Reveals Key Regulatory Mechanisms. *J Am Soc Nephrol*.

Kaplan, J. M., Kim, S. H., North, K. N., Renke, H., Correia, L. A., Tong, H. Q., Mathis, B. J., Rodriguez-Perez, J. C., Allen, P. G., Beggs, A. H. & Pollak, M. R. 2000. Mutations in ACTN4, encoding alpha-actinin-4, cause familial focal segmental glomerulosclerosis. *Nat Genet*, 24, 251-6.

Katada, T. & Sakurai, H. 2016. Proper Notch activity is necessary for the establishment of proximal cells and differentiation of intermediate, distal, and connecting tubule in *Xenopus* pronephros development. *Dev Dyn*, 245, 472-82.

Kaverina, N. V., Eng, D. G., Largent, A. D., Daehn, I., Chang, A., Gross, K. W., Pippin, J. W., Hohenstein, P. & Shankland, S. J. 2017. WT1 Is Necessary for the Proliferation and Migration of Cells of Renin Lineage Following Kidney Podocyte Depletion. *Stem Cell Reports*, 9, 1152-1166.

Kerjaschki, D. 1994. Dysfunctions of cell biological mechanisms of visceral epithelial cell (podocytes) in glomerular diseases. *Kidney Int*, 45, 300-13.

Kestila, M., Lenkkeri, U., Mannikko, M., Lamerdin, J., Mccready, P., Putaala, H., Ruotsalainen, V., Morita, T., Nissinen, M., Herva, R., Kashtan, C. E., Peltonen, L., Holmberg, C., Olsen, A. & Tryggvason, K. 1998. Positionally cloned gene for a novel glomerular protein--nephrin--is mutated in congenital nephrotic syndrome. *Mol Cell*, 1, 575-82.

Khurana, S., Chakraborty, S., Lam, M., Liu, Y., Su, Y. T., Zhao, X., Saleem, M. A., Mathieson, P. W., Bruggeman, L. A. & Kao, H. Y. 2012. Familial focal segmental glomerulosclerosis (FSGS)-linked alpha-actinin 4 (ACTN4) protein mutants lose ability to activate transcription by nuclear hormone receptors. *J Biol Chem*, 287, 12027-35.

- Kikkawa, Y., Sanzen, N. & Sekiguchi, K. 1998. Isolation and characterization of laminin-10/11 secreted by human lung carcinoma cells. laminin-10/11 mediates cell adhesion through integrin alpha3 beta1. *J Biol Chem*, 273, 15854-9.
- Kim, D., Lim, S., Park, M., Choi, J., Kim, J., Han, H., Yoon, K., Kim, K., Lim, J. & Park, S. 2014. Ubiquitination-dependent CARM1 degradation facilitates Notch1-mediated podocyte apoptosis in diabetic nephropathy. *Cell Signal*, 26, 1774-82.
- Klamt, B., Koziell, A., Poulat, F., Wieacker, P., Scambler, P., Berta, P. & Gessler, M. 1998. Frasier syndrome is caused by defective alternative splicing of WT1 leading to an altered ratio of WT1 +/-KTS splice isoforms. *Hum Mol Genet*, 7, 709-14.
- Kolobov, V. V., Storozheva, Z. I., Gruden, M. A. & Sherstnev, V. V. 2012. Regional features of the expression of genes involved in neurogenesis and apoptosis in the brain of adult rats. *Bull Exp Biol Med*, 153, 746-9.
- Komaki, F., Miyazaki, Y., Niimura, F., Matsusaka, T., Ichikawa, I. & Motojima, M. 2013. Foxc1 gene null mutation causes ectopic budding and kidney hypoplasia but not dysplasia. *Cells Tissues Organs*, 198, 22-7.
- Kopan, R., Cheng, H. T. & Surendran, K. 2007. Molecular insights into segmentation along the proximal-distal axis of the nephron. *J Am Soc Nephrol*, 18, 2014-20.
- Kopan, R. & Ilagan, M. X. 2009. The canonical Notch signaling pathway: unfolding the activation mechanism. *Cell*, 137, 216-33.
- Kovall, R. A. & Blacklow, S. C. 2010. Mechanistic insights into Notch receptor signaling from structural and biochemical studies. *Curr Top Dev Biol*, 92, 31-71.
- Koziell, A., Grech, V., Hussain, S., Lee, G., Lenkkeri, U., Tryggvason, K. & Scambler, P. 2002. Genotype/phenotype correlations of NPHS1 and NPHS2 mutations in nephrotic syndrome advocate a functional inter-relationship in glomerular filtration. *Hum Mol Genet*, 11, 379-88.
- Koziell, A. & Grundy, R. 1999. Frasier and Denys-Drash syndromes: different disorders or part of a spectrum? *Arch Dis Child*, 81, 365-9.
- Krall, P., Canales, C. P., Kairath, P., Carmona-Mora, P., Molina, J., Carpio, J. D., Ruiz, P., Mezzano, S. A., Li, J., Wei, C., Reiser, J., Young, J. I. & Walz, K. 2010. Podocyte-specific overexpression of wild type or mutant trpc6 in mice is sufficient to cause glomerular disease. *PLoS One*, 5, e12859.

- Krebs, L. T., Deftos, M. L., Bevan, M. J. & Gridley, T. 2001. The Nrarp gene encodes an ankyrin-repeat protein that is transcriptionally regulated by the notch signaling pathway. *Dev Biol*, 238, 110-9.
- Krebs, L. T., Xue, Y., Norton, C. R., Shutter, J. R., Maguire, M., Sundberg, J. P., Gallahan, D., Closson, V., Kitajewski, J., Callahan, R., Smith, G. H., Stark, K. L. & Gridley, T. 2000. Notch signaling is essential for vascular morphogenesis in mice. *Genes Dev*, 14, 1343-52.
- Kreidberg, J. A. 2000. Functions of alpha3beta1 integrin. *Curr Opin Cell Biol*, 12, 548-53.
- Kreidberg, J. A. 2003. Podocyte differentiation and glomerulogenesis. *J Am Soc Nephrol*, 14, 806-14.
- Kreidberg, J. A. 2010. WT1 and kidney progenitor cells. *Organogenesis*, 6, 61-70.
- Kreidberg, J. A., Donovan, M. J., Goldstein, S. L., Rennke, H., Shepherd, K., Jones, R. C. & Jaenisch, R. 1996. Alpha 3 beta 1 integrin has a crucial role in kidney and lung organogenesis. *Development*, 122, 3537-47.
- Kreidberg, J. A., Sariola, H., Loring, J. M., Maeda, M., Pelletier, J., Housman, D. & Jaenisch, R. 1993. WT-1 is required for early kidney development. *Cell*, 74, 679-91.
- Krendel, M., Kim, S. V., Willinger, T., Wang, T., Kashgarian, M., Flavell, R. A. & Mooseker, M. S. 2009. Disruption of Myosin 1e promotes podocyte injury. *J Am Soc Nephrol*, 20, 86-94.
- Kriz, W., Shirato, I., Nagata, M., Lohr, M. & Lemley, K. V. 2013. The podocyte's response to stress: the enigma of foot process effacement. *Am J Physiol Renal Physiol*, 304, F333-47.
- Kucinkas, L., Rudaitis, S., Pundziene, B. & Just, W. 2005. Denys-Drash syndrome. *Medicina (Kaunas)*, 41, 132-4.
- Kume, T., Deng, K. & Hogan, B. L. 2000. Minimal phenotype of mice homozygous for a null mutation in the forkhead/winged helix gene, Mf2. *Mol Cell Biol*, 20, 1419-25.
- Ladomery, M., Sommerville, J., Woolner, S., Slight, J. & Hastie, N. 2003. Expression in *Xenopus* oocytes shows that WT1 binds transcripts in vivo, with a central role for zinc finger one. *J Cell Sci*, 116, 1539-49.

- Lake, R. J., Grimm, L. M., Veraksa, A., Banos, A. & Artavanis-Tsakonas, S. 2009. In vivo analysis of the Notch receptor S1 cleavage. *PLoS One*, 4, e6728.
- Larsson, S. H., Charlieu, J. P., Miyagawa, K., Engelkamp, D., Rassoulzadegan, M., Ross, A., Cuzin, F., Van Heyningen, V. & Hastie, N. D. 1995. Subnuclear localization of WT1 in splicing or transcription factor domains is regulated by alternative splicing. *Cell*, 81, 391-401.
- Lasagni, L., Ballerini, L., Angelotti, M. L., Parente, E., Sagrinati, C., Mazzinghi, B., Peired, A., Ronconi, E., Becherucci, F., Bani, D., Gacci, M., Carini, M., Lazzeri, E. & Romagnani, P. 2010. Notch activation differentially regulates renal progenitors proliferation and differentiation toward the podocyte lineage in glomerular disorders. *Stem Cells*, 28, 1674-85.
- Lee, K. J. & Jessell, T. M. 1999. The specification of dorsal cell fates in the vertebrate central nervous system. *Annu Rev Neurosci*, 22, 261-94.
- Lefebvre, J., Clarkson, M., Massa, F., Bradford, S. T., Charlet, A., Buske, F., Lacas-Gervais, S., Schulz, H., Gimpel, C., Hata, Y., Schaefer, F. & Schedl, A. 2015. Alternatively spliced isoforms of WT1 control podocyte-specific gene expression. *Kidney Int*, 88, 321-31.
- Leimeister, C., Schumacher, N. & Gessler, M. 2003. Expression of Notch pathway genes in the embryonic mouse metanephros suggests a role in proximal tubule development. *Gene Expr Patterns*, 3, 595-8.
- Li, G., Li, Y., Liu, S., Shi, Y., Chi, Y., Liu, G. & Shan, T. 2013. Gremlin aggravates hyperglycemia-induced podocyte injury by a TGFbeta/smad dependent signaling pathway. *J Cell Biochem*, 114, 2101-13.
- Li, X., Chuang, P. Y., D'agati, V. D., Dai, Y., Yacoub, R., Fu, J., Xu, J., Taku, O., Premisrut, P. K., Holzman, L. B. & He, J. C. 2015. Nephrin Preserves Podocyte Viability and Glomerular Structure and Function in Adult Kidneys. *J Am Soc Nephrol*, 26, 2361-77.
- Li, X., Tao, H., Xie, K., Ni, Z., Yan, Y., Wei, K., Chuang, P. Y., He, J. C. & Gu, L. 2014. cAMP signaling prevents podocyte apoptosis via activation of protein kinase A and mitochondrial fusion. *PLoS One*, 9, e92003.

- Li, Y., Kang, Y. S., Dai, C., Kiss, L. P., Wen, X. & Liu, Y. 2008. Epithelial-to-mesenchymal transition is a potential pathway leading to podocyte dysfunction and proteinuria. *Am J Pathol*, 172, 299-308.
- Liapis, H. 2008. Molecular pathology of nephrotic syndrome in childhood: a contemporary approach to diagnosis. *Pediatr Dev Pathol*, 11, 154-63.
- Liapis, H., Romagnani, P. & Anders, H. J. 2013. New insights into the pathology of podocyte loss: mitotic catastrophe. *Am J Pathol*, 183, 1364-1374.
- Liebeskind, D. S. 2014. Nephrotic syndrome. *Handb Clin Neurol*, 119, 405-15.
- Lim, S. & Kaldis, P. 2013. Cdks, cyclins and CKIs: roles beyond cell cycle regulation. *Development*, 140, 3079-93.
- Lipska, B. S., Ranchin, B., Iatropoulos, P., Gellermann, J., Melk, A., Ozaltin, F., Caridi, G., Seeman, T., Tory, K., Jankauskiene, A., Zurowska, A., Szczepanska, M., Wasilewska, A., Harambat, J., Trautmann, A., Peco-Antic, A., Borzecka, H., Moczulska, A., Saeed, B., Bogdanovic, R., Kalyoncu, M., Simkova, E., Erdogan, O., Vrljicak, K., Teixeira, A., Azocar, M., Schaefer, F. & Podonet, C. 2014. Genotype-phenotype associations in WT1 glomerulopathy. *Kidney Int*, 85, 1169-78.
- Little, M., Holmes, G., Bickmore, W., Van Heyningen, V., Hastie, N. & Wainwright, B. 1995. DNA binding capacity of the WT1 protein is abolished by Denys-Drash syndrome WT1 point mutations. *Hum Mol Genet*, 4, 351-8.
- Little, N. A., Hastie, N. D. & Davies, R. C. 2000. Identification of WTAP, a novel Wilms' tumour 1-associating protein. *Hum Mol Genet*, 9, 2231-9.
- Liu, Y. H., Tsai, J. W., Chen, J. L., Yang, W. S., Chang, P. C., Cheng, P. L., Turner, D. L., Yanagawa, Y., Wang, T. W. & Yu, J. Y. 2017. Ascl1 promotes tangential migration and confines migratory routes by induction of Ephb2 in the telencephalon. *Sci Rep*, 7, 42895.
- Liu, Z., Chen, S., Boyle, S., Zhu, Y., Zhang, A., Piwnica-Worms, D. R., Ilagan, M. X. & Kopan, R. 2013. The extracellular domain of Notch2 increases its cell-surface abundance and ligand responsiveness during kidney development. *Dev Cell*, 25, 585-98.
- Lopez-Hellin, J., Cantarell, C., Jimeno, L., Sanchez-Fructuoso, A., Puig-Gay, N., Guirado, L., Vilarino, N., Gonzalez-Roncero, F. M., Mazuecos, A., Lauzurica, R., Burgos, D., Plumed, J. S., Jacobs-Cacha, C., Jimenez, C., Fernandez, A., Fernandez-Alvarez,

P., Torregrosa, V., Nieto, J. L., Meseguer, A., Alonso, A. & Group, G. S. 2013. A form of apolipoprotein a-I is found specifically in relapses of focal segmental glomerulosclerosis following transplantation. *Am J Transplant*, 13, 493-500.

Lu, J., Richardson, J. A. & Olson, E. N. 1998. Capsulin: a novel bHLH transcription factor expressed in epicardial progenitors and mesenchyme of visceral organs. *Mech Dev*, 73, 23-32.

Maezawa, Y., Onay, T., Scott, R. P., Keir, L. S., Dimke, H., Li, C., Eremina, V., Maezawa, Y., Jeansson, M., Shan, J., Binnie, M., Lewin, M., Ghosh, A., Miner, J. H., Vainio, S. J. & Quaggin, S. E. 2014. Loss of the podocyte-expressed transcription factor Tcf21/Pod1 results in podocyte differentiation defects and FSGS. *J Am Soc Nephrol*, 25, 2459-70.

Magnusson, J. P., Goritz, C., Tatarishvili, J., Dias, D. O., Smith, E. M., Lindvall, O., Kokaia, Z. & Frisen, J. 2014. A latent neurogenic program in astrocytes regulated by Notch signaling in the mouse. *Science*, 346, 237-41.

Malaga-Diequez, L., Bouhassira, D., Gipson, D. & Trachtman, H. 2015. Novel therapies for FSGS: preclinical and clinical studies. *Adv Chronic Kidney Dis*, 22, e1-6.

Markus, M. A., Heinrich, B., Raitskin, O., Adams, D. J., Mangs, H., Goy, C., Ladomery, M., Sperling, R., Stamm, S. & Morris, B. J. 2006. WT1 interacts with the splicing protein RBM4 and regulates its ability to modulate alternative splicing in vivo. *Exp Cell Res*, 312, 3379-88.

Marshall, C. B. & Shankland, S. J. 2006. Cell cycle and glomerular disease: a minireview. *Nephron Exp Nephrol*, 102, e39-48.

Martin, C. E. & Jones, N. 2018. Nephrin Signaling in the Podocyte: An Updated View of Signal Regulation at the Slit Diaphragm and Beyond. *Front Endocrinol (Lausanne)*, 9, 302.

Martin, L. A., Ribas, R., Simigdala, N., Schuster, E., Pancholi, S., Tenev, T., Gellert, P., Buluwela, L., Harrod, A., Thornhill, A., Nikitorowicz-Buniak, J., Bhamra, A., Turgeon, M. O., Poulogiannis, G., Gao, Q., Martins, V., Hills, M., Garcia-Murillas, I., Fribbens, C., Patani, N., Li, Z., Sikora, M. J., Turner, N., Zwart, W., Oesterreich, S., Carroll, J., Ali, S. & Dowsett, M. 2017. Discovery of naturally occurring ESR1 mutations in breast cancer cell lines modelling endocrine resistance. *Nat Commun*, 8, 1865.

May, C. J., Saleem, M. & Welsh, G. I. 2014. Podocyte dedifferentiation: a specialized process for a specialized cell. *Front Endocrinol (Lausanne)*, 5, 148.

- Mcconnell, M. J., Cunliffe, H. E., Chua, L. J., Ward, T. A. & Eccles, M. R. 1997. Differential regulation of the human Wilms tumour suppressor gene (WT1) promoter by two isoforms of PAX2. *Oncogene*, 14, 2689-700.
- Mccright, B., Gao, X., Shen, L., Lozier, J., Lan, Y., Maguire, M., Herzlinger, D., Weinmaster, G., Jiang, R. & Gridley, T. 2001. Defects in development of the kidney, heart and eye vasculature in mice homozygous for a hypomorphic Notch2 mutation. *Development*, 128, 491-502.
- Mccright, B., Lozier, J. & Gridley, T. 2006. Generation of new Notch2 mutant alleles. *Genesis*, 44, 29-33.
- Mckinney, P. A., Feltbower, R. G., Brocklebank, J. T. & Fitzpatrick, M. M. 2001. Time trends and ethnic patterns of childhood nephrotic syndrome in Yorkshire, UK. *Pediatr Nephrol*, 16, 1040-4.
- Mclaughlin, K. A., Ronnes, M. S. & Mercola, M. 2000. Notch regulates cell fate in the developing pronephros. *Dev Biol*, 227, 567-80.
- Meehan, S. M., Chang, A., Gibson, I. W., Kim, L., Kambham, N. & Laszik, Z. 2013. A study of interobserver reproducibility of morphologic lesions of focal segmental glomerulosclerosis. *Virchows Arch*, 462, 229-37.
- Meyer, T. W., Bennett, P. H. & Nelson, R. G. 1999. Podocyte number predicts long-term urinary albumin excretion in Pima Indians with Type II diabetes and microalbuminuria. *Diabetologia*, 42, 1341-4.
- Miles, C. G., Slight, J., Spraggon, L., O'sullivan, M., Patek, C. & Hastie, N. D. 2003. Mice lacking the 68-amino-acid, mammal-specific N-terminal extension of WT1 develop normally and are fertile. *Mol Cell Biol*, 23, 2608-13.
- Miller-Hodges, E. & Hohenstein, P. 2012. WT1 in disease: shifting the epithelial-mesenchymal balance. *J Pathol*, 226, 229-40.
- Mimura, I. & Nangaku, M. 2010. The suffocating kidney: tubulointerstitial hypoxia in end-stage renal disease. *Nat Rev Nephrol*, 6, 667-78.
- Miner, J. H. 1998. Developmental biology of glomerular basement membrane components. *Curr Opin Nephrol Hypertens*, 7, 13-9.
- Miner, J. H. 2012. The glomerular basement membrane. *Exp Cell Res*, 318, 973-8.

Miner, J. H. & Sanes, J. R. 1994. Collagen IV alpha 3, alpha 4, and alpha 5 chains in rodent basal laminae: sequence, distribution, association with laminins, and developmental switches. *J Cell Biol*, 127, 879-91.

Misra, K., Luo, H., Li, S., Matisse, M. & Xiang, M. 2014. Asymmetric activation of Dll4-Notch signaling by Foxn4 and proneural factors activates BMP/TGFbeta signaling to specify V2b interneurons in the spinal cord. *Development*, 141, 187-98.

Miura, K., Kurihara, H., Horita, S., Chikamoto, H., Hattori, M., Harita, Y., Tsurumi, H., Kajiho, Y., Sawada, Y., Sasaki, S., Igarashi, T., Kunishima, S. & Sekine, T. 2013. Podocyte expression of nonmuscle myosin heavy chain-IIA decreases in idiopathic nephrotic syndrome, especially in focal segmental glomerulosclerosis. *Nephrol Dial Transplant*, 28, 2993-3003.

Moellering, R. E., Cornejo, M., Davis, T. N., Del Bianco, C., Aster, J. C., Blacklow, S. C., Kung, A. L., Gilliland, D. G., Verdine, G. L. & Bradner, J. E. 2009. Direct inhibition of the NOTCH transcription factor complex. *Nature*, 462, 182-8.

Mollet, G., Ratelade, J., Boyer, O., Muda, A. O., Morisset, L., Lavin, T. A., Kitzis, D., Dallman, M. J., Bugeon, L., Hubner, N., Gubler, M. C., Antignac, C. & Esquivel, E. L. 2009. Podocin inactivation in mature kidneys causes focal segmental glomerulosclerosis and nephrotic syndrome. *J Am Soc Nephrol*, 20, 2181-9.

Moloney, D. J., Panin, V. M., Johnston, S. H., Chen, J., Shao, L., Wilson, R., Wang, Y., Stanley, P., Irvine, K. D., Haltiwanger, R. S. & Vogt, T. F. 2000. Fringe is a glycosyltransferase that modifies Notch. *Nature*, 406, 369-75.

Morello, R. & Lee, B. 2002. Insight into podocyte differentiation from the study of human genetic disease: nail-patella syndrome and transcriptional regulation in podocytes. *Pediatr Res*, 51, 551-8.

Moriguchi, T., Hamada, M., Morito, N., Terunuma, T., Hasegawa, K., Zhang, C., Yokomizo, T., Esaki, R., Kuroda, E., Yoh, K., Kudo, T., Nagata, M., Greaves, D. R., Engel, J. D., Yamamoto, M. & Takahashi, S. 2006. MafB is essential for renal development and F4/80 expression in macrophages. *Mol Cell Biol*, 26, 5715-27.

Morimoto, M., Myung, C., Beirnes, K., Choi, K., Asakura, Y., Bokenkamp, A., Bonneau, D., Brugnara, M., Charrow, J., Colin, E., Davis, A., Deschenes, G., Gentile, M., Giordano, M., Gormley, A. K., Govender, R., Joseph, M., Keller, K., Lerut, E., Levtschenko, E., Massella, L., Mayfield, C., Najafian, B., Parham, D., Spranger, J., Stenzel, P., Yis, U., Yu, Z., Zonana, J., Henderson, G. & Boerkoel, C. F. 2016. Increased Wnt and Notch

signaling: a clue to the renal disease in Schimke immuno-osseous dysplasia? *Orphanet J Rare Dis*, 11, 149.

Morito, N., Yoh, K., Ojima, M., Okamura, M., Nakamura, M., Hamada, M., Shimohata, H., Moriguchi, T., Yamagata, K. & Takahashi, S. 2014. Overexpression of Mafb in podocytes protects against diabetic nephropathy. *J Am Soc Nephrol*, 25, 2546-57.

Morohashi, Y. & Tomita, T. 2013. Protein trafficking and maturation regulate intramembrane proteolysis. *Biochim Biophys Acta*, 1828, 2855-61.

Morrison, A. A., Viney, R. L. & Lodomery, M. R. 2008. The post-transcriptional roles of WT1, a multifunctional zinc-finger protein. *Biochim Biophys Acta*, 1785, 55-62.

Morrissey, J., Guo, G., Moridaira, K., Fitzgerald, M., Mccracken, R., Tolley, T. & Klahr, S. 2002. Transforming growth factor-beta induces renal epithelial jagged-1 expression in fibrotic disease. *J Am Soc Nephrol*, 13, 1499-508.

Motamedi, F. J., Badro, D. A., Clarkson, M., Lecca, M. R., Bradford, S. T., Buske, F. A., Saar, K., Hubner, N., Brandli, A. W. & Schedl, A. 2014. WT1 controls antagonistic FGF and BMP-pSMAD pathways in early renal progenitors. *Nat Commun*, 5, 4444.

Motojima, M., Kume, T. & Matsusaka, T. 2017. Foxc1 and Foxc2 are necessary to maintain glomerular podocytes. *Exp Cell Res*, 352, 265-272.

Motojima, M., Ogiwara, S., Matsusaka, T., Kim, S. Y., Sagawa, N., Abe, K. & Ohtsuka, M. 2016a. Conditional knockout of Foxc2 gene in kidney: efficient generation of conditional alleles of single-exon gene by double-selection system. *Mamm Genome*, 27, 62-9.

Motojima, M., Tanimoto, S., Ohtsuka, M., Matsusaka, T., Kume, T. & Abe, K. 2016b. Characterization of Kidney and Skeleton Phenotypes of Mice Double Heterozygous for Foxc1 and Foxc2. *Cells Tissues Organs*, 201, 380-9.

Mukherjee, A., Veraksa, A., Bauer, A., Rosse, C., Camonis, J. & Artavanis-Tsakonas, S. 2005. Regulation of Notch signalling by non-visual beta-arrestin. *Nat Cell Biol*, 7, 1191-201.

Mundlos, S., Pelletier, J., Darveau, A., Bachmann, M., Winterpacht, A. & Zabel, B. 1993. Nuclear localization of the protein encoded by the Wilms' tumor gene WT1 in embryonic and adult tissues. *Development*, 119, 1329-41.

- Munro, S. & Freeman, M. 2000. The notch signalling regulator fringe acts in the Golgi apparatus and requires the glycosyltransferase signature motif DXD. *Curr Biol*, 10, 813-20.
- Murea, M., Park, J. K., Sharma, S., Kato, H., Gruenwald, A., Niranjana, T., Si, H., Thomas, D. B., Pullman, J. M., Melamed, M. L. & Susztak, K. 2010. Expression of Notch pathway proteins correlates with albuminuria, glomerulosclerosis, and renal function. *Kidney Int*, 78, 514-22.
- Muto, R., Yamamori, S., Ohashi, H. & Osawa, M. 2002. Prediction by FISH analysis of the occurrence of Wilms tumor in aniridia patients. *Am J Med Genet*, 108, 285-9.
- Nakada, Y., Hunsaker, T. L., Henke, R. M. & Johnson, J. E. 2004. Distinct domains within Mash1 and Math1 are required for function in neuronal differentiation versus neuronal cell-type specification. *Development*, 131, 1319-30.
- Nakatani, T., Kumai, M., Mizuhara, E., Minaki, Y. & Ono, Y. 2010. Lmx1a and Lmx1b cooperate with Foxa2 to coordinate the specification of dopaminergic neurons and control of floor plate cell differentiation in the developing mesencephalon. *Dev Biol*, 339, 101-13.
- Natoli, T. A., Liu, J., Eremina, V., Hodgens, K., Li, C., Hamano, Y., Mundel, P., Kalluri, R., Miner, J. H., Quaggin, S. E. & Kreidberg, J. A. 2002a. A mutant form of the Wilms' tumor suppressor gene WT1 observed in Denys-Drash syndrome interferes with glomerular capillary development. *J Am Soc Nephrol*, 13, 2058-67.
- Natoli, T. A., McDonald, A., Alberta, J. A., Taglienti, M. E., Housman, D. E. & Kreidberg, J. A. 2002b. A mammal-specific exon of WT1 is not required for development or fertility. *Mol Cell Biol*, 22, 4433-8.
- Nellesen, D. T., Lai, E. C. & Posakony, J. W. 1999. Discrete enhancer elements mediate selective responsiveness of enhancer of split complex genes to common transcriptional activators. *Dev Biol*, 213, 33-53.
- Nelson, B. R., Hartman, B. H., Ray, C. A., Hayashi, T., Birmingham-McDonogh, O. & Reh, T. A. 2009. Acheate-scute like 1 (Ascl1) is required for normal delta-like (Dll) gene expression and notch signaling during retinal development. *Dev Dyn*, 238, 2163-78.
- Nelson, B. R. & Reh, T. A. 2008. Relationship between Delta-like and proneural bHLH genes during chick retinal development. *Dev Dyn*, 237, 1565-80.

- Nicolay, D. J., Doucette, J. R. & Nazarali, A. J. 2006. Transcriptional regulation of neurogenesis in the olfactory epithelium. *Cell Mol Neurobiol*, 26, 803-21.
- Niranjan, T., Bielez, B., Gruenwald, A., Ponda, M. P., Kopp, J. B., Thomas, D. B. & Susztak, K. 2008. The Notch pathway in podocytes plays a role in the development of glomerular disease. *Nat Med*, 14, 290-8.
- Niranjan, T., Murea, M. & Susztak, K. 2009. The pathogenic role of Notch activation in podocytes. *Nephron Exp Nephrol*, 111, e73-9.
- Nurmemmedov, E., Yengo, R. K., Lodomery, M. R. & Thunnissen, M. M. 2010. Kinetic behaviour of WT 1's zinc finger domain in binding to the alpha-actinin-1 mRNA. *Arch Biochem Biophys*, 497, 21-7.
- O'brien, L. L., Grimaldi, M., Kostun, Z., Wingert, R. A., Selleck, R. & Davidson, A. J. 2011. Wt1a, Foxc1a, and the Notch mediator Rbpj physically interact and regulate the formation of podocytes in zebrafish. *Dev Biol*, 358, 318-30.
- O'brien, L. L. & McMahon, A. P. 2014. Induction and patterning of the metanephric nephron. *Semin Cell Dev Biol*, 36, 31-8.
- Okajima, T., Xu, A. & Irvine, K. D. 2003. Modulation of notch-ligand binding by protein O-fucosyltransferase 1 and fringe. *J Biol Chem*, 278, 42340-5.
- Orloff, M. S., Iyengar, S. K., Winkler, C. A., Goddard, K. A., Dart, R. A., Ahuja, T. S., Mokrzycki, M., Briggs, W. A., Korbet, S. M., Kimmel, P. L., Simon, E. E., Trachtman, H., Vlahov, D., Michel, D. M., Berns, J. S., Smith, M. C., Schelling, J. R., Sedor, J. R. & Kopp, J. B. 2005. Variants in the Wilms' tumor gene are associated with focal segmental glomerulosclerosis in the African American population. *Physiol Genomics*, 21, 212-21.
- Ortega, A., Niksic, M., Bachi, A., Wilm, M., Sanchez, L., Hastie, N. & Valcarcel, J. 2003. Biochemical function of female-lethal (2)D/Wilms' tumor suppressor-1-associated proteins in alternative pre-mRNA splicing. *J Biol Chem*, 278, 3040-7.
- Ozdemir, D. D. & Hohenstein, P. 2014. Wt1 in the kidney--a tale in mouse models. *Pediatr Nephrol*, 29, 687-93.
- Pacary, E., Heng, J., Azzarelli, R., Riou, P., Castro, D., Lebel-Potter, M., Parras, C., Bell, D. M., Ridley, A. J., Parsons, M. & Guillemot, F. 2011. Proneural transcription factors regulate different steps of cortical neuron migration through Rnd-mediated inhibition of RhoA signaling. *Neuron*, 69, 1069-84.

- Palmer, W. H. & Deng, W. M. 2015. Ligand-Independent Mechanisms of Notch Activity. *Trends Cell Biol*, 25, 697-707.
- Parenti, R., Salvatorelli, L., Musumeci, G., Parenti, C., Giorlandino, A., Motta, F. & Magro, G. 2015. Wilms' tumor 1 (WT1) protein expression in human developing tissues. *Acta Histochem*, 117, 386-96.
- Park, N. I., Guilhamon, P., Desai, K., Mcadam, R. F., Langille, E., O'connor, M., Lan, X., Whetstone, H., Coutinho, F. J., Vanner, R. J., Ling, E., Prinos, P., Lee, L., Selvadurai, H., Atwal, G., Kushida, M., Clarke, I. D., Voisin, V., Cusimano, M. D., Bernstein, M., Das, S., Bader, G., Arrowsmith, C. H., Angers, S., Huang, X., Lupien, M. & Dirks, P. B. 2017. ASCL1 Reorganizes Chromatin to Direct Neuronal Fate and Suppress Tumorigenicity of Glioblastoma Stem Cells. *Cell Stem Cell*, 21, 411.
- Patek, C. E., Little, M. H., Fleming, S., Miles, C., Charlieu, J. P., Clarke, A. R., Miyagawa, K., Christie, S., Doig, J., Harrison, D. J., Porteous, D. J., Brookes, A. J., Hooper, M. L. & Hastie, N. D. 1999. A zinc finger truncation of murine WT1 results in the characteristic urogenital abnormalities of Denys-Drash syndrome. *Proc Natl Acad Sci U S A*, 96, 2931-6.
- Patel, S. R., Ranghini, E. & Dressler, G. R. 2014. Mechanisms of gene activation and repression by Pax proteins in the developing kidney. *Pediatr Nephrol*, 29, 589-95.
- Patrakka, J. & Tryggvason, K. 2007. Nephrin--a unique structural and signaling protein of the kidney filter. *Trends Mol Med*, 13, 396-403.
- Pavenstadt, H., Kriz, W. & Kretzler, M. 2003. Cell biology of the glomerular podocyte. *Physiol Rev*, 83, 253-307.
- Peden, A. A., Oorschot, V., Hesser, B. A., Austin, C. D., Scheller, R. H. & Klumperman, J. 2004. Localization of the AP-3 adaptor complex defines a novel endosomal exit site for lysosomal membrane proteins. *J Cell Biol*, 164, 1065-76.
- Pelletier, J., Schalling, M., Buckler, A. J., Rogers, A., Haber, D. A. & Housman, D. 1991. Expression of the Wilms' tumor gene WT1 in the murine urogenital system. *Genes Dev*, 5, 1345-56.
- Perico, L., Conti, S., Benigni, A. & Remuzzi, G. 2016. Podocyte-actin dynamics in health and disease. *Nat Rev Nephrol*, 12, 692-710.

- Philippe, A., Weber, S., Esquivel, E. L., Houbron, C., Hamard, G., Ratelade, J., Kriz, W., Schaefer, F., Gubler, M. C. & Antignac, C. 2008. A missense mutation in podocin leads to early and severe renal disease in mice. *Kidney Int*, 73, 1038-47.
- Piscione, T. D., Wu, M. Y. & Quaggin, S. E. 2004. Expression of Hairy/Enhancer of Split genes, Hes1 and Hes5, during murine nephron morphogenesis. *Gene Expr Patterns*, 4, 707-11.
- Preston, R., Stuart, H. M. & Lennon, R. 2017. Genetic testing in steroid-resistant nephrotic syndrome: why, who, when and how? *Pediatr Nephrol*.
- Qin, X. S., Tsukaguchi, H., Shono, A., Yamamoto, A., Kurihara, H. & Doi, T. 2009. Phosphorylation of nephrin triggers its internalization by raft-mediated endocytosis. *J Am Soc Nephrol*, 20, 2534-45.
- Quaggin, S. E. 2002. Transcriptional regulation of podocyte specification and differentiation. *Microsc Res Tech*, 57, 208-11.
- Quaggin, S. E. & Kreidberg, J. A. 2008. Development of the renal glomerulus: good neighbors and good fences. *Development*, 135, 609-20.
- Quaggin, S. E., Schwartz, L., Cui, S., Igarashi, P., Deimling, J., Post, M. & Rossant, J. 1999. The basic-helix-loop-helix protein pod1 is critically important for kidney and lung organogenesis. *Development*, 126, 5771-83.
- Quaggin, S. E., Vanden Heuvel, G. B. & Igarashi, P. 1998. Pod-1, a mesoderm-specific basic-helix-loop-helix protein expressed in mesenchymal and glomerular epithelial cells in the developing kidney. *Mech Dev*, 71, 37-48.
- Ramidi, G. B., Kurukumbi, M. K. & Sealy, P. L. 2011. Collapsing glomerulopathy in sickle cell disease: a case report. *J Med Case Rep*, 5, 71.
- Rana, N. A. & Haltiwanger, R. S. 2011. Fringe benefits: functional and structural impacts of O-glycosylation on the extracellular domain of Notch receptors. *Curr Opin Struct Biol*, 21, 583-9.
- Raposo, A. A., Vasconcelos, F. F., Drechsel, D., Marie, C., Johnston, C., Dolle, D., Bithell, A., Gillotin, S., Van Den Berg, D. L., Ettwiller, L., Flicek, P., Crawford, G. E., Parras, C. M., Berninger, B., Buckley, N. J., Guillemot, F. & Castro, D. S. 2015. Ascl1 Coordinately Regulates Gene Expression and the Chromatin Landscape during Neurogenesis. *Cell Rep*.

- Reiser, J., Kriz, W., Kretzler, M. & Mundel, P. 2000. The glomerular slit diaphragm is a modified adherens junction. *J Am Soc Nephrol*, 11, 1-8.
- Relle, M., Cash, H., Brochhausen, C., Strand, D., Menke, J., Galle, P. R. & Schwarting, A. 2011. New perspectives on the renal slit diaphragm protein podocin. *Mod Pathol*, 24, 1101-10.
- Rheault, M. N. & Gbadegesin, R. A. 2016. The Genetics of Nephrotic Syndrome. *J Pediatr Genet*, 5, 15-24.
- Rink, J., Ghigo, E., Kalaidzidis, Y. & Zerial, M. 2005. Rab conversion as a mechanism of progression from early to late endosomes. *Cell*, 122, 735-49.
- Robb, L., Mifsud, L., Hartley, L., Biben, C., Copeland, N. G., Gilbert, D. J., Jenkins, N. A. & Harvey, R. P. 1998. epicardin: A novel basic helix-loop-helix transcription factor gene expressed in epicardium, branchial arch myoblasts, and mesenchyme of developing lung, gut, kidney, and gonads. *Dev Dyn*, 213, 105-13.
- Ronco, P. 2007. Proteinuria: is it all in the foot? *J Clin Invest*, 117, 2079-82.
- Roselli, S., Gribouval, O., Boute, N., Sich, M., Benessy, F., Attie, T., Gubler, M. C. & Antignac, C. 2002. Podocin localizes in the kidney to the slit diaphragm area. *Am J Pathol*, 160, 131-9.
- Rosenberg, A. Z. & Kopp, J. B. 2017. Focal Segmental Glomerulosclerosis. *Clin J Am Soc Nephrol*, 12, 502-517.
- Ruf, R. G., Schultheiss, M., Lichtenberger, A., Karle, S. M., Zalewski, I., Mucha, B., Everding, A. S., Neuhaus, T., Patzer, L., Plank, C., Haas, J. P., Ozaltin, F., Imm, A., Fuchshuber, A., Bakaloglu, A., Hildebrandt, F. & Group, A. P. N. S. 2004. Prevalence of WT1 mutations in a large cohort of patients with steroid-resistant and steroid-sensitive nephrotic syndrome. *Kidney Int*, 66, 564-70.
- Ruotsalainen, V., Ljungberg, P., Wartiovaara, J., Lenkkeri, U., Kestila, M., Jalanko, H., Holmberg, C. & Tryggvason, K. 1999. Nephrin is specifically located at the slit diaphragm of glomerular podocytes. *Proc Natl Acad Sci U S A*, 96, 7962-7.
- Ryu, M., Kulkarni, O. P., Radomska, E., Miosge, N., Gross, O. & Anders, H. J. 2011. Bacterial CpG-DNA accelerates Alport glomerulosclerosis by inducing an M1 macrophage phenotype and tumor necrosis factor-alpha-mediated podocyte loss. *Kidney Int*, 79, 189-98.

Sachs, N., Kreft, M., Van Den Bergh Weerman, M. A., Beynon, A. J., Peters, T. A., Weening, J. J. & Sonnenberg, A. 2006. Kidney failure in mice lacking the tetraspanin CD151. *J Cell Biol*, 175, 33-9.

Sadl, V., Jin, F., Yu, J., Cui, S., Holmyard, D., Quaggin, S., Barsh, G. & Cordes, S. 2002. The mouse Kreisler (Krm1/MafB) segmentation gene is required for differentiation of glomerular visceral epithelial cells. *Dev Biol*, 249, 16-29.

Sadowski, C. E., Lovric, S., Ashraf, S., Pabst, W. L., Gee, H. Y., Kohl, S., Engelmann, S., Vega-Warner, V., Fang, H., Halbritter, J., Somers, M. J., Tan, W., Shril, S., Fessi, I., Lifton, R. P., Bockenhauer, D., El-Desoky, S., Kari, J. A., Zenker, M., Kemper, M. J., Mueller, D., Fathy, H. M., Soliman, N. A., Group, S. S. & Hildebrandt, F. 2015. A single-gene cause in 29.5% of cases of steroid-resistant nephrotic syndrome. *J Am Soc Nephrol*, 26, 1279-89.

Salant, D. J. 1994. The structural biology of glomerular epithelial cells in proteinuric diseases. *Curr Opin Nephrol Hypertens*, 3, 569-74.

Sanna-Cherchi, S., Burgess, K. E., Nees, S. N., Caridi, G., Weng, P. L., Dagnino, M., Bodria, M., Carrea, A., Allegretta, M. A., Kim, H. R., Perry, B. J., Gigante, M., Clark, L. N., Kisselev, S., Cusi, D., Gesualdo, L., Allegri, L., Scolari, F., D'agati, V., Shapiro, L. S., Pecoraro, C., Palomero, T., Ghiggeri, G. M. & Gharavi, A. G. 2011. Exome sequencing identified MYO1E and NEIL1 as candidate genes for human autosomal recessive steroid-resistant nephrotic syndrome. *Kidney Int*, 80, 389-96.

Saran, R., Li, Y., Robinson, B., Abbott, K. C., Agodoa, L. Y., Ayanian, J., Bragg-Gresham, J., Balkrishnan, R., Chen, J. L., Cope, E., Eggers, P. W., Gillen, D., Gipson, D., Hailpern, S. M., Hall, Y. N., He, K., Herman, W., Heung, M., Hirth, R. A., Hutton, D., Jacobsen, S. J., Kalantar-Zadeh, K., Kovesdy, C. P., Lu, Y., Molnar, M. Z., Morgenstern, H., Nallamothu, B., Nguyen, D. V., O'hare, A. M., Plattner, B., Pisoni, R., Port, F. K., Rao, P., Rhee, C. M., Sakhuja, A., Schaubel, D. E., Selewski, D. T., Shahinian, V., Sim, J. J., Song, P., Streja, E., Kurella Tamura, M., Tentori, F., White, S., Woodside, K. & Hirth, R. A. 2016. US Renal Data System 2015 Annual Data Report: Epidemiology of Kidney Disease in the United States. *Am J Kidney Dis*, 67, Svii, S1-305.

Saran, R., Li, Y., Robinson, B., Ayanian, J., Balkrishnan, R., Bragg-Gresham, J., Chen, J. T., Cope, E., Gipson, D., He, K., Herman, W., Heung, M., Hirth, R. A., Jacobsen, S. S., Kalantar-Zadeh, K., Kovesdy, C. P., Leichtman, A. B., Lu, Y., Molnar, M. Z., Morgenstern, H., Nallamothu, B., O'hare, A. M., Pisoni, R., Plattner, B., Port, F. K., Rao, P., Rhee, C. M., Schaubel, D. E., Selewski, D. T., Shahinian, V., Sim, J. J., Song, P.,

Streja, E., Kurella Tamura, M., Tentori, F., Eggers, P. W., Agodoa, L. Y. & Abbott, K. C. 2015. US Renal Data System 2014 Annual Data Report: Epidemiology of Kidney Disease in the United States. *Am J Kidney Dis*, 66, Svii, S1-305.

Savin, V. J., Sharma, M., Zhou, J., Gennoch, D., Fields, T., Sharma, R., McCarthy, E. T., Srivastava, T., Domen, J., Tormo, A. & Gauchat, J. F. 2015. Renal and Hematological Effects of CLCF-1, a B-Cell-Stimulating Cytokine of the IL-6 Family. *J Immunol Res*, 2015, 714964.

Saxen, L. & Sariola, H. 1987. Early organogenesis of the kidney. *Pediatr Nephrol*, 1, 385-92.

Saylam, K. & Simon, P. 2003. WT1 gene mutation responsible for male sex reversal and renal failure: the Frasier syndrome. *Eur J Obstet Gynecol Reprod Biol*, 110, 111-3.

Schell, C. & Huber, T. B. 2017. The Evolving Complexity of the Podocyte Cytoskeleton. *J Am Soc Nephrol*, 28, 3166-3174.

Schell, C., Wanner, N. & Huber, T. B. 2014. Glomerular development--shaping the multi-cellular filtration unit. *Semin Cell Dev Biol*, 36, 39-49.

Schiffer, M., Bitzer, M., Roberts, I. S., Kopp, J. B., Ten Dijke, P., Mundel, P. & Bottinger, E. P. 2001. Apoptosis in podocytes induced by TGF-beta and Smad7. *J Clin Invest*, 108, 807-16.

Schiffer, M., Mundel, P., Shaw, A. S. & Bottinger, E. P. 2004. A novel role for the adaptor molecule CD2-associated protein in transforming growth factor-beta-induced apoptosis. *J Biol Chem*, 279, 37004-12.

Schumacher, V. A., Jeruschke, S., Eitner, F., Becker, J. U., Pitschke, G., Ince, Y., Miner, J. H., Leuschner, I., Engers, R., Everding, A. S., Bulla, M. & Royer-Pokora, B. 2007. Impaired glomerular maturation and lack of VEGF165b in Denys-Drash syndrome. *J Am Soc Nephrol*, 18, 719-29.

Schwanbeck, R., Martini, S., Bernoth, K. & Just, U. 2011. The Notch signaling pathway: molecular basis of cell context dependency. *Eur J Cell Biol*, 90, 572-81.

Schwarz, K., Simons, M., Reiser, J., Saleem, M. A., Faul, C., Kriz, W., Shaw, A. S., Holzman, L. B. & Mundel, P. 2001. Podocin, a raft-associated component of the glomerular slit diaphragm, interacts with CD2AP and nephrin. *J Clin Invest*, 108, 1621-9.

- Scott, R. P. & Quaggin, S. E. 2015. Review series: The cell biology of renal filtration. *J Cell Biol*, 209, 199-210.
- Seely, J. C. 2017. A brief review of kidney development, maturation, developmental abnormalities, and drug toxicity: juvenile animal relevancy. *J Toxicol Pathol*, 30, 125-133.
- Sellin, L., Huber, T. B., Gerke, P., Quack, I., Pavenstadt, H. & Walz, G. 2003. NEPH1 defines a novel family of podocin interacting proteins. *FASEB J*, 17, 115-7.
- Sha, W. G., Shen, L., Zhou, L., Xu, D. Y. & Lu, G. Y. 2015. Down-regulation of miR-186 contributes to podocytes apoptosis in membranous nephropathy. *Biomed Pharmacother*, 75, 179-84.
- Shan, J., Jokela, T., Skovorodkin, I. & Vainio, S. 2010. Mapping of the fate of cell lineages generated from cells that express the Wnt4 gene by time-lapse during kidney development. *Differentiation*, 79, 57-64.
- Shankland, S. J. 2006. The podocyte's response to injury: role in proteinuria and glomerulosclerosis. *Kidney Int*, 69, 2131-47.
- Sharma, M., Magenheimer, L. K., Home, T., Tamano, K. N., Singhal, P. C., Hyink, D. P., Klotman, P. E., Vanden Heuvel, G. B. & Fields, T. A. 2013. Inhibition of Notch pathway attenuates the progression of human immunodeficiency virus-associated nephropathy. *Am J Physiol Renal Physiol*, 304, F1127-36.
- Sharma, R., Sanchez-Ferras, O. & Bouchard, M. 2015. Pax genes in renal development, disease and regeneration. *Semin Cell Dev Biol*, 44, 97-106.
- Shih, N. Y., Li, J., Cotran, R., Mundel, P., Miner, J. H. & Shaw, A. S. 2001. CD2AP localizes to the slit diaphragm and binds to nephrin via a novel C-terminal domain. *Am J Pathol*, 159, 2303-8.
- Shih, N. Y., Li, J., Karpitskii, V., Nguyen, A., Dustin, M. L., Kanagawa, O., Miner, J. H. & Shaw, A. S. 1999. Congenital nephrotic syndrome in mice lacking CD2-associated protein. *Science*, 286, 312-5.
- Shimojo, H., Ohtsuka, T. & Kageyama, R. 2008. Oscillations in notch signaling regulate maintenance of neural progenitors. *Neuron*, 58, 52-64.
- Simrick, S., Masse, K. & Jones, E. A. 2005. Developmental expression of Pod 1 in *Xenopus laevis*. *Int J Dev Biol*, 49, 59-63.

- Sir Elkhatim, R., Li, J. Y., Yong, T. Y. & Gleadle, J. M. 2014. Dipping your feet in the water: podocytes in urine. *Expert Rev Mol Diagn*, 14, 423-37.
- Sirin, Y. & Susztak, K. 2012. Notch in the kidney: development and disease. *J Pathol*, 226, 394-403.
- Sjoqvist, M. & Andersson, E. R. 2017. Do as I say, Not(ch) as I do: Lateral control of cell fate. *Dev Biol*.
- Srivastava, T., Garola, R. E., Whiting, J. M. & Alon, U. S. 2003. Cell-cycle regulatory proteins in podocyte cell in idiopathic nephrotic syndrome of childhood. *Kidney Int*, 63, 1374-81.
- Stanley, P. & Okajima, T. 2010. Roles of glycosylation in Notch signaling. *Curr Top Dev Biol*, 92, 131-64.
- Stark, K., Vainio, S., Vassileva, G. & McMahon, A. P. 1994. Epithelial transformation of metanephric mesenchyme in the developing kidney regulated by Wnt-4. *Nature*, 372, 679-83.
- Steffes, M. W., Schmidt, D., Mccrery, R., Basgen, J. M. & International Diabetic Nephropathy Study, G. 2001. Glomerular cell number in normal subjects and in type 1 diabetic patients. *Kidney Int*, 59, 2104-13.
- Stephenson, N. L. & Avis, J. M. 2012. Direct observation of proteolytic cleavage at the S2 site upon forced unfolding of the Notch negative regulatory region. *Proc Natl Acad Sci U S A*, 109, E2757-65.
- Subramanian, B., Sun, H., Yan, P., Charoonratana, V. T., Higgs, H. N., Wang, F., Lai, K. V., Valenzuela, D. M., Brown, E. J., Schlondorff, J. S. & Pollak, M. R. 2016. Mice with mutant Inf2 show impaired podocyte and slit diaphragm integrity in response to protamine-induced kidney injury. *Kidney Int*, 90, 363-372.
- Suresh, S. & Irvine, A. E. 2015. The NOTCH signaling pathway in normal and malignant blood cell production. *J Cell Commun Signal*, 9, 5-13.
- Susztak, K., Raff, A. C., Schiffer, M. & Bottinger, E. P. 2006. Glucose-induced reactive oxygen species cause apoptosis of podocytes and podocyte depletion at the onset of diabetic nephropathy. *Diabetes*, 55, 225-33.

- Sweeney, E., Fryer, A., Mountford, R., Green, A. & McIntosh, I. 2003. Nail patella syndrome: a review of the phenotype aided by developmental biology. *J Med Genet*, 40, 153-62.
- Sweetwyne, M. T., Gruenwald, A., Niranjana, T., Nishinakamura, R., Strobl, L. J. & Susztak, K. 2015. Notch1 and Notch2 in Podocytes Play Differential Roles During Diabetic Nephropathy Development. *Diabetes*, 64, 4099-111.
- Taelman, V., Van Campenhout, C., Solter, M., Pieler, T. & Bellefroid, E. J. 2006. The Notch-effector HRT1 gene plays a role in glomerular development and patterning of the *Xenopus* pronephros anlagen. *Development*, 133, 2961-71.
- Takemoto, M., He, L., Norlin, J., Patrakka, J., Xiao, Z., Petrova, T., Bondjers, C., Asp, J., Wallgard, E., Sun, Y., Samuelsson, T., Mostad, P., Lundin, S., Miura, N., Sado, Y., Alitalo, K., Quaggin, S. E., Tryggvason, K. & Betsholtz, C. 2006. Large-scale identification of genes implicated in kidney glomerulus development and function. *EMBO J*, 25, 1160-74.
- Tanaka, E., Asanuma, K., Kim, E., Sasaki, Y., Oliva Trejo, J. A., Seki, T., Nonaka, K., Asao, R., Nagai-Hosoe, Y., Akiba-Takagi, M., Hidaka, T., Takagi, M., Koyanagi, A., Mizutani, S., Yagita, H. & Tomino, Y. 2014. Notch2 activation ameliorates nephrosis. *Nat Commun*, 5, 3296.
- Tanigaki, K. & Honjo, T. 2010. Two opposing roles of RBP-J in Notch signaling. *Curr Top Dev Biol*, 92, 231-52.
- Tasic, V., Gucev, Z. & Polenakovic, M. 2015. Steroid Resistant Nephrotic Syndrome- Genetic Consideration. *Pril (Makedon Akad Nauk Umet Odd Med Nauki)*, 36, 5-12.
- Taylor, P., Takeuchi, H., Sheppard, D., Chillakuri, C., Lea, S. M., Haltiwanger, R. S. & Handford, P. A. 2014. Fringe-mediated extension of O-linked fucose in the ligand-binding region of Notch1 increases binding to mammalian Notch ligands. *Proc Natl Acad Sci U S A*, 111, 7290-5.
- Thiery, J. P. & Sleeman, J. P. 2006. Complex networks orchestrate epithelial-mesenchymal transitions. *Nat Rev Mol Cell Biol*, 7, 131-42.
- Tolvanen, T. A., Dash, S. N., Polianskyte-Prause, Z., Dumont, V. & Lehtonen, S. 2015. Lack of CD2AP disrupts Glut4 trafficking and attenuates glucose uptake in podocytes. *J Cell Sci*, 128, 4588-600.

- Tomar, R., Mudumana, S. P., Pathak, N., Hukriede, N. A. & Drummond, I. A. 2014. *osr1* is required for podocyte development downstream of *wt1a*. *J Am Soc Nephrol*, 25, 2539-45.
- Topaloglu, R., Denamur, E., Akyuz, C., Kale, G. & Bakkaloglu, A. 1999. Wilms' tumour-associated late nephrotic syndrome responsive to treatment. *Nephrol Dial Transplant*, 14, 954-6.
- Toska, E. & Roberts, S. G. 2014. Mechanisms of transcriptional regulation by WT1 (Wilms' tumour 1). *Biochem J*, 461, 15-32.
- Totaro, A., Castellan, M., Battilana, G., Zanconato, F., Azzolin, L., Giulitti, S., Cordenonsi, M. & Piccolo, S. 2017. YAP/TAZ link cell mechanics to Notch signalling to control epidermal stem cell fate. *Nat Commun*, 8, 15206.
- Tryggvason, K., Patrakka, J. & Wartiovaara, J. 2006. Hereditary proteinuria syndromes and mechanisms of proteinuria. *N Engl J Med*, 354, 1387-401.
- Ueki, Y., Wilken, M. S., Cox, K. E., Chipman, L., Jorstad, N., Sternhagen, K., Simic, M., Ullom, K., Nakafuku, M. & Reh, T. A. 2015. Transgenic expression of the proneural transcription factor *Ascl1* in Muller glia stimulates retinal regeneration in young mice. *Proc Natl Acad Sci U S A*, 112, 13717-22.
- Ueno, T., Kobayashi, N., Nakayama, M., Takashima, Y., Ohse, T., Pastan, I., Pippin, J. W., Shankland, S. J., Uesugi, N., Matsusaka, T. & Nagata, M. 2013. Aberrant Notch1-dependent effects on glomerular parietal epithelial cells promotes collapsing focal segmental glomerulosclerosis with progressive podocyte loss. *Kidney Int*, 83, 1065-75.
- Ullmark, T., Montano, G. & Gullberg, U. 2018. DNA and RNA binding by the Wilms' tumour gene 1 (WT1) protein +KTS and -KTS isoforms-From initial observations to recent global genomic analyses. *Eur J Haematol*, 100, 229-240.
- Urban, N., Van Den Berg, D. L., Forget, A., Andersen, J., Demmers, J. A., Hunt, C., Ayrault, O. & Guillemot, F. 2016. Return to quiescence of mouse neural stem cells by degradation of a proactivation protein. *Science*, 353, 292-5.
- Valcourt, U., Kowanetz, M., Niimi, H., Heldin, C. H. & Moustakas, A. 2005. TGF-beta and the Smad signaling pathway support transcriptomic reprogramming during epithelial-mesenchymal cell transition. *Mol Biol Cell*, 16, 1987-2002.
- Van Tetering, G. & Vooijs, M. 2011. Proteolytic cleavage of Notch: "HIT and RUN". *Curr Mol Med*, 11, 255-69.

- Vasconcelos, F. F. & Castro, D. S. 2014. Transcriptional control of vertebrate neurogenesis by the proneural factor *Ascl1*. *Front Cell Neurosci*, 8, 412.
- Verma, R., Kovari, I., Soofi, A., Nihalani, D., Patrie, K. & Holzman, L. B. 2006. Nephrin ectodomain engagement results in Src kinase activation, nephrin phosphorylation, Nck recruitment, and actin polymerization. *J Clin Invest*, 116, 1346-59.
- Vivarelli, M., Colucci, M., Bonanni, A., Verzani, M., Serafinelli, J., Emma, F. & Ghiggeri, G. 2017. Ofatumumab in two pediatric nephrotic syndrome patients allergic to rituximab. *Pediatr Nephrol*, 32, 181-184.
- Wagner, K. D., Wagner, N., Guo, J. K., Elger, M., Dallman, M. J., Bugeon, L. & Schedl, A. 2006. An inducible mouse model for PAX2-dependent glomerular disease: insights into a complex pathogenesis. *Curr Biol*, 16, 793-800.
- Wagner, K. D., Wagner, N., Vidal, V. P., Schley, G., Wilhelm, D., Schedl, A., Englert, C. & Scholz, H. 2002. The Wilms' tumor gene *Wt1* is required for normal development of the retina. *Embo j*, 21, 1398-405.
- Wagner, N., Wagner, K. D., Hammes, A., Kirschner, K. M., Vidal, V. P., Schedl, A. & Scholz, H. 2005. A splice variant of the Wilms' tumour suppressor *Wt1* is required for normal development of the olfactory system. *Development*, 132, 1327-36.
- Waldman, M., Crew, R. J., Valeri, A., Busch, J., Stokes, B., Markowitz, G., D'agati, V. & Appel, G. 2007. Adult minimal-change disease: clinical characteristics, treatment, and outcomes. *Clin J Am Soc Nephrol*, 2, 445-53.
- Wang, P., Pereira, F. A., Beasley, D. & Zheng, H. 2003. Presenilins are required for the formation of comma- and S-shaped bodies during nephrogenesis. *Development*, 130, 5019-29.
- Wang, S., Kim, J. H., Moon, K. C., Hong, H. K. & Lee, H. S. 2004. Cell-cycle mechanisms involved in podocyte proliferation in cellular lesion of focal segmental glomerulosclerosis. *Am J Kidney Dis*, 43, 19-27.
- Wang, S. C., Lin, X. L., Wang, H. Y., Qin, Y. J., Chen, L., Li, J., Jia, J. S., Shen, H. F., Yang, S., Xie, R. Y., Wei, F., Gao, F., Rong, X. X., Yang, J., Zhao, W. T., Zhang, T. T., Shi, J. W., Yao, K. T., Luo, W. R., Sun, Y. & Xiao, D. 2015. *Hes1* triggers epithelial-mesenchymal transition (EMT)-like cellular marker alterations and promotes invasion and metastasis of nasopharyngeal carcinoma by activating the PTEN/AKT pathway. *Oncotarget*, 6, 36713-30.

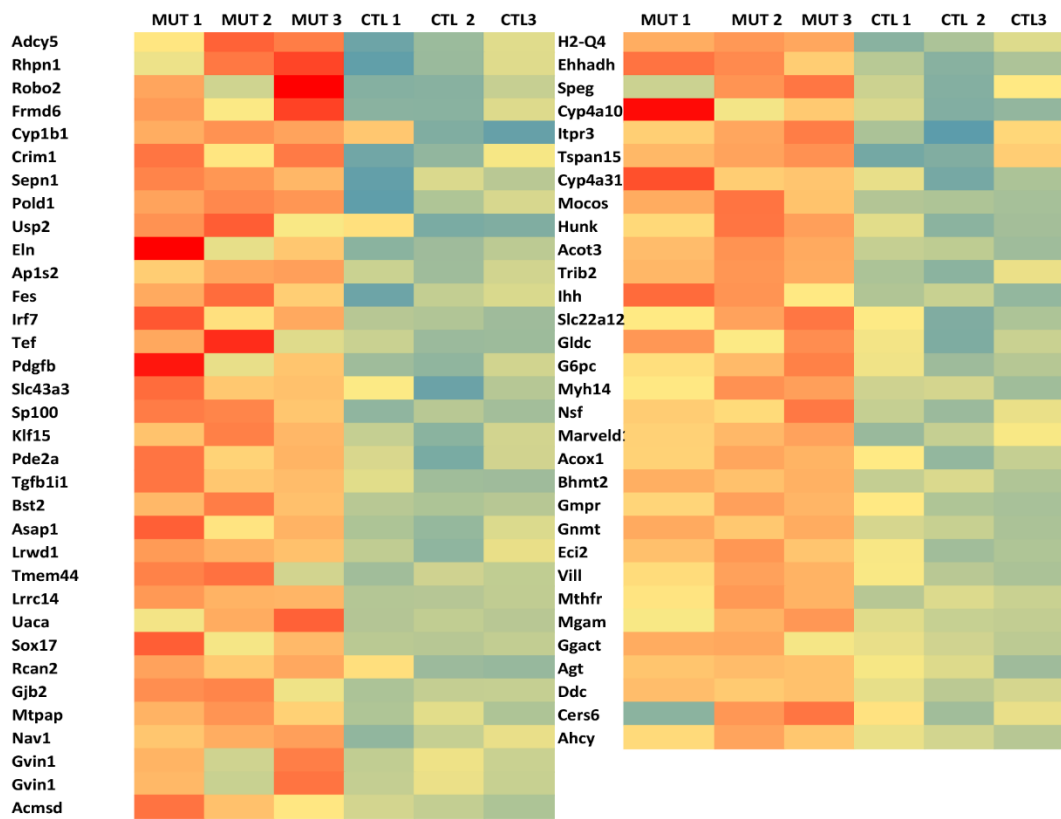
- Wang, X. M., Yao, M., Liu, S. X., Hao, J., Liu, Q. J. & Gao, F. 2014. Interplay between the Notch and PI3K/Akt pathways in high glucose-induced podocyte apoptosis. *Am J Physiol Renal Physiol*, 306, F205-13.
- Wang, Y., Zhou, C. J. & Liu, Y. 2018. Wnt Signaling in Kidney Development and Disease. *Prog Mol Biol Transl Sci*, 153, 181-207.
- Wang, Z. Y., Qiu, Q. Q., Enger, K. T. & Deuel, T. F. 1993. A second transcriptionally active DNA-binding site for the Wilms tumor gene product, WT1. *Proc Natl Acad Sci U S A*, 90, 8896-900.
- Wartiovaara, J., Ofverstedt, L. G., Khoshnoodi, J., Zhang, J., Makela, E., Sandin, S., Ruotsalainen, V., Cheng, R. H., Jalanko, H., Skoglund, U. & Tryggvason, K. 2004. Nephrin strands contribute to a porous slit diaphragm scaffold as revealed by electron tomography. *J Clin Invest*, 114, 1475-83.
- Waters, A. M., Wu, M. Y., Onay, T., Scutaru, J., Liu, J., Lobe, C. G., Quaggin, S. E. & Piscione, T. D. 2008. Ectopic notch activation in developing podocytes causes glomerulosclerosis. *J Am Soc Nephrol*, 19, 1139-57.
- Wei, C., El Hindi, S., Li, J., Fornoni, A., Goes, N., Sageshima, J., Maignel, D., Karumanchi, S. A., Yap, H. K., Saleem, M., Zhang, Q., Nikolic, B., Chaudhuri, A., Daftarian, P., Salido, E., Torres, A., Salifu, M., Sarwal, M. M., Schaefer, F., Morath, C., Schwenger, V., Zeier, M., Gupta, V., Roth, D., Rastaldi, M. P., Burke, G., Ruiz, P. & Reiser, J. 2011. Circulating urokinase receptor as a cause of focal segmental glomerulosclerosis. *Nat Med*, 17, 952-60.
- Weinmaster, G. & Fischer, J. A. 2011. Notch ligand ubiquitylation: what is it good for? *Dev Cell*, 21, 134-44.
- Welsch, T., Endlich, N., Kriz, W. & Endlich, K. 2001. CD2AP and p130Cas localize to different F-actin structures in podocytes. *Am J Physiol Renal Physiol*, 281, F769-77.
- Wharram, B. L., Goyal, M., Wiggins, J. E., Sanden, S. K., Hussain, S., Filipiak, W. E., Saunders, T. L., Dysko, R. C., Kohno, K., Holzman, L. B. & Wiggins, R. C. 2005. Podocyte depletion causes glomerulosclerosis: diphtheria toxin-induced podocyte depletion in rats expressing human diphtheria toxin receptor transgene. *J Am Soc Nephrol*, 16, 2941-52.

- Wharton, K. A., Yedvobnick, B., Finnerty, V. G. & Artavanis-Tsakonas, S. 1985. opa: a novel family of transcribed repeats shared by the Notch locus and other developmentally regulated loci in *D. melanogaster*. *Cell*, 40, 55-62.
- White, J. T., Zhang, B., Cerqueira, D. M., Tran, U. & Wessely, O. 2010. Notch signaling, wt1 and foxc2 are key regulators of the podocyte gene regulatory network in *Xenopus*. *Development*, 137, 1863-73.
- Wiggins, J. E., Goyal, M., Sanden, S. K., Wharram, B. L., Shedden, K. A., Misek, D. E., Kuick, R. D. & Wiggins, R. C. 2005. Podocyte hypertrophy, "adaptation," and "decompensation" associated with glomerular enlargement and glomerulosclerosis in the aging rat: prevention by calorie restriction. *J Am Soc Nephrol*, 16, 2953-66.
- Wilkin, M., Tongngok, P., Gensch, N., Clemence, S., Motoki, M., Yamada, K., Hori, K., Taniguchi-Kanai, M., Franklin, E., Matsuno, K. & Baron, M. 2008. Drosophila HOPS and AP-3 complex genes are required for a Deltex-regulated activation of notch in the endosomal trafficking pathway. *Dev Cell*, 15, 762-72.
- Wilkinson, G., Dennis, D. & Schuurmans, C. 2013. Proneural genes in neocortical development. *Neuroscience*, 253, 256-73.
- Wong, G. T., Manfra, D., Poulet, F. M., Zhang, Q., Josien, H., Bara, T., Engstrom, L., Pinzon-Ortiz, M., Fine, J. S., Lee, H. J., Zhang, L., Higgins, G. A. & Parker, E. M. 2004. Chronic treatment with the gamma-secretase inhibitor LY-411,575 inhibits beta-amyloid peptide production and alters lymphopoiesis and intestinal cell differentiation. *J Biol Chem*, 279, 12876-82.
- Wong, P. C., Zheng, H., Chen, H., Becher, M. W., Sirinathsinghji, D. J., Trumbauer, M. E., Chen, H. Y., Price, D. L., Van Der Ploeg, L. H. & Sisodia, S. S. 1997. Presenilin 1 is required for Notch1 and Dll1 expression in the paraxial mesoderm. *Nature*, 387, 288-92.
- Woroniecki, R. P. & Kopp, J. B. 2007. Genetics of focal segmental glomerulosclerosis. *Pediatr Nephrol*, 22, 638-44.
- Xiao, Z., Zhang, J., Peng, X., Dong, Y., Jia, L., Li, H. & Du, J. 2014. The Notch gamma-secretase inhibitor ameliorates kidney fibrosis via inhibition of TGF-beta/Smad2/3 signaling pathway activation. *Int J Biochem Cell Biol*, 55, 65-71.
- Xu, J., Nie, X., Cai, X., Cai, C. L. & Xu, P. X. 2014. Tbx18 is essential for normal development of vasculature network and glomerular mesangium in the mammalian kidney. *Dev Biol*, 391, 17-31.

- Yaddanapudi, S., Altintas, M. M., Kistler, A. D., Fernandez, I., Moller, C. C., Wei, C., Peev, V., Flesche, J. B., Forst, A. L., Li, J., Patrakka, J., Xiao, Z., Grahammer, F., Schiffer, M., Lohmuller, T., Reinheckel, T., Gu, C., Huber, T. B., Ju, W., Bitzer, M., Rastaldi, M. P., Ruiz, P., Tryggvason, K., Shaw, A. S., Faul, C., Sever, S. & Reiser, J. 2011. CD2AP in mouse and human podocytes controls a proteolytic program that regulates cytoskeletal structure and cellular survival. *J Clin Invest*, 121, 3965-80.
- Yamamoto, S., Charng, W. L., Rana, N. A., Kakuda, S., Jaiswal, M., Bayat, V., Xiong, B., Zhang, K., Sandoval, H., David, G., Wang, H., Haltiwanger, R. S. & Bellen, H. J. 2012. A mutation in EGF repeat-8 of Notch discriminates between Serrate/Jagged and Delta family ligands. *Science*, 338, 1229-32.
- Yamamoto, S., Schulze, K. L. & Bellen, H. J. 2014. Introduction to Notch signaling. *Methods Mol Biol*, 1187, 1-14.
- Yang, A. H., Chen, J. Y. & Chen, B. F. 2004a. The dysregulated glomerular cell growth in Denys-Drash syndrome. *Virchows Arch*, 445, 305-14.
- Yang, L. T., Nichols, J. T., Yao, C., Manilay, J. O., Robey, E. A. & Weinmaster, G. 2005. Fringe glycosyltransferases differentially modulate Notch1 proteolysis induced by Delta1 and Jagged1. *Mol Biol Cell*, 16, 927-42.
- Yang, X., Klein, R., Tian, X., Cheng, H. T., Kopan, R. & Shen, J. 2004b. Notch activation induces apoptosis in neural progenitor cells through a p53-dependent pathway. *Dev Biol*, 269, 81-94.
- Yu, H., Kistler, A., Faridi, M. H., Meyer, J. O., Trynieszewska, B., Mehta, D., Yue, L., Dyer, S. & Reiser, J. 2016. Synaptopodin Limits TRPC6 Podocyte Surface Expression and Attenuates Proteinuria. *J Am Soc Nephrol*, 27, 3308-3319.
- Yuan, Y., Zhao, C., An, X., Wu, L., Wang, H., Zhao, M., Bai, M., Duan, S., Zhang, B., Zhang, A. & Xing, C. 2016. A vital role for myosin-9 in puromycin aminonucleoside-induced podocyte injury by affecting actin cytoskeleton. *Free Radic Res*, 50, 627-37.
- Zemel, S., Bartolomei, M. S. & Tilghman, S. M. 1992. Physical linkage of two mammalian imprinted genes, H19 and insulin-like growth factor 2. *Nat Genet*, 2, 61-5.
- Zhang, M., Qin, Y., Zuo, B., Gong, W., Zhang, S., Gong, Y., Quan, Z. & Chu, B. 2017. Overexpression of NOTCH-regulated Ankyrin Repeat Protein is associated with papillary thyroid carcinoma progression. *PLoS One*, 12, e0167782.

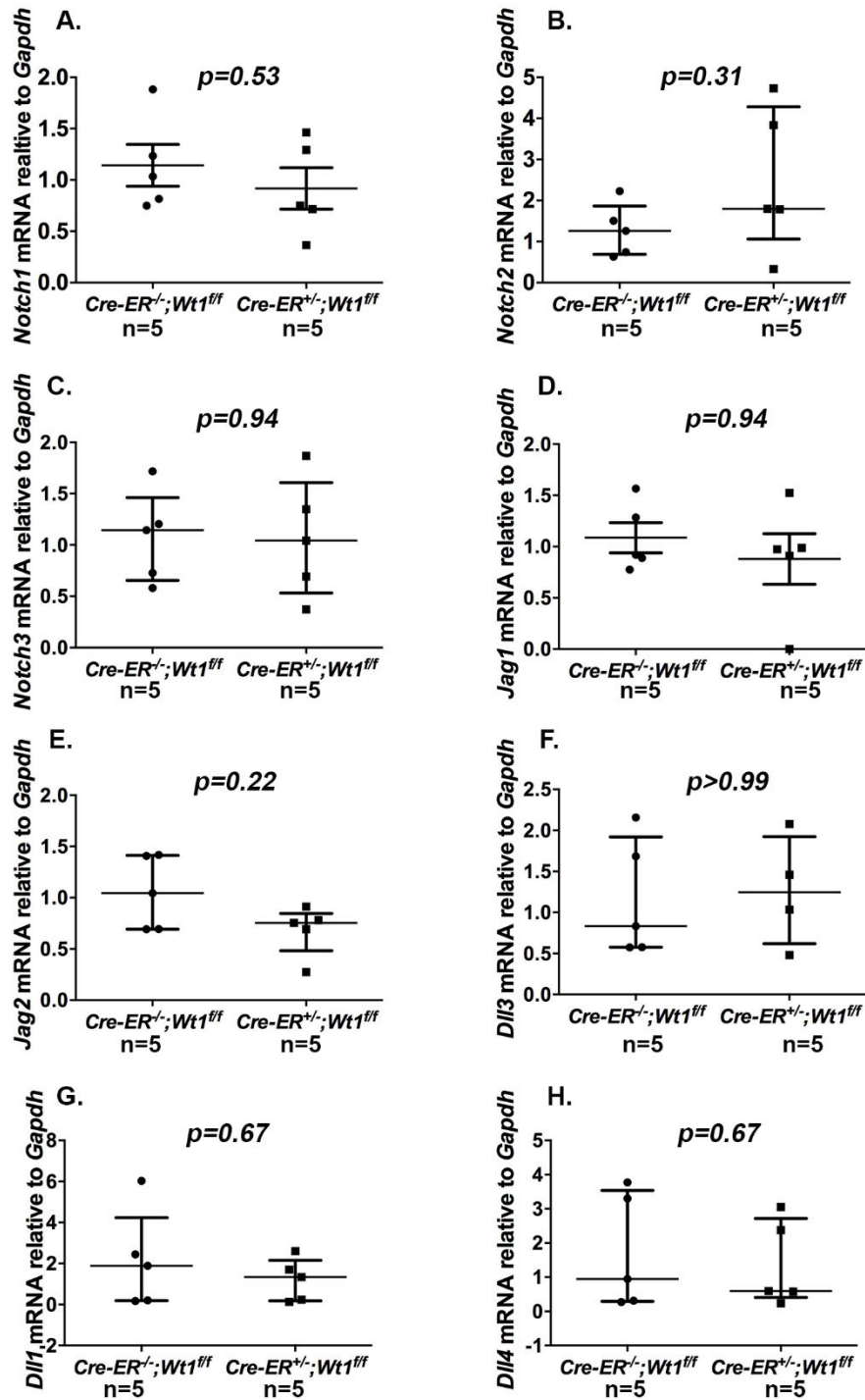
Zhou, T. B. & Qin, Y. H. 2012. The signaling pathways of LMX1B and its role in glomerulosclerosis. *J Recept Signal Transduct Res*, 32, 285-9.

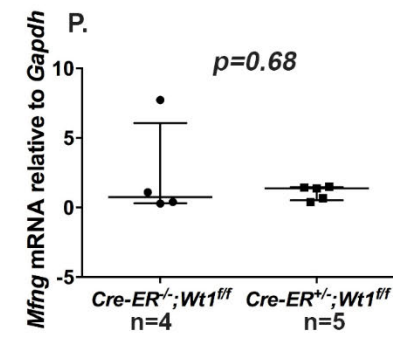
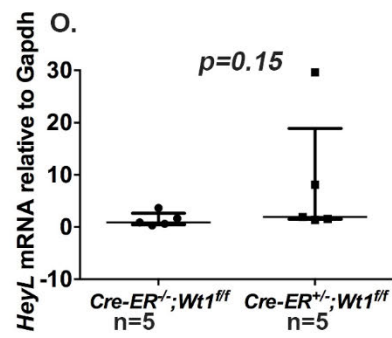
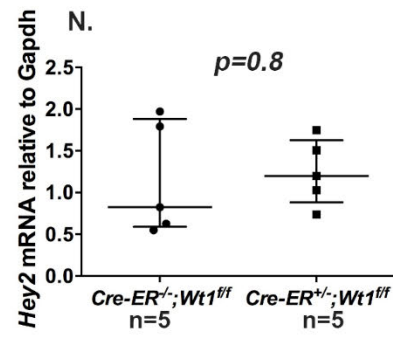
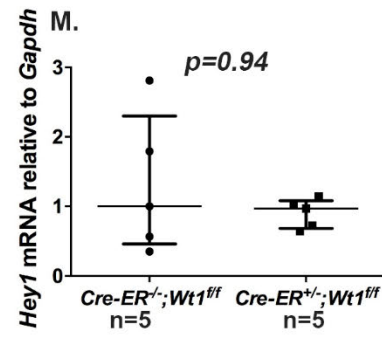
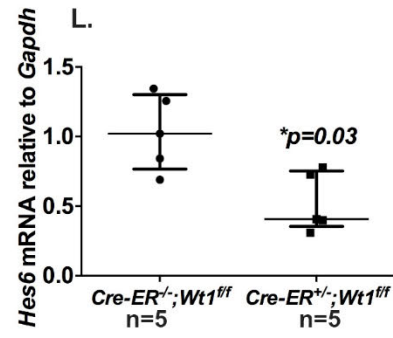
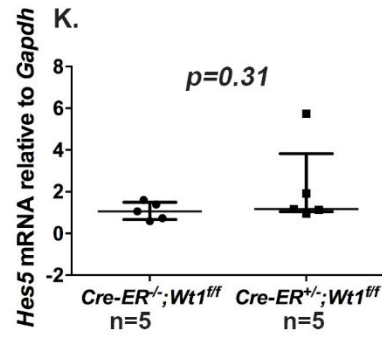
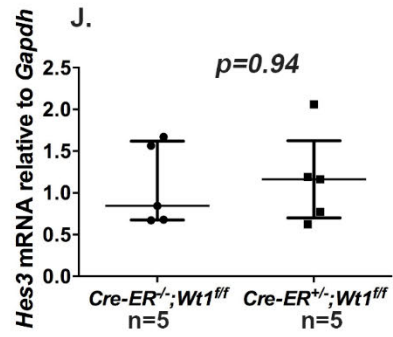
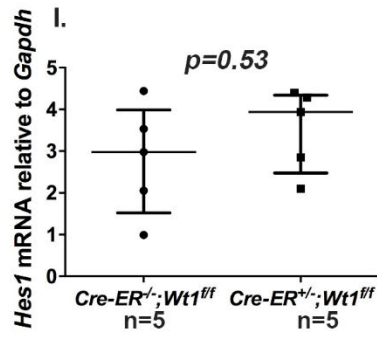
Zou, J., Yaoita, E., Watanabe, Y., Yoshida, Y., Nameta, M., Li, H., Qu, Z. & Yamamoto, T. 2006. Upregulation of nestin, vimentin, and desmin in rat podocytes in response to injury. *Virchows Arch*, 448, 485-92.



Appendix B

Figure B.1. Dot plot analyses showing each gene of the Notch pathway at D4 P.I. (*Cre-ERTM/-;Wt1^{ff}* vs. *Cre-ERTM/+;Wt1^{ff}*). Middle horizontal lines mark median mRNA transcript levels relative to *Gapdh*, upper and lower horizontal lines mark the IQR.





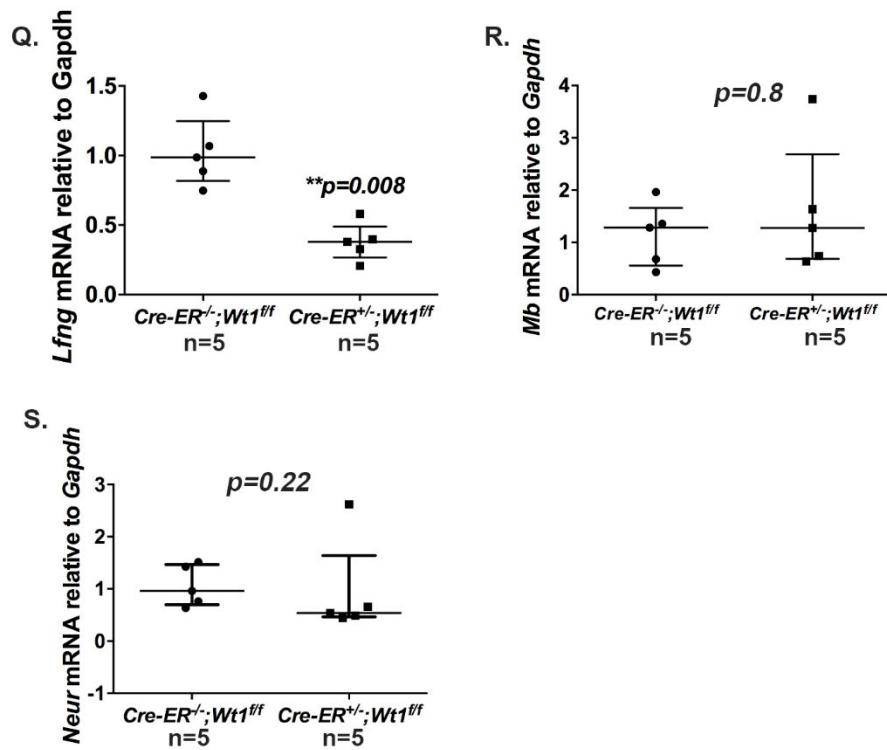
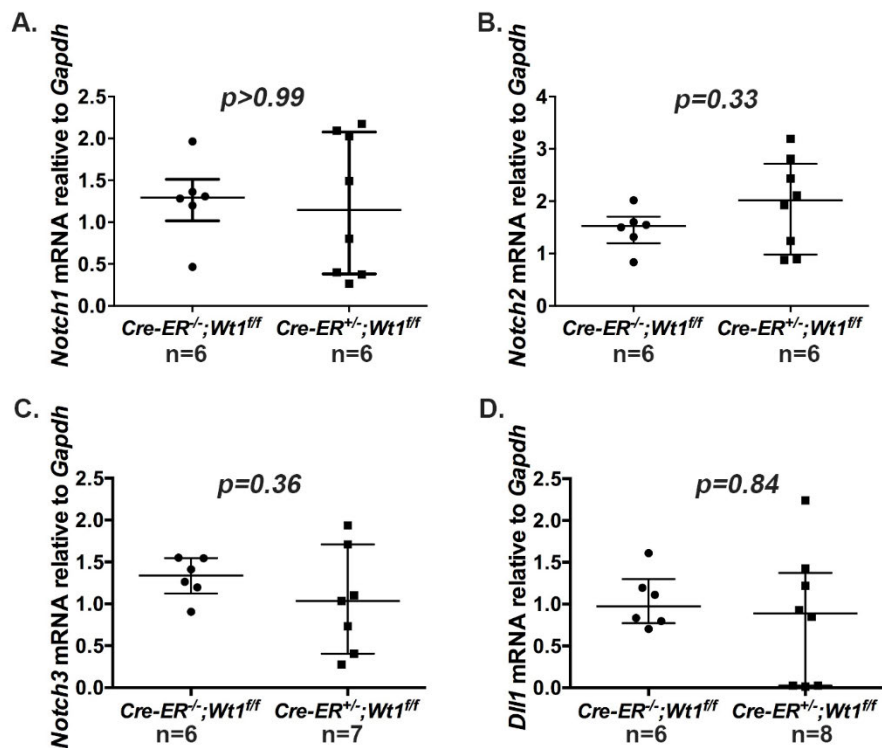
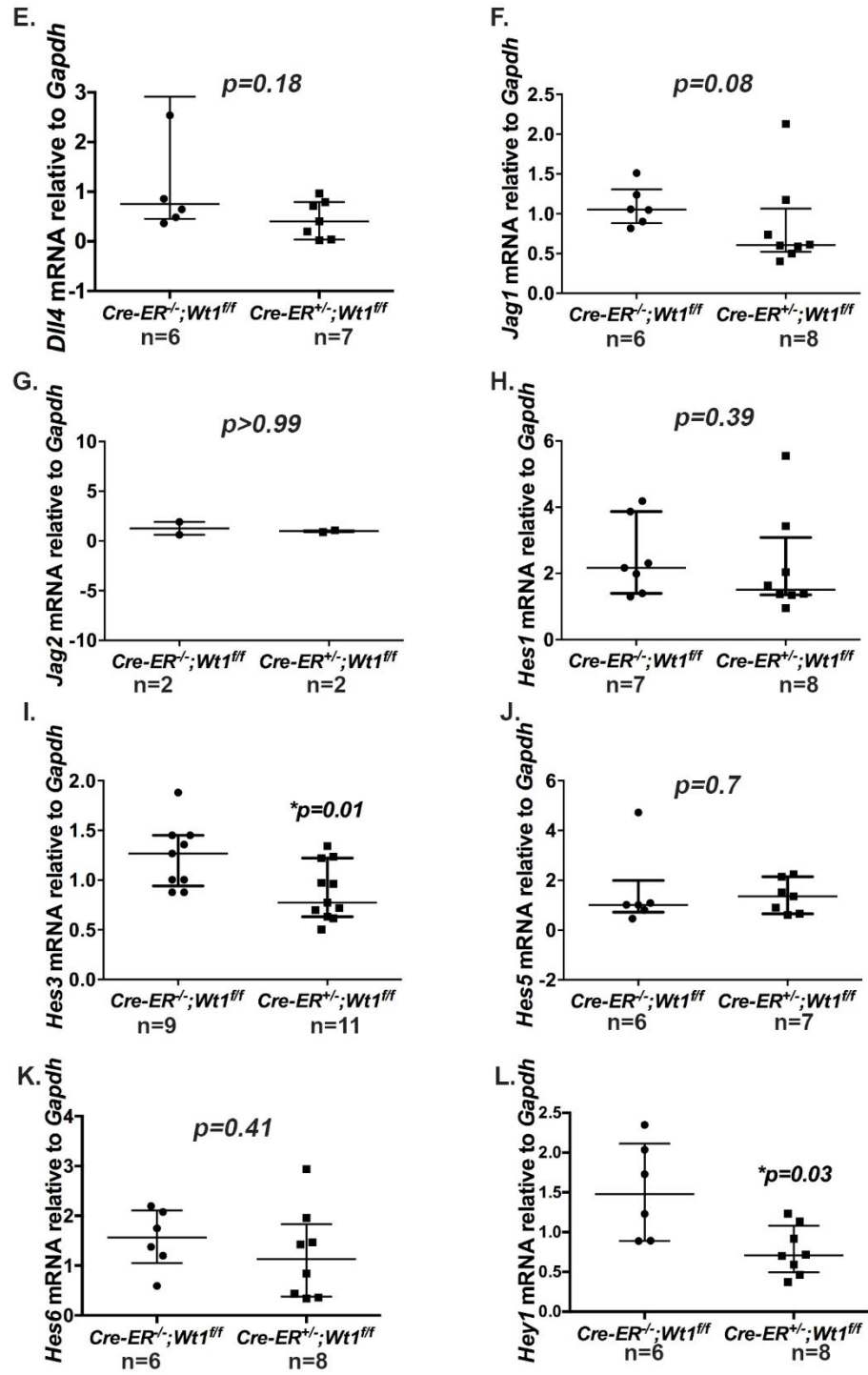


Figure B.2. Dot plot analyses showing each gene of the Notch pathway at D5 P.I. (*Cre-ER^{TM-/-};Wt1^{ff}* vs. *Cre-ER^{TM+/-};Wt1^{ff}*). Middle horizontal lines mark median mRNA transcript levels relative to *Gapdh*, upper and lower horizontal lines mark the IQR.





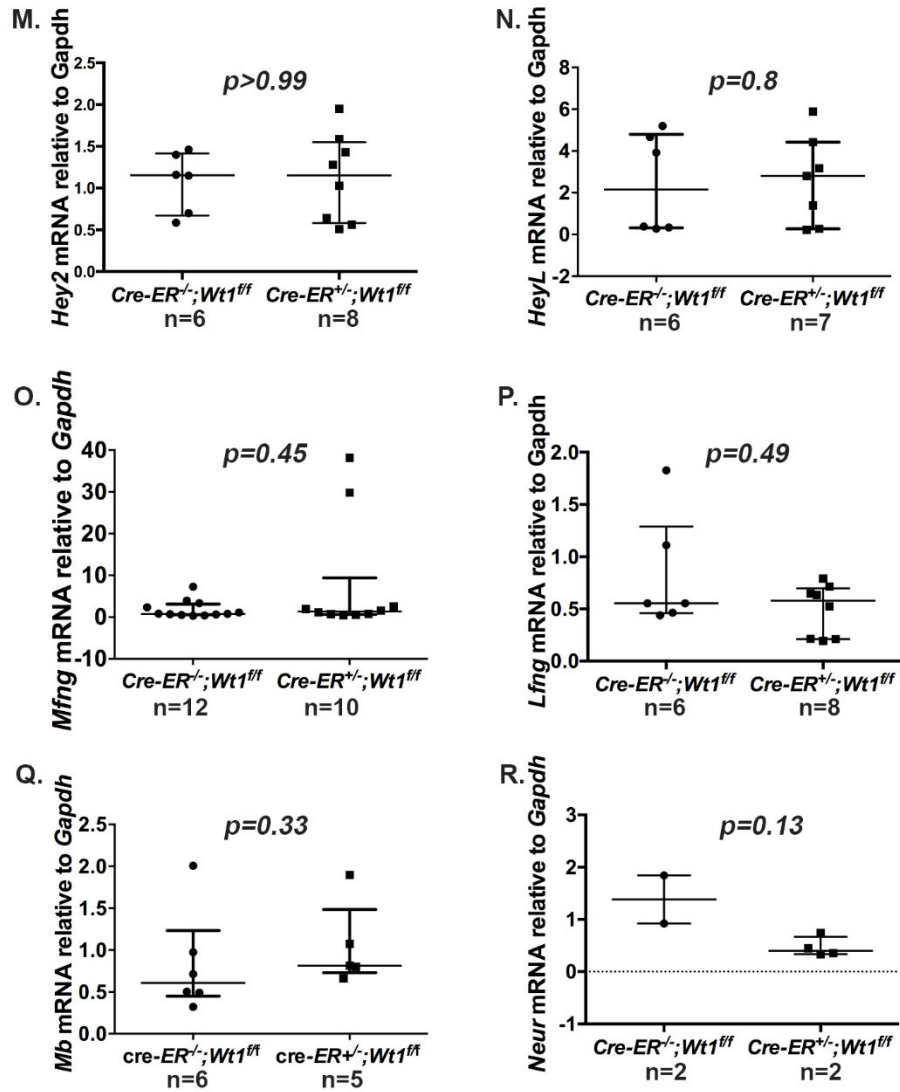


Figure B.3. Dot plot analyses showing each gene of the Notch pathway at D6 P.I. (*Cre-ER^{TM-/-};Wt1^{fl/fl}* vs. *Cre-ER^{TM+/-};Wt1^{fl/fl}*). Middle horizontal lines mark median mRNA transcript levels relative to *Gapdh*, upper and lower horizontal lines mark the IQR

